SCUOLA NORMALE SUPERIORE - PISA

Tesi
di
Perfezionamento

Linear and nonlinear optics of Bose fields: light waves in dielectric structures, matter waves in optical lattices

Candidato:
Iacopo Carusotto

Relatore:
Prof. G. C. La Rocca

Contents

Preface 1

I Semiconductor optics 5

Introduction 7

1 Linear optics of semiconductor DBR microcavities 11

1.1 The Photonic Band Gap (PBG) crystal 12

1.2 The Distributed Bragg Reflector (DBR) as a one-dimensional PBG . . 16

1.3 The DBR microcavity 18

1.4 The DBR cavity as an impurity in a PBG crystal 20

1.5 Strong exciton-photon coupling effects in DBR microcavities 22

1.5.1 A simple two-mode model 22

1.5.2 An *ab initio* calculation via transfer matrices 27

1.6 The microcavity polaritons: quantum coherence effects in the transmission spectra 30

1.7 Linear optics of coupled microcavities 33

2 Nonlinear optics of microcavities I: intensity-dependent refractive index 37

2.1 The nonlinear Fabry-Perot interferometer 38

2.2 The single mode model 42

2.3 The nonlinear DBR microcavity 44

2.4 Nonlinear DBR microcavity containing excitonic resonances 47
2.5 Two-beam nonlinear interactions: pump and probe optics and optical switching 49
2.6 Nonlinear optics of coupled DBR microcavities 51

3 Nonlinear optics of microcavities II: two-photon processes 55
3.1 The model 57
3.2 Transmission and second harmonic generation spectra: two-photon Rabi splitting 60
3.2.1 Physical interpretation of the results 63
3.2.2 Comparison with another quadratically nonlinear system. . . 64
3.3 Two-photon optical Stark effect: probing the dressed system 65
3.4 Discussion of material and geometrical parameters 74

Conclusions and perspectives 81

II Atom optics 85

Introduction 87

4 Atom optics fundamentals from a quantum optics point of view 91
4.1 Field-theoretical approach to atom optics 92
4.2 The many-body problem of the interacting Bose gas 98
4.2.1 Coherent matter waves, Bose condensates and the mean-field approximation 101

5 Atom optics in optical lattices and the atomic Fabry-Perot interferometer 105
5.1 The simple optical lattice: localized modes and tunneling resonances 107
5.2 The bichromatic optical lattice 113
5.3 Nonlinear atom optics: optical limiting and optical bistability 117

5.4 Atom laser coherence length determination 120
5.4.1 A simple atom laser model 121
5.4.2 Velocity filtering 123
5.4.3 Atomic standing wave 126

Conclusions and perspectives **133**

III Quantum (atom) optics 137

Introduction **139**

6 Quantum theory of the single-mode nonlinear (atomic) Fabry-Perot cavity 143
6.1 The model 145
6.2 Weak nonlinearity case: mean field theory and linearized fluctuations 151
6.3 Strong nonlinearity: the *(atom) blockade* effect 158
6.4 Quantum tunneling effects in optical bistability 166
6.5 Conclusions and perspectives 171

7 A stochastic macroscopic wavefunction approach to the interacting Bose gas 173
7.1 Stochastic formulation of the N-boson problem using Hartree functions 176
7.1.1 A stochastic Hartree Ansatz with Fock states 176
7.1.2 Stochastic evolution of a Fock state Hartree dyadic 179
7.1.3 Exact evolution of a Fock state Hartree dyadic 181
7.1.4 Validity conditions for the stochastic Fock state Hartree ansatz 182
7.1.5 A stochastic Hartree ansatz with coherent states 183
7.2 Particular implementations of the stochastic approach 184
7.2.1 Growth of the statistical errors 185
7.2.2 The *simple* schemes 187

7.2.3 The *constant trace* schemes 192
7.3 Stochastic vs. exact approach for a two-mode model 193
7.4 Stochastic approach for a one-dimensional Bose gas 198
7.5 Conclusions and perspectives 199

Conclusions and future developments **203**

List of publications **209**

Other research activities **211**

Bibliography **217**

Acknowledgments **241**

Preface

This thesis summarizes the main topics of the research activity performed during the three years of the *Corso di Perfezionamento* at the *Scuola Normale Superiore* in Pisa under the supervision of prof. Giuseppe La Rocca: it has been my great pleasure to have the possibility of exploring several different fields of physics and the main conclusion that I may be tempted to get from this experience is certainly that physics is still much more unified than people generally say. Indeed, it seems to me still possible as well as very fascinating to try to keep track of the main ideas of neighboring fields so as to mutually exchange techniques and physical pictures; in this way, all fields can profit from a strong cross-fertilization effect.

Even if completely different physical systems have been examined during these three years, most of the thesis can be considered as the discussion of a pair of different realizations of the same physical concept, the *interacting bosonic field*: both light waves and bosonic atoms can be in fact described in terms of a quantum field with Bose commutation relations. The different pictures that we generally have in mind of the two systems derive not only from the different dispersion laws of the two particles and, in particular, the massive nature of the atomic field with respect to the massless electromagnetic field, but also from the much shorter wavelength of room temperature matter waves with respect to visible light. Of course, the atom is here considered as a single entity and its composite nature generally neglected: this simplified description is clearly correct only provided its internal degrees of freedom are not involved in the dynamics.

The different historical development of human knowledge about the matter and the light fields closely reflects these points: the relatively long wavelength of visible light has allowed a rather early observation of the interference and diffraction effects typical of a wave, while the smallness of the single photon energy has hidden the quantum nature of the light field until the beginning of the century when

the photoelectric effect was discovered. On the other hand, the discrete nature of the matter field, already guessed by the ancient Greeks, has been the base of all atomistic theories of matter, whereas the shortness of the atomic wavelength has hidden the wavy character until the first atomic interference experiments in the late twenties. Both the particle and the wave character of the quantum Bose field have therefore been known for centuries, but only very recently it has been realized that they are different aspects of the same entity; only the advent of modern quantum mechanics and, in particular, of quantum field theory has led to the unification of the wave and particle concepts into the unified concept of quantum field so that matter and light have ceased to be considered completely distinct physical entities.

Very remarkably, the field-theoretical description of collisional atom-atom interactions is analogous to the description of optical nonlinearities in dielectric media with an intensity dependent refraction index: in both cases, in fact, the Hamiltonian has to include an interaction term quartic in the field operators. This means that any physical consideration on an interacting atomic Bose gas is easily extended to an interacting gas of photons which propagate in a nonlinear medium and vice versa. Thanks to the recent progress in the realization of coherent sources of matter waves, the analogy of atom optics with photon optics is now complete: such atom laser beams are in fact the atomic analogs of optical laser beams and have very similar all-order coherence properties; for this reason, nonlinear atom optics with atom laser beams is now the subject of a very intense research. In particular, the much stronger atom-atom interaction strength with respect to the effective photon-photon one in nonlinear media is expected to allow for appreciable nonlinear optical effects with just a very small number of quanta, so that definitely quantum effects such as non-classical beams and quantum entanglements should be more easily observed with matter waves.

The first part of the thesis is devoted to a discussion of nonlinear optical effects in the presence of dielectric systems which modify the mode structure of the electromagnetic field, in particular distributed Bragg reflector microcavities. In the presence of discrete states, the light field can be described in terms of a finite number of harmonic oscillators and the nonlinearities are included as additional anharmonic terms in the Hamiltonian; damping terms account for the coupling to the continuum of propagating states external to the dielectric structure. At the classical level, the description in terms of such discrete modes is shown to be equivalent to Maxwell's wave equations in a nonlinear dielectric medium but leads to much simpler calcu-

lations; instead of working with nonlinear partial differential equations, a simple system of a few ordinary differential equations is able to give accurate quantitative predictions as well as a deeper insight in the physical behavior. In this approach, all the details of the specific system under examination are summarized in a small number of parameters governing the dynamics of the system. In particular, we shall discuss two different kinds of optical nonlinearities: an intensity-dependent refraction index and resonant two-photon processes; in both cases, the transmission spectra of the microcavity are characterized for growing values of the incident intensity and the possibility of observing optical bistability and optical limiting pointed out. In addition, we shall study the linear optical response of the cavity to a weak probe field when it is optically dressed by a strong pump beam: the control of the probe transmission by the pump beam can be interpreted as an optical transistor behavior, while the shift and splitting of the excitonic spectral features which appear in the case of two-photon absorption can be seen as a two-photon optical Stark effect.

Given the strict analogy between Maxwell's equations for the electromagnetic field in nonlinear materials and the Gross-Pitaevskii equation for the coherent interacting matter waves of a Bose condensate or an atom laser, much of the results of the first part are applied in the second part to the propagation of a coherent atomic beam through an optical lattice; the periodic optical potential of the laser field is in fact a sort of distributed Bragg reflector for matter waves and a microcavity can be obtained using a spatially modulated lattice. The discrete modes which appear in the numerically predicted transmission spectra are interpreted in terms of an effective mass approximation: since the atomic mass at the gap edge is much lighter than the free-space mass, the mode spacing can be as large as one tenth of the atomic recoil energy. This fact, together with the narrow linewidth of the modes, suggests the use of such atomic Fabry-Perot cavities for nonlinear atom optics experiments: collisional atom-atom interactions will be shown to allow for (atom) optical limiting and (atom) optical bistability.

Since the strength of atom-atom interactions is generally orders of magnitude larger than the effective strength of the photon-photon interactions induced by the nonlinear dielectric material, the mean-field approach underlying the Gross-Pitaevskii equation for the atomic field is more likely to fail than Maxwell's equation of classical electrodynamics. In other terms, the appearance of an appreciable nonlinear optical effect generally requires a smaller number of quanta in the atomic case, so that nonclassical effects should be better observed with matter waves rather than

light waves.

The third part of the thesis is devoted to the exact study of a strongly interacting Bose field beyond the mean field approximation and, in particular, of the quantum coherence properties of the field. In the case of a single-mode cavity, such a calculation can be exactly performed in terms of the quantum master equation for the field: for low values of the nonlinear coupling, the behavior is close to the one predicted by the mean-field theory: quantum effects are only a small correction and can be treated in a perturbative way. For strong nonlinearities, definitely quantum effects appear in the coherence properties of the transmitted beam: for the case of an incident beam exactly on resonance with the empty cavity, a sort of *atom blockade* effect will be discussed; for the case of a blue-detuned incident beam (and repulsive interactions), a bimodal shape is found for the steady-state atom distribution in the cavity mode, which is the quantum generalization of optical bistability.

While the simple structure of the Hilbert space of the single-mode system has allowed the quantum master equation to be numerically solved, an analogous task becomes quickly unfeasible as soon as a few modes of the field have to be included: as most relevant examples, the dynamics of an atomic cloud in a magnetic trap as well as the coherence properties of light in a strongly nonlinear planar microcavity are very hardly determined unless we limit ourselves to a mean-field approximation. The thesis is concluded by the discussion of a novel reformulation of the time-evolution of an interacting Bose gas in terms of the stochastic evolution of Hartree states; this work has been mainly performed at the *Laboratoire Kastler-Brossel* in Paris[(a)] during the first months of 1999 under the supervision of proff. Jean Dalibard and Yvan Castin. Among the many possible implementations of the method, schemes can be found, which are not subject to the divergences typical of Positive-P calculations since they lead to stochastic differential equations with a regular solution for all times; the stochastic scheme of Positive-P representation is itself recovered as another specific scheme of our general framework. Although the numerical calculations performed so far have dealt only with very simple systems, the approach looks very promising for the numerical study of multimode systems involving a relatively small number of strongly interacting particles.

[(a)]Partial financial support from EC (TMR network ERB FMRX-CT96-0002) is acknowledged.

Part I

Semiconductor optics

Introduction

A substantial progress in the investigation of fundamental effects in light-matter interaction has followed the development of laser sources, which are able to generate fields of remarkable monochromaticity and intensity. Most experiment were initially carried out on gaseous samples, which have optical transitions with a homogeneous linewidth very close to the natural radiative one.[1,2] In this way it is possible to perform the experiments of interest without being disturbed by spurious damping effects which could hide the process under examination. Very recently, laser cooling and trapping techniques have allowed to overcome even Doppler broadening effects: in this way it is now possible to cool the atoms down to temperatures for which the Doppler linewidth is much smaller than the natural one.[3] However, all these experiments require an apparatus which is far from being simple and portable: several laser sources are in fact needed to manipulate the atoms and the alignment of the experimental setup can be problematic.

Since the recent progress in growing semiconductor samples with optical features sufficiently sharp and free from unwanted damping effects, there has been much interest in trying to export all the nonlinear and quantum optics formalism to the description of optical processes in solid-state samples. From the experimental point of view it is in fact much simpler to work with a solid-state sample than with an atomic one: once the sample has been grown, there is no need for complicate manipulations but for its cooling down to a few Kelvin via conventional techniques. From the point of view of applications, optical elements as small and as portable as semiconductor ones have an enormous utility, since light-emitting diodes, harmonic generators and bistable elements are widely applied in all sorts of optical setups. Also from a fundamental point of view the study of optical properties of solid-state materials can bring to a deeper understanding of the dynamics of the material excitations which are made to interact with the electromagnetic field, e.g.

phonons, free electron-hole pairs, excitons and even biexcitons.

The recent developments in the controlled growth of heterostructures of different semiconducting materials on the nanometer scale have opened the possibility of having the carrier motion quantized in some spatial directions and hence of studying electronic systems with reduced dimensionalities such as quantum wells (2D), quantum wires (1D) and even quantum dots (0D).[4] Since the confinement of carriers makes the excited electron-hole pairs to interact more strongly among them, such systems are very interesting from the point of view of nonlinear optics: sharp excitonic resonances can be observed in the optical response even at room temperature and the corresponding susceptibilities show a strong dependence on the excitation level.[5,6]

But semiconductor heterostructures not only can affect the carrier motion in the material, but can also modify the structure of photonic modes; in particular, it has been shown as possible to have a photonic density of states which vanishes in a certain window as well as a sharply peaked one. A vanishing density of states can be observed in a photonic band gap (PBG) crystal: thanks to the periodic modulation of the refraction index, light is effectively forbidden from propagating at frequencies comprised within the gap and spontaneous emission can not occur at such frequencies. Sharp peaks in the density of states can be observed in microcavity systems, in which light is confined by a pair of distributed Bragg reflectors (DBR): the presence of the cavity mode gives a sharply peaked density of states at the resonance frequency with a spatially localized photonic wavefunction. Provided the damping is weak enough, the strong enhancement of the light-matter interaction which follows the spatial localization of both the photonic and the excitonic modes can eventually lead to a strong coupling regime in which the eigenmodes of the system are mixed exciton-polariton modes.

Much of the published literature on semiconductor microcavities deals with linear optical processes; only recently nonlinear and quantum effects in such structures have been studied and observed. This field obviously deserves a greater attention, both because it can provide new informations on the dynamics of carriers in heterostructures and because the specific nonlinear properties of the material may allow for new optical processes.

This first part of the thesis is devoted to the study of the optical properties of semiconductor DBR microcavities at both linear and nonlinear regime: in chap.1, we give

a short and simple review of the linear regime behavior; the two following chaps.2 and 3 summarize our original results on the nonlinear response of semiconductor microcavities in the presence of either an intensity-dependent refractive index or resonant two-photon processes such as second-harmonic generation or two-photon absorption.

Chapter 1

Linear optics of semiconductor DBR microcavities

This first chapter contains a short review of the linear optical properties of photonic band gap (PBG) crystals, distributed Bragg reflectors (DBR) and finally DBR microcavities: in all these systems, a spatial modulation of the dielectric properties is exploited in order to strongly modify the photonic mode structure with respect to the free-space one.

Sec.1.1 discusses the photonic dispersion in systems in which the dielectric constant has a periodic spatial modulation, such as PBG crystals: the typical features of wave dispersion in periodic systems are recovered, such as allowed bands and forbidden gaps.

Sec.1.2 applies these ideas to the so-called distributed Bragg reflectors (DBR): a light beam which incides on the finite slab of PBG forming the DBR mirror is transmitted if the frequency corresponds to a band while it is nearly totally reflected if the light frequency corresponds to a forbidden gap in the photonic dispersion.

The two following sections introduce the concept of a DBR microcavity from two different points of view: in sec.1.3 we shall consider the optical cavity formed by a pair of DBR mirrors separated by a cavity layer of dielectric. As it is well-known from classical electromagnetism, the mirrors impose boundary conditions to the electromagnetic field in the cavity and the frequencies of the resulting localized modes depend on the thickness of the cavity layer. From a different point of view (sec.1.4), these same modes can be interpreted as defect states in an otherwise pe-

riodic PBG crystal in exactly the same way as the bound states of the carriers in a doped semiconducting material.

The localization of the photonic mode wavefunction can be used to enhance the interaction of the light field with matter: as discussed in sec.1.5, if an excitonic transition is coupled to the cavity mode, a strong coupling regime can be achieved, in which the eigenmodes of the coupled system are a pair of polaritonic mixed states, i.e. linear superposition of matter and light excitations; in the transmission spectra, the mixing reflects into a splitting of the cavity transmission peak into a doublet of peaks.

In the case the excitonic linewidth is much smaller than the photonic one, quantum coherence effects between the polaritons are predicted to give rise to peculiar sharp features in the linear transmission spectrum in the weak-coupling regime (sec.1.6). This effect can be interpreted as the microcavity analog of the Fano interference profile of electromagnetically induced transparency.

Sec.1.7 completes the picture with a brief discussion of the properties of coupled DBR microcavities, i.e. a pair of DBR microcavities sharing a (generally less reflecting) central mirror. Such a system is characterized by a pair of localized cavity modes which are mutually coupled by the tunneling through the central mirror and the eigenmodes consist of a doublet of delocalized modes over the two cavities.

1.1 The Photonic Band Gap (PBG) crystal

As it is well known for electrons in a crystalline solid,[7–9] the dispersion of any particle or excitation in a system with a spatial periodicity is characterized by *allowed bands* and *forbidden gaps*. In particular, this is valid for the photonic dispersion in a material medium with spatially periodic refractive properties.[10,11]

The discrete translational symmetry of the system allows in fact for the application of Bloch's theorem[7] so that the energy states can be classified in terms of a *quasimomentum* k which spans the first Brillouin zone (FBZ) of the lattice, and a *band index*. Great effort has been recently devoted to the realization of structures showing a complete *photonic band gap* (PBG), i.e. a finite energy window in which the photonic density of states vanishes and light propagation is forbidden, irrespective of its propagation direction. In such systems, in fact, spontaneous emission processes

such as electron-hole recombination would be inhibited if the photonic band gap overlaps the electronic band edge leading to increased efficiencies of a semiconductor laser as well as to a squeezing of the output field.[11]

Although its conceptual simplicity, this complete PBG has been very elusive; a great deal of both theoretical and experimental works have appeared on the subject, some of them using even sophisticated group theory techniques;[12–15] a complete PBG has been finally obtained in the microwave frequency range using a fcc lattice with an asymmetrical Wigner-Seitz unit cell.[16,17]

Given a lattice with a periodicity L and a mean refraction index $\bar{n}$, the first gap opens up at a frequency of the order of the Bragg frequency

$$\omega_{Br} = \frac{c\pi}{L\bar{n}}. \tag{1.1}$$

A photonic crystal with the PBG located in the microwave range can be fabricated just by drilling an array of appropriately oriented holes in a solid dielectric material;[17] the required spacing being of the order of a few millimeters, the holes can in fact be easily obtained by means of ordinary microfabrication techniques.[11]

On the other hand, the realization of a structure showing a PBG at optical frequencies is still an open problem, since it requires a spatial modulation of the dielectric properties with a periodicity of the order of 100nm in all three dimensions. For such a purpose, a number of different systems are actually being investigated, such as polystirene colloidal crystals,[18,19] synthetic opals[20] and even atoms trapped in optical lattices.[21,22]

If we limit ourselves to one-dimensional geometries, structures with periodicities in the optical range are easily fabricated by means of *molecular beam epitaxy (MBE)* techniques allowing for Bragg mirrors as well as single and coupled microcavities to be grown; very recently, similar structures with periodicities as short as a few nanometers are beginning to be used as mirrors in the soft X-ray domain.[23]

The analogy between the electrons in a crystalline solid and the photons in a periodic dielectric structure can be further clarified by rewriting Maxwell's wave equation in a dielectric medium in the following Schrödinger-like form:[4]

$$-\frac{\hbar^2}{2m_o}\vec{\nabla}^2\vec{E}(x) - \hbar\omega\left[\epsilon(x)-1\right]\vec{E}(x) - \frac{\hbar^2}{2m_o}\vec{\nabla}\left[\left(\vec{\nabla}\log\epsilon(x)\right)\cdot\vec{E}(x)\right] = \hbar\omega\vec{E}(x); \tag{1.2}$$

ω is the photon frequency, $E(x)$ the electric field and $\epsilon(x)$ the local dielectric constant; the mass m_o has been defined according to $m_o = \hbar\omega/2c^2$. The first term of

eq.(1.2) describes a sort of kinetic energy of the photon, which takes into account the free-space photon dispersion; the second and third terms depend on the refractive properties of the material medium. In particular, the former term can be interpreted as giving a sort of dielectric potential V_{diel}

$$V_{diel}(x) = -\hbar\omega\left[\epsilon(x) - 1\right]; \tag{1.3}$$

to which photons are subjected. For the one-dimensional geometries which are matter of the following sections the electric field is everywhere parallel to the interfaces between different materials so that the last term, which would otherwise couple the spin and the translational degrees of freedom, results exactly vanishing.

The well-known total internal reflection at a dielectric-vacuum interface[24] can be interpreted as arising from the dielectric potential V_{diel} of eq.(1.3): if the longitudinal kinetic energy of the photon in the dielectric material $\hbar\omega\epsilon\cos^2\theta$ is not large enough for surmounting the potential step $\hbar\omega(\epsilon - 1)$ with respect to external free-space, the photon is reflected back. The condition for total internal reflection which follows from this approach agrees with the usual condition $\sin^2\theta > \epsilon^{-1}$.

Fig.1.1 reproduces the band structures for a one-dimensional periodic system: the calculations have been performed using the usual *transfer matrix* algorithm for the propagation of linearly polarized electromagnetic waves at normal incidence in a one-dimensional structure.[4,25] If we denote as

$$E(x,t) = v_1 e^{in_o(x-x_o)\omega/c} e^{-i\omega t} + v_2 e^{-in_o(x-x_o)\omega/c} e^{-i\omega t} \tag{1.4}$$

the resulting electric field of the two waves which propagate in respectively the forward and backward directions inside a slab of material of refraction index n_o, the field amplitude can be summarized in the two component complex vector

$$\mathbf{v} = \begin{pmatrix} v_1 \\ v_2 \end{pmatrix}. \tag{1.5}$$

In this formalism, both the boundary conditions at the interface between two layers with different refractive index and the propagation through an homogeneous slab are described by linear matricial equations of the form

$$\begin{pmatrix} v_1' \\ v_2' \end{pmatrix} = \begin{pmatrix} M_{11} & M_{12} \\ M_{21} & M_{22} \end{pmatrix} \begin{pmatrix} v_1 \\ v_2 \end{pmatrix} = \mathbf{M} \begin{pmatrix} v_1 \\ v_2 \end{pmatrix}. \tag{1.6}$$

In the first case, the *transfer matrix* M has the form

$$\mathbf{M}_{\text{int}} = \begin{pmatrix} \frac{n_1+n_2}{2n_2} & \frac{n_2-n_1}{2n_2} \\ \frac{n_2-n_1}{2n_2} & \frac{n_1+n_2}{2n_2} \end{pmatrix}, \tag{1.7}$$

$n_{1,2}$ being the refraction indices of the materials separated by the interface, while in the other case, it has the form

$$\mathbf{M}_{\text{pr}} = \begin{pmatrix} e^{in\omega l/c} & 0 \\ 0 & e^{-in\omega l/c} \end{pmatrix}. \tag{1.8}$$

In the next chapter (sec.2.3), this method will be generalized and applied to nonlinear materials in which the refractive index depends on the local light intensity.

For each value of the frequency ω, the wavevector of each mode k_i is given by $\lambda_i = e^{ik_iL}$, $\lambda_{1,2}$ being the eigenvalues of the 2x2 transfer matrix corresponding to propagation along the unit cell. The real part of k_i clearly refers to propagation, while the imaginary one to extinction (and, eventually, absorption, if the lattice is dissipative).[26]

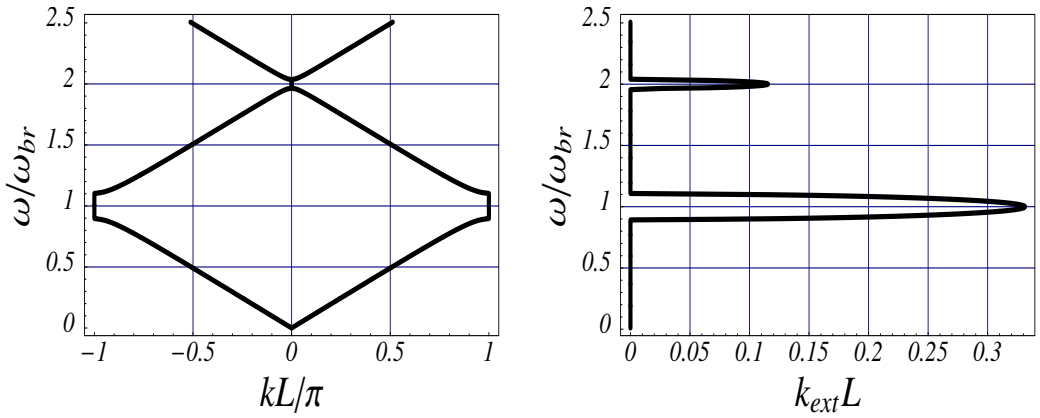

FIGURE 1.1: Photonic structure of a one-dimensional periodic non-absorbing structure composed of alternated $n_1 = 3.5$ and $n_2 = 2.5$ layers; $d_1/d_2 = 2/3.5$. The gaps open at frequencies which are integer multiples of the Bragg frequency ω_{Br}. The presence of the second gap at $2\omega_{Br}$ is a clear signature of non-$\lambda/4$ layers. Left panel: photonic dispersion (real part of the wavevector). Right panel: extinction coefficient (imaginary part).

For a two-layer unit cell of refraction indices $n_{1,2}$ and thicknesses $d_{1,2}$, the gap width is generally an increasing function of the refractive index contrast, i.e. the amplitude

of the modulation of the potential V_{diel}; for given values of $n_{1,2}$, the maximal width of the lowest gap is achieved in the case of $\lambda/4$ layers, i.e. when $d_1 n_1 = d_2 n_2 = \lambda_{Br}/4$. Unfortunately, symmetry reasons make this condition incompatible with the opening of a second gap around $2\omega_{Br}$.[27]

An *effective mass* can be defined for the photons at band edge according to the general rule

$$m_{eff} = \left(\frac{1}{\hbar} \frac{\partial^2 \omega}{\partial k^2} \right)^{-1} ; \tag{1.9}$$

as in the electronic case, *conduction band* photons have a *positive* effective mass, while *valence* band ones have a negative mass; consequently, a defect which is attractive in the sense of eq.(1.3), e.g. a more refracting layer, can bind conduction band photons, while valence band photons are bound by repulsive defects, e.g. additional holes in the material.[10,11]

1.2 The Distributed Bragg Reflector (DBR) as a one-dimensional PBG

Consider a monochromatic light beam normally inciding on a finite slab of one-dimensional PBG crystal; in fig.1.2 we have plotted the transmittivity as function of its frequency ω_L. Most of its features can be explained starting from the simple band dispersion of the previous section.

If the incident frequency ω_L corresponds to a forbidden gap, light can not propagate through such a dielectric lattice and would be totally reflected back by an infinite structure;[4] this because the photonic dispersion inside the PBG gives a purely imaginary wavevector for frequencies inside the gap. In the case of a finite sample, a small part of the incident flux can instead tunnel across the system: the transmitted beam has an intensity which is an exponentially decreasing function of the number of periods of the structure with a characteristic length given by the inverse of the *extinction* coefficient k_{ext}. Anyway, since absorption is absent, the process is purely reactive and conserves energy; this means that the sum of the transmitted and reflected intensities exactly equals the incident one.

A similar extinction process occurs when light falls onto the interface between a dielectric and the vacuum with an angle larger than the critical angle $\theta > \theta_{cr} =$

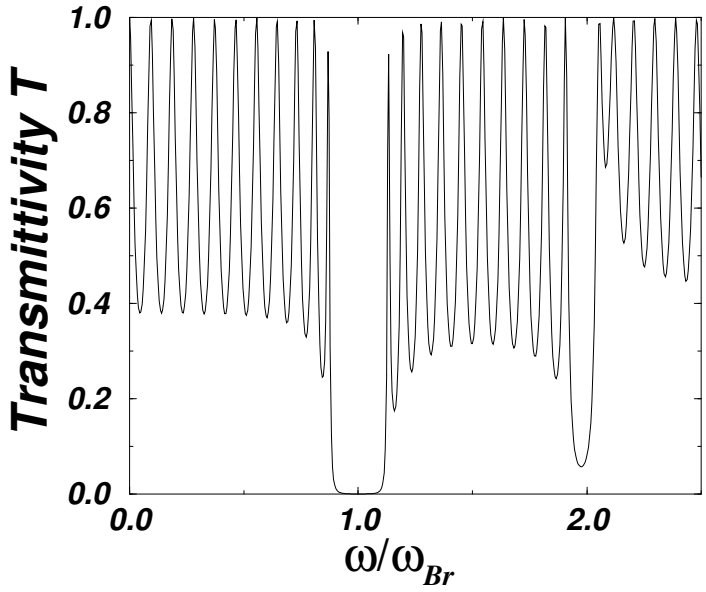

FIGURE 1.2: Transmission spectrum of a 10 periods PBG crystal. Same parameters as in fig.1.1.

$\arcsin 1/\sqrt{\epsilon}$: in this case, the photon dispersion in free-space does not allow for propagating states with a real wavevector if the transverse wavevector $k_\perp > \omega/c$. Light has therefore to be totally reflected at the interface, leaving only a non-propagating exponential tail in the vacuum. If two dielectric bodies with parallel interfaces are separated by a thin vacuum layer of thickness d, the tunneling amplitude for $\theta > \theta_{cr}$ has the same exponentially decreasing behavior as a function of d as the transmission through of finite slab of PBG. This effect is currently used in practice for tuning the in- and out-coupling intensity of a whispering gallery dielectric resonator.[28]

If the frequency ω_L corresponds to an allowed band, incident light couples to propagating modes and can be transmitted across the lattice; as it happens for a finite dielectric slab, the presence of an impedance mismatch at the abrupt interfaces of the PBG crystal causes partial reflections and hence oscillations in the transmittivity spectrum with a period inversely proportional to the lattice thickness.

Given their good reflection performances at frequencies lying inside an energy gap, finite slabs of PBG are commonly used as high quality *distributed Bragg reflector* (DBR) mirrors; in most cases, the lattice is formed by a stack of $\lambda/4$ layers tuned to the desired frequency, in order to maximize both the extinction coefficient and the

reflection spectral range at a given refraction index contrast. Other configurations are sometimes adopted for specific purposes: doubly resonant second harmonic generation, e.g., requires high reflectivity at both ω_L and $2\omega_L$, which can not be obtained with usual $\lambda/4$ mirrors. A detailed discussion on such FASH (fundamental and second harmonic) mirrors can be found in.[27]

The materials most commonly used for DBR mirrors are certainly $Al_xGa_{1-x}As$ alloys, whose refractive index can be varied changing the relative proportion of Ga and Al atoms from a value of about $n_{\mathrm{AlAs}} \simeq 2.95$ up to a value of about $n_{\mathrm{GaAs}} \simeq 3.56$; such materials allow in fact for an easy growth of the DBR mirror structure by means of MBE techniques as well as for the integration in the same monolithic sample of the electronic confinement structures, e.g. quantum wells, which are required in order to have strong and sharp excitonic optical lines. Given the limited refractive index contrast of such compounds, other classes of materials are actually investigated in order to get enhanced refractive index contrasts, e.g. II-VI inorganic semiconductors,[29,30] alternate layers of ZnS ($n_{\mathrm{ZnS}} \simeq 2.3$), MgF_2 ($n_{\mathrm{MgF_2}} \simeq 1.35$) and organic materials[31] as well as many others.[32–34]

1.3 The DBR microcavity

Consider now a pair of DBR mirrors separated by a dielectric layer of refraction index n_{cav} and thickness d_{cav} grown on a substrate of refraction index n_{sub} as in fig.1.3: such a system can be considered as an optical cavity, since light is confined in the central *cavity layer* by the pair of mirrors which surround it. If the DBR mirrors are formed by $\lambda/4$ layers and the cavity one is a $\lambda/2$ layer, the Fabry-Perot mode has a frequency very close to the Bragg frequency ω_{Br}. Examples of transmission spectra through such structures, calculated using the transfer matrix formalism, are reproduced in fig.1.4).

For frequencies lying outside the reflection window of the DBR mirrors, there is appreciable transmission since light can propagate through the whole structure. The complicate modulation is the result of the multiple reflections at the interfaces and can be interpreted in terms of the so-called *leaky modes*.[35]

For frequencies lying inside the gap of the DBR mirrors, transmission is nearly vanishing at all frequencies comprised within the forbidden gap of the DBR mirrors, but for the narrow Fabry-Perot peak which corresponds to a *resonant tunneling* pro-

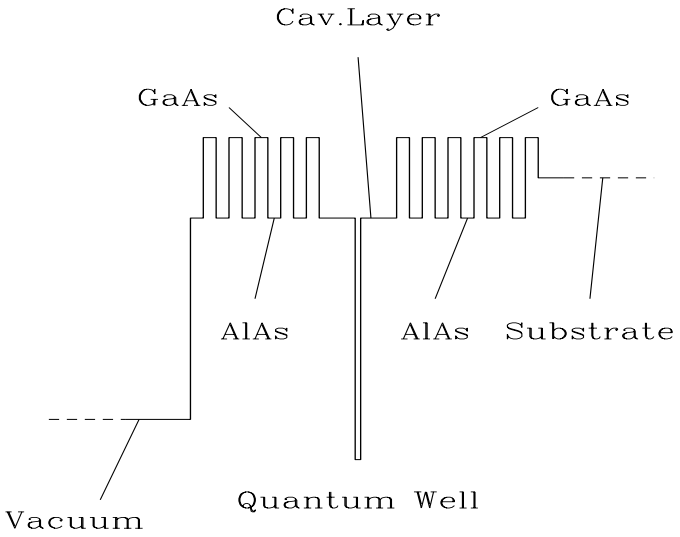

FIGURE 1.3: Scheme of a DBR microcavity; the heights of the lines correspond to the refraction index of the different layers.

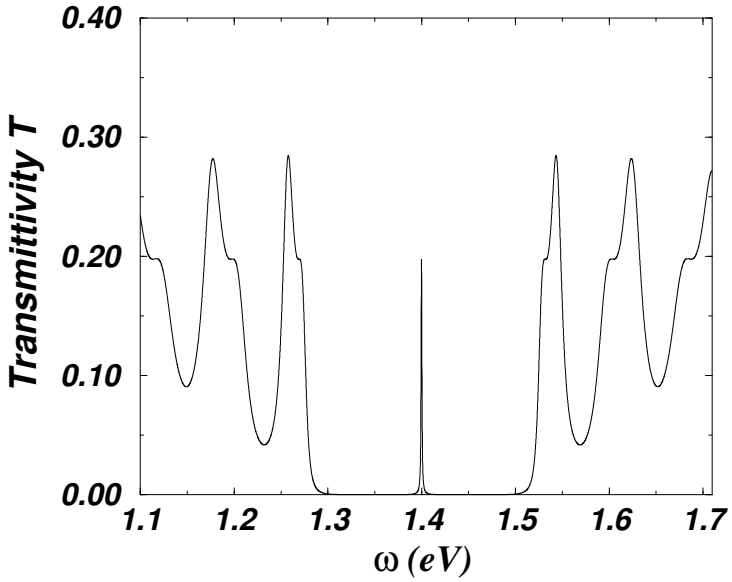

FIGURE 1.4: Transmission spectra of an empty microcavity. The DBR mirrors are formed by 10 periods of a $\lambda/4$ lattice; the cavity layer is a $\lambda/2$ one. The Bragg frequency is $\hbar\omega_{Br} = 1.40$eV; $n_1 = 2.9$, $n_2 = 3.6$, $n_{cav} = 2.9$ and $n_{sub} = 3.5$.

cess on the localized cavity mode: the peak center is at the mode frequency and its linewidth γ is given by the radiative lifetime $\gamma = \tau^{-1}$; this latter being proportional to the (small) mirror transmittivity, the more lattice periods are present in the DBR mirrors, the narrower is the resonance. In general, the sharpness of an optical resonance is measured in terms of the *quality factor* Q, defined as the ratio $Q = \omega_{lin}/\gamma$ of the frequency and the linewidth; in physical terms it is equal to 2π times the number of oscillations required to damp the energy of a factor $1/e$. Since the reflectivity of DBR mirrors can be very close to 1, very high quality cavity modes should be obtainable: experimentally, Q factors as high as 10^4 have been observed or, equivalently, linewidths as narrow as 0.13meV.[36] Differently from the case of metallic cavities, the transmittivity of DBR microcavities is smaller than unity even at exact resonance with a FP mode because of the presence of the substrate material on just one side of the structure.

The fact that DBR microcavities are monolithic objects is very interesting from the point of view of the applications: the mechanically stable geometrical alignment allows in fact for an easy manipulation; furthermore, the reduced volume of the cavity mode, together with the possibility of integrating active layers such as quantum wells in the same monolithic object, allows for the investigation of the physics of strongly coupled photon-exciton systems.[37–40]

1.4 The DBR cavity as an impurity in a PBG crystal

The photonic mode localized inside the cavity by reflections on the two DBR mirrors forming the microcavity can also be considered as a defect state in an otherwise periodic system: the two DBR mirrors surrounding the cavity layer can be in fact seen as a single one-dimensional periodic array in which an extra layer with different characteristics (the cavity layer) has been inserted, i.e. a *doped* PBG crystal.

As it is well-known from semiconductor physics,[7,8] when an impurity atom is present in a otherwise periodic crystalline lattice, a localized *defect* state appears for carriers at frequencies comprised within the gap between the valence and the conduction band. Depending on the strength of the impurity potential, the defect state can be either *deep*, if the carrier is tightly bound and the energy level is far inside the gap, or *shallow*, if the carrier wavefunction is delocalized over many unit cells and the energy level is close to a neighboring band. Depending on whether the sign of the

electric potential is positive or negative, the defect can be respectively classified as a *donor* or an *acceptor*: in the first case, the potential results attractive for positive mass electrons and the energy of the bound state is located just below the conduction band; in the second case, instead, the potential results attractive for negative mass holes and the energy of the bound state is located just above the valence band.

A similar behavior is expected to occur in PBG crystals when some dielectric material is either added or removed at a certain location in the crystal:[41] in the first case, the extra dielectric generates a negative defect potential which can bind positive mass conduction band photons; in the other case, the removed dielectric generates a positive potential which can bind negative mass valence band photons.

Such a prediction can be immediately verified by simply calculating the transmission properties of a doped PBG crystal for different values of the thickness of the central (cavity) layer d_{cav};[42] the energy of the defect state corresponds to the line-center of the resonant tunneling peak.

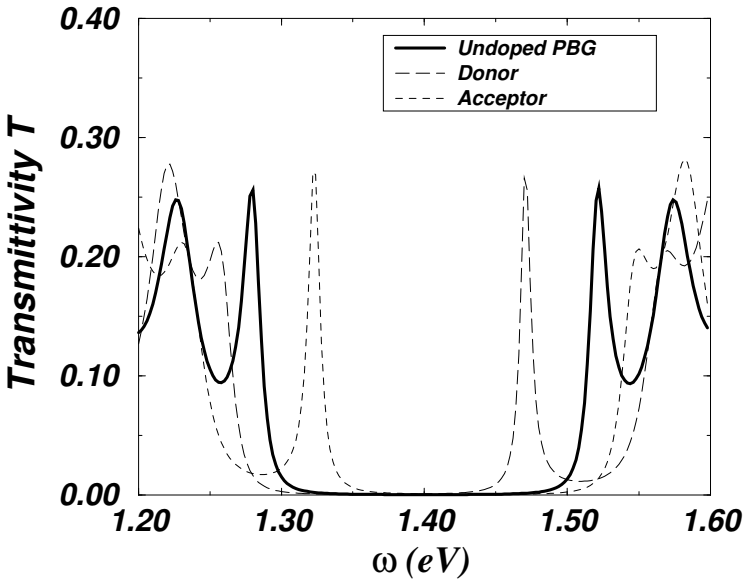

FIGURE 1.5: Transmission spectra of microcavities for different values of the cavity layer thickness; the DBR mirrors are $\lambda/4$ mirrors, each formed by 10 periods of alternated $n_1 = 2.9$ and $n_2 = 3.6$ layers. The cavity layer ($n_{cav} = 2.9$) is respectively a $\lambda/8$ (acceptor), a $\lambda/4$ (undoped PBG) or a $3\lambda/8$ (donor) layer.

For $d_{cav} = d^o_{cav} = \frac{\pi\, c}{2 n_{cav} \omega_{Br}}$, the central layer is itself a $\lambda/4$ one and therefore identical

to its neighbors; in this case, the PBG crystal is not doped and the transmission spectrum shows no resonant tunneling peaks. For $d_{cav} > d^o_{cav}$, a transmission peak appears just below the conduction band edge: it corresponds to resonant tunneling on a *donor* impurity state. For $d_{cav} < d^o_{cav}$, the resonant tunneling peak appears instead just above the valence band edge; it corresponds to an *acceptor* impurity state. In both cases the distance from the band is initially an increasing function of $|d_{cav} - d^o_{cav}|$.

Impurities have been studied extensively also in two and three dimensional PBG crystals from both the theoretical and the experimental point of view; several authors[41,43–45] have in fact shown that a localized addition of removal of dielectric material in a slab of otherwise periodic photonic crystal provides localized photonic states which can have Q-values as high as 10^4 and very tightly bound wavefunctions, with mode volumes of the order of a few square or cubic wavelengths. As expected, the coupling efficiency to externally incident fields decreases exponentially with the distance of the impurity from the crystal surface, as it is expected for tunneling on a localized mode.

1.5 Strong exciton-photon coupling effects in DBR microcavities

1.5.1 A simple two-mode model

Consider a single-mode DBR microcavity containing in the cavity layer a stack of N_w identical quantum wells with strong electric-dipole excitonic transitions radiatively coupled to the photonic mode of the cavity. At low excitation densities, when the excitons can be considered as non-interacting bosons, such a system can be simply modeled as a pair of coupled harmonic oscillators.

The Hamiltonian of such a model can be written in terms of the photonic and excitonic field operators $\hat{a}_{ph}$ and $\hat{a}_{exc}$ as

$$\begin{aligned} \mathcal{H} &= \hbar\omega_{ph}\hat{a}^\dagger_{ph}\hat{a}_{ph} + \hbar\omega_{exc}\hat{a}^\dagger_{exc}\hat{a}_{exc} + \hbar k_c\hat{a}^\dagger_{ph}\hat{a}_{exc} + \hbar k^*_c\hat{a}^\dagger_{exc}\hat{a}_{ph} + \\ &+ \hbar k_{inc}E_{inc}(t)\hat{a}^\dagger_{ph} + \hbar k^*_{inc}E^*_{inc}(t)\hat{a}_{ph}; \end{aligned} \tag{1.10}$$

the first two terms account for the linear oscillations of the photonic and excitonic

fields respectively at ω_{ph} and ω_{exc}. The $\hbar k_c \hat{a}^\dagger_{ph}\hat{a}_{exc} + \hbar k^*_c \hat{a}^\dagger_{exc}\hat{a}_{ph}$ coupling terms respectively describe excitonic stimulated emission and absorption processes from and into the cavity mode; the coupling coefficient k_c depends on the matrix element of the excitonic transition and will be related in sec.1.5.2 to the excitonic contribution to the macroscopic dielectric constant. Since only a specific linear combination of the N_w excitonic states is effectively coupled to the photonic mode radiation while the other $N_w - 1$ dark[46] states are not directly involved in optical processes, the exciton-photon coupling strength for a stack of N_w equivalently located wells is proportional to $\sqrt{N_w}$.[47,48]

The $\hbar k_{inc} E_{inc}(t)\hat{a}^\dagger_{ph} + \hbar k^*_{inc} E^*_{inc}(t)\hat{a}_{ph}$ term describes the effect on the microcavity of an incident laser beam which forces the photonic cavity mode to oscillate. Thanks to its all-order coherence, the incident laser field is well modeled as a classical C-number field $E_{inc}(t)$. The coupling coefficient k_{inc} is proportional to the transmission amplitude of the front cavity mirror; analogously, the amplitude of the transmitted field through the cavity E_{tr} is proportional to the internal photonic amplitude $\hat{a}_{ph}$ times a η_{tr} coefficient proportional to the transmission amplitude of the back mirror.

From the point of view of the sole microcavity, the coupling of the photonic mode to the continuum of propagating external modes through the non-perfectly reflecting mirrors as well as the exciton damping due to phonon and disorder induced scattering or ionization are dissipative processes and thus can not be included in a simple Hamiltonian formalism. From the general theory of damping,[1,49] it follows that the dynamics of the two-mode system is completely described by the following *master equation* for the density matrix $\hat{\rho}$

$$\frac{\partial \hat{\rho}}{\partial t} = \frac{i}{\hbar}\left[\hat{\rho}, \mathcal{H}\right] + \gamma_{ph} D\left[\hat{a}_{ph}\right]\hat{\rho} + \gamma_{exc} D\left[\hat{a}_{exc}\right]\hat{\rho} \tag{1.11}$$

in which we have added to the usual Hamiltonian evolution terms which account for the damping of respectively the photonic and excitonic modes

$$D\left[\hat{a}_{ph}\right]\hat{\rho} = \hat{a}_{ph}\hat{\rho}\hat{a}^\dagger_{ph} - \frac{1}{2}\left(\hat{a}^\dagger_{ph}\hat{a}_{ph}\hat{\rho} + \hat{\rho}\hat{a}^\dagger_{ph}\hat{a}_{ph}\right) \tag{1.12}$$

$$D\left[\hat{a}_{exc}\right]\hat{\rho} = \hat{a}_{exc}\hat{\rho}\hat{a}^\dagger_{exc} - \frac{1}{2}\left(\hat{a}^\dagger_{exc}\hat{a}_{exc}\hat{\rho} + \hat{\rho}\hat{a}^\dagger_{exc}\hat{a}_{exc}\right); \tag{1.13}$$

as usual, the coefficients $\gamma_{ph,exc}$ have the usual meaning of damping rates of respectively the photonic and excitonic oscillations. If we define $\eta_{inc,tr}$ as the proportionality factors between the cavity field and the emitted fields respectively in front and behind the cavity, the contribution of radiative escape of photons from the cavity to

the cavity damping can be written as

$$\gamma_{ph}^{(rad)} = \frac{c}{8\pi}\left(|\eta_{inc}|^2 + |\eta_{tr}|^2\right); \tag{1.14}$$

in addition, the η_{inc} coefficient can be related [(a)] to the coupling coefficient k_{inc} of the incident beam to the cavity mode:

$$\eta_{inc} = \frac{8\pi}{c} k_{inc}. \tag{1.15}$$

For a symmetric structure, $\eta_{inc} = \eta_{tr}$ and $k_{inc} = k_{tr}$, and therefore

$$k_{inc} = \sqrt{4\pi\gamma_{ph}^{(rad)}/c} \tag{1.16}$$

$$\eta_{tr} = \sqrt{c\gamma_{ph}^{(rad)}/16\pi}. \tag{1.17}$$

Another contribution to γ_{ph} may arise from light absorption processes in the dielectric material forming the DBR mirrors and the cavity layer. Exciton damping is instead caused by phonon and disorder scattering or ionization. Since the decay channels of the excitonic and photonic modes are expected to be distinct,[51] no coupling of the excitonic and photonic modes is expected to arise from damping effects; in other words, non-diagonal damping terms have not to be included in the master equation eq.(1.11).

Inserting the explicit form of the Hamiltonian eq.(1.10) into the master equation eq.(1.11), we can obtain a closed set of motion equations for the mean-values of the field operators $a_{ph,exc} = \langle \hat{a}_{ph,exc} \rangle$:

$$\frac{da_{ph}}{dt} = -i\omega_{ph}a_{ph} - ik_c a_{exc} - \frac{1}{2}\gamma_{ph}a_{ph} - ik_{inc}E_{inc}(t) \tag{1.18}$$

$$\frac{da_{exc}}{dt} = -i\omega_{exc}a_{exc} + ik_c^* a_{ph} - \frac{1}{2}\gamma_{exc}a_{exc}; \tag{1.19}$$

differently from the case of nonlinear optical systems treated in the next chapters, the equations for the mean-field amplitudes are in the present case exact: the quadratic form of the Hamiltonian eq.(1.10) guarantees in fact that the all-order coherence of the incident laser beam is transferred to the cavity field as well as to the excitonic field.

[(a)] This is easily proven by remembering that the transmission through any symmetric, linear and non-absorbing structure is, at exact resonance, exactly one [50, chap.9]

If the incident field is a monochromatic one $E_{inc}(t) = E^o_{inc}e^{-i\omega_L t}$, we can analytically find the steady-state transmitted amplitude E^o_{tr}:

$$E^o_{tr} = \frac{k_{inc}\eta_{tr}E^o_{inc}}{\omega_{ph} - \omega_L - i\gamma_{ph}/2 - \frac{|k_c|^2}{\omega_{exc}-\omega_L-i\gamma_{exc}/2}}. \tag{1.20}$$

In absence of photon-exciton coupling $k_c = 0$, we recover the typical expression for the single resonance of the bare cavity mode at ω_{ph} with linewidth γ_{ph}.

In currently grown microcavities, the excitonic linewidth is generally comparable or even larger than the photonic one: $\gamma_{exc} > \gamma_{ph}$; in the resonant case $\Delta = \omega_{exc} - \omega_{ph} = 0$, depending on whether $4\,|k_c|$ is smaller or larger than $|\gamma_{exc} - \gamma_{ph}|$, we can be either in a *weak* coupling regime or in a *strong* coupling regime. The transmission spectrum shows in fact a pair of poles at the (complex) eigenfrequencies

$$\tilde{\omega}_{1,2} = \omega_{1,2} - i\gamma_{1,2} = \omega_{ph} - i\frac{\gamma_{ph}+\gamma_{exc}}{4} \pm \sqrt{|k_c|^2 - \left(\frac{\gamma_{exc}-\gamma_{ph}}{4}\right)^2} \tag{1.21}$$

of the linear system eqs.(1.18-1.19). In the weak coupling regime, the real parts of the poles, which define the resonance frequencies, coincide and are equal to $\omega_{1,2} = \omega_{ph} = \omega_{exc}$, so that the transmission spectrum has a single peak at ω_{ph}. In the strong coupling regime, a doublet of Rabi-split peaks appears, symmetrically located with respect to $\omega_{ph} = \omega_{exc}$. From a physical point of view, the doublet of peaks arises from resonant tunneling processes on the two *dressed* eigenstates of the cavity, the so-called *exciton polaritons*, which are linear superpositions of the excitonic and photonic modes and can be determined from the diagonalization of the cavity Hamiltonian eq.(1.10).

The transition from the weak to the strong coupling regime can be observed in fig.1.6: transmission spectra for growing coupling strengths k_c have been plotted in the resonant case $\Delta = 0$: the transition from a single peak to a doublet of peaks is apparent. On the other hand, if we vary the detuning Δ in the strong coupling regime, the polaritonic peaks show the typical anticrossing behavior of a coupled two-modes system:[37,38,52] since only the photonic mode is actually coupled to the incident and transmitted beams, the oscillator strength of each peak reflects the weight of its photonic component. An explicit calculation in the *optical Stark effect (OSE)* regime in which the linewidths are negligible with respect to the Rabi splitting Ω_R, leads to the polariton frequencies

$$\omega_{1,2} = \frac{\Delta}{2} \pm \left(\frac{\Delta^2}{4} + |k_c|^2\right)^{1/2} = \frac{\Delta}{2} \pm \frac{\Omega_R}{2} \tag{1.22}$$

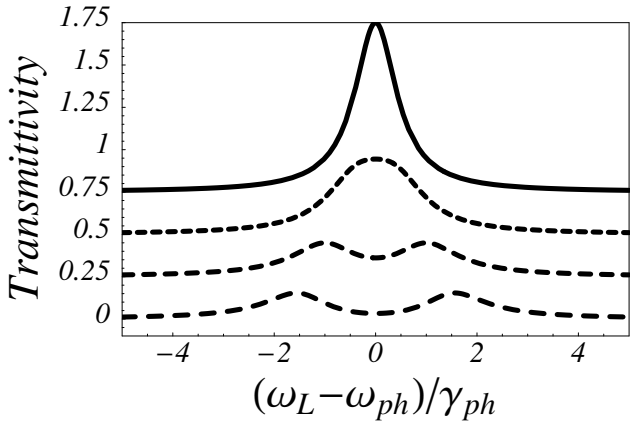

FIGURE 1.6: Transmission spectra for different values of the exciton-photon coupling k_c. To clarify the picture, each spectrum has been shifted upwards of 0.25. The solid line refer to the empty cavity case $k_c = 0$; a longer dashing means a stronger coupling k_c. The weak- to strong-coupling transition is evident. $k_c/\gamma_{ph} = 0, 0.5, 1, 1.5$; $\gamma_{exc} = \gamma_{ph}$, $\Delta = 0$.

and to the oscillator strengths

$$f_1 \propto |k_{inc}\eta_{tr}| \frac{\omega_1 - \Delta}{\omega_1 - \omega_2} \tag{1.23}$$

$$f_2 \propto |k_{inc}\eta_{tr}| \frac{\omega_2 - \Delta}{\omega_2 - \omega_1}, \tag{1.24}$$

where the oscillator strength of a peak is defined as the integrated intensity of its lineshape.

Such a behavior can be observed in the spectra of fig.1.7, in which transmission spectra for different values of Δ have been plotted in the strong coupling regime. For $\Delta = 0$, the peaks are located at symmetrical positions with respect to $\omega_{ph} = \omega_{exc}$ and have equal strengths. For $\Delta < 0$ the weak lower peak, mainly excitonic, is located just below ω_{exc} while strong upper peak, mainly photonic, is located just above ω_{ph}; the redistribution of the oscillator strength, as well as the frequency shift from the bare frequencies ω_{exc} and ω_{ph} are a consequence of the coupling which mixes the exciton and photon states into polaritonic ones. A symmetric behavior occurs for $\Delta > 0$.

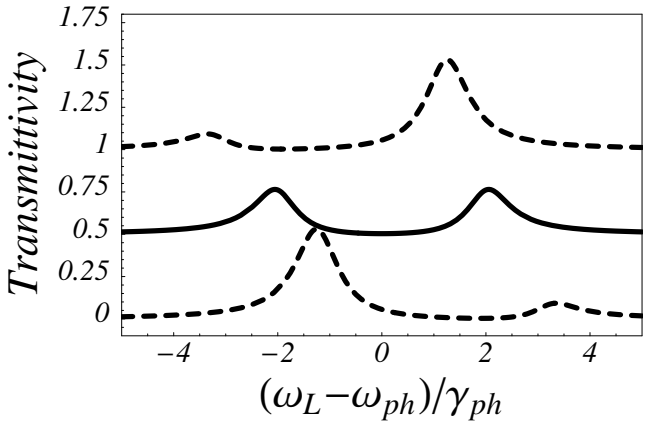

FIGURE 1.7: Transmission spectra for different values of the exciton-photon detuning Δ. To clarify the picture, each spectrum has been shifted upwards of 0.5. The solid line refers to the resonant case $\Delta = 0$; the dashed lines refer to the symmetric $\Delta/\gamma_{ph} = \pm 2$ cases; anticrossing behavior is apparent. $\gamma_{exc} = \gamma_{ph}$, $k_c/\gamma_{ph} = 2$.

1.5.2 An *ab initio* calculation via transfer matrices

The predictions of the previous subsection are based on a simple two-mode model which takes into account only one photonic and one excitonic mode. Now, we shall check their validity by comparing them to the predictions obtained by integrating Maxwell's equations for the electromagnetic field in the dielectric structure. This can be done within the transfer matrix formalism[4,25] already used in the previous sections; the quantum wells can in fact be modeled as very thin layers with a Drude-Lorentz dielectric constant

$$\epsilon_{QW}(\omega) = \frac{4\pi e^2}{m} \frac{f_{exc}^{(2D)}}{\omega_{exc}^2 - \omega^2 - i\gamma_{exc}\omega} \delta(z - z_{QW}); \tag{1.25}$$

as an example, for 10nm wide InGaAs quantum wells, the 2D oscillator strength $f_{osc}^{(2D)}$ has a value of about $5 \cdot 10^{-4} \mathring{A}^{-2}$.[53]

Performing such a calculation for the structure described in sec.1.3 when a few quantum wells are inserted in the cavity layer brings to the transmission spectra of fig.1.8, which closely resemble the ones already obtained within the simple two mode model.

The oscillator strength of the quantum well exciton $f_{osc}^{(2D)}$ to be used in the transfer matrix calculation can be either experimentally measured[54] or theoretically com-

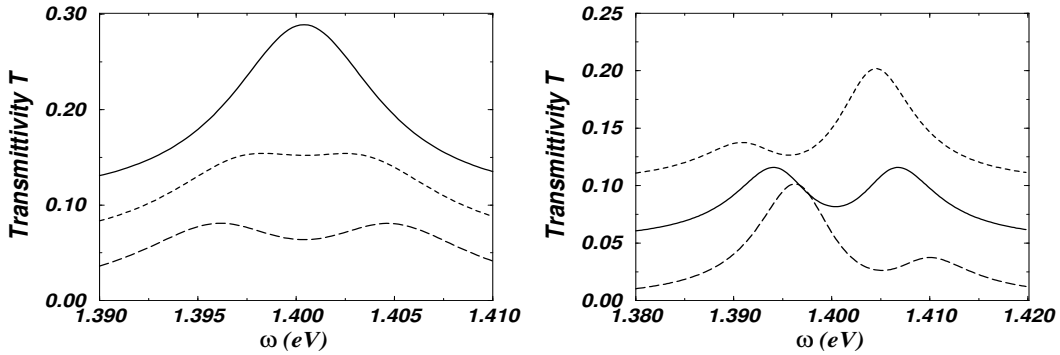

FIGURE 1.8: Transmission spectra through DBR microcavities containing an excitonic resonance: each DBR is formed by 10 periods of $\lambda/4$ PBG with $n_{1,2} = 2.9, 3.6$ and the cavity layer is a $\lambda/2$ layer with $n_{cav} = 2.9$, giving a cavity mode close to 1.40eV. The excitonic linewidth $\hbar\gamma_{exc} = 0.01$eV is comparable to the cavity linewidth. Left panel: resonant case for different excitonic oscillator strengths. Right panel: anticrossing of photonic and excitonic modes during a scan of $\hbar\omega_{exc} = 1.395, 1.4, 1.405$eV. In both panels, each curve is shifted upwards of 0.05.

puted starting from the electronic structure of the well.[55] On the other hand, the k_c coefficient of the two-mode model summarizes information on the geometry of the whole cavity system and, in particular, on the wavefunction of the photonic cavity mode.

Given any linear and non-absorptive dielectric profile $\epsilon(x)$, the electromagnetic field can be developed in eigenmodes of the wave equation

$$E(x,t) = \sum_i \mathcal{E}_i(x) a_i(t) e^{-i\omega_i t} + \mathcal{E}_i^*(x) a_i^*(t) e^{i\omega_i t}; \tag{1.26}$$

if we choose the normalization

$$\int dx \, \frac{\epsilon(x)}{2\pi} \mathcal{E}_i^*(x) \mathcal{E}_i(x) = \hbar\omega_i \delta_{i,j}, \tag{1.27}$$

the field intensities $|a_i|^2$ get the meaning of photonic surface density.

In the so-called SVEA (slowly varying envelope) approximation which consists of assuming a temporal variation of the mode amplitudes $a_i(t)$ much slower than the free oscillation frequency ω_i, the time evolution of the mode amplitudes [6, pag.216] can be written as

$$\sum_i \frac{2i\epsilon(x)\omega_i}{c^2} \frac{da_i}{dt} \mathcal{E}_i(x) e^{-i\omega_i t} = \frac{4\pi}{c^2} \frac{\partial^2 \mathcal{P}(x,t)}{\partial t^2} \tag{1.28}$$

where the polarization $\mathcal{P}(x,t)$ contains contributions from all processes which have not been included in the background dielectric constant $\epsilon(x)$, i.e. all nonlinear effects, as well as our resonant excitonic polarization.

Multiplying both members of eq.(1.28) by $\mathcal{E}_j(x)$ and integrating over dx, the modes result separated

$$i\frac{da_i}{dt} = -\int dx\, \mathcal{E}_i^*(x)\, 4\pi\mathcal{P}_{\omega_i}(x); \tag{1.29}$$

within the SVEA approximation, only the terms which oscillating at a frequency close to the mode frequency ω_i have to be kept in the right-hand sides of the motion equations eq.(1.29).

In our specific case, only one photonic mode a_{ph} is involved and the polarization $\mathcal{P}(x)$ contains the excitonic contribution only; assuming monochromatic oscillation at ω_L, this can be written as

$$4\pi\mathcal{P}_{\omega_L}(x) = \epsilon_{QW}(x)\mathcal{E}_{ph}(x)a_{ph} = \frac{4\pi e^2}{m}\frac{f_{osc}^{(2D)}}{\omega_{exc}^2 - \omega_L^2 - i\gamma_{exc}\omega_L}\mathcal{E}_{ph}(x_{QW})a_{ph} \tag{1.30}$$

leading to an excitonic term in the motion equation for the photonic field amplitude a_{ph} of the form

$$i\left.\frac{da_{ph}}{dt}\right|_{exc} = -\left(\frac{e^2}{m}\frac{f_{osc}^{(2D)}}{\omega_{exc}^2 - \omega_L^2 - i\gamma_{exc}\omega}\left|\mathcal{E}_{ph}(x_{QW})\right|^2\right)a_{ph}. \tag{1.31}$$

On the other hand, the excitonic polarization introduces in the photonic motion equation of the two-mode model a term

$$i\left.\frac{da_{ph}}{dt}\right|_{exc} = -\frac{|k_c|^2}{\omega_{exc} - \omega_L - i\gamma_{exc}/2}\,a_{ph} \simeq -\frac{2\omega_{exc}\,|k_c|^2}{\omega_{exc}^2 - \omega_L^2 - i\gamma_{exc}\omega_L}\,a_{ph}; \tag{1.32}$$

comparing the photonic motion equations eq.(1.32) and eq.(1.31) of the two approaches, an explicit expression for k_c can be obtained in terms of the quantum well oscillator strength and the photonic wavefunction $\mathcal{E}_{ph}(x)$

$$|k_c|^2 = \frac{e^2}{2m\hbar\omega_2}f_{osc}^{(2D)}\left|\mathcal{E}_{ph}(x_{QW})\right|^2; \tag{1.33}$$

the phase of k_c refers to the (generally unobservable) absolute phase of the excitonic field and can be arbitrarily chosen without affecting the physical predictions.

More generally, if the cavity contains several quantum wells located at different spatial positions, $|k_c|^2$ is the sum of the contribution of each single well; if the well

spacing is much shorter than the photonic wavelength, or the wells are located at equivalent positions within the cavity layer, the effective coupling k_c results proportional to the square root of the number of wells,[47,48] as expected from general arguments starting from the concept of bright and dark states.

1.6 The microcavity polaritons: quantum coherence effects in the transmission spectra

Although the largest part of the works that have appeared up to now on microcavity optics refer to the $\gamma_{exc} > \gamma_{ph}$ case, very interesting behaviors are expected to occur in the opposite $\gamma_{ph} \gg \gamma_{exc}$ case. From an experimental point of view, very narrow excitonic transitions can be obtained by working at low temperature with high-quality quantum wells with a very small interface roughness. As previously stated, control over the cavity linewidth is instead obtained by simply varying the number of lattice periods in the DBR mirrors.

In the deep strong coupling regime, when the Rabi splitting of the poles is much larger than both their linewidths, the physical behavior is the same as the one described in the previous section and the polaritonic peaks have a linewidth which is the average of the excitonic and photonic linewidths.[52]

When the strength k_c of the exciton-photon coupling is intermediate between the photonic and the excitonic linewidths, qualitatively new features in the transmission spectra are predicted by the same eq.(1.20):

All the spectra plotted in fig.1.9 show a broad peak centered at the photonic mode frequency ω_{ph} and, superimposed, a narrow feature around ω_{exc}, whose qualitative shape strongly depends on the detuning Δ; the width of the narrow feature can be as small as the excitonic linewidth γ_{exc}.

In the resonant $\Delta = 0$ case, the transmitted amplitude eq.(1.20) can be approximated in the $|\omega_L - \omega_{exc}| \ll \gamma_{ph}$ window as

$$E^o_{tr} = k_{inc}\eta_{tr}E^o_{inc}\left(\frac{i}{\gamma_{ph}/2} - \frac{\frac{4|k_c|^2}{\gamma^2_{exc}}}{\omega_{exc} - \omega_L - i\Gamma/2}\right), \tag{1.34}$$

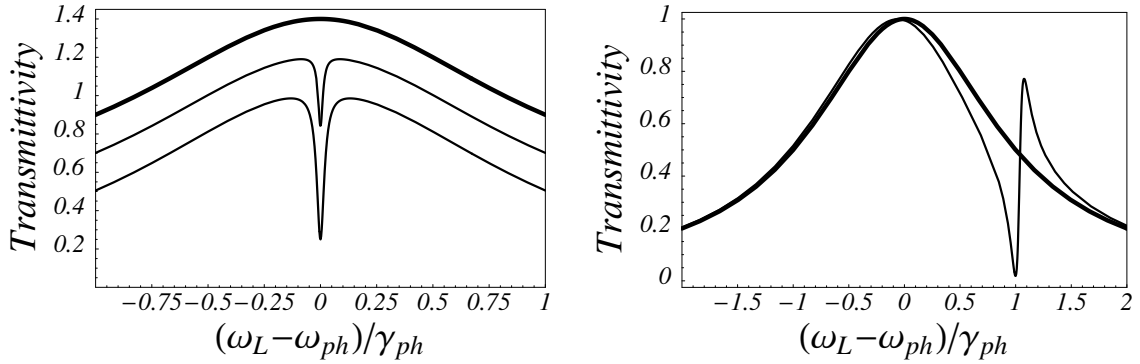

FIGURE 1.9: Transmission spectra in the $\gamma_{ph} \gg \gamma_{exc} = 10^{-2}\gamma_{ph}$ case. Left panel, resonant $\Delta = 0$ case; $k_c/\gamma_{ph} = 0, 0.05, 0.1$; each of the curves is shifted upwards of 0.2. Right panel, non-resonant $\Delta/\gamma_{ph} = 1$ case; $k_c/\gamma_{ph} = 0, 0.25$.

where the linewidth Γ of the narrow central feature is defined as

$$\Gamma = \gamma_{exc}\left(1 + \frac{4\left|k_c\right|^2}{\gamma_{ph}\gamma_{exc}}\right). \tag{1.35}$$

Such a lineshape corresponds to a very flat and broad pedestal with a narrow hole at ω_{exc} of linewidth Γ whose visibility is given by

$$\beta = \frac{|E_{tr}^{max}| - |E_{tr}^{min}|}{|E_{tr}^{max}|} = \frac{4\left|k_c\right|^2}{\gamma_{ph}\Gamma} = \frac{1}{1 + \frac{\gamma_{exc}\gamma_{ph}}{4|k_c|^2}}. \tag{1.36}$$

Depending on the value of the adimensional parameter $\eta = 4\left|k_c\right|^2/\gamma_{ph}\gamma_{exc}$, the linewidth Γ can be as small as γ_{exc}, provided $\eta \ll 1$; in this limit, however, also its visibility results very small. In the opposite limit $\eta \gg 1$, the transmission at ω_{exc} results almost vanishing, but the dip linewidth becomes large and equal to $4\left|k_c\right|^2/\gamma_{ph} \gg \gamma_{exc}$. The narrow dip which appears in the intermediate regime $\eta \simeq 1$ is strictly related to the well-known *electromagnetically induced transparency (EIT)* of coherently driven three-level atoms:[56,57] as in the atomic case the excitation is coherently trapped in a metastable state so that absorption is effectively canceled out, in our microcavity system the incident laser drives both polaritons in a coherent way with a well-definite relative phase in such a way that their superposition has a nearly vanishing photonic component for $\omega_L = \omega_{ph}$. Since the transmitted amplitude is proportional to the photonic component of the excitation, the transmission spectrum shows a dip around ω_{ph} whose narrow linewidth is a consequence of the

strong dependence of the relative phase of the two polaritons on the laser frequency ω_L.

In the case of a finite detuning Δ, the transmission amplitude in the $|\omega_L - \omega_{exc}| \ll \gamma_{ph}$ limit can be approximated by

$$E^o_{tr} = \frac{k_{inc}\eta_{tr}E^o_{inc}}{z}\left(1 + \frac{|k_c|^2/z}{\omega_{exc} - \omega_L - i\gamma_{exc} - |k_c|^2/z}\right), \tag{1.37}$$

where $z = \Delta + i\gamma_{ph}/2$; as expected, for $\Delta = 0$ we have $z = i\gamma_{ph}/2$ and eq.(1.34) is recovered. This lineshape corresponds to a very broad pedestal (whose slope is not included in the approximate expression), with superimposed a dispersion-like curve centered at a frequency close to ω_{exc}; the transition from a simple dip to a dispersion-like curve is controlled by the argument of the complex number z, which is purely imaginary for $\Delta = 0$ and real in the $\Delta \gg \gamma_{ph}$ limit. In the former case, the broad pedestal interferes with the imaginary part of the resonant second term, giving a dip-like shape; in the latter case, the broad pedestal interferes with its real part, giving a dispersion-like shape.

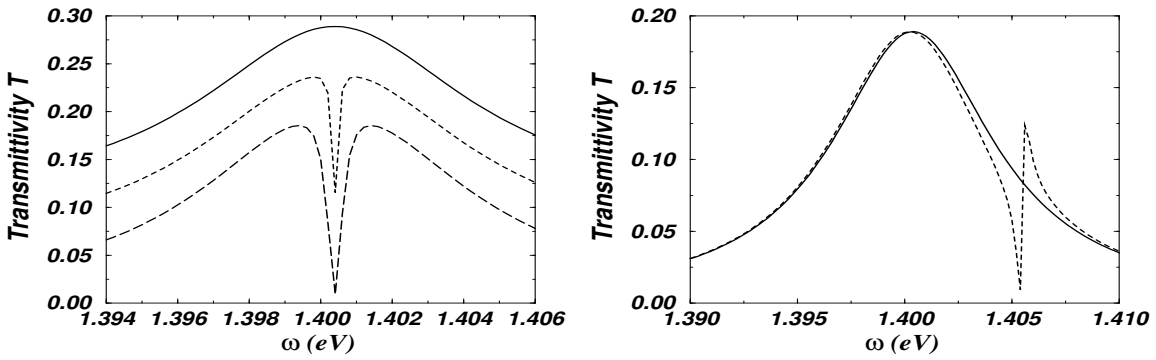

FIGURE 1.10: Transmission spectra through DBR microcavities containing a narrow excitonic resonance: each DBR is formed by 10 periods of $\lambda/4$ PBG with $n_{1,2} = 2.9, 3.6$ and the cavity layer is a $\lambda/2$ layer with $n_{cav} = 2.9$, giving a cavity mode close to 1.40eV. The excitonic linewidth $\hbar\gamma_{exc} = 0.1$meV is much smaller than the cavity linewidth. Left panel: resonant case for different excitonic oscillator strengths; each curve has been shifted upwards of 0.05. Right panel: non-resonant case $\hbar\omega_{exc} = 1.405$eV.

A physical interpretation of such lineshapes can be put forward in terms of *Fano interference profiles*[1,58,59] in the transmission process: this can in fact be interpreted as a quantum-mechanical transition from a state in which there is a photon in front of the

cavity to the continuum of states in which there is a photon propagating beyond the cavity. Since such process can occur along two different paths, quantum mechanical interference between the two amplitudes occurs, which causes the appearance of the peculiar features in the transmission spectra.

As in the previous section, we can compare the predictions of the two mode model to the predictions obtained by direct integration of Maxwell's equations: the agreement of the two approaches is apparent from fig.1.10, giving further evidence to the validity of the two-mode model.

1.7 Linear optics of coupled microcavities

In the last years, several authors have considered the more complicated configuration of fig.1.11, in which two DBR microcavities are grown on top of each other sharing the central mirror.[60–62]

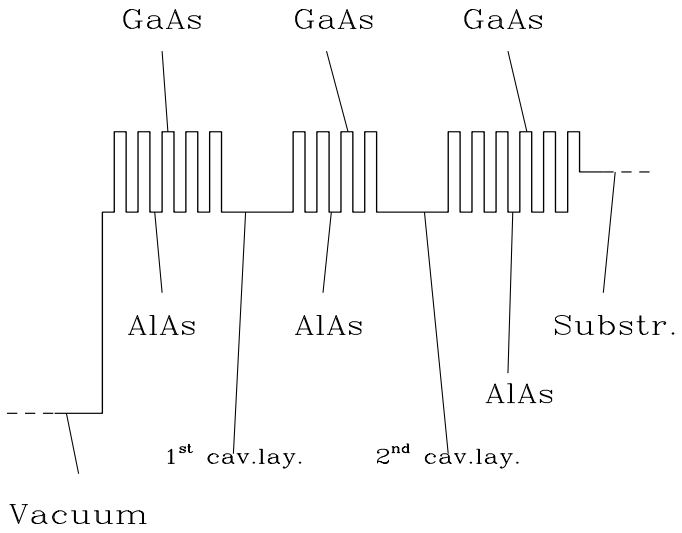

FIGURE 1.11: Scheme of a coupled DBR microcavity configuration; the heights of the lines correspond to the refraction index of the different layers.

Given the finite transmittivity of the central mirror, generally less reflecting than the external ones, the optical modes of each cavity are coupled to each other by tunneling processes through the central mirror, so that the system behaves according to

the same coupled two-mode mode used in the previous sections. In that case, the resulting eigenmodes were polaritons, i.e. coherent superpositions of excitonic and photonic modes; now, they are delocalized optical excitations which involve the two cavities at a time with a well-definite relative phase.

In order to check the validity of such a description, we have numerically calculated the transmission spectra through coupled cavity systems using the transfer matrix formalism.[4,25] As it can be observed in fig.1.12, the behavior is the expected one: in the left panel, the two single cavity modes are resonant with each other and the transmittivity of the central mirror is varied by tuning the number of lattice periods of the central DBR mirror: the spacing of the transmission peaks results a strongly decreasing function of the number of periods, i.e. an increasing function of the central mirror transmittivity.

In the right panel, we keep a constant coupling, while we vary the detuning of the single cavity modes by changing the thickness of the cavity layers: while one of the cavity modes is swept across the other, the two transmission peaks show the typical anticrossing behaviour of coupled two-level systems.

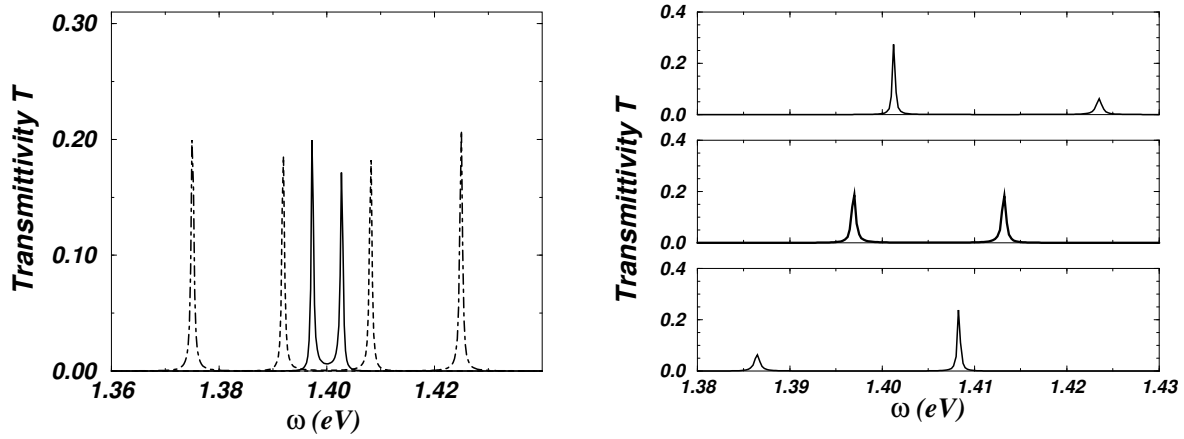

FIGURE 1.12: Transmission spectra for coupled microcavity systems. Left panel:resonant case for different numbers of lattice periods in the central mirror $N_c = 5$ (solid), 10 (dashed) and 15 (dot-dashed). Right panel: the cavity modes are detuned from each other. The external DBR mirrors contain 15 periods; all mirrors are formed of alternating $n_{1,2} = 2.9, 3.6$ $\lambda/4$ layers. The system is grown on a $n_{sub} = 3.5$ substrate.

Such coupled cavities systems can be further complicated adding a few quantum

wells in one or both the cavity layers: if the excitonic frequencies are close to the cavity modes and the coupling is sufficiently strong, the resulting eigenstates of the system are complicated linear combinations of the different excitonic and photonic modes and each eigenstate corresponds to a resonant tunneling peak in the transmission spectrum. For the interested reader, a more detailed discussion of such systems can be found in ref.61, 62.

Chapter 2

Nonlinear optics of microcavities I: intensity-dependent refractive index

The discussion of the linear optical properties of DBR microcavities contained in the previous chapter is the starting point of the present chapter, which is focussed on the nonlinear optical effects which arise in a microcavity geometry from a spatially distributed intensity-dependent refractive index. In the presence of such a nonlinearity, the spectral position of the main features of the transmission spectrum depends on light intensity as well as the effective transmittivity at a given frequency. In other terms, the transmission of a beam suffers a feedback from optical nonlinearity which can be either negative or positive; depending on this sign, *optical limiting* or *optical bistability* effects can be observed.

Sec.2.1 will review the simplest case of a metallic mirror cavity filled of a nonlinear material and sec.2.2 will present a simple analytical single-mode model which well reproduces the underlying physics and can be applied to any geometry, all the information on the detailed structure being summarized in a few parameters which can be computed from the photonic structure at linear regime and the nonlinear optical susceptibility of the material medium.

In the following sections, we shall describe the predictions of numerical simulations for a few specific DBR microcavity configurations: sec.2.3 and sec.2.4 discuss the case of a single cavity; a generalization of the transfer matrix algorithm to nonlinear systems has been used for the calculations. If parameters are appropriately chosen, optical bistability and optical limiting are obtained, in agreement with the

single-mode model. When a quantum well is inserted in the cavity layer in such a way its excitonic transition is strongly coupled to the cavity mode, the interplay of nonlinearity and Rabi splitting gives rise to peculiar features that can be well explained by a two-mode model with intensity-dependent parameters.

In sec.2.5, a more complicated two-beam configuration is considered, in which the refractive index profile of the system is modified by a strong *pump* beam and then probed by another weak *probe* beam; in this sort of *optical transistor*, the intensity of the pump beam (the base current) controls the transmission of the probe (the collector current). Unfortunately, the operation of an optical transistor based on a single nonlinear DBR microcavity requires the probe beam to be much weaker than the pump one, so that its amplification properties are not well suited for applications.

In sec.2.6 a possible way to overcome this difficulty is discussed, using the coupled nonlinear DBR microcavities introduced in sec.1.7 instead of a single cavity; in this case the system really behaves as an optical transistor, since a rather weak pump beam is capable to modulate a stronger probe beam and hence amplify the carried signal. As the only limitation of this arrangement, the probe beam has to be slightly red-detuned with respect to the pump one.

2.1 The nonlinear Fabry-Perot interferometer

Consider a pair of metallic plane mirrors of reflectivity $R_m \lesssim 1$ separated by a slab of thickness d of a non absorbing material whose refractive index n_{eff} depends on the local light intensity.

In fig.2.1 we have plotted the transmission spectrum of such a cavity at linear regime:

$$I_{tr} = \frac{I_{inc}}{1 + 4/T_m^2 \sin^2 \delta_{lin}/2}; \tag{2.1}$$

δ_{lin} is the (linear regime) round-trip phase shift $\delta_{lin} = 2n_{lin}\omega_L d/c$ and T_m is the transmittivity $T_m = 1 - R_m$ of the mirrors.

Resonant tunneling peaks occur at the FP mode frequencies

$$\omega_{FP}^{(j)} = \frac{\pi c}{n_{lin} d}(j+1) \tag{2.2}$$

and have linewidths given by

$$\gamma = \frac{cT_m}{n_{lin} d}. \tag{2.3}$$

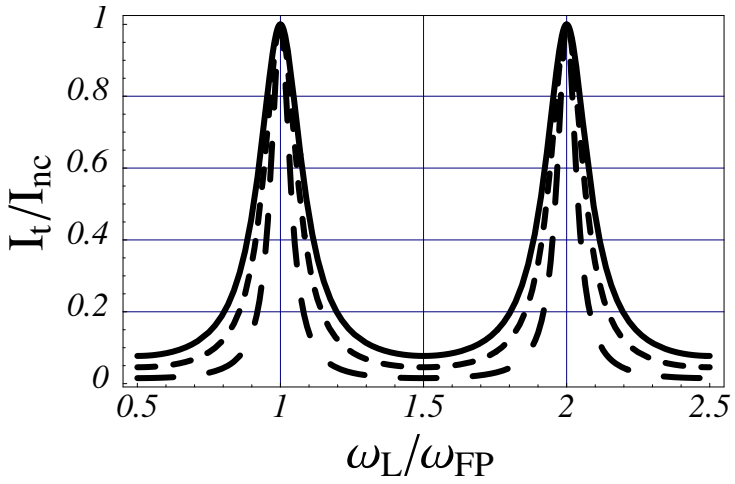

FIGURE 2.1: Transmission spectrum of a non-absorbing FP cavity at linear regime. The longer the dashing, the smaller the mirror transmittivity T_m.

Since $I_{int} = I_{tr}/T_m$, the internal intensity at resonance is generally much larger than the incident one for sufficiently good cavity mirrors, making optical cavities useful devices for the observation of nonlinear optical effects. In this case, we have to substitute in eq.(2.2) the effective refractive index corresponding to the internal intensity I_{int}; assuming, for simplicity

$$n_{eff} = n_{lin} + \tilde{n}_{nl} I_{int}. \tag{2.4}$$

the effective round-trip phase shift can be written as

$$\delta_{eff} = \delta_{lin} + \delta_{nl} = \delta_{lin} + \frac{2d\omega_L}{c}\tilde{n}_{nl} I_{int}. \tag{2.5}$$

Inserting such a result into eq.(2.1), we are led to the final constitutive relation for the nonlinear FP cavity:

$$\frac{I_{tr}}{I_{inc}} = \frac{1}{1 + 4/T_m^2 \sin^2 \delta_{eff}/2} \tag{2.6}$$

which can be analytically studied [63, pag.268]. In particular, for high enough incident intensity

$$I_{inc} > I_{thres} = \frac{4\pi}{3\sqrt{3}} \frac{n_{lin}^2}{\tilde{n}_{nl}} \frac{\gamma^2}{\omega_L^2} = \frac{4\pi n_{lin}^2}{3\sqrt{3}\tilde{n}_{nl} Q^2}. \tag{2.7}$$

several solutions to eq.(2.6) are possible and the system shows optical multistability.

In physical terms, the effect of the nonlinearity can be interpreted as a frequency shift $\Delta\omega$ of the cavity resonance from its linear regime frequency ω_{FP} equal to

$$\frac{\Delta\omega}{\omega_{FP}} = -\frac{\tilde{n}_{nl} I_{int}}{n_{lin}} = \frac{2\omega_{nl} I_{int}}{\omega_{FP}} \tag{2.8}$$

which explains the proportionality of the threshold intensity I_{thres} on the square of the linewidth γ: one factor of γ comes from the sharpness of the spectral features with respect to frequency shifts (i.e. $dT/d\omega$), while the other one from the resonance enhancement of the internal intensity with respect to the incident one.

Depending on the relative sign of the nonlinear refractive index $\tilde{n}_{nl}$ and the incident frequency ω_L it is possible to achieve both *optical limiting* and *optical bistability*; assuming for simplicity $\tilde{n}_{nl} < 0$, as in most semiconducting materials at frequencies below the electronic band gap, the sign of the nonlinear frequency shift will be positive $\Delta\omega > 0$.

If the incident frequency is located just above a resonance peak, the nonlinearity will push the resonance peak closer to the incident frequency and the transmittivity will be reinforced: such a *positive* feedback can eventually lead to *optical bistability*. On the other hand, if the incident frequency is already on the resonance peak or is located just below it, the nonlinearity will push the resonance peak further away from the incident frequency, giving a *negative* feedback on the transmission and, consequently, an *optical limiter* behavior.

In fig.2.2 we have plotted a few examples of characteristic I_t vs I_{inc} curves for both optical limiting and optical bistability cases; in this second case, the central branch, characterized by a negative value of the differential transmittivity dI_t/dI_{inc} corresponds to unstable fixed points of the dynamical system and can not be explored experimentally in a continuous wave (cw) experiment.

All such results are summarized in fig.2.3, which shows the transmitted intensity I_{tr} spectra as function of the incident frequency ω_L at different values of incident intensity I_{inc}; white regions correspond to unstable solutions. Bistable behavior is here described by a triple intersection of one of the fixed I_{inc} curves with the vertical line defining ω_L; the two external intersections are stable, while the central solution lies always in the instability region which is under the tilted resonance peak.

If the mirror reflectivity is high enough for the resonance peaks to be well spaced from each other and we limit to the case of nonlinear shifts much smaller than the mode spacing, the sine in the denominator of the right-hand side of eq.(2.6) can be

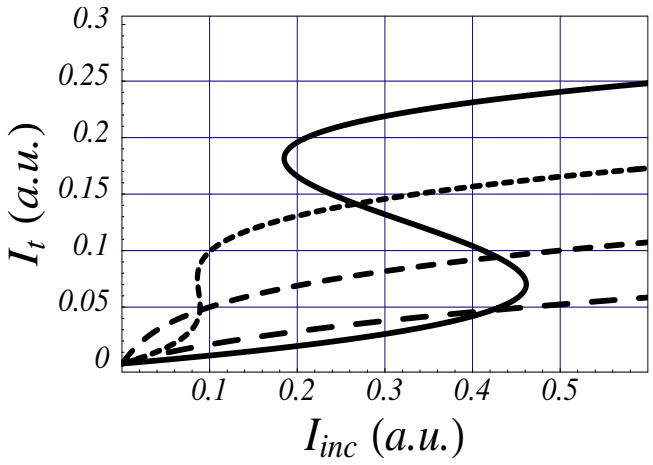

FIGURE 2.2: Characteristic I_t vs. I_{inc} curves for different values of incident frequency $\omega_L/\omega_{FP} = 0.97, 1.00, 1.03, 1.06$. Notice optical limiting for $\omega_L \leq \omega_{FP}$ (the longer the dashing, the lower the frequency) and optical bistability for $\omega_L > \omega_{FP}$ (solid line).

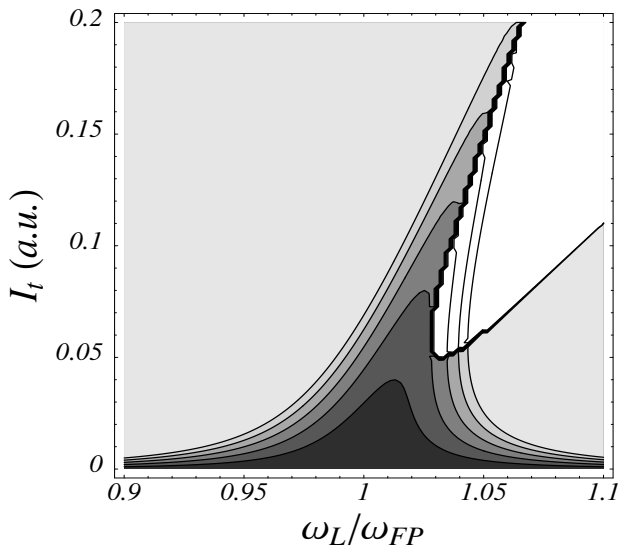

FIGURE 2.3: Transmitted intensity I_t spectra for different values of incident intensity I_{inc} as a function of the incident frequency ω_L. The grey scale corresponds to the incident intensity: lighter shadowing means higher intensity; white regions correspond to unstable behavior.

linearized around an effective resonance at $\omega_{FP} + 2\omega_{nl} I_{int}$

$$\frac{I_{tr}}{I_{inc}} = \frac{\gamma^2/4}{\left(\omega_L - \omega_{FP} - 2\omega_{nl} I_{int}\right)^2 + \gamma^2/4}. \tag{2.9}$$

In physical terms, this is equivalent to stating that only a single resonance is effectively relevant to the transmission of the cavity, while the others are too far detuned to contribute. On the other hand, if the intensity is so large that the nonlinear shift becomes comparable to the mode separation, several optical limiting stages alternated to multistability loops can be observed for increasing I_{inc}.

2.2 The single mode model

Starting from the discussion of the previous section, we can try to develop a model which from the beginning takes into account only a single mode of the cavity and introduces the nonlinearity simply as a dependence of the mode frequency on light intensity.

In analogy to what has been done in sec.1.5.1, we can describe the conservative dynamics of the cavity with an Hamiltonian of the form

$$\hat{\mathcal{H}} = \hbar\omega_o \hat{a}^\dagger \hat{a} + \hbar\omega_{nl} \hat{a}^\dagger \hat{a}^\dagger \hat{a}\hat{a} + \hbar k_{inc} E_{inc}(t) \hat{a}^\dagger + \hbar k^*_{inc} E^*_{inc}(t) \hat{a} \tag{2.10}$$

in which the nonlinearity is taken into account by the quartic term $\hbar\omega_{nl} \hat{a}^\dagger \hat{a}^\dagger \hat{a}\hat{a}$ which gives a nonlinear shift $\Delta\omega = 2\omega_{nl} \hat{a}^\dagger \hat{a}$ of the cavity mode frequency. Cavity damping is described by damping terms in the master equation for the density matrix of the cavity field.

As we have done in sec.1.5.2 for the exciton-photon coupling coefficient, the nonlinear coupling ω_{nl} can be expressed in terms of experimentally accessible properties of the cavity, such as the nonlinear susceptibility of the material and the wavefunction of the photonic mode at linear regime.

The nonlinear polarization term appearing in the SVEA motion equation eq.(1.29) for the cavity field is easily written in terms of the nonlinear dielectric constant $\chi^{(3)}$ (or equivalently the nonlinear refractive index $n_{nl} = \frac{3}{8n_{lin}} \mathrm{Re}\left[\chi\right]^{(3)}$); from such a calculation, a simple expression for the nonlinear frequency shift in terms of the wavefunction $\mathcal{E}(x)$ of the photonic mode can be obtained

$$\omega_{nl} = -\frac{3}{8\hbar} \int dx \ |\mathcal{E}(x)|^4 \chi^{(3)} = -\frac{n_{lin}}{\hbar} \int dx \ |\mathcal{E}(x)|^4 n_{nl}(x); \tag{2.11}$$

such an expression can be used to determine ω_{nl} of any actual dielectric structure.

For the most relevant case of a metallic plane-mirror cavity, the wavefunction $\mathcal{E}(x)$ has a standing wave profile

$$\mathcal{E}(x) = \sqrt{\frac{4\pi\hbar\omega_o}{Sd\, n_{lin}^2}} \sin\left[n_{lin}\omega_o x/c\right], \tag{2.12}$$

where n_{lin} is the linear refractive index of the material and d is the cavity length; in order to give to the quantity $\left\langle \hat{a}^\dagger \hat{a} \right\rangle$ the meaning of photon number, eq.(2.12) has been normalized in a three-dimensional way, assuming a transverse area S for the cavity mode. Inserting this expression into eq.(2.11), we recover the result eq.(2.8), which gives further evidence to the validity of the single-mode model.

Since optical nonlinearities in current semiconducting materials usually require a large number of photons to be present in the cavity mode in order to have an appreciable nonlinear modulation of the transmittivity, a *mean-field* (MF) approximation can be performed. This approximation, which corresponds to replacing all operators with their mean values and assuming all operator products appearing in the motion equations to be factorizable, is equivalent to using classical rather than quantum electrodynamics and is valid in the limit of high photon number $\left\langle \hat{a}^\dagger \hat{a} \right\rangle \gg 1$. A detailed discussion of the validity and the limitations of MF theory will be given in chap.6.

In this mean-field approximation, the operator-valued master equation is replaced by a simple ordinary differential equation for the field mean value $a = \langle \hat{a} \rangle$

$$i\frac{da}{dt} = -i\omega_o a - 2i\omega_{nl} \left|a\right|^2 a - \frac{1}{2}\gamma_{ph} a - ik_{inc} E_{inc}(t); \tag{2.13}$$

unlike for the case of the exciton-photon coupling described in sec.1.5.1, this evolution equation is now only an approximation, since for its derivation we have assumed

$$\left\langle \hat{a}^\dagger \hat{a} \hat{a} \right\rangle = \left|a\right|^2 a; \tag{2.14}$$

as we shall see in detail in chap.6, the weaker the nonlinearity ω_{nl}, the better the approximation.

In the case of a monochromatic excitation $E_{inc}(t) = E_{inc}^{(o)} e^{-i\omega_L t}$, if we switch to a slow variable $b(t) = \bar{a}(t) e^{i\omega_L t}$, we are led to a homogeneous equation

$$\frac{db}{dt} = -i\left(\omega_L - \omega_o - 2\omega_{nl}\left|b\right|^2\right) b - \frac{1}{2}\gamma_{ph} b - ik_{inc} E_o \tag{2.15}$$

which has a stationary state b_{ss} as a long time limit

$$b_{ss} = \frac{ik_{inc}E_{inc}^{(o)}}{i\left(\omega_L - \omega_o - 2\omega_{nl}\left|b_{ss}\right|^2\right) - \gamma_{ph}/2}. \tag{2.16}$$

From the point of view of the physical field $a(t)$, the steady-state corresponds to a monochromatic oscillation of the cavity field at ω_L

$$a_{ss}(t) = b_{ss}e^{-i\omega_L t}. \tag{2.17}$$

Since the amplitude of the transmitted field is proportional to the internal field $E_{tr}^{(o)} = \eta_{tr}b_{ss}$, eq.(2.16) can be used to characterize the transmission properties of the cavity as function of both the incident frequency ω_L and the incident intensity; in this way, the result eq.(2.9) is immediately recovered as well as all its physical predictions, such as optical bistability and optical limiting.

The stability of each of the steady-states of eq.(2.16) can be determined using classical linearization techniques: dynamical stability requires all eigenvalues of the linearized system to have a negative real part. In our specific case, the linearization of eq.(2.15) around a steady-state $b = b_{ss}$ leads to an equation of the form

$$\frac{\partial \delta b}{\partial t} = -i\left(\omega_L - \omega_o\right)\delta b - 4i\omega_{nl}\left|b_{ss}\right|^2\delta b - 2i\omega_{nl}b_{ss}^2\delta b^* - \frac{1}{2}\gamma_{ph}\delta b; \tag{2.18}$$

switching to the δb, δb^* basis, the characteristic equation of the linear system has the form

$$\left(\lambda + \gamma_{ph}/2\right)^2 + \left(\omega_L - \omega_{FP} - 4\omega_{nl}\left|b_{ss}\right|^2\right)^2 - 2\omega_{nl}^2\left|b_{ss}\right|^4 = 0. \tag{2.19}$$

Imposing that both eigenvalues have a negative real part leads to the condition

$$\left(2\omega_{nl}\left|b_{ss}\right|^2\right)^2 - \left(\omega_L - \omega_{FP} - 4\omega_{nl}\left|b_{ss}\right|^2\right)^2 < \frac{\gamma_{ph}^2}{4}, \tag{2.20}$$

which can be shown to be equivalent to the usual one

$$\frac{dI_t}{dI_{inc}} > 0 \tag{2.21}$$

which has been used for determining the stability region in fig.2.3.

2.3 The nonlinear DBR microcavity

As we have seen in the previous section, all the qualitative features discussed in sec.2.1 for the case of a metallic mirror nonlinear Fabry-Perot interferometer charac-

terize the behavior of any nonlinear system which can be described by the single-mode model.

The DBR microcavities of sec.1.3 fall in this category, since they show well separated optical modes and the relatively large nonlinear polarizability of the semiconducting material can provide an appreciable nonlinear shift of the cavity mode.[64] This suggests that a numerical integration of the nonlinear wave equation for the electromagnetic field should give results in qualitative agreement with the predictions of the single-mode model. In order to do this, a direct generalization of the transfer matrix algorithm[4,25] to systems with an intensity dependent refractive index can be used:[26] the structure is divided in layers much thinner than the wavelength in the material so that the light intensity can be considered as constant within each layer; at each step, the local refractive index is determined using the refraction index value which corresponds to the local value of the light intensity and then inserted in the standard transfer matrix algorithm.

Since the main room-temperature nonlinear susceptibility of semiconducting materials come from the excitation of free pairs and the consequent reduction of the refractive index by electron-hole plasma and Pauli exclusion principle effects, the closer is the operating frequency to the gap edge, the stronger the absorption and therefore the effective nonlinear susceptibility.[5,65–67] This means that both the refractive index, the absorption and the nonlinear susceptibility can all be controlled by tuning the energy gap position by means of the chemical composition of the material. In the most relevant case of $Al_xGa_{(1-x)}As$ alloys, a larger amount of Al atoms corresponds a larger energy gap and therefore the optical nonlinearity is the strongest in pure GaAs layers.

In tab.2.1, we have summarized the experimental values[68,69] actually used in numerical simulations; although the refractive index variation following the presence of excited carriers can be somewhat varied by tuning the operating frequency closer of further from the energy gap, the strongest frequency dependence of the nonlinear susceptibility comes from the frequency dependence of absorption.

In the actual simulations, we have assumed a functional dependence of the refractive index on intensity of the form:

$$n_{eff} = n_{lin} + \delta n^{max} \frac{I/I_{sat}}{1 + I/I_{sat}}, \tag{2.22}$$

with the frequency-dependent parameters n_{lin}, δn^{max} and I_{sat} which have to be fitted

GaAs	Refractive index n	3.6
	Absorption coefficient k	≈ 0.001
	Gap energy E_g	1.425 eV
	Carrier saturation density N_s	$\approx 10^{18}$ cm^{-3}
	Nonlinear variation refractive index δn^{max}	≈ -0.03
AlAs	Refractive index n	2.95
	Absorption coefficient k	≈ 0
AlGaAs	Refractive Index n	$3.6 > n > 2.95$
InGaAs Quantum Well	2D Oscillator strength f_{osc}	$5 \cdot 10^{-4}$Å^{-2}
	Resonance energy E_0	1.415 eV
	Linewidth Γ	1 meV
	Carrier saturation density N_s	$\approx 5 \cdot 10^{11}$ cm^{-2}

TABLE 2.1: Summary of experimentally determined[68,69] optical constants of GaAs based materials.

on experimental data.

Since the optical modes of a DBR microcavity are not confined in the cavity layer, but do penetrate also inside the mirrors, we expect that a nonlinear polarizability localized in the cavity layer should be less effective than a nonlinearity distributed along the whole structure; this guess has been verified studying the transmission properties of two different structures. In the first case the external mirrors are formed of non-absorbing wide gap AlAs/AlGaAs layers, while the cavity layer is formed by a strongly nonlinear GaAs layer; in the second case all the system is nonlinear, being formed by AlGaAs/GaAs mirrors with a GaAs cavity layer. As expected, the nonlinear mode shift results much larger in the second case, while it is very small in the first case (fig.2.4); as usual, the mode shift leads to optical bistability or optical limiting effects depending on the relative position of the incident laser frequency and the cavity mode.

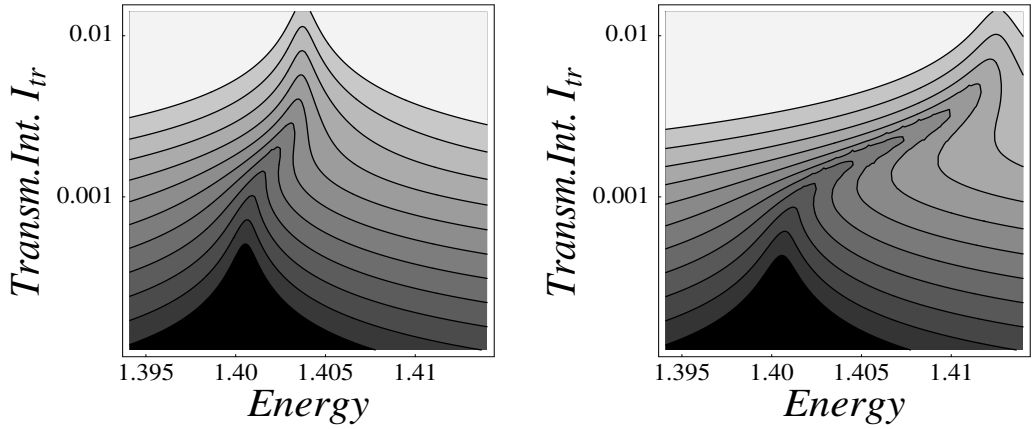

FIGURE 2.4: Simple nonlinear DBR microcavity: transmitted intensity I_{tr} spectra at different values of the incident intensity I_{inc}; the grey scale corresponds to the incident intensity: lighter shadowing means higher intensity. Transmitted intensity is measured in kW/cm^2; energy in eV. Left panel: nonlinearity concentrated in the cavity layer; Right panel: nonlinearity distributed along the whole structure.

2.4 Nonlinear DBR microcavity containing excitonic resonances

The nonlinear frequency shift of a cavity mode described in the previous sections can be exploited to vary in an *all optical* way the detuning of the cavity mode with respect to an excitonic resonance to which it is strongly coupled[70] and therefore observe an anticrossing behavior which should closely resemble the one depicted in fig.1.7.

Provided the excitonic resonance is not yet *bleached* at the large light intensities which are required to shift the cavity mode across the excitonic resonance, the transmission spectra are characterized by the peculiar structures reproduced in the left panel of fig.2.5. At low light intensities, the photonic mode is on the red side of the excitonic transition, while it is shifted on its blue side at large intensities; in between, the two modes are strongly mixed.

Such a behavior clearly relies on the assumption that the excitonic saturation density is much larger than the excitonic density which is generated by the strong laser beam at the intensities which are required for the shift of the photonic resonance.

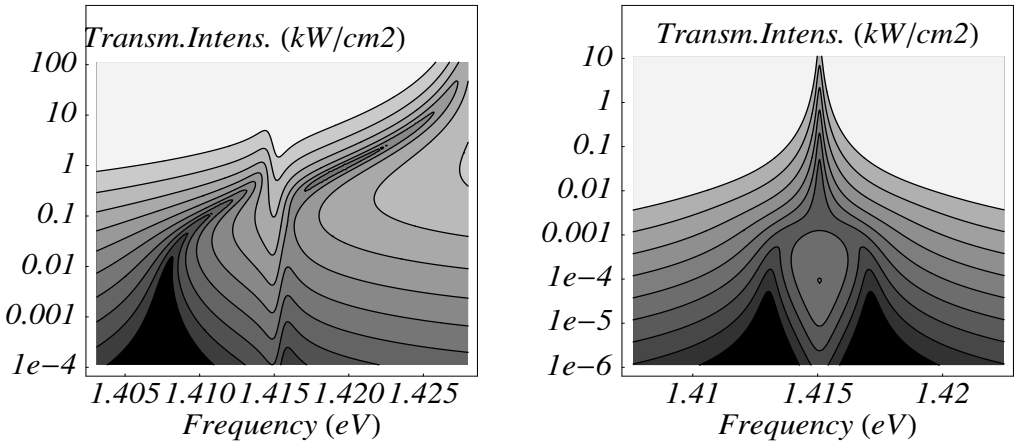

FIGURE 2.5: DBR microcavity containing a few quantum wells: transmitted intensity I_{tr} spectra at different values of incident intensity I_{inc}. The grey scale corresponds to the incident intensity: lighter shadowing means higher intensity. Transmitted intensity is measured in kW/cm^2. Left panel: the cavity mode is swept across an unbleachable excitonic transition by the optical nonlinearity. Right panel: the photonic mode does not appreciably shift while the exciton is bleached.

Unfortunately, neither InGaAs quantum well excitons nor bulk GaAs excitons can be used for such purpose, since their large Bohr radii reflect into a rather low saturation density.[65] The same electron-hole plasma which is responsible for the nonlinear polarizability of the dielectric medium is in fact able to bleach the excitonic transition in the quantum well. On the other hand, organic semiconductors, having excitonic states much more localized in space, may be good candidates for the observation of such effects.[71,72]

However, as it has been already pointed out by several authors, the nonlinear properties of a bleachable excitonic[73] or atomic[74] transition strongly coupled to a photonic resonance can lead to interesting patterns in the nonlinear transmission spectra as well. In the right panel of fig.2.5 we have reproduced a typical example of such effects: the excitonic and photonic modes are initially at resonance and the frequency shift of the optical mode is assumed to be still very small at the light intensities which are required for the bleaching of the excitonic resonance.

As it has been done for the simple nonlinear cavity, the study of such systems can be performed in terms of simple effective Hamiltonians which generalize eq.(1.10) adding appropriately chosen nonlinear terms. For the description of the nonlin-

ear shift of the photonic mode across the excitonic mode, it is sufficient to add the usual term $\hbar\omega_{nl}\hat{a}^\dagger\hat{a}^\dagger\hat{a}\hat{a}$ to the Hamiltonian eq.(1.10). Exciton bleaching at densities of the order of the saturation density n_{sat} is instead well described by an intensity-dependent exciton-light coupling

$$k_c^{(eff)} = \frac{n_{sat}}{n_{sat} + |a_{exc}|^2} k_c \tag{2.23}$$

in the motion equations eqs.(1.18-1.19).

2.5 Two-beam nonlinear interactions: pump and probe optics and optical switching

In the previous sections we have discussed the effect of an intensity dependence of the refractive index on the transmission properties of a single beam; the resulting feedback on the transmittivity can result either positive or negative, depending on the details of the configuration and the operating frequency; in particular, optical bistability can be observed in the former case, while optical limiting can be observed in the latter case.

The present section is devoted to the analysis of the effect of a, generally strong, *pump* beam on the transmission of a second, generally weaker, *probe* beam. At the simplest level, the nonlinear interactions of the two beams can be described in the following way: the pump beam creates some excitation in the material, e.g. free electron-hole pairs, the presence of which modifies the refraction index profile experienced by the probe beam as well as by the pump beam itself. Since the probe beam is assumed not to be coupled to the optical polarization created by the pump beam but only to the produced excitation density, the relative phase of the two beams is not involved in the process and the nonlinear process can be said to be an incoherent one; such an assumption is generally well verified in semiconducting materials at room temperature, in which the optical polarization of the electron-hole pairs is quickly washed out by the interaction with the thermal bath of phonons. As we shall discuss in the next chapter, coherent processes can however be observed in semiconductor microcavities provided we dispose of sharp excitonic or photonic resonances resonantly coupled by the nonlinearity to the fundamental cavity mode.

While the probe beam, assumed to be weak, can be treated at linear regime neglect-

ing its self-interactions as well as its effect onto the pump beam, the pump beam amplitude has to be taken into account at all orders by means of the generalized transfer matrix algorithm previously used. As in the previous section, the refraction index experienced by the probe beam is modeled by

$$n_{pump}^{eff} = n_{pump}^{lin} + \delta n_{self}^{max} \frac{I^{(pump)}/I_{self}^{sat}}{1 + I^{(pump)}/I_{self}^{sat}} \tag{2.24}$$

while the one experienced by the probe is given by

$$n_{probe}^{eff} = n_{probe}^{lin} + \delta n_{mut}^{max} \frac{I^{(pump)}/I_{mut}^{sat}}{1 + I^{(pump)}/I_{mut}^{sat}}. \tag{2.25}$$

The coefficients n_{pump}^{lin} and n_{probe}^{lin}, δn_{self}^{max} and δn_{mut}^{max}, I_{self}^{sat} and I_{mut}^{sat} are in general different, but of the same order of magnitude, provided both frequencies are sufficiently far from all excitonic and interband transitions of the material medium.

In this framework, the transmission of the probe is a function of the intensity of the pump beam: such a behaviour is equivalent to a sort of *all optical transistor*, in which the pump beam plays the role of the *base* current and the probe plays the role of the *collector* current. As in the conventional electronic transistors, the collector current, i.e. the probe transmission, is controlled by the intensity of the base current, i.e. the intensity of the pump beam.

In fig.2.6 we have reproduced the evolution of the transmission spectra for the probe beam as the pump beam intensity is increased: the nonlinear frequency shift of the optical mode is apparent; at a given frequency, the transmittivity of the probe can be varied of more than one order of magnitude just by sweeping a resonance across its operating frequency. Eventually, if the pump beam has itself a bistable behavior, the *bit* of information stored in its hysteresis loop can be read by the probe beam.

In summary, such a device shows all the main features required from an optical memory: write operations are performed by modulating the intensity of the pump beam, read operations by monitoring the transmission of the probe beam. Unfortunately, the upper bound on the probe beam intensity in order not to perturb the pump beam is rather stringent in the present case of single DBR cavities: if both the pump and the probe beams are intended to interact with the cavity mode, their frequency difference can not be large and therefore both of them are able to create an excitation in the material. This means that the probe beam has to be much weaker than the pump beam and significant amplification of the pump signal onto the probe beam can not be achieved.

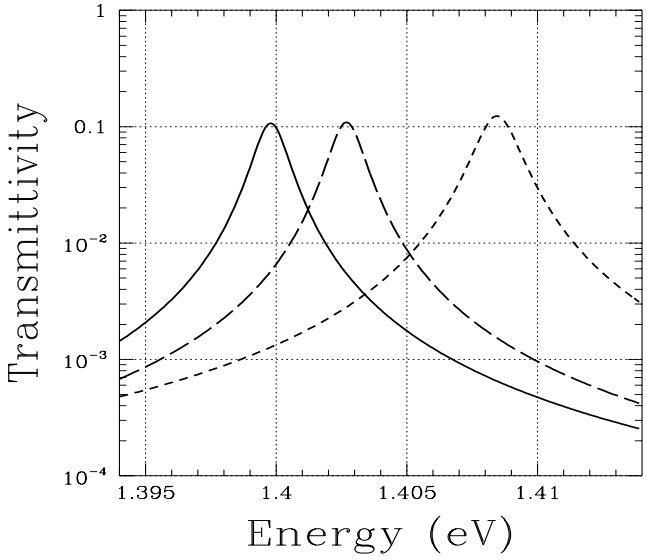

FIGURE 2.6: Simple DBR microcavity: transmission spectra of a (weak) probe beam. Pump intensity grows from the solid line to the short-dashed line. A contrast of more than one order of magnitude in the probe transmittivity is apparent.

2.6 Nonlinear optics of coupled DBR microcavities

In the previous section we have discussed the simplest example of all-optical switch, in which the intensity of a strong pump beam controls the transmission of a probe beam, assumed weak enough not to perturb the refraction properties of the material. Depending on the specific choices made for the operating frequencies and the geometrical configuration, the actual extent of such a linear regime can be completely different; in particular, we have seen that the use of a single DBR microcavity requires the probe beam to be much weaker than the pump one.

Since in a semiconducting material absorption is a fast decreasing function of the distance from the electronic gap edge, this difficulty can be overcome by tuning the pump beam close to such edge and the probe well inside the gap. In this way, probe absorption results negligible as well as its nonlinear effect on the pump, while the pump can create a substantial excitation even at moderate intensities. The probe beam intensity can therefore be comparable or even larger than the pump beam intensity so that the device truly behaves as an optical amplifier: a signal encoded in a small modulation of the pump beam intensity is amplified into a stronger modu-

lation of the probe beam.

In order for both beams to be resonantly coupled to the nonlinear device, the coupled cavity configuration introduced in sec.1.7 is very useful, since its transmittivity shows two resonance peaks: the pump beam can in fact be tuned close to the upper one and the probe beam close to the lower one. This means that the pump intensity inside the structure can be resonantly enhanced thanks to the resonance with the upper cavity mode, while the probe transmittivity has a sharp dependence on the pump intensity thanks to the resonance on the lower cavity mode.

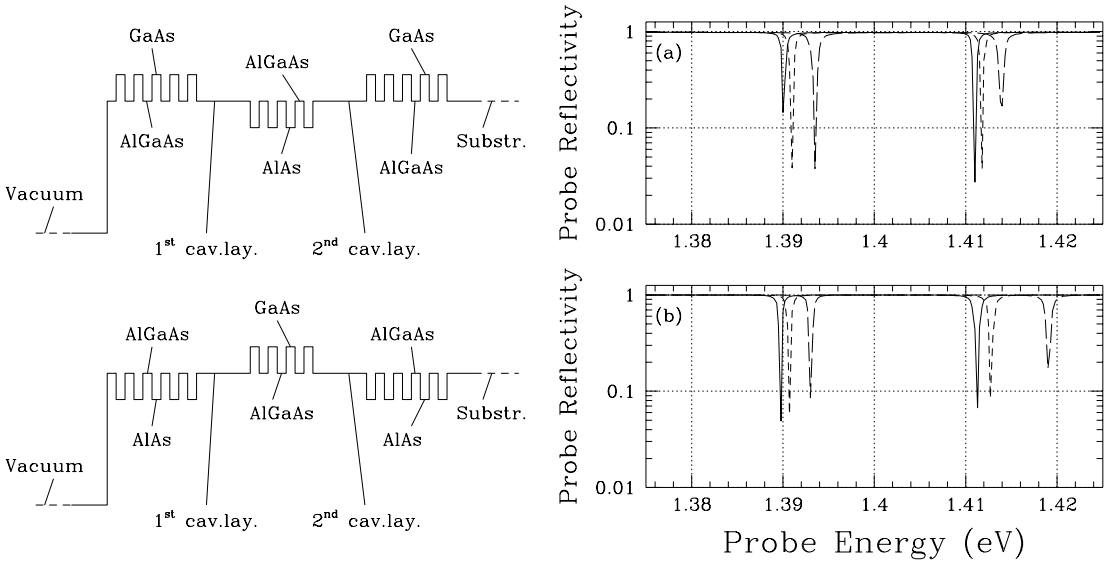

FIGURE 2.7: Nonlinear coupled DBR microcavities. Left panels: sketch of the system under examination; the heights of the lines represent the refraction index of the different layers. Right panels: reflectivity of a probe beam for different values of the pump intensity which grows from very low (solid line) to very high (long dashed line). Upper panels: nonlinearity in the external mirrors. Lower panels: nonlinearity in the central mirror.

From an immediate extension of the general theory of sec.1.5.2, it is easy to see how the nonlinear *cross*-frequency shift of one mode on the other is, at lowest order, proportional to the matrix element

$$\int dx\, \chi^{(3)}(x)\ |E_1(x)|^2\ |E_2(x)|^2\,, \tag{2.26}$$

which quantifies the spatial overlap of the mode *intensities*; in the single beam case, the *self*-frequency shift of eq.(2.11) is recovered. Coupled cavities (sec.1.7) look very

promising systems from the point of view of giving a large cross-frequency shift, since the eigenfunctions in the resonant case are the symmetric and antisymmetric combinations of the single cavity wavefunctions. By appropriately choosing the cavity parameters, the upper and lower cavity modes can be tuned respectively close to the band edge and far inside the gap, as required for the optical amplifier operation.[75]

As in the single cavity case, it is better not to concentrate the nonlinearity in the cavity layers, but to distribute it along the whole DBR mirrors: fig.2.7 shows the evolution of probe reflectivity spectra as pump intensity is increased; the main feature is a frequency shift of both resonance peaks. In the upper panel, nonlinearity is situated in the external mirrors: in this case, both modes result shifted of a similar amount by the nonlinearity. In the lower panel, the nonlinearity is concentrated in the central mirror, whose transmission tends to be reinforced with growing light intensities; the spacing of the doublet is therefore enhanced so that the nonlinear shift is larger on the upper cavity resonance.

Chapter 3

Nonlinear optics of microcavities II: two-photon processes

All the discussion contained in the previous chapter has been focussed on the nonlinear effects which arise in semiconducting materials at room temperature; in this case, the optical polarization of the electron-hole pairs is quickly washed out by the interaction with the thermal bath of phonons and the nonlinear effect is due to the incoherent excitation density created in the material by absorptive effects.

The present chapter is instead devoted to the discussion of a new class of nonlinear optical effects which arise from *two-photon* processes in the presence of sharp excitonic or photonic resonances nonlinearly coupled to the fundamental photonic mode;[76,77] more specifically, our attention will be focussed on a pair of different systems, the mathematical description of which is however identical. The first of them consists in a microcavity supporting two photonic modes at frequencies ω_1 and $\omega_2 \approx 2\omega_1$; assuming an appreciable *second harmonic generation* (SHG) in the material medium, the two photonic modes result nonlinearly coupled to each other by a term which corresponds to the mutual conversion of two fundamental photons into an harmonic photon and vice versa. The second system consists in a microcavity supporting one photonic mode at a frequency ω_1 approximately equal to half the frequency ω_2 of an excitonic transition; if this latter allows for *two-photon absorption* (TPA), the excitonic mode and the photonic mode result coupled by a term which converts two photons into an exciton and vice versa which is formally identical to the second harmonic generation coupling term.

After the general discussion of the model contained in sec.3.1, the following sec.3.2 is devoted to the analysis of transmission spectra through our system when it is illuminated by a single beam at a frequency close to the lower mode frequency ω_1. At linear regime the spectrum is characterized by a single peak at ω_1, while at high intensities the main effect is either the appearance of a new peak at half the higher mode frequency $\omega_2/2$ or a *two-photon Rabi splitting* in the resonant case $\omega_1 \simeq \omega_2/2$.

Sec.3.3 is devoted to the linear optical response of our system when it is *dressed* by a strong pump beam; such a case is much similar to the usual optical Stark effect, in which an atomic transition is driven by a pump beam and probed by a weak probe beam. Differently from that case, in which the nonlinearity was intrinsic in the two-level structure of the material excitation, we are now dealing with a pair of linear oscillators interacting with each other by means of a two-photon coupling term; for this reason we shall refer to it as a *two-photon optical Stark effect* (TPOSE).

Because of this similarity, our results are physically most interesting in the two-photon absorption case; hence we shall concentrate on the absorption spectra in the case the system is driven at a frequency near the lower photonic mode and probed near the upper excitonic mode. The main feature that we shall discuss is the strong dependence of probe absorption spectra on pump intensity. When the intensity of the pump is low enough, the spectra show a single excitonic peak at ω_2; at moderate intensities, the dressing gives origin to an additional peak at $\omega_1+\omega_L$. For even higher intensities, the response is more complicated and, in particular, gain is predicted at some specific frequencies because of hyper-Raman scattering processes.

To make the discussion complete, an explicit expression for the coupling coefficient between the modes has to be given in terms of the experimentally accessible nonlinear optical susceptibilities $\chi^{(2)}$ and $\chi^{(3)}$. This is done in sec.3.4, together with a numerical estimate of the light intensity needed for the actual experimental observations of two-photon Rabi splitting or two-photon optical Stark effect in GaAs based microstructures.

3.1 The model

Consider a system with two bosonic degrees of freedom nonlinearly coupled by cubic interaction terms and driven by classical external fields:

$$\begin{aligned}\mathcal{H} &= \hbar\omega_1\,\hat{b}_1^\dagger\hat{b}_1 + \hbar\omega_2\,\hat{b}_2^\dagger\hat{b}_2 + \hbar\beta\,\hat{b}_2^\dagger\hat{b}_1^2 + \hbar\beta^*\,\hat{b}_1^{\dagger 2}\hat{b}_2 + \hbar k_1 E_1(t)\hat{b}_1^\dagger + \hbar k_1^* E_1^*(t)\hat{b}_1 + \\ &+ \hbar k_2 E_2(t)\hat{b}_2^\dagger + \hbar k_2^* E_2^*(t)\hat{b}_2. \end{aligned} \tag{3.1}$$

Such an Hamiltonian,[78–82] supplemented by the usual damping terms, can describe a few different nonlinear optical effects: our attention will be concentrated upon the two cases of resonant two-photon absorption (TPA) and of doubly resonant second harmonic generation (SHG) inside a microcavity. In the TPA case one boson is a cavity photon and the other is an exciton, while in the SHG both bosons are cavity photons. The nonlinear coupling is supposed to be nearly resonating, i.e. $2\omega_1$ is supposed to be close to ω_2; apart from the inclusion of phenomenological damping terms, all other modes of the system will be neglected.

The origin of the nonlinear coupling term $\hbar\beta\hat{b}_2^\dagger\hat{b}_1^2$ is different in the two cases: in the TPA case, in fact, it describes coherent optical transitions in the material which bring to the absorption of two cavity photons and the consequent creation of an exciton. The β coefficient is thus proportional to the effective matrix element for a two-photon absorption process, which, according to the general formula of second-order perturbation theory

$$M_{fi} = \sum_j \frac{\langle f|\mathcal{H}|j\rangle\,\langle j|\mathcal{H}|i\rangle}{E_i - E_j}, \tag{3.2}$$

contains a sum over all intermediate virtual states in which a matter excitation is created after absorption of a first photon. In sec.3.4, we shall relate β to the third-order nonlinear optical susceptibility $\chi^{(3)}(-\omega;-\omega,\omega,\omega)$ which in the specific case of resonant excitonic TPA can be written in the form:

$$\chi^{(3)}\left(-\omega;\omega,-\omega,\omega\right) = \frac{f^{(3)}}{\hbar\left(\omega_2 - 2\omega - i\gamma_2\right)}; \tag{3.3}$$

This will allow us to extract β from experimental data or theoretical calculations for the TPA cross-section which are present in the literature.

On the other hand, a nonlinear coupling term of the same form describes in the SHG case an optical process in which two photons of the fundamental cavity mode are

converted into a single harmonic cavity mode at approximately twice the fundamental frequency. This means that a complete adiabatical elimination of the matter degrees of freedom has been performed and all the matter dynamics has been summarized in the effective matrix element of the process; according to perturbation theory, this is now a third order one: absorption of the first fundamental photon, absorption of the second one and final emission of the harmonic photon; at each step, a sum over all virtual matter states analogous to the one in eq.(3.2) is required. In sec.3.4 we shall relate β to the familiar second-order nonlinear susceptibility of the material $\chi^{(2)}(-2\omega;\omega,\omega)$.

The $\hbar k_i E_i(t)\hat{b}_i^\dagger + \hbar k_i^* E_i^*(t)\hat{b}_i$ terms describe the driving of the $\hat{b}_1$ and $\hat{b}_2$ modes by external classical fields $E_1(t)$ and $E_2(t)$, e.g. laser beams incident on the cavity: a photonic mode can be driven by the external light field which leaks into the cavity through the non-perfectly reflecting front mirror, while an excitonic mode can be driven by an external radiation provided the cavity mirrors are nearly transparent at its frequency in order for the photonic mode structure of the cavity not to affect the (linear) coupling of the external radiation to the exciton. In the following we shall simplify the notation by letting $F_i(t) = k_i E_i(t)$.

Because of the coupling to several continua of external modes, the eigenmodes of our system have a finite lifetime and their energy is dissipated out in several different ways. Since these effects are dissipative, they are not included in the Hamiltonian above, but have to be introduced at the level of the quantum master equation as done in sec.1.5.1 giving $-\gamma_i\hat{b}_i$ terms in the equations of motions eqs.(3.4-3.5) for the field amplitudes. The damping of the photonic modes has to include the radiative escape of photons from the cavity as well as free pair absorption, while phonon and disorder scattering or ionization contribute to the damping of excitonic modes. Other possible forms of damping terms, which can arise, e.g., from two-photon free pair absorption, will not be considered in the following of this chapter, although they could result necessary for a refined fit of experimental data.

In the high intensity limit $\left\langle \hat{b}_1^\dagger \hat{b}_1 \right\rangle, \left\langle \hat{b}_2^\dagger \hat{b}_2 \right\rangle \gg 1$ the same *mean field* approximation can be performed as in sec.2.2, in which all operators are replaced by their mean values and their products are assumed to factorize; within such an approximation, the equations of motion for the field amplitudes $b_i = \left\langle \hat{b}_i \right\rangle$ can be written as:

$$\dot{b}_1 = -i\omega_1 b_1 - \gamma_1 b_1 - 2i\beta^* b_2 b_1^* - iF_1(t) \tag{3.4}$$

$$\dot{b}_2 = -i\omega_2 b_2 - \gamma_2 b_2 - i\beta b_1^2 - iF_2(t). \tag{3.5}$$

Such a description clearly does not take into account all those effects which arise from the quantum nature of the fields and their quantum and thermal fluctuations;[83,84] as discussed in chap.6, we expect such an approximation to be valid for small values of the nonlinear coupling β.

Leaving aside sub-harmonic generation effects[80,85] which take place when the system is driven on the harmonic mode, we shall concentrate our attention on the case in which the driving is only on the fundamental mode and it is monochromatic at frequency ω_L: $F_1(t) = F_o e^{-i\omega_L t}$ and $F_2 = 0$. It is convenient to introduce the slowly varying variables $a_1 = b_1 e^{i\omega_L t}$ and $a_2 = b_2 e^{2i\omega_L t}$; putting $\delta_M = (\omega_2 - 2\omega_1)/2$ and $\delta_L = \omega_L - \omega_1$, the evolution of the system will be given by:

$$\dot{a}_1 = i\delta_L a_1 - \gamma_1 a_1 - 2i\beta^* a_2 a_1^* - iF_o \tag{3.6}$$

$$\dot{a}_2 = 2i(\delta_L - \delta_M)a_2 - \gamma_2 a_2 - i\beta a_1^2. \tag{3.7}$$

A great deal of information about the physical behavior of our system can be obtained by looking for stationary solutions of the system of differential equations eq.(3.6) and eq.(3.7); the system being dissipative, it can, in fact, be expected to generally converge to a stationary solution at least for weak drivings. In any case, the stability of the solution found can be verified by means of the usual linearization techniques.

The stationary solutions (A_1 and A_2) are given by the equations:

$$A_1 \left[\delta_L + i\gamma_1 - \frac{|\beta A_1|^2}{\delta_L - \delta_M + i\gamma_2/2}\right] = F_o \tag{3.8}$$

$$A_2 = \frac{\beta A_1^2/2}{\delta_L - \delta_M + i\gamma_2/2} \tag{3.9}$$

and the stability can be determined from the eigenvalues of the linearized system[78]

$$\frac{d}{dt}\delta\vec{\alpha} = \mathbf{M}\cdot\delta\vec{\alpha}; \tag{3.10}$$

where we have introduced the displacement from the steady state solution:

$$\begin{aligned}\delta\vec{\alpha} &= (a_1 - A_1, a_1^* - A_1^*, a_2 - A_2, a_2^* - A_2^*)^T = \\ &= (\delta a_1, \delta a_1^*, \delta a_2, \delta a_2^*)^T\end{aligned} \tag{3.11}$$

and the linearized evolution matrix

$$\mathbf{M} = \begin{pmatrix} -\gamma_1 + i\delta_L & -2i\beta^* A_2 & -2i\beta^* A_1^* & 0 \\ 2i\beta A_2^* & -\gamma_1 - i\delta_L & 0 & 2i\beta A_1 \\ -2i\beta A_1 & 0 & -\gamma_2 + 2i(\delta_L - \delta_M) & 0 \\ 0 & 2i\beta^* A_1^* & 0 & -\gamma_2 - 2i(\delta_L - \delta_M) \end{pmatrix} \tag{3.12}$$

3.2 Transmission and second harmonic generation spectra: two-photon Rabi splitting

Such a simple theory can predict exactly the transmission properties of the structure under continuous wave (cw) illumination: to visualize their behavior, in fig.3.1 we have reproduced a few spectra of the internal intensity parameter $\Omega^2 = |\beta A_1|^2$ (which is proportional to the internal intensity as well as to the transmitted one) as function of the driving frequency δ_L, for different values of incident (driving) intensity: the upper panel refers to the exact resonance $\delta_M = 0$ case, the lower panel to the detuned case $\delta_M = 4\gamma$. The whitened regions correspond to unstable behavior. We have supposed $\gamma_1 = \gamma_2 = \gamma$.

In the latter case ($\delta_M = 4\gamma$), the transmitted intensity at low incident intensity, i.e. in the linear regime limit, is characterized by a single peak at $\delta_L = 0$ (i.e. at $\omega_L = \omega_1$); at higher intensities, a new peak appears close to $\delta_L = \delta_M$ (i.e. at $\omega_L \simeq \omega_2/2$) and for growing intensities the peaks bend in the external direction repelling each other and tend to have the same strength. In the $\delta_M = 0$ case, the transmitted intensity shows initially a single peak at $\delta_L = 0$, which at higher intensities splits in two; for growing intensities the two components bend again towards the external direction, their strengths staying equal.

Thanks to the bending of the transmission peaks with growing intensity, dispersive optical bistability can be obtained:[80] a multiple intersection of the vertical straight line corresponding to a given δ_L with the transmission spectrum at a given incident intensity has the the physical meaning of optical multistability already encountered in sec.2.1. The instability region present under the bended peak correspond to the central unstable branch of the hysteresis loop. The instability predicted in the region between the two peaks correspond instead to a so-called hard-mode transition: the eigenvalues of the stability matrix M having a non-vanishing imaginary part at the threshold, the system goes from a stable solution to a limit cycle, which physically

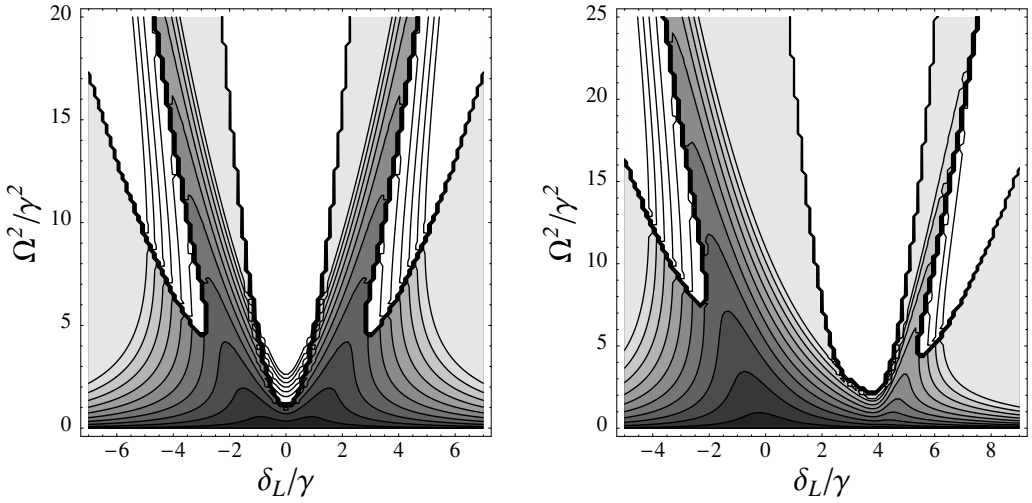

FIGURE 3.1: Internal intensity parameter ($\Omega^2 = |\beta A_1|^2$, proportional to the internal as well as to the transmitted intensity) for different values of (constant) incident intensity as a function of the detuning of the incident field δ_L. Left panel: exact resonance case $\delta_M = 0$. Right panel: $\delta_M = 4\gamma$. The grey scale corresponds to the incident intensity: lighter shadowing means higher intensity; white regions correspond to unstable behavior.

corresponds to self-pulsing of the transmission with time; a detailed discussion of such phenomena is beyond the scope of the present discussion and can be found in.[78,80,82]

Since resonant enhancement of SHG by means of an optical cavity is actually considered as a most useful way for improving the performances of devices,[27,86–88] it can be interesting to investigate the intensity of the generated harmonic field as a function of the incident frequency and detuning; in our formalism, this is proportional to

$$I_h = |A_2|^2 = \left| \frac{\beta A_1^2/2}{\delta_L - \delta_M + i\gamma_2/2} \right|^2 , \tag{3.13}$$

i.e. to the square of the fundamental mode internal intensity times a *temporal phase matching* factor $(\delta_L - \delta_M + i\gamma_2/2)^{-1}$, whose physical meaning will be clarified in the following.

In fig.3.2 we have represented the spectra of harmonic intensity as function of the incident frequency δ_L, for different values of incident intensity; again the upper panel corresponds to the exact resonance $\delta_M = 0$ case, while the lower panel to the de-

tuned $\delta_M = 4\gamma$ case. As done previously, instability regions have been whitened. The principal features are analogous to the previously analyzed transmission case: optical bistability and self pulsing can thus be observed also by looking at the harmonic field intensity. Notice the typical quadratic dependence of the harmonic intensity on the *internal* fundamental intensity: all the bistability and self-pulsing effects are in fact due simply to the coupling of the incident beam with the cavity mode at the fundamental frequency.

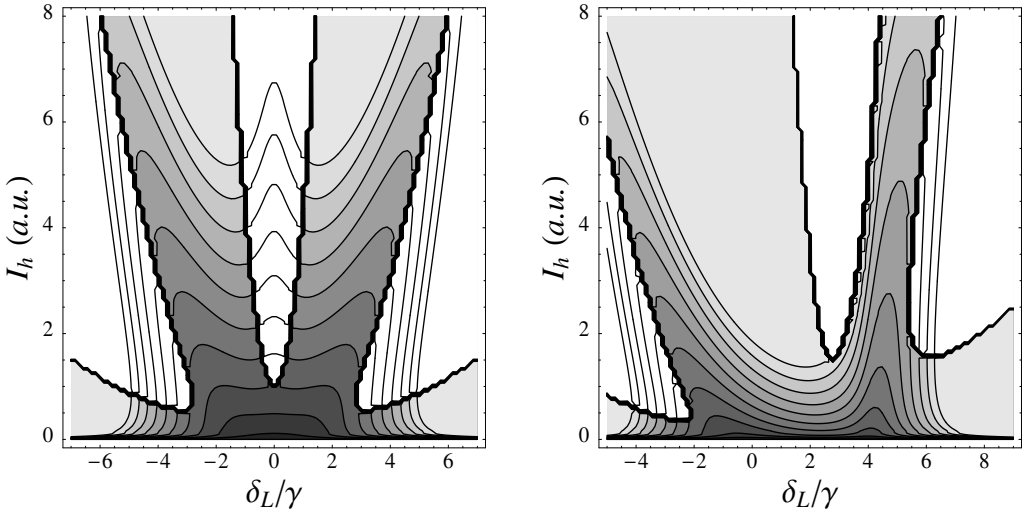

FIGURE 3.2: Second harmonic intensity spectra for different values of (constant) incident intensity. Left panel: exact resonance case $\delta_M = 0$. Right panel: $\delta_M = 4\gamma$. The grey scale corresponds to the incident intensity: lighter shadowing means higher intensity; white regions correspond to unstable behavior.

The *undepleted pump* approximation, currently done in nonlinear optics when the generated harmonic field is supposed to be weak compared to the fundamental one corresponds in our formalism to neglecting back-action of the harmonic field on the fundamental one, i.e. to assuming $b_2 = 0$ in eq.(3.4) or, equivalently, A_1 in the square braket of eq.(3.8). In this scheme, the fundamental beam is not affected by nonlinear effects, while the harmonic one is still described by eq.(3.5) and eq.(3.9). For current experimental parameters, such an approximation is generally a good one; first evidence of pump depletion phenomena in resonant SHG is however present in the spectra of [89, fig.3].

3.2.1 Physical interpretation of the results

The relatively simple structure of eq.(3.8) allows for a clear physical interpretation of the spectra of fig.3.1; since the transmittivity of the system τ is proportional to the ratio of the internal amplitude A_1 and the incident amplitude F_o, we can focus our attention on its rescaled version:

$$\tilde{\tau} = \frac{A_1}{F_o} = \left[\delta_L + i\gamma_1 - \frac{\Omega^2}{\delta_L - \delta_M + i\gamma_2/2}\right]^{-1} \tag{3.14}$$

which has a form much similar to the one described by eq.(1.20), but for the dependence of the transmittivity τ on the transmitted intensity Ω^2 which is a typical signature of nonlinear effects: for the moment we shall consider Ω as an independent parameter and we shall study the behavior of the transmission spectrum at fixed Ω.

Assuming for the sake of simplicity the damping coefficients $\gamma_{1,2}$ to be negligible, the transmittivity (as function of the incident frequency δ_L) shows two closely spaced poles at:

$$\delta_{1,2} = \left[\frac{\delta_M}{2} \pm \left(\frac{\delta_M^2}{4} + \Omega^2\right)^{1/2}\right]; \tag{3.15}$$

with oscillator strengths given by:

$$f_1 = \frac{\delta_1 - \delta_M}{\delta_1 - \delta_2} \tag{3.16}$$

$$f_2 = \frac{\delta_2 - \delta_M}{\delta_2 - \delta_1}; \tag{3.17}$$

the total strength $f_1 + f_2$ being constant and equal to 1.

These results are easily interpreted in the two-level system framework as a nonlinear Rabi splitting of two quasi-resonant states, detuned of $2\delta_M$ and coupled to each other through the intensity dependent Ω term.[85] We refer to it as *two-photon* Rabi splitting because it is due to the cubic interaction term $\hbar\beta\hat{b}_2^\dagger\hat{b}_1^2 + \text{h.c.}$. At linear regime, i.e. when the coupling is vanishing, one eigenstate corresponds to a pair of photons in the fundamental mode and the other to a single boson on the harmonic mode; clearly only the former is *bright* in a transmission experiment at low intensity. At higher intensities, when the nonlinear interaction begins to be important, the modes are mixed up and the bright component is redistributed among them. Thanks to such a redistribution, the spectrum start to show a pair of peaks:

the stronger one is initially at ω_1, while the weaker one appears at $\omega_2/2$ (the factor $1/2$ accounts for the fact that *two* fundamental bosons must be destroyed to create an harmonic one). For growing coupling Ω their mutual interaction make them repel in energy and equalize in strength; at very high intensities, the detuning δ_M becomes small as compared with the coupling Ω and thus we have a doublet of equally strong peaks with a splitting equal to 2Ω (we can neglect δ_M in eq.(3.15)). When $\delta_M = 0$ the poles are equally bright at any intensity, since the resonance condition guarantees an equal distribution of the bright component. Moreover the two peaks are symmetrically placed with respect to $\omega_1 = \omega_2/2$ with a splitting equal to 2Ω.

From the structure of eq.(3.14), in analogy with the discussion following eq.(1.20), we could expect for $\gamma_2 \ll \gamma_1$ the appearance of the peculiar spectral features given by quantum coherence effects. Unfortunately, as we can see in fig.3.1, this is not the case because they generally lye inside the instability regions and thus are not experimentally accessible in a cw experiment.

So far, we have discussed the behavior of the transmittivity spectra as they depend on the intensity parameter Ω: in physical terms this means that we have studied the behavior of the transmittivity at a fixed value of the transmitted intensity. From an experimental point of view, however, we would rather be interested in spectra at constant incident intensity whose calculation requires an inversion of the functional relation between the incident intensity and the transmitted intensity. The curves of fig.3.1 and 3.2 have been plotted after performing such an inversion, the sawtooth appearance of the instability being due to finite numerical resolution.

3.2.2 Comparison with another quadratically nonlinear system.

The equations 3.6 and 3.7, which describe the time-evolution of our system, are very similar to the ones describing spatial propagation of a monochromatic wave through a second harmonic generating medium when the undepleted pump approximation is not made. If we denote E_ω and $E_{2\omega}$ the slowly varying field amplitudes respectively of the fundamental and the harmonic field, n_ω and $n_{2\omega}$ the refraction indices and Δk the wave vector mismatch $2k_\omega - k_{2\omega}$ and we switch to the new variable $\hat{E}_{2\omega} = \frac{1}{\sqrt{2}} E_{2\omega}\, e^{-i\,\Delta k\, z}$, the propagation equations in the so-called slowly

varying envelope approximation (SVEA) have the form:[6]

$$\frac{\partial}{\partial z}E_\omega = \frac{i\omega\sqrt{2}}{2n_\omega c}\left[\chi^{(2)}\left(-2\omega;\omega,\omega\right)E_\omega^*\hat{E}_{2\omega}\right] - \gamma_1 E_\omega \tag{3.18}$$

$$\frac{\partial}{\partial z}\hat{E}_{2\omega} = \frac{i\omega\sqrt{2}}{2n_{2\omega}c}\left[\frac{1}{2}\chi^{(2)}\left(-2\omega;\omega,\omega\right)E_\omega^2\right] - i\,\Delta k\,\hat{E}_{2\omega} - \gamma_2\hat{E}_{2\omega} \tag{3.19}$$

which have the same formal structure as equations 3.6 and 3.7, apart from the forcing term E_o; in particular the wave vector mismatch Δk plays the role of the mode detuning $2\delta_M$; for this reason the factor $\left(\delta_L - \delta_M + i\gamma_2/2\right)^{-1}$ above can be considered as a *temporal phase matching* factor: at a given fundamental (internal) intensity, the amplitude of the generated harmonic field is proportional to the inverse of the mismatch, i.e. the coherence time. Of course, despite the mathematical similarity of the equations, the physical informations which have to be extracted is different: in the present case, we are looking for the steady state in the presence of driving terms, while in the case of equations 3.18 and 3.19 the driving term is absent and boundary conditions at the interfaces of the nonlinear slab have to be imposed.

3.3 Two-photon optical Stark effect: probing the dressed system

In the previous section we have described the steady-state response to a monochromatic strong driving and we have focussed on stable equilibria, at the expense of other features, like self-pulsing. The stability of such solutions has been verified checking that all the eigenvalues of the linearized evolution matrix M have negative real part. But the linearized theory can also give a lot of other information on the dynamical behavior of the system when it is illuminated by a strong beam: besides quantum fluctuation effects in the spectra of transmitted and sub/second harmonic light, which have been already studied in detail by Drummond et al.,[81] the linearized evolution can be used to determine the (linear) response of this *dressed* system to weak additional *probe* fields; the response of our system to the probe will in fact be different according to the intensity of the pump beam. Such an analysis is clearly restricted to pump intensities and frequencies which lie inside the stability region. The result we shall obtain are strictly related to Drummond's ones, since the general linear response theory connects the response of a system to its fluctuations (fluctuation-dissipation theorem[90]).

Calling again $\delta\vec{\alpha}$ the displacements of the slowly varying field amplitudes from the steady state (in the absence of the probe) and $\mathbf{M}$ the linearized evolution matrix in the rotating frame (see eq.(3.11) and eq.(3.12)), the equations of motion can be written as

$$\frac{d}{dt}\delta\vec{\alpha} = \mathbf{M}\cdot\delta\vec{\alpha} + \vec{f}(t); \tag{3.20}$$

where the $\vec{f}(t)$ term accounts for the probe field (again in the rotating frame) and corresponds to additional driving terms in eq.(3.6) and eq.(3.7).

The solution of eq.(3.20) is immediately obtained in the most simple case of a monochromatic driving term $\vec{f}(t) = \vec{f}_o e^{-i\omega t}$. Putting $\delta\vec{\alpha}(t) = \delta\vec{\alpha}_o\, e^{-i\omega t}$, it is easy to verify that

$$\delta\vec{\alpha}_o = -\left[\mathbf{M} + i\omega\mathbf{1}\right]^{-1}\cdot\vec{f}_o; \tag{3.21}$$

in this way the eigenvalues of $\mathbf{M}$ get the physical meaning of frequencies of the *dressed* modes of the system as driven by the pump beam: since $\mathbf{M}$ depends on the pump intensity F_o via the fields A_1 and A_2 that the pump generates inside the structure, the energies of the dressed modes and their weights (i.e. their oscillator strengths) will depend on the pump intensity as well. So the spectral features of the response to the probe beam will suffer remarkable qualitative changes when the pump intensity is varied. Without the cubic interaction term $\hbar\beta\,\hat{b}_2^\dagger\hat{b}_1^2 + \text{h.c.}$ in the Hamiltonian, this effect would not be present and the response would be independent of the presence of the pump beam F_o.

Effects of this kind, which involve nonlinear interactions between a strong dressing (pump) beam and a weak probe have been the subject of active study for a couple of decades, but the interest has been for the greatest part focussed on the intrinsic nonlinearities of two or three level atoms. The Mollow triplet of fluorescence[91,92] and the stimulated emission and absorption lineshapes of nearly resonantly driven two level atoms (optical Stark effect, OSE)[93–95] are among the most celebrated examples. Very recently, there has been much interest on excitonic Mollow spectra in semiconductor microcavities: both experimental[96] and theoretical[97] work has been devoted to the observation of changes in the probe absorption spectrum when the exciton is resonantly dressed.

Such an effect stems from the fermionic nature of the electron-hole pair forming the exciton, in the sense that at high excitation densities the exciton can not be considered a true boson anymore.[5,65] In the present work we are considering a somewhat different case: instead of dealing with an intrinsically nonlinear material excitation,

the nonlinearity is now concentrated in the mutual interaction between two rigorously bosonic modes. The predicted effect in the TPA case, in particular, does not require any deviation of the exciton from bosonic behavior,[97] but only the possibility of two photon processes; for this reason it will be called *two photon* optical Stark effect (TPOSE).

A most interesting quantity which can be calculated by means of this linear response theory is the excitonic polarization created in a TPA configuration by a weak probe (test) field at a frequency ω_t close to ω_2: depending on the intensity F_o and the frequency ω_L of the pump, its spectral features can be radically different. For simplicity we shall suppose that the cavity mirrors do not confine light at ω_2, so that the coupling of the exciton to the incident probe beam is not affected by the photonic mode structure of the cavity. An experimental observation of such effects clearly requires some violation of parity selection rules, so as to make the excitonic transition allowed for both one-photon and two-photon absorption: a single quantum well under a strong static electric field perpendicular to the QW layers[98] or an asymmetric quantum well [99–101] structures could be good choices.

In the slow variables, the additional driving term corresponding to the probe has the form:

$$\vec{f}(t) = iF_t \begin{pmatrix} 0 \\ 0 \\ 1 \\ 0 \end{pmatrix} e^{-i(\omega_t - 2\omega_L)t} - iF_t^* \begin{pmatrix} 0 \\ 0 \\ 0 \\ 1 \end{pmatrix} e^{i(\omega_t - 2\omega_L)t}; \tag{3.22}$$

we have set $F_t = k_t E_t$ where E_t is the amplitude of the probe beam and k_t is a coupling coefficient proportional to the dipole matrix element of the one-photon transition. In the following we shall also use the reduced probe frequency defined as $\delta_t = \omega_t - 2\omega_L$. The polarization of the system is determined by the third element of the response δa_2. Since the additional driving term contains two different frequencies $\pm\delta_t$, the response of the system will also have two spectral components

$$\delta\vec{\alpha}(t) = \delta\vec{\alpha}^{(+)}e^{-i\delta_t t} + \delta\vec{\alpha}^{(-)}e^{+i\delta_t t} \tag{3.23}$$

which result in an actual excitonic polarization oscillating at both ω_t and $4\omega_L - \omega_t$

$$\begin{aligned} P_{exc}(t) &= \left\{\delta a_2^{(+)}e^{-i\delta_t t} + \delta a_2^{(-)}e^{i\delta_t t}\right\} e^{-2i\omega_L t} + \text{h.c.} \\ &= \left\{\delta a_2^{(+)}e^{-i\omega_t t} + \delta a_2^{(-)}e^{-i(4\omega_L - \omega_t)t}\right\} + \text{h.c.}. \end{aligned} \tag{3.24}$$

The first term derives from the linear polarization of the (dressed) system and has the same frequency ω_t as the forcing field; the second term instead describes a polarization at a frequency which is symmetrical of ω_t with respect to the oscillation frequency $2\omega_L$ of the dressing field A_2. This last term, which is present in atomic systems as well, arises from nonlinear wave-mixing effects of the (weak) probe with the (strong) pump beam.

The expression eq.(3.24) for the polarization can be rearranged as

$$P_{exc}(t) = e^{-i\omega_t t}\left\{\delta a_2^{(+)} + \delta a_2^{(-)} e^{2i\delta_t t}\right\} + \text{h.c.}; \tag{3.25}$$

physically this means that the resulting polarization can be seen as an oscillating polarization at ω_t amplitude-modulated at δ_t. Since the modulation frequency δ_t is generally rather high, the most relevant quantity is the *mean* absorption suffered by the probe beam, and then only the first term in brackets $\delta a_2^{(+)}$ must be retained. The susceptibility is then given by $\chi_{exc} \propto \delta a_2^{(+)}/E_t$ and probe absorption is proportional to its imaginary part.

Its most peculiar physical features can be predicted in a rather simple way by looking at the explicit form of the equation of motion for the actual (not the slowly varying) displacements of the fields from equilibrium δb_1, δb_1^*, δb_2, and δb_2^* (cfr.eq.(3.4) and eq.(3.5))

$$\begin{aligned}
\delta\dot{b}_1 &= -i\omega_1\delta b_1 - \gamma_1\delta b_1 - 2i\beta^* A_1^* e^{i\omega_L t}\delta b_2 - 2i\beta^* A_2 e^{-2i\omega_L t}\delta b_1^* && (3.26)\\
\delta\dot{b}_2 &= -i\omega_2\delta b_2 - \gamma_2\delta b_2 - 2i\beta A_1 e^{-i\omega_L t}\delta b_1 + iF_t e^{-i\omega_t t} && (3.27)\\
\delta\dot{b}_1^* &= i\omega_1\delta b_1^* - \gamma_1\delta b_1^* + 2i\beta A_1 e^{-i\omega_L t}\delta b_2^* + 2i\beta A_2^* e^{2i\omega_L t}\delta b_1 && (3.28)\\
\delta\dot{b}_2^* &= i\omega_2\delta b_2^* - \gamma_2\delta b_2^* + 2i\beta A_1^* e^{i\omega_L t}\delta b_1^* - iF_t^* e^{i\omega_t t}; && (3.29)
\end{aligned}$$

two different sorts of time-dependent coupling terms are present: the first one, whose intensity is proportional to $\Omega = |\beta A_1|$, connects the δb_1 and δb_2 fields to each other; the other one, whose intensity is instead proportional to $|\beta A_2|$ and thus to Ω^2, connects the δb_1 field to its complex conjugate δb_1^*.

For moderate pump intensities only the former one will be important and thus the pair of fields $\delta a_{1,2}$ will be decoupled from the complex conjugate fields $\delta a_{1,2}^*$. From the numerical calculations, it results that the fields and their conjugates are effectively decoupled only for pump intensities below the instability regions. If we neglect the latter coupling (i.e. the one $\propto |\beta A_2|$), the system can be described as a pair of linearly coupled oscillators at ω_1 and ω_2 with a time-dependent coupling term

$-2i\beta A_1 e^{-i\omega_L t}$; by setting $\delta\tilde{b}_1 = e^{-i\omega_L t}\delta b_1$, the time-dependence of the coupling term can be eliminated: in this way the equations of motion eq.(3.26) and eq.(3.27) can be simply rewritten as

$$\dot{\delta\tilde{b}_1} = -i(\omega_1+\omega_L)\delta\tilde{b}_1 - \gamma_1\delta\tilde{b}_1 - 2i\beta^* A_1^*\delta b_2 \quad (3.30)$$

$$\delta\dot{b}_2 = -i\omega_2\delta b_2 - \gamma_2\delta b_2 - 2i\beta A_1\delta\tilde{b}_1 + iF_t e^{-i\omega_t t}. \quad (3.31)$$

The eigenmodes of this system depend on the bare frequencies $\omega_1+\omega_L$ and ω_2 and the coupling $-2i\beta A_1$ in the usual way for a two-level system: a pair of modes at frequencies ω_α and ω_β which start respectively at $\omega_1+\omega_L$ and ω_2 and tend to mix and repel as the intensity of the coupling grows up. Since the driving is only on the second mode, at low coupling intensity the brightness is concentrated in this mode, while for growing intensity it tends to redistribute equally among both eigenmodes. The probe absorption spectra will show peaks at the oscillation frequencies of the modes and the intensity of each peak will be proportional to its brightness.

Fig.3.3 and fig.3.4 contain two series of spectra which differ from each other for the choice of detuning parameters δ_L and δ_M: in each series the absorption spectra are plotted as a function of probe frequency at growing dressing intensities A_1 (and hence couplings); the frequency zero has been set at the excitonic frequency ω_2. Consider the first spectrum, reproduced in the upper-left panel of fig.3.3 ($\delta_M/\gamma = -2$ and $\delta_L/\gamma = 8$): at very low dressing intensity (a), we recover the linear spectrum, with a single peak at the frequency of the bare excitonic mode ω_2; at slightly higher intensity (b) a new peak appears at a frequency $\omega_t = \omega_1+\omega_L$ (i.e., $(\omega_t-\omega_2)/\gamma = (\delta_L - 2\delta_M)/\gamma = 12$); as intensity grows up (c,d), the strengths of these two peaks tend to equalize and their energies to repel each other. This is a clear signature of mixing and repelling of two (one dark and one bright) coupled modes in a two-level system.

The physical meaning of the peak at $\omega_1+\omega_L$ instead of $2\omega_1$ can be understood if we think at the nature of the oscillating coupling; this is in fact due to the dressing field $A_1 e^{-i\omega_L t}$ and in quantum terms it converts an exciton in the harmonic (ω_2) mode into a photon in the fundamental (ω_1) mode plus one more photon in the dressing field. Differently from the previously analyzed single beam nonlinear optics, the coupling is now linear in the fields $\delta b_{1,2}$, so that the spectral features do not depend on the intensity of the probe beam, provided this is weak enough not to perturb appreciably the system. This is again due to the fact we are not dealing anymore with the conversion of one harmonic boson in two fundamental ones, as we were

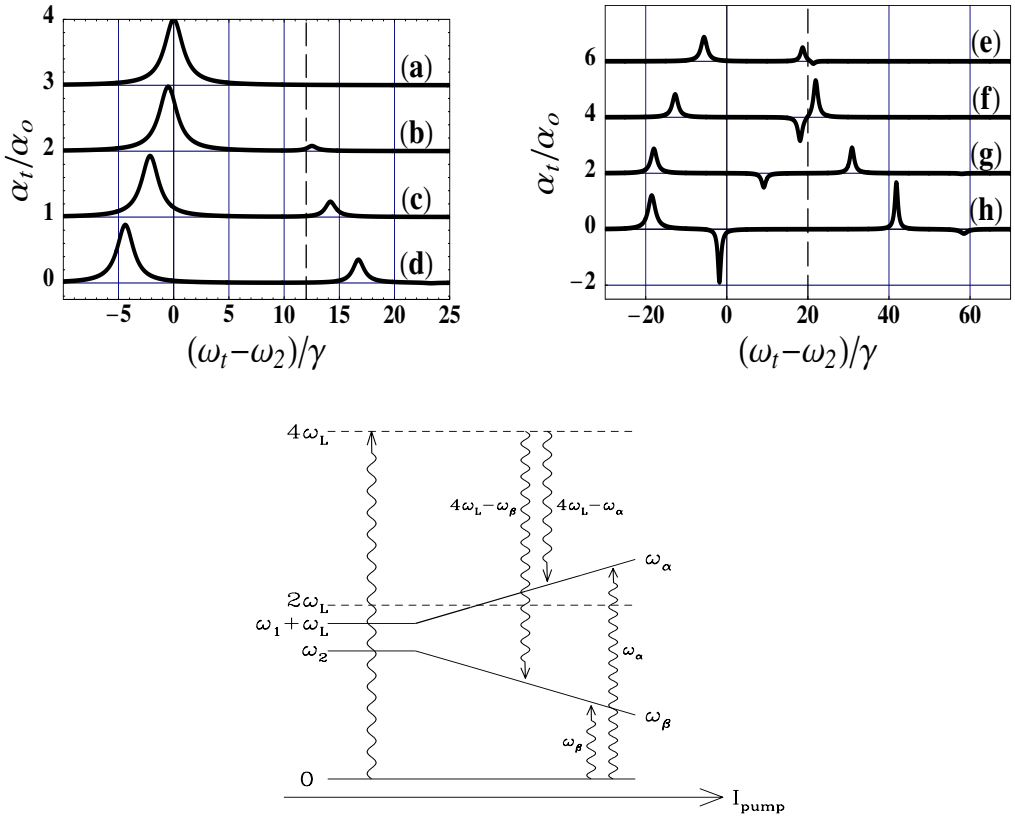

FIGURE 3.3: In the two upper frames, probe absorption spectra at different dressing intensities. Absorption has been normalized to the bare exciton absorption. Dressing intensity grows from (a) to (h); instabilities are between (e) and (f) and above (h). Notice the change of frequency scale. Non-resonant case $\omega_1 + \omega_L - \omega_2 = 12\gamma$, $2\omega_L - \omega_2 = 20\gamma$: $\delta_M/\gamma = -2$, $\delta_L/\gamma = 8$. In the lower frame, schematic plot of the energy levels involved in the optical processes: the frequencies ω_α and ω_β of the dressed states shift with increasing pump intensity.

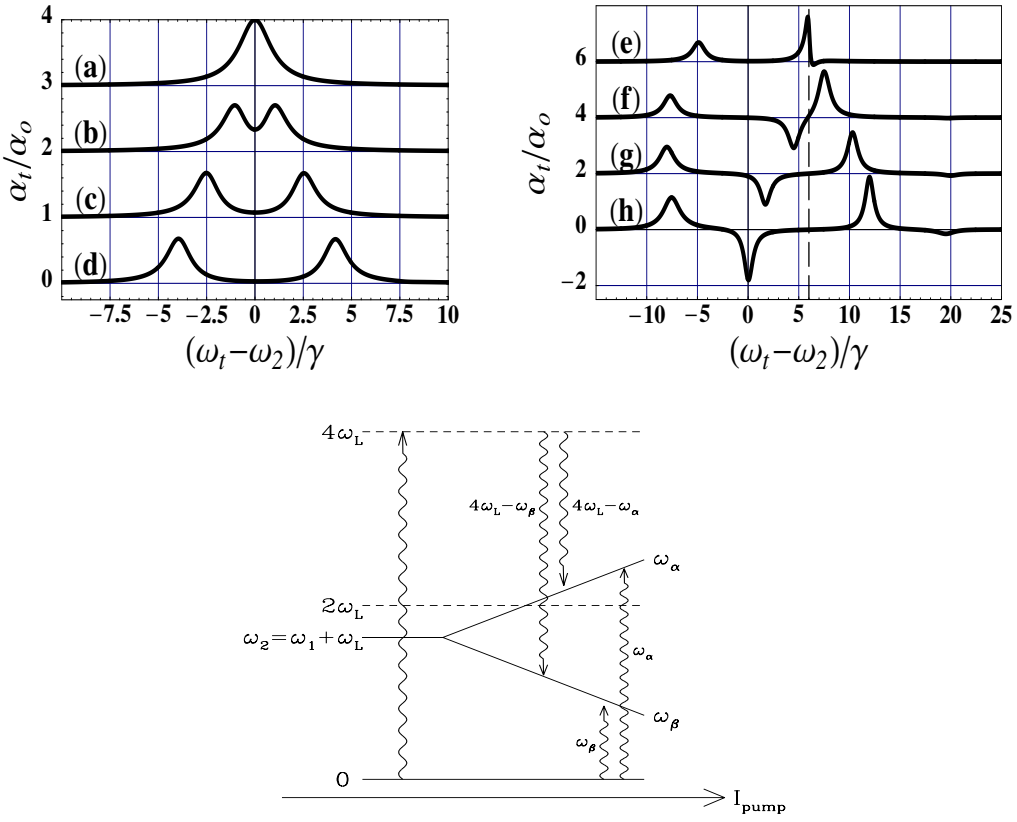

FIGURE 3.4: In the two upper frames, probe absorption spectra at different dressing intensities. Absorption has been normalized to the bare exciton absorption. Dressing intensity grows from (a) to (h); instabilities are between (e) and (f) and above (h). Notice the change of frequency scale. Resonant case $\omega_1+\omega_L=\omega_2$, $2\omega_L-\omega_2=6\gamma$: $\delta_M/\gamma=3$, $\delta_L/\gamma=6$. In the lower frame, schematic plot of the energy levels involved in the optical processes: the frequencies ω_α and ω_β of the dressed states shift with increasing pump intensity.

doing in the one-beam case, but with a conversion of a harmonic exciton into a single fundamental photon plus a dressing A_1 photon (ω_L).

Analogous considerations can be repeated in order to explain the structure of the spectrum reproduced in the upper-left panel of fig.3.4 ($\delta_L/\gamma = 6$ and $\delta_M/\gamma = 3$), though the resonance condition $\omega_2 = \omega_1 + \omega_L$ makes the spectra look somewhat different: the bare modes at ω_2 and $\omega_1 + \omega_L$ are in fact resonant and hence the coupling does not introduce a new peak, but only split the existing one in a symmetric doublet of peaks. This is still centered at $\delta_t = 0$ and its spacing grows with growing dressing field intensity.

As it can be observed in the upper-right panels of fig.3.3 and fig.3.4, at higher pump intensities the $-2i\beta^* A_2 e^{-2i\omega_L t}$ coupling terms start to be relevant as well. In particular, its effect begins to be dramatic when one of the absorption peaks (the upper one at ω_α, in our specific cases) is close to $2\omega_L$ (i.e. $\omega_t - \omega_2 = 2\delta_L - 2\delta_M$), frequency at which it resonates. This is verified when the dressing intensity is close to the lower edge of the bistability unstable region. In this case, the peak narrows (the threshold corresponds to the vanishing of the real part of one eigenvalue of M), its shape is modified and some gain (i.e. negative absorption) appears (see spectra (e)) at a frequency just above the resonance frequency $2\omega_L$.

Increasing the dressing intensity above the bistability unstable region, i.e. in the upper branch of the hysteresis curve, the spectra result radically different. The two absorptive peaks are still present at frequencies ω_α and ω_β and keep on repelling themselves as the pump intensity grows up. At the same time, a gain peak is present at a frequency $4\omega_L - \omega_\alpha$, which is the symmetric of the upper absorption peak frequency ω_α with respect to the resonance frequency $2\omega_L$. For growing pump intensity, as the absorption peak frequency ω_α shifts towards higher frequencies because of the coupling term $-2i\beta A_1 e^{-i\omega_L t}$, the gain peak shifts towards lower frequencies in order to satisfy the symmetry condition with respect to $2\omega_L$. Near the threshold of the self-pulsing instability, the other absorptive peak at ω_β begins to have a gain counterpart at $4\omega_L - \omega_\beta$ as well: in fig.3.3 this gain peak is hardly visible near $(\omega_t - \omega_2)/\gamma \simeq 60$, while in fig.3.4 it is located near $(\omega_t - \omega_2)/\gamma \simeq 20$.

Such qualitatively new features, are stable with respect to variations of detunings and linewidths as we have verified; in analogy to the gain appearing in the classical OSE,[1,94,95] a simple physical interpretation can be put forward in terms of stimulated hyper-Raman scattering[102] in a dressed system picture; the main effect of the

$-2i\beta^* A_2 e^{-2i\omega_L t}$ coupling term is in fact to induce conversion of a few quanta of the dressing fields A_1 and A_2 (for a total frequency $4\omega_L$) into a dressed excitation (at ω_α or ω_β) plus one more photon in the probe beam (at ω_t), which thus results amplified. Indeed, for such a process, energy conservation imposes that $\omega_t = 4\omega_L - \omega_{\alpha,\beta}$: in this way it is possible to explain the symmetry condition empirically found in the calculated spectra.

In order to understand why the hyper-Raman process takes place involving the $4\omega_L$ frequency, it is useful to reformulate the dynamics of the dressed system in the usual Hamiltonian formalism of quantum optics; in terms of the field displacements δb_1 and δb_2, the effective Hamiltonian of the (dressed) system can be written as

$$\begin{aligned}\mathcal{H}_d &= \hbar\omega_1\,\delta\hat{b}_1^\dagger\delta\hat{b}_1 + \hbar\omega_2\,\delta\hat{b}_2^\dagger\delta\hat{b}_2 + 2\hbar\beta\,A_1 e^{-i\omega_L t}\delta\hat{b}_2^\dagger\delta\hat{b}_1 + 2\hbar\beta^*\,A_1^* e^{i\omega_L t}\delta\hat{b}_1^\dagger\delta\hat{b}_2 + \\ &+ \hbar\beta^*\,A_2 e^{-2i\omega_L t}\delta\hat{b}_1^{\dagger 2} + \hbar\beta\,A_2^* e^{2i\omega_L t}\delta\hat{b}_1^2 + \hbar k_t E_t e^{-i\omega_t t}\delta\hat{b}_2^\dagger + \hbar k_t^* E_t^* e^{i\omega_t t}\delta\hat{b}_2.\end{aligned} \tag{3.32}$$

If we neglect for the moment the last two terms, we are left with two bosonic modes, linearly coupled to each other; this approximation is valid at low pump intensity, i.e. when the A_1 coupling is much greater than the A_2 coupling. As previously described, the probe absorption spectra are in this case characterized by a pair of absorptive peaks corresponding to the dressed modes at ω_α and ω_β, which result from diagonalization of the Hamiltonian.

The appearance of gain at higher pump intensities is due to the terms proportional to $\delta\hat{b}_1^2$ and $\delta\hat{b}_1^{\dagger 2}$, which allow for the conversion of one harmonic dressing exciton A_2 at $2\omega_L$ into a pair of quanta of the fundamental mode $\delta b_1'$ and $\delta b_1''$ of frequencies respectively equal to ω_1' and ω_1''. One of these quanta then merges with a A_1 dressing photon at ω_L into an excitation at ω_α or ω_β which is left inside the system; the other one, together with a A_1 dressing photon, is instead converted into an additional photon in the probe beam at ω_t. In conclusion, two A_1 dressing photons and one A_2 dressing exciton (for a total frequency equal to $4\omega_L$) are converted into a dressed excitation at ω_α or ω_β, plus a probe beam photon at ω_t: this kind of optical process, in which some quanta of a strong pump beam are scattered into an excitation of the material system plus an escaping photon, is called *hyper-Raman scattering*;[6] furthermore, since the emission of the escaping photon is stimulated by the probe beam, we shall say it is a *stimulated* hyper-Raman scattering.

As a final remark, it is interesting to notice that the sum rules demonstrated at all orders of perturbation theory in[103,104] are well verified even by our model, which

allows for non-perturbative nonlinear optical effects, like optical bistability and optical self-pulsing; in particular the absorption sum rule, which states that the integral of the probe absorption coefficient over all frequency is independent of pump intensity, has been numerically verified in the stability regions. According to this sum rule the appearance of gain in some spectral region must compensates for an increased absorption in other spectral regions.

3.4 Discussion of material and geometrical parameters

Until now we have not paid attention to the absolute value of the nonlinear coupling β; all the effects described in the previous sections depend only on the product $\Omega = |\beta A_1|$. Indeed it seems theoretically possible to compensate for a small β by the use of high intensities; however very high light intensities are not handy because of high heat production inside the structure and the possibility of other competing nonlinear effects. A high β would thus allow for the observation of our specific two-photon processes at intensities at which other processes, like non-resonant Kerr nonlinearities, exciton bleaching or higher harmonic generation are negligible; furthermore, if β is large enough for nonlinear effects to be important with just a few excitation quanta in the modes, quantum fluctuations give important corrections to the present mean-field results and peculiar quantum coherence effects can be observed.

An explicit calculation of the parameter β can be performed starting from the usual optical constants of the materials forming the structure; as we have already pointed out, in the SHG configuration β is related to the $\chi^{(2)}$ susceptibility of the materials, while in the TPA case it depends on the generalized oscillator strength of the two-photon absorptive transition, or, in other words, on the resonant part of the $\chi^{(3)}$ susceptibility. In the following, we limit our attention to planar structures, in which all the equations reduce to one-dimensional ones; the general case does not introduce in principle new different features, apart from the geometrical complications due to the vectorial character of the fields and the tensorial character of the susceptibilities.

If we expand the electromagnetic field in eigenvectors of the wave equation in a

linear refractive background medium of dielectric constant $\epsilon(x)$

$$E(x,t) = \sum_i \left\{ \mathcal{E}_i(x) e^{-i\omega_i t} a_i(t) + \mathcal{E}_i^*(x) e^{i\omega_i t} a_i^\dagger(t) \right\} \tag{3.33}$$

and we perform the so-called SVEA approximation (sec.1.5.2), which correspond to supposing the temporal variation of the mode amplitudes to be much slower than the oscillation frequency, we get to the explicit expression for the coupling constant β in the SHG case:[89]

$$\beta_{SHG} = -\frac{1}{\hbar} \int \mathcal{E}_2(x)^* \chi^{(2)}(x) \mathcal{E}_1(x)^2 \, dx. \tag{3.34}$$

The physical interpretation of such an expression is evident: it is the overlap integral of the square of the fundamental wavefunction with the harmonic wavefunction weighted by the $\chi^{(2)}$ nonlinear susceptibility of the material; in a quantum field theoretical language, this expression corresponds to the matrix element of a three-photon vertex in which two fundamental photons annihilate into a harmonic photon. Since we are dealing with planar structures, the wavefunction normalization has been chosen to be the natural one-dimensional one, i.e.

$$\int \frac{\epsilon(x)}{2\pi} \mathcal{E}_i(x)^* \mathcal{E}_j(x) \, dx = \delta_{i,j} \hbar \omega_i; \tag{3.35}$$

in this way the mode intensities $|b_i|^2$ have the meaning of mean photon density per unit surface. From this choice it follows that the photonic wavefunction has the dimensions of an electric field times a length while β is the product of a frequency times a length. From eq.(3.34) it is evident how the arbitrariness in the definition of the global phase of the wavefunctions reflects on the nonlinear coupling β (and analogously on the external couplings $k_{1,2}$): a change in the phase definition of the wavefunctions must in fact correspond to a change in the system parameters in a way to leave the Hamiltonian invariant.

In the presence of an isolated two-photon absorption transition, the $\chi^{(3)}$ susceptibility can be written as[6]

$$\chi^{(3)}\left(-\omega;\omega,-\omega,\omega\right) = \frac{f^{(3)}}{\hbar\left(\omega_2 - 2\omega - i\gamma_2\right)}; \tag{3.36}$$

because of its similarity with the well known oscillator strength of a linear transition, the quantity $f^{(3)}$ can be called generalized oscillator strength of a (two-photon) transition. The nonlinear excitonic polarization can be written as

$$P_{NL}(x,t) = 3 e^{-i\omega_L t} \chi^{(3)}(x) \left|\mathcal{E}_1(x)\right|^2 \mathcal{E}_1(x) \left|a_1\right|^2 a_1. \tag{3.37}$$

Inserting this result in Maxwell's equations and performing the SVEA approximation as previously, we get to a motion equation for the field amplitude of the form

$$\frac{\partial a_1}{\partial t} = -\gamma_1 a_1 - iF_o e^{-i(\omega_L - \omega_1)} + i\frac{3\left|a_1\right|^2 a_1}{\hbar^2\left(\omega_{exc} - 2\omega_L - i\gamma_{exc}\right)} \int \left|\mathcal{E}_1(x)\right|^4 f^{(3)}(x)\, dx. \quad (3.38)$$

Comparing these term with the analogous equation that can be derived from our Hamiltonian formalism:

$$\frac{\partial a_1}{\partial t} = -\gamma_1 a_1 - iF_o e^{-i(\omega_L - \omega_1)} + i\frac{2\left|\beta\right|^2}{\omega_2 - 2\omega_L - i\gamma_2} \left|a_1\right|^2 a_1 \quad (3.39)$$

we get to the final result:

$$\left|\beta_{TPA}\right|^2 = \frac{3}{2\hbar^2} \int \left|\mathcal{E}_1(x)\right|^4 f^{(3)}(x)\, dx; \quad (3.40)$$

the phase of β, which is still undetermined, is not physically important, since it determines only the relative phase of the fundamental and harmonic fields (see e.g. eq.(3.9)); when we are driving the system on both modes, the phase of β fixes the phase of the amplitude oscillations in the excitonic polarization eq.(3.25). The physical meaning of the remaining indetermination in the absolute phase of β_{TPA} depends on the fact that we have used as input only the oscillator strength of the two-photon transition, which correspond to the square modulus of the effective matrix element; since the absolute phase of an excitonic field is generally not observed, such an indeterminacy does not have physical consequences (sec.1.5.2). The proportionality of the coupling β to the square root of the generalized oscillator strength is analogous to the classical vacuum Rabi splitting, in which the Rabi frequency is proportional to the square root of the density of resonant atoms or quantum wells.[48]

After having determined the general expressions for the coupling constant β in both SHG and TPA cases, it can be interesting to compute quantitatively the magnitude of the predicted effect in a couple of specific experimental arrangements. We shall concentrate our attention on the nonlinear Rabi frequency $\Omega = |\beta B_1|$ as function of the internal intensity on the fundamental mode. For a simple metallic planar cavity of length L and dielectric constant ϵ, the wavefunction of a photonic mode is given by the expression

$$\mathcal{E}_j = \sqrt{\frac{4\pi\hbar\omega_j}{L\epsilon}} \sin k_j x \quad (3.41)$$

with

$$k_j = \frac{\pi j}{L} \quad (3.42)$$

and the internal light intensity in each propagation direction can be written as:

$$I_{int} = \frac{c\sqrt{\epsilon}}{4\pi} |\mathcal{E}_1 b_1|^2 = \frac{\hbar\omega_1 c}{L\sqrt{\epsilon}} |A_1|^2 , \tag{3.43}$$

where $\mathcal{E}_1$ has been taken at an antinode of the cavity mode. It is important to remember that, since we are working close to resonance, the internal intensity can be several orders of magnitude higher than the incident one, the proportionality constant between the two being as large as the Q factor of the cavity.[105]

According to the considerations worked out by Berger,[27] second harmonic generation in a metallic mirror microcavity is most effective when the cavity length L equals the second harmonic generation coherence length L_{coh} of the nonlinear material; for GaAs at the technologically useful wavelength of 10.6μm the coherence length amounts to 108μm. In this specific geometrical arrangement, explicit integration of eq.(3.34) brings to the result:

$$\beta_{SHG} = 4\chi^{(2)} \sqrt{\frac{2\pi\hbar\omega_1}{L\epsilon^3}} \omega_1. \tag{3.44}$$

Using eq.(3.43) and eq.(3.41), the nonlinear Rabi frequency $\Omega = |\beta A_1|$ can be written in terms of the internal light intensity I_{int} as:

$$\frac{\Omega}{\omega_1} = 4\sqrt{\frac{2\pi I_{int}}{\epsilon^{5/2} c}} \chi^{(2)}. \tag{3.45}$$

The experimental value of $\chi^{(2)}$ for GaAs at 10.6μm is about $2.4 \cdot 10^{-7}$esu.[88,106] So, in order to observe the splitting in the case the cavity Q-factor is 10^4, it is necessary to have Ω/ω_1 at least equal to 10^{-4}; this is satisfied provided the internal power is about $1\,\mathrm{GW\,cm^{-2}}$. As long as the nonlinear material fills the entire cavity, a change in the cavity length does not affect β; to increase β we thus have to increase $\chi^{(2)}$ shifting the operating frequency closer to the gap edge or changing the nonlinear medium.

The validity of the present calculation is in any case limited to case of well-localized modes inside the cavity; the case of a dielectric microcavity with DBR mirrors optimized for reflection at both the fundamental and at the harmonic frequency (FASH mirrors[27]) would give much more freedom in the choice of the reflection phase at the two mirrors, but at the same time the optical modes would penetrate inside the mirrors and an active material concentrated in the cavity layer would not be the

best alternative any more; in this case it may be better to distribute the nonlinearity along the whole structure. Although such an arrangement has revealed to be useful for optical bistability and optical "transistor" effect (sec.2.3-2.6 and ref. 64,70,75), it has not been studied yet for optimizing second harmonic generation.

Two-photon absorption spectroscopy has been an important tool for the characterization of electron-hole states in quantum wells: the two-photon absorption spectra taken at $\omega \simeq E_G/2$ show in fact sharp features due to subband quantization and excitonic effects.[107–109] In particular it has been possible to clearly resolve some excitonic peaks. Provided their linewidth is sufficiently small, these transitions seems to be a good candidate for the observation of our coherent two-photon effects.

Since the sharpest features are present in TM polarization ($\hat{\epsilon} \parallel \hat{z}$), it can be favorable to work at oblique incidence. This is not a problem, indeed it gives the possibility of tuning the photonic fundamental mode with the angle, while the excitonic frequency stays nearly constant. A detailed calculation of the two-photon absorption cross-section in GaAs/AlGaAs heterostructures has been performed by Shimizu.[98] For example, conversion of his results for the $c_1lh_2, 1S$ exciton into generalized oscillator strengths brings to the result of about $f_{2D}^{(3)} \simeq 2 \cdot 10^{-29}\,\mathrm{cm}^4$. It can be interesting to notice that, if we assume a linewidth of 1 meV for the exciton and a well spacing of 10nm, this value corresponds to a resonant $\chi^{(3)}$ of $1.2 \cdot 10^{-8}$esu.

Moreover, under a strong static electric field parallel to the growth axis, some excitonic transitions can be allowed for both one- and two-photon absorption because of parity symmetry breaking.[98] But an externally applied static electric field is not the only solution: several papers have appeared which investigate the problem of breaking the symmetry of a material system in order to make some optical susceptibility non-vanishing. In particular, asymmetrically grown quantum wells[99,100] and indirect excitons in polytype double-quantum-well structures[101] have recently received much interest.

Let's consider a microcavity of length L and dielectric constant ϵ bounded by metallic mirrors and containing N_w identical quantum wells situated at positions $x_{1\ldots N_w}$ all corresponding to antinodes of the electric field; in this case the generalized oscillator strength $f^{(3)}(x)$ is given by

$$f^{(3)}(x) = \sum_{i=1} N_w f_{2D}^{(3)} \delta(x - x_i) \tag{3.46}$$

Explicit integration of eq.(3.40) then brings to the result:

$$\beta_{TPA} = \frac{\pi\omega_1}{L\epsilon}\sqrt{24 f_{2D}^{(3)} N_w}. \tag{3.47}$$

Using again eq.(3.43) and eq.(3.41), the Rabi frequency can be written as function of internal light intensity I_{int} as:

$$\frac{\Omega}{\omega_1} = \sqrt{\frac{24 f_{2D}^{(3)} N_w \pi^2 I_{int}}{L\epsilon^{3/2}\hbar\omega_1 c}} \tag{3.48}$$

As previously, let's quantify the effect in terms of the internal intensity needed in order to have $\Omega/\omega_1 = 10^{-3}$. Inserting the numerical values for the quantum well excitonic transition and supposing the cavity to be a $\lambda/2$ cavity containing about 10 quantum wells, we obtain an internal intensity of about $600\,\mathrm{MW\,cm^{-2}}$.

While in the SHG case the main limitation on light intensity comes from unavoidable heating effects, in the TPA case it is necessary to pay attention also to the fact that excitons behave in a bosonic way only at low densities $n_{exc} \ll n_{sat}$, i.e. when their mean spacing is much larger than their radius. As we have already discussed in sec.2.4, at higher densities, both screening effects and the fermionic nature of the underlying electrons and holes contribute to bleach the excitonic transition. Remembering that the total population of excitons per unit area is given by $|A_2|^2$ and assuming the excitons are equally distributed among the wells, it follows from eq.(3.9) that the excitonic density in each well has the expression

$$n_{exc} = |A_2|^2 / N_w = \left|\frac{\Omega^2}{2\omega_L - \omega_2 + i\gamma_2}\right|^2 \frac{1}{N_w |\beta|^2}; \tag{3.49}$$

inserting in this expression a realistic value for β in GaAs structures, it results that the two-photon Rabi splitting should be observable in GaAs structures before the exciton is bleached, while for the instabilities and the TPOSE gain the required excitonic density seems much higher than the typical saturation density of about $n_{sat} = 3 \cdot 10^{11}\mathrm{cm^{-2}}$. However, an increased value of the nonlinear coupling β and of the number of wells N_w should allow for the same nonlinear effects at a lower excitonic density.

Conclusions and perspectives

This first part of the thesis has been devoted to the study of a few interesting nonlinear optical effects which can be observed in semiconductor DBR microcavities; after a short review on their most important properties at linear regime (chap.1), we have discussed the behavior of microcavities grown with materials showing an intensity-dependent refractive index (chap.2). Depending on the geometrical and the material properties of the system, as well as on the operating frequency, both optical limiting and optical bistability have been predicted to occur for reasonable values of the light intensity. With an eye to applications, we have briefly discussed how such effects can be eventually exploited for an all-optical processing of signals: specific configurations which may result useful for either the amplification of an optical signal (optical transistor) or the realization of an all-optical bit of memory have been pointed out.[64,70,75]

In the last chapter (chap.3) we have given a detailed analysis of resonant two-photon nonlinear processes such as second harmonic generation and two-photon absorption and, in particular, we have discussed their signatures in the single-beam transmission spectrum through the microcavity as well as in two-beam pump-and-probe experiments.[76,77] Although the calculations have been performed using a very simple model which involves only two bosonic modes nonlinearly coupled by a cubic term, we have shown how this approach can be applied to describe any experimental arrangement: all the relevant details of the actual configuration are in fact summarized in a small number of parameters.

Since the nonlinear optical susceptibility of current materials is in general very weak, a large number of photons is generally required in the cavity mode in order for nonlinear effects to be important; for the single-mode nonlinear cavity of sec.2.2, the critical number $N_o = \gamma_{ph}/\omega_{nl}$ is a good estimate of this quantity, since it gives the number of photons which have to be present in the cavity mode in order

for the nonlinear shift to be equal to γ_{ph} and therefore for the transmission to be substantially modified.

Starting from such a consideration, it has been natural to perform the calculations neglecting the discrete, quantum, nature of the field and apply classical electrodynamics in continuous media with a nonlinear polarizability; with respect to the operator-valued quantum master equation which is required for the description of a quantum field, classical electrodynamics leads to much simpler and physically transparent calculations. The use of classical electrodynamics can be justified as arising from a mean-field (MF) approximation on the light field: the field operators are replaced by their mean values and all their products are assumed to factorize; this is equivalent to neglecting all fluctuations around the mean values of the fields, which is generally true provided the population of the modes under examination is very large.

Although conventional semiconductor DBR microcavities are well within such a $N_o \gg 1$ regime, the recent developments of photonic cavities with very large Q-factors and very small mode volumes and of optical materials with very strong nonlinearities has pushed the optical community towards the study of systems in which the critical number $N_o \leq 1$ and therefore the nonlinear effects are triggered by a very small number of photons. In such systems, in fact, the quantum state of the light field can be manipulated down to the single quantum level and definitely nonclassical states can be generated.

As we shall discuss in detail in chap.4, the light field in a nonlinear material and the interacting atomic Bose gas can be both described as a Bose field with a quartic interaction term in the Hamiltonian; despite the profound physical differences between the two systems, analogous results have therefore to hold for the transmission of such Bose waves through single-mode cavities. In the case of atomic matter waves, single-mode DBR cavities showing well separated cavity modes with narrow linewidths and tight longitudinal confinement can be obtained using optical lattices (chap.5). Thanks to the very strong intensity of collisional atom-atom interactions, very low values of the incident atomic flux are required for the observation of nonlinear atom optical effects. Provided transverse motion is appropriately frozen by a single mode waveguide, the nonlinear coupling coefficient $\omega_{\rm nl}$ of the cavity resonance can be comparable or even larger than the mode linewidth γ.

Given the strict analogy of the behavior of light and matter waves, we shall post-

pone to the third part of the thesis the detailed discussion of the validity range of the mean-field approximation and the nonclassical effects that can be observed when this approximation breaks down; the same physical model can in fact be successfully applied to both Bose fields, irrespective of their profoundly different physical nature. Thanks to its formal simplicity, the single mode system of sec.2.2 is well suited for a direct numerical integration of the quantum master equation (chap.6). For the case of a weak nonlinearity $N_o \gg 1$, the mean-field results will be recovered; for the case of a strong nonlinearity $N_o \leq 1$, peculiar quantum features will be found in the correlation functions of the transmitted beam.

Part II

Atom optics

Introduction

In the last years, several authors have emphasized the close analogy between the recent developments in the field of coherent atom optics and the fundamental steps of nonlinear and quantum optics following the realization in the late fifties of the first optical *lasers*. The coherence properties of atomic *Bose-Einstein condensates* (BECs) are in fact very similar to the coherence properties of laser light: both of them are in fact well described by *classical* C-number fields and fluctuations can in most cases be neglected; in the case of light, the field under examination is the electromagnetic field, while in the atomic case it is a Schrödinger matter field.

Since the development of laser cooling techniques, both the luminosity, the monochromaticity and the collimation of atomic beams has been substantially improved in the last decades and most of the fundamental elements of the optical bench are now available for applications, such as atomic beam splitters and diffraction gratings for matter waves; atomic interferometers look in fact very promising as gravitational and inertial sensors. Since all these experiments do not involve atom-atom interactions, they are not sensitive to the higher-order coherence functions of the incident atomic beam and are well observed with thermal atomic beams which are the matter analog of the light emitted by a conventional lamp.

On the other hand, nonlinear atom optics has started to be considered only in the last years, after the realization of atomic BECs and the consequent extraction of coherent matter waves: nonlinear optical effects require in fact a larger luminosity and are sensitive to the coherence of the input beams; for this reason, they could not be easily observed with non-degenerate thermal sources. While temporally finite pulses can be obtained by coherently extracting atoms from a previously formed trapped BEC, a continuous wave source has not been realized yet, although it is actually the subject of active work, the main difficulty obviously consisting in the lack of an efficient refilling mechanism for the parent condensate.

This second part of the thesis is devoted to the study of the atom optical properties of the massive atomic bosonic field; in particular, thanks to the fundamental analogy between light and matter waves, we shall try to export into the realm of atom optics all the concepts we have discussed in the previous part of the thesis for the case of photon optics in dielectric structures such as DBR microcavities.

In the first chap.4, we shall review the main points of the analogy between light and matter waves; in particular, we shall see how each of the terms appearing in the Hamiltonian for the atomic field has a simple physical interpretation in optical terms. The external optical or magnetic potential to which atoms are subjected can be seen as a dielectric constant for matter waves; the atomic spin corresponds to the polarization of an electromagnetic wave; the s-wave atom-atom collisional interactions can be reinterpreted as a local nonlinear intensity-dependent refraction index.

As in the first part of the thesis we have always approximated the electromagnetic field as a classical field, a similar mean-field theory is currently adopted for the description of a coherent atomic field, leading to the well-known Gross-Pitaevskii equation, which gives accurate predictions for the dynamics of dilute Bose condensed clouds at very low temperatures, when the non-condensed fraction can be considered as negligible. After a brief review of the most relevant exact approaches to the complete many-body problem together with their difficulties, the chapter is concluded with a detailed discussion on the main points of mean-field theory, in particular the underlying all-order coherence assumptions, the experimental confirmations and the validity limits.

In the following chap.5, the interaction of atomic waves with optical lattices is discussed and the transmission and reflection properties of an atomic beam characterized in terms of atomic Bloch waves in the nearly periodic potential of the lattice: this periodicity allows in fact for a substantial reduction of the effective atomic mass, while the spatial modulation of the lattice parameters provides the confinement needed for the quantization of atomic motion and the consequent appearance of discrete localized states which are the atomic analog of the optical modes of DBR microcavities. At linear regime, the transmission spectrum of such a system when driven by a coherent atomic beam is characterized by a rather large reflecting window corresponding to the forbidden energy gap of the lattice and sharp peaks corresponding to resonant tunneling processes on the discrete states. Given the rather large mode spacing and the tight confinement of the mode wavefunction, for grow-

ing incident intensities nonlinear effects are expected to give rise to atom optical limiting or atom optical bistability; thanks to the much stronger collisional atom-atom interactions with respect to photon-photon interactions in a nonlinear material, the bistability threshold is predicted to occur at a very low value of the atomic flux.

We conclude the chapter discussing two possible methods for the experimental determination of the coherence length of an actual atom laser source: while the coherence of a trapped BEC is now a well-established fact, a direct measurement of the coherence properties of a propagating beam is not avaiable yet and, in particular, it is still an open question whether the atom laser can have a coherence length longer than the parent condensate. Both the schemes we propose are based of the reflection properties of atomic mirrors; the first one exploits the frequency dependence of the transmittivity of an optical lattice in order to separate the different velocity classes in the beam and thus determine its spectral distribution. The second scheme is based on the diffraction of light on the density profile of the atomic standing wave which is formed in front of a nearly perfect atomic mirror: since the coherence length of the standing wave is related to the coherence length of the atom laser, a measurement of the latter can be performed just by looking at the angular linewidth of the diffraction peaks.

Chapter 4

Atom optics fundamentals from a quantum optics point of view

This chapter is devoted to a brief review of some concepts of atom optics, Bose-Einstein condensation and atom lasers from the point of view of quantum optics; this approach to the properties of ultra-cold Bose gases is complementary to the many-body approach more familiar to condensed matter physicists. The main purpose of the discussion will be to stress the fundamental analogy between the behaviour of light waves in dielectric (eventually nonlinear) media and the behaviour of interacting matter waves in external (optical or magnetic) potentials: the strong cross-fertilization effect which has arisen from such parallelism has in fact helped us to get a deeper as well as more intuitive picture of both systems.

In sec.4.1, the Hamiltonian for an interacting Bose gas subjected to an external potential is introduced and a simple physical interpretation of each term is given from the point of view of optics: the external potential is show to give a sort of refractive index for matter waves, the atomic spin is the analog of the polarization vector and the atom-atom interactions provide the optical nonlinearity for matter waves. This discussion will be completed in sec.4.2 with a review of the different approaches that can be adopted for the solution of the bosonic many-body problem: after some general words on the available exact methods together with their limitations, a specific attention will be paid to the mean-field theory together with the all-order coherence assumptions which underlie it. A more detailed study of the nonclassical effects and the dynamics beyond the mean-field is postponed to chap.6, while the discussion of our stochastic wavefunction approach to the bosonic many-body problem is

the subject of chap.7.

4.1 Field-theoretical approach to atom optics

The Hamiltonian of an interacting Bose gas is usually written in terms of the Bose field operator $\hat{\Psi}(x)$ as:

$$\mathcal{H} = \int dx\, \hat{\Psi}^\dagger(x) \left[-\frac{\hbar^2}{2m}\nabla^2 + V^{\rm ext}(x) \right] \hat{\Psi}(x) + \\ + \frac{1}{2}\int\int dx\, dx'\, \hat{\Psi}^\dagger(x)\hat{\Psi}^\dagger(x') V^{\rm int}(x-x')\hat{\Psi}(x')\hat{\Psi}(x); \quad (4.1)$$

the first two terms describe the single particle dynamics in an external potential $V^{\rm ext}$; the third term accounts for atom-atom interactions, modeled by a two-particle interaction potential $V^{int}(x-x')$. As usual, the field operators are assumed to satisfy the Bose commutation relations $\left[\hat{\Psi}(x), \hat{\Psi}^\dagger(x')\right] = \delta(x-x')$.

Immediate is the generalization to the case of a multicomponent gas, in which atoms in different internal states coexist:

$$\mathcal{H} = \left(-\frac{\hbar^2}{2m}\right) \sum_i \int dx\, \hat{\Psi}_i^\dagger(x)\nabla^2\hat{\Psi}_i(x) + \sum_{i,j}\int dx\, \hat{\Psi}_i^\dagger(x) V_{i,j}^{\rm ext}(x)\hat{\Psi}_j(x) + \\ + \frac{1}{2}\sum_{i,j,k,l}\int\int dx\, dx'\, \hat{\Psi}_i^\dagger(x)\hat{\Psi}_j^\dagger(x') V_{i,j,k,l}^{\rm int}(x-x')\hat{\Psi}_k(x')\hat{\Psi}_l(x); \quad (4.2)$$

the atom field is now described by multicomponent field operators $\hat{\Psi}_i(x)$ satisfying the Bose commutation relations $\left[\hat{\Psi}_i(x), \hat{\Psi}_j^\dagger(x')\right] = \delta(x-x')\delta_{i,j}$. The index i runs over the possible internal states, which can be either different Zeeman sublevels of a single hyperfine level, or sublevels belonging to different hyperfine levels, or even different atomic species.

As a very simple example, a spin $F = 1$ atom is described by a three-component atom field $\hat{\Psi}_i(x)$; in this case, besides the usual angular momentum $m_F = 1, 0, -1$ basis, a Cartesian x, y, z basis can be adopted, in which the three components transform as the three components of a vectorial quantity like the electric or the magnetic field.[110] Atoms with larger values of the spin, are instead described by more complex tensorial quantities: spin $F = 2$ atoms correspond, e.g., to traceless symmetric second-rank tensors.

While the kinetic term generally has a diagonal form[(a)]

$$-\sum_i \frac{\hbar^2}{2m}\hat{\Psi}_i^\dagger(x)\nabla^2\hat{\Psi}_i(x), \tag{4.3}$$

the external potential term

$$\sum_{i,j}\hat{\Psi}_i^\dagger(x)V_{i,j}^{\mathrm{ext}}(x,t)\hat{\Psi}_j(x), \tag{4.4}$$

involves a two-indices quantity $V_{i,j}^{\mathrm{ext}}(x,t)$: the diagonal terms $V_{i,i}^{\mathrm{ext}}$ account for the external potential to which each sublevel is subjected, while off-diagonal terms $V_{i\neq j}^{\mathrm{ext}}$ account for transitions between different sublevels induced by stationary or time-dependent optical, microwave or rf fields.

The interaction term, involving the product of four field operators has an even more complicate structure

$$\sum_{i,j,k,l} V_{i,j,k,l}^{\mathrm{int}}(x-x')\hat{\Psi}_i^\dagger(x)\hat{\Psi}_j^\dagger(x')\hat{\Psi}_k(x')\hat{\Psi}_l(x), \tag{4.5}$$

with the interaction potential $V_{i,j,k,l}^{\mathrm{int}}(x-x')$ being a four-indices quantity. If the limit our attention to the case of ultra-low collisions, we are allowed to neglect all collision channels other than the s-wave one and to replace the interaction potential with a simple contact potential

$$V_{i,j,k,l}^{\mathrm{int}}(x-x') = V_{i,j,k,l}^{\mathrm{int}}\delta(x-x'); \tag{4.6}$$

the detailed shape of the interaction potential starts in fact to be important only at larger values of the kinetic energy.

Thanks to the isotropy of space, symmetry arguments allow to considerably reduce the number of the independent components of the tensorial quantity $V_{i,j,k,l}^{\mathrm{int}}$; as an example, in the case of two spin 1 atoms,[110,112] s-wave collisions are described on just two scattering lengths, a_o for the $J_{tot}=0$ channel and a_2 for the $F_{tot}=2$ channel

$$V^{\mathrm{int}} = \frac{4\pi\hbar^2}{M}\left(a_2\mathcal{P}_2 + a_0\mathcal{P}_0\right) = \left(c_0 + c_2\vec{\mathbf{F}}_1\cdot\vec{\mathbf{F}}_2\right); \tag{4.7}$$

[(a)]More precisely, the kinetic term is diagonal only if we choose the same basis for the polarization states at all spatial positions. In photon and atom optics, this is generally the case, but for the case of magnetically trapped atoms. In this case, a polarization axis parallel to the local magnetic field is instead chosen: at low temperatures, however, the non-diagonal kinetic terms result much smaller than the Zeeman splittings and can be then safely neglected thanks to an adiabaticity assumption.[111]

$\mathcal{P}_s$ denote the projector operators which project the pair of colliding atoms into a total spin s state, $\vec{\mathbf{F}}_\alpha$ is the spin operator of the α^{th} atom and the c_α are defined according to

$$c_0 = \frac{4\pi\hbar^2}{M}\left(a_0 + 2a_2\right)/3 \tag{4.8}$$

$$c_2 = \frac{4\pi\hbar^2}{M}\left(a_2 - a_0\right)/3. \tag{4.9}$$

The scattering length a_1 for the $F_{tot} = 1$ channel is actually not relevant, since the bosonic nature of the undistinguishable colliding atoms fixes the wavefunction to be symmetric with respect to the exchange of the two colliding atoms.

The Heisenberg equation of motion for the Bose field

$$i\hbar\frac{\partial\hat{\Psi}_i(x)}{\partial t} = -\frac{\hbar^2}{2m}\nabla^2\hat{\Psi}_i(x) + \sum_j V^{\text{ext}}_{i,j}(x)\hat{\Psi}_j(x) + \sum_{j,k,l} V^{\text{int}}_{i,j,k,l}\hat{\Psi}^\dagger_j(x)\hat{\Psi}_k(x)\hat{\Psi}_l(x) \tag{4.10}$$

which follows from the Hamiltonian eq.(4.1) has a form which is very similar to Maxwell's equation eq.(1.2) for the electromagnetic field in a nonlinear material medium with an intensity dependent refractive index; in this analogy, the external potential $V^{\text{ext}}_{i,j}(x)$ corresponds to the dielectric constant $\epsilon_{i,j}(x)$ of the material medium and the interaction term $V^{\text{int}}_{i,j,k,l}$ to a spatially uniform, local and frequency-flat third-order nonlinear susceptibility $\chi^{(3)}_{i,j,k,l}$.[113]

In eq.(4.7), we have exploited the isotropy of space in order to write the interaction potential of spin 1 atoms in terms of the two only independent parameters a_0 and a_2 which characterize its strength; given the analogy with a third-order nonlinear susceptibility, this writing provides a simple way to determine the independent parameters which define the $\chi^{(3)}_{i,j,k,l}(-\omega;\omega,-\omega,\omega)$ of an isotropic material.

As photons are bosonic particles, the $F_{tot} = 1$ channel is irrelevant if the frequencies of the four photons which are involved in the optical process are equal, as it happens in the $\chi^{(3)}_{i,j,k,l}(-\omega;\omega,-\omega,\omega)$ susceptibility. We are therefore free to fix the corresponding scattering length a_1 to any value without changing the physical predictions;[114] in other words, adding to $V^{\text{int}}_{i,j,k,l}$ the terms which correspond to an $F_{tot} = 1$ channel does not change the interaction energy, since their contributions are canceled out in the final sum over the three polarization indices j, k, l. In particular, if we choose $a_1 = a_2$, the interaction matrix can be rewritten as

$$V^{\text{int}} = \frac{4\pi\hbar^2}{M}\Big(a_2\mathcal{P}_2 + a_2\mathcal{P}_1 + a_0\mathcal{P}_0\Big) = \frac{4\pi\hbar^2}{M}\Big(a_2\mathbf{1} + (a_0 - a_2)\mathcal{P}_0\Big); \tag{4.11}$$

given the simple form of the $\mathcal{P}_0$ projector in the Cartesian basis

$$\mathcal{P}_0 = \frac{1}{3}|xx+yy+zz\rangle\langle xx+yy+zz|, \tag{4.12}$$

it is immediate to rewrite the interaction matrix as

$$V^{\rm int} = \frac{4\pi\hbar^2}{M}\left[a_2\sum_{i,j}|i,j\rangle\langle i,j| + \frac{(a_0-a_2)}{3}|xx+yy+zz\rangle\langle xx+yy+zz|\right]. \tag{4.13}$$

This result can be immediately translated in the language of susceptibilities

$$\epsilon_{xxxx} = \epsilon_{yyyy} = \epsilon_{zzzz} = \frac{b_0+2b_2}{3} \tag{4.14}$$

$$\epsilon_{xxyy} = \epsilon_{yyxx} = \epsilon_{xxzz} = \epsilon_{zzxx} = \epsilon_{zzyy} = \epsilon_{yyzz} = \frac{b_0-b_2}{3} \tag{4.15}$$

$$\epsilon_{xyxy} = \epsilon_{yxyx} = \epsilon_{xzxz} = \epsilon_{zxzx} = \epsilon_{zyzy} = \epsilon_{yzyz} = b_2 \tag{4.16}$$

$$\epsilon_{xyyx} = \epsilon_{yxxy} = \epsilon_{xzzx} = \epsilon_{zxxz} = \epsilon_{yzzy} = \epsilon_{zyyz} = 0, \tag{4.17}$$

where $b_{0,2}$ are proportional respectively to $a_{0,2}$.

On the other hand, the $F_{tot} = 1$ term may result important if we are interested in interactions which involve distinguishable particles for which Bose exchange symmetry does not hold; in particular, this is the case for a nonlinear susceptibility $\chi^{(3)}(-\omega_1;\omega_2,-\omega_3,\omega_4)$ which involves different frequencies. In this case, a term proportional to the projector

$$\mathcal{P}_1 = \frac{1}{2}\Big[|yz-zy\rangle\langle yz-zy| + |zx-xz\rangle\langle zx-xz| + |xy-yx\rangle\langle xy-yx|\Big] \tag{4.18}$$

has to be introduced in $V^{\rm int}_{i,j,k,l}$ and its effect is no more canceled in the sum. Such results are in perfect agreement with the tables of susceptibilities that can be found in nonlinear optics books such as [6, pag.302] and that have been determined by means of completely different arguments. In particular, the three independent matrix elements which characterize the third-order nonlinear susceptibility of an isotropic material are nothing else than linear combinations of a_0, a_1 and a_2.

In actual experiments, a static and conservative external potential $V_{\rm ext}(x)$ can be applied to the atoms in two different ways,[3] using either a magnetic field, or a far off-resonance laser field. In *magnetic traps*, the atoms are subjected to a magnetic potential given by $-\vec{\mu}\cdot\vec{B}$, where $\vec{\mu}$ is the magnetic dipole moment of the atomic state under exam. Such a potential has a different sign according to the internal state of the atom: states in which the magnetic moment is anti-parallel to the field are called

weak-field seekers since the atom results attracted by field minima; states in which the magnetic moment is parallel to the field, are instead *strong-field seeker* ones since the atom results attracted by field maxima. In practical cases, since local maxima of the magnetic field modulus can not be achieved in regions of space where current vanishes, only weak-field seeker states can be actually trapped.

Provided the atomic motion is slow enough, the orientation of the atomic magnetic moment adiabatically follows the direction of the magnetic field: in such a case, spin-polarized atoms preserve their polarization during their motion and a description in terms of a single (yet spatially dependent) internal state subjected to a local potential proportional to the field magnitude is accurate.[111] Quantitatively, such an approximation is valid provided the variation rate of the magnetic field experienced by the atoms during their motion is much slower than the Larmor precession frequency of the magnetic moment, i.e. the Zeeman splitting of the magnetic sublevels. This is generally the case but at the points at which the magnetic field vanishes: here Majorana spin-flip transitions to untrapped states occur which result in atom losses from the trap.

In *optical traps*, atoms are subjected to an optical potential arising from the optical Stark shift of the atomic levels dressed by the laser field: if light is blue-detuned from the atomic transition, the ground state is raised in frequency, while it is lowered if light is red-detuned. This means that an atom is attracted towards high field regions in case of red detuning and towards low field regions in case of blue detuning.[1] From a different point of view, laser light induces an oscillating electric dipole $\vec{d}$ in the atom which, depending on the relative detuning $\delta = \omega_L - \omega_{at}$, can be either parallel ($\delta < 0$) or anti-parallel ($\delta > 0$) to the electric field $\vec{E}$; from these considerations, together with the explicit form of the atom-field interaction energy $-\vec{d} \cdot \vec{E}$, the sign of the optical force is immediately explained.

In the case of far-off resonance laser fields, the detuning δ is almost the same for all Zeeman sublevels of a same hyperfine state so that the potentials experienced by each of them have the same sign and therefore spin-flip transitions are no longer dangerous for trapping. At the same time, spontaneous emission effects are themselves depressed in far-off resonance traps: since the optical potential V_{opt} is proportional to $I_L \delta^{-1}$ while the spontaneous emission rate Γ_{sp} is proportional to the excited level population P_e and hence to $I_L \delta^{-2}$, the spontaneous emission rate Γ_{sp} can be made negligible at a constant value of V_{opt} just by compensating the enhanced detuning δ with a stronger laser intensity I_L.

The recent experiments on Bose-Einstein condensations have mostly used magnetic traps for confining the atom cloud and performing evaporative cooling: such a use relies on the possibility of having a large depth (up to 1mK) and selectively extracting the most energetic atoms. In order to avoid Majorana spin-flip processes with the consequent losses of atoms, clever magnetic field configurations have been envisaged, such as the *cloverleaf*,[115,116] the *baseball*[117,118] and the *TOP*[119] traps; reducing appropriately the background pressure, lifetimes as long as a few ten minutes has been observed. The typical oscillation frequency of atoms around the bottom of magnetic traps are generally at most of the order of hundreds of hertz, with a spatial size for the ground state of the order of a few microns.

The use of optical dipole traps looks promising from several points of view: first of all, all spin states can be trapped in the same trap[120,121] with a trapping frequency generally higher than the one of magnetic traps; in addition, three dimensional standing wave patterns can be obtained in which the trap sizes are comparable or even smaller than the laser wavelength.[122,123] Depending on the lattice intensity, atoms can be either bound at the minima of the optical potential or move with a dispersion law typical of periodic systems, with allowed bands and forbidden gaps; most remarkably, the effective masses of the atoms in such lattices can be much smaller than the free-space one.[124,125] Disadvantages of the optical potentials are the unavoidable spontaneous emission processes and the inability of performing evaporative cooling in the traditional way; cooling techniques based on different ideas are however being actually developed.[3,126]

While the photon-photon interactions which are described by a Kerr nonlinear susceptibility result from the interaction of light with matter and can hence be tuned by an appropriate choice of the material in which light propagates, atom-atom interactions are determined by the internal electronic structure of colliding atoms. However, by applying external magnetic[127–129] or optical fields,[130,131] it is possible to induce slight changes in the internal electronic structure of the atoms which can eventually result into dramatic changes of the collisional properties. Very remarkably, in the presence of a quasi-bound molecular state, the scattering length can be resonantly enhanced of several orders of magnitude just by tuning the energy of the quasi-bound state close to the energy of the colliding pair. As in optical media dissipative processes are generally associated to any resonantly enhanced optical susceptibility, such Feshbach resonances in the elastic s-wave collision cross-section are generally associated to enhanced three-body recombination rates,[132–134] which

are the atomic analog of nonlinear absorption in photon optics.

4.2 The many-body problem of the interacting Bose gas

Whenever the nonlinear interaction term in the wave equation eq.(4.10) for the matter field $\hat{\Psi}_i(x)$ can be considered as negligible with respect to the other kinetic and external potential terms, the Bose field can be approximated as a free field so that the theory, being now a single particle one, can be exactly solved irrespective to the specific quantum state of the field; more precisely, the evolution equations for any correlation function of the field give at each order a closed set of Schrödinger-like partial differential equations. As simplest examples, the mean-field $\psi_i(x,t) = \left\langle \hat{\Psi}_i(x,t) \right\rangle$ satisfies the Schrödinger equation

$$i\hbar \frac{\partial \psi_i(x,t)}{\partial t} = -\frac{\hbar^2}{2m}\nabla^2 \psi_i(x,t) + \sum_j V_{i,j}^{\mathrm{ext}}(x)\psi_j(x,t), \tag{4.19}$$

while the one-body density matrix $\rho_{i,j}(x',t';x,t) = \left\langle \hat{\Psi}_i^\dagger(x',t')\hat{\Psi}_j(x,t) \right\rangle$ satisfies the more complicate equation

$$i\hbar \frac{\partial \rho_{k,i}(x',t';x,t)}{\partial t} = -\frac{\hbar^2}{2m}\nabla_x^2 \rho_{k,i}(x',t';x,t) + \sum_j V_{i,j}^{\mathrm{ext}}(x)\rho_{k,j}(x',t';x,t). \tag{4.20}$$

In sec.5.4.2 we shall make use of this equation in order to determine how the transmission of an atom laser beam through an optical lattice depends on its first-order coherence length. If the initial state is a coherent one, its all-order coherence is not destroyed by the interaction with any sort of conservative external potential.

On the other hand, a general and tractable theory able to give exact results for the the interacting Bose gas described by the complete Hamiltonian eq.(4.1) is still not available in the general case; only simplified models which involve only a few modes of the atomic field have been solved in an exact and complete way. Among these, the most relevant ones are the Josephson junction, modeled as a double trap,[135] and the phase conjugation mirror;[136] in both cases, only two modes of the Bose field are in fact involved.

For the general case of spatially distributed gases in which a large number of modes are actually involved in the dynamics, several approaches have been developed,

each with its specific purposes and range of applicability: some of them are exact, other approximated; some of them are analytical, other numerical.

For the study of thermodynamical equilibrium properties, quantum Monte Carlo (QMC) techniques are currently used,[137–140] based on Feynman's path integral formulation of quantum mechanics. Besides their well-known computational difficulty, such methods have several limitations: since they explicitely work in coordinate space, Hamiltonians which are not real in such a representation can not be handled: unfortunately, this is the case of vortices in Bose-condensed clouds.

For study of dynamical properties, QMC techniques, based on an imaginary-time evolution, are not suited and completely different approaches have to be used: quantum kinetic theories have been recently developed for the study of the formation of the condensate and of the dynamics of the non-condensed fraction;[141–150] unfortunately the corresponding calculations are quite heavy for spatially distributed systems.

In quantum optics, the study of interactions between light fields in nonlinear media has been often performed using the so-called "semiclassical" distribution functions for the Bose field;[49,151,152] depending on the ordering of the operators we are interested in, either Glauber's P-distribution,[153–155] Wigner's W-distribution or the Q-distributions can be used. In such approaches, the dynamics of the nonlinear system under examination is reduced to a Fokker-Planck (FP) system of partial differential equations which is in practice solved by means of the corresponding stochastic (Langevin) equation; in this way the numerical complexity of the problem is sensibly reduced with respect to the original FP equation. Unfortunately, for some most relevant systems such as the nonlinear single-mode Fabry-Perot cavity of sec.2.2, the FP equation does not have a positive-definite diffusion term, so that the usual rewriting in terms of stochastic evolution is not possible and the numerical treatment has to be done directly on the FP equation;[156] in addition, the P- and the W-distributions are in general not positive and sometimes even not real, so that it is not possible to give them an interpretation in term of a probability distribution.

These difficulties have been overcome by the introduction of the Positive-P representation by Drummond and Gardiner,[157,158] which gives positive-definite diffusion terms for the most relevant physical systems as well as a distribution function which, being always positive, can be interpreted as a true probability distribution;[159] this at the expense of doubling the number of variables involved in the

theory. The Positive-P method has revealed to be a fundamental tool for the study of a number of quantum optical systems,[49] such as the nonlinear FP cavity,[160] the optical parametric oscillator,[161,162] quantum solitons,[163,164] . As the only limitation of the Positive-P approach, for sufficiently strong nonlinearities, the solution of the stochastic equations exists only for a short time interval, after which divergences occur in the sense that the trajectory is expelled towards infinity in a finite time.[165–169]

In the last years, the positive-*P* distribution has been applied to the study of interacting atomic gases: since atom-atom collisional interactions are generally much stronger than photon-photon ones in a nonlinear medium, the divergences are even more problematic in the atomic case than in the photonic case.[170] Interesting results on the formation of the condensate can however be obtained with such a technique provided the system has an intrinsic damping mechanism; in particular, this is the case for the formation of a condensate from a evaporatively cooled an atomic cloud.[171]

In addition to the Langevin equations which arise from the representations of the Bose field in terms of semiclassical distribution functions, stochastic methods have been widely applied to quantum optics for the description of quantum noise effects. The most celebrated of this methods is certainly the so-called Monte Carlo wavefunction method,[172–176] in which the usual master equation for the density matrix of the system is replaced by a stochastic Schrödinger-like evolution equation for the wavefunction: fluctuation and dissipation effects due to the coupling with the external reservoir are taken into account by quantum jumps which occur at random times during the otherwise conservative evolution of the system. This stochastic wave-function method provides new insight in the phenomena and allows for actual calculations on problems which would otherwise be exceedingly complicated if treated via the master equation.

In chap.7, the principles of a new exact and numerically tractable approach to the problem of the interacting Bose gas are discussed,[177] an approach which is not restricted to thermal equilibrium of the gas but allows for the description of its time-evolution. In this approach, all the atoms share a same wavefunction which is let evolve according to a stochastic differential equation; under appropriate conditions on the specific form of the stochastic evolution, the exact dynamics of the many-body system is recovered, together with all the quantum correlations which may appear in the quantum gas following the atom-atom interactions. Thanks to the fact that the conditions for recovering the exact dynamics do not completely determine

the form of the stochastic equation, we can find different schemes with profoundly different statistical and stability properties. One of such schemes is a reformulation from a different point of view of Positive-*P* representation and therefore leads to stochastic differential equations which suffer from divergence problems; the generality of our method however allows for other schemes to be found which can be mathematically proven to have a regular solution for all times. For such schemes, the only limitation turns out to be the computational time: in particular, the numerical effort increases almost exponentially with the duration of the time evolution. A few examples of application of this method to simple systems are discussed in sec.7.3 and 7.4.

4.2.1 Coherent matter waves, Bose condensates and the mean-field approximation

Throughout all the discussion of nonlinear optical effects contained in the first part of the present thesis we have always assumed all-order coherence for both the light and the excitonic fields which were involved in the effect under examination. It is a well-known result of quantum optics that a laser above threshold emits light whose statistical properties closely resemble the ones of a classical all-order coherent beam;[49,151,152,178] as we shall see in more detail in sec.6, if we furthermore assume that the nonlinear coupling inside the cavity is small enough, it can be proven that the coherence of the incident beam is transferred to the cavity as well as to the transmitted fields. Such an assumption has the immediate consequence that all operator products involved in the theory are factorizable and all the dynamics can be expressed in terms of the mean value of the field alone. In this way, a complicate operatorial-value master equation is replaced by C-number nonlinear partial differential equations which can be treated by conventional techniques; for the case of light, such *mean field* (MF) equations are nothing else than Maxwell's equations in a nonlinear dielectric medium.

A similar approximation is currently done for the description of the matter waves which are associated to a Bose condensate: if the nonlinear interaction term in eq.(4.10) is assumed to be factorizable, the resulting MF equation for the mean value $\psi(x,t) = \left\langle \hat{\Psi}(x,t) \right\rangle$ of the atomic matter field is the well-known Gross-Pitaevskii

equation:[179–181]

$$i\hbar\frac{\partial}{\partial t}\psi(x) = -\frac{\hbar^2}{2m}\nabla^2\psi(x) + V_{ext}(x)\psi(x) + V_{int}\left|\psi(x)\right|^2\psi(x). \tag{4.21}$$

As it is well known from equilibrium thermodynamics, a Bose gas well below the condensation temperature is correctly described as a coherent field provided it is *dilute* enough:[182] in terms of the density n and the scattering length a, the diluteness condition reads as $\sqrt{na^3} \ll 1$. Current trapped atomic Bose-Einstein condensates (BEC) well satisfy such a limit, while in the case of superfluid helium the interactions are too strong.

From the experimental point of view, the assumptions of mean-field theory have been confirmed by the direct measurement[183] of a few low-order coherence functions of trapped BECs: in the framework of Glauber's coherence functions,[153,154] the all-order coherence can be reformulated as[184–186]

$$g^{(n)}(x_1,t_1;\ldots;x_{2n},t_{2n}) = \\ = \frac{\left\langle \hat{\Psi}^\dagger(x_1,t_1)\ldots\hat{\Psi}^\dagger(x_n,t_n)\hat{\Psi}(x_{n+1},t_{n+1})\ldots\hat{\Psi}(x_{2n},t_{2n})\right\rangle}{\left\langle \hat{\Psi}^\dagger(x_1,t_1)\hat{\Psi}(x_1,t_1)\right\rangle^{1/2}\ldots\left\langle \hat{\Psi}^\dagger(x_{2n},t_{2n})\hat{\Psi}(x_{2n},t_{2n})\right\rangle^{1/2}} = 1. \tag{4.22}$$

Historically, the first signature of the presence of a Bose condensate in a trapped gas has been the appearance of a narrow peak in the momentum distribution; in terms of coherence, this corresponds to the presence of a long-range tail in the first-order coherence function $g^{(1)}$.

The second-order coherence $g^{(2)}(0) = 1$ of a condensed cloud has been verified measuring the release energy after switching off the trapping potential:[183] the potential energy stored in the interactions between atoms in the BEC is in fact predicted by MFT to be equal to the integral

$$U_{\rm int} = \frac{V_{\rm int}}{2}\int dx\ \left|\psi(x)\right|^4. \tag{4.23}$$

For a non-degenerate beam the measurement[187] of the same coherence function has instead given the expected[178] $g^{(2)}(0) = 2$ value for a thermal system. The third order coherence has been measured[188] comparing the three-body recombination rates of trapped Bose gas in the degenerate and non-degenerate cases: the measured ratio $g^{(3)}_{th}(0)/g^{(3)}_{BEC(0)} = 7.4 \pm 2$ agrees with the theoretical[178] prediction of $3! = 6$.

Besides these measurements, the validity of the mean field approach has been indirectly verified in many other circumstances, just by comparing the experimental results with the predictions of Gross-Pitaevskii equation eq.(4.21): as a few examples, it is worth mentioning the frequencies of the collective excitations of the trapped BEC,[182] the interference patterns of overlapping Bose condensates,[189] the Rabi oscillations between different internal states,[190,191] the Bragg scattering of matter waves[192] and the Bloch oscillations in the periodic potential of optical lattices.[193,194] Very recently, four-wave mixing[110,136,195] of matter waves has been demonstrated,[196] giving a first evidence of *nonlinear atom optical* effect.

Although a direct measurement of the coherence length of an atom laser pulse has not been performed yet, from the well-established coherence properties of a trapped BEC it is quite fair to infer an analogous all-order coherence for the output beam; all the output coupling mechanisms actually used to couple atoms out of a trap are in fact based on coherently driven electromagnetical transitions,[197–200] which are well described by time-dependent non-diagonal terms in the external potential $V_{i,j}^{\mathrm{ext}}$ and are the atomic analog of the partially transmitting mirrors which are currently used to generate coherent light beams from laser cavities. On such a basis, an atom laser beam will be always modeled in the following of the thesis as a classical C-number pulse of Schrödinger field; a pair of possible methods for the experimental verification of such an assumption are discussed in sec.5.4.

Depending on the specific output coupling scheme and on whether gravity is acting or not on the atom laser beam, very different regimes can be obtained for the atom laser frequency. Raman output coupling devices[198] impart the extracted atoms a momentum kick which is of the order of the single-photon recoil and can be tuned by varying the geometrical angle between the Raman beams; also the output direction is freely selected. Radio-frequency and microwave output coupling schemes impart a negligible momentum kick to the atoms, which separate from the parent BEC because of mean-field repulsion and gravity. In the presence of gravity,[199] atoms are accelerated while they fall down; a kinetic energy equal to the recoil energy is reached after a free fall $1.7\,\mu$m long for the case of Rb atoms and $40\,\mu$m long for the case of Na atoms. Using, e.g., an atomic waveguide, the strong effect of gravity can be counterbalanced and, in absence of an initial momentum kick, output coupled atoms expand following the mean-field repulsion of the trapped cloud. The imparted kinetic energy is in this case of the order of the chemical potential and therefore generally much smaller than the recoil energy.

In addition to the temporally finite atom laser pulses that can be extracted from a previously formed trapped condensate, a number of theoretical works have appeared in the last years on possible schemes for generating a continuous wave (cw) coherent atom beam.[201–204] For this purpose, the trapped condensate has to be continuously refilled in order to maintain a stationary state in which the losses due to the formation of the output beam are compensated by the continuous loading of new atoms from a thermal cloud. Unfortunately, although several experimental groups are actually involved in such a research, none of the refilling mechanisms proposed so far has been yet realized.

While in the non-interacting case the propagation of a beam through any sort of arrangement has been shown not to destroy the coherence of a classical beam, atom-atom interactions can eventually modify the statistical properties of the beam in a non-trivial way and possibly lead to nonclassical behaviours.[136, 205–208] As in the photonic case, the weaker the interactions, the more accurate the predictions of mean field theory: for the homogeneous gas, this condition is equivalent to the diluteness condition $\sqrt{na^3} \ll 1$; for a driven atomic cavity, we shall see in sec.6 that nonclassical effects can be important if just a small number of atoms in the cavity mode are enough for the transmission to be appreciably affected.

Chapter 5

Atom optics in optical lattices and the atomic Fabry-Perot interferometer

The main topic of the first part of the present thesis has been the study of the properties of optical cavities with well-spaced modes which are driven by a coherent incident laser field. Depending on their energy, photons from the incident beam can be resonantly coupled into the localized cavity mode and then transmitted on the other side of the system.

In order for such cavities to be useful devices for nonlinear optics experiments, two principal features are required: a transmission spectrum showing well separated narrow peaks and a resonant enhancement of the internal intensity with respect to the incident one; the latter is necessary for enhancing the nonlinear interactions inside the cavity, the former makes the transmittivity a very sensitive function of the nonlinear frequency shift.

Although magnetic and optical traps are widely used for the manipulation of atoms, it is not clear how to get large level spacings and narrow linewidths as well as an appreciable coupling of the cavity mode to the incident and transmitted beams.

A very simple proposal have been put forward by Wilkens *et al.*[209] and, independently, by other authors:[210,211] their model of atomic Fabry-Perot interferometer, shown in fig.5.1, is composed by a pair of parallel and blue detuned laser beams; in this configuration, atoms are confined in the space between the laser beams thanks to the repulsive optical potential. In- and out-coupling is provided by tunneling processes across the beam waists.

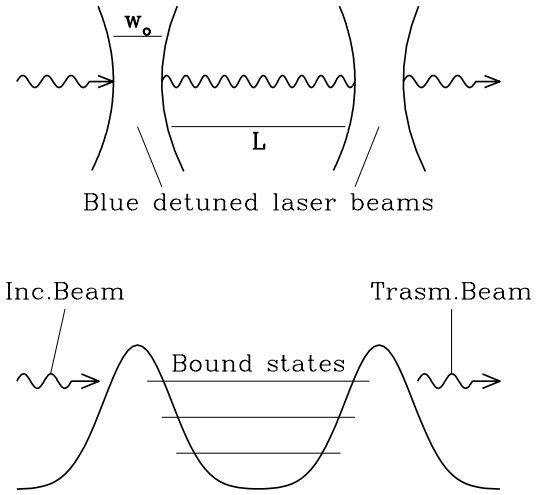

FIGURE 5.1: Schematic plot of the atomic Fabry-Perot interferometer originally proposed by Wilkens *et al.*[209] Upper panel: optical arrangement. Lower panel: optical potential experienced by the atoms.

Two are the main problems presented by such an arrangement: since the characteristic size L of the cavity region is at least of a few laser wavelengths, the spacing of the discrete modes generally turns out to be much smaller than the recoil energy. The energy of the FP modes in a cavity of length L is in fact given by

$$\omega_{FP}^{(n)} \simeq \frac{\hbar\pi^2}{2mn^2L^2}, \tag{5.1}$$

which, for moderate values of the mode order n, satisfies $\hbar\omega_{FP}^{(n)} \ll \epsilon_{rec}$.

Furthermore, since the in- and out-coupling processes depend on tunneling processes across the barriers, the coupling of the cavity modes to the incident driving beam is generally very weak so that the corresponding transmission peaks are very weak as well as very sensitive to asymmetries in the mirror reflectivities.[50,105]

Our proposals[124,125] are based on the idea that an *effective mass* m_{eff} much smaller than the free space mass m can be found in eq.(5.1) provided the atoms propagate in the periodic potential of an optical lattice. As in the electronic and photonic cases (sec.1.1), the atomic dispersion in a periodic potential is in fact characterized by allowed bands and forbidden gaps and its curvature near the gap edge can be made much sharper than the free-space one; in this case, the mode spacing for a given L is much larger than in free space.

As independently [(a)] suggested by Santos and Roso,[212,213] such atomic Bloch waves can be confined by a slow modulation of the lattice parameters on a length scale L much longer than the lattice period. This modulation can either be due to the finite lattice size or even applied from the exterior using a bichromatic lattice; within the envelope function picture, the local potential for the atoms is in fact given by the local band edge. Conduction band atoms, for which the effective mass is positive, are attracted by low potential regions, while valence band atoms, for which the effective mass is negative, are instead attracted by high potential regions. If such a potential is strong enough to give discrete quasi-bound states, transmission spectra will be characterized by resonant tunneling peaks: both their spacing and their intensity can be controlled acting on the intensity, the wavevector and the spatial size of the lattice. As we shall see in the following, bichromatic lattices look more promising than simple lattices from the point of view of applications, since they allow for quantized states in both conduction and valence bands with an enhanced coupling to the incident beam.

Nonlinear atom optical experiments can be carried out with such atomic cavities in close analogy to what has been done for light using DBR microcavities (chap.2): since the atom optical nonlinearity arising from atom-atom interactions is generally much stronger than optical nonlinearities, *atom optical bistability* and *atom optical limiting* are predicted to occur at very low values of the incident atomic flux. In addition, atomic reflection on optical lattices can be used at linear regime for a direct measurement of the coherence length of an atom laser beam without involving the parent condensate.

5.1 The simple optical lattice: localized modes and tunneling resonances

Consider[125,212,213] a linearly polarized Gaussian laser beam of frequency ω_L and beam waist w_o, back reflected by a system of mirrors along a nearly counterpropagating direction with the same linear polarization as in the lower panel of fig.5.2; let θ be the (small) angle between the two beams, $\lambda_L = 2\pi/k_L = 2\pi c/\omega_L$ their wavelength and E_L their central amplitude.

[(a)] We regret we have become aware of such papers only long after the publication of our results.

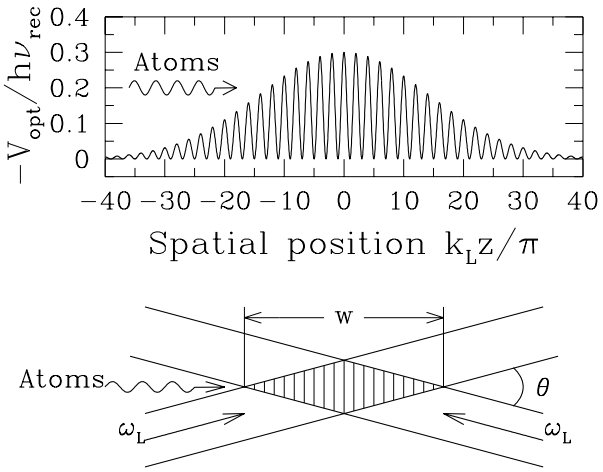

FIGURE 5.2: The simple optical lattice. Lower panel: sketch of the proposed arrangement. Upper panel: qualitative behaviour of the optical potential experienced by the atoms.

In the region of space where they overlap, a $lin \parallel lin$ standing wave pattern is formed, with a spatial profile similar to the one reproduced in the upper panel of fig.5.2: a periodic potential of wavevector $k_l = k_L \cos\theta/2$ with a broad Gaussian envelope of length $w = w_o/\sin\theta/2$[212,214]

$$|E(z)|^2 = 2\,|E_L|^2\, e^{-z^2/2w^2} \cos^2 k_l z. \tag{5.2}$$

A monochromatic and collimated atomic beam is sent on the optical lattice along its axis; assuming the laser frequency ω_L to be far from resonance with the atomic optical transition frequency ω_{at}, each Zeeman sublevel i is decoupled from the others and experiences a conservative optical potential

$$\begin{aligned} V_{i,j}^{\rm ext}(z) &= V_i^{\rm ext}(z)\,\delta_{i,j} = \frac{2\,|d_i E_L|^2}{\hbar\,(\omega_L - \omega_a t)}\delta_{i,j}\, e^{-z^2/2w^2} \cos^2 k_l z = \\ &= \hbar\Omega_i^o\,\delta_{i,j}\frac{1+\cos 2k_l z}{2} e^{-z^2/2w^2} \end{aligned} \tag{5.3}$$

proportional to the square modulus of the matrix element of the optical transition d_i. The atomic dynamics in the transverse plane can be neglected assuming a transversally wide optical lattice and modeling the atomic beam as a plane wave: this allows the calculations to be performed in a one-dimensional longitudinal approximation. A truly one-dimensional geometry can however be obtained by using an atomic

waveguide to confine the transverse motion; several methods have been proposed to obtain such a configuration, the most promising being based on hollow-core optical fibers[215–219] or magnetic fields[220–225]

At linear regime, a simple numerical integration of the Schrödinger equation eq.(4.19) in the potential $V_i^{\rm ext}(z)$ leads to the transmission spectrum for atoms in each polarization. Two examples of such spectra are reproduced in the left panel of fig.5.4. Since the atoms are subjected to a potential which is a periodic one with a slow modulation, we can try to explain the main features of the spectra shown using concepts typical of solid state physics.[7,8]

If the potential does not show any modulation, the atom dispersion in a periodic potential of the form

$$V^{\rm opt}(z) = V_{av} + \frac{1}{2}\,{\rm Re}\left[\left(V_l\, e^{2ik_l z}\right)\right], \tag{5.4}$$

is characterized by *allowed bands* and *forbidden gaps*,[226,227] as shown in fig.5.3.

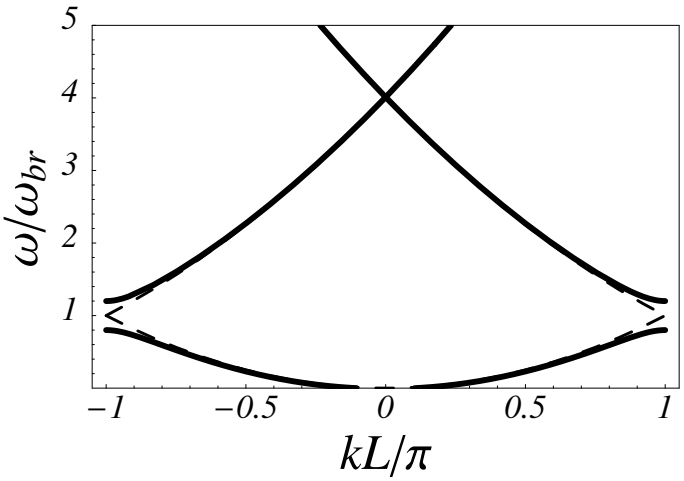

FIGURE 5.3: Atomic dispersion in a periodic optical lattice with $V_l/\omega_{Br} = 0.8$, $V_{av} = 0$.

In the *nearly free atom* approximation, in which the lattice potential $V_{opt}(z)$ is assumed to be weak with respect to the Bragg frequency of the lattice $\omega_{Br} = \hbar k_l^2/2m$, the dispersion of the two lowest bands results given by

$$\hbar\omega_{c,v}(k) = \frac{\hbar^2 k_l^2}{2m} + V_{av} + \frac{\hbar(k-k_l)^2}{2m} \pm \sqrt{\left(\frac{\hbar^2 k_l (k-k_l)}{m}\right)^2 + \left(\frac{V_l}{4}\right)^2}. \tag{5.5}$$

Remarkably, the curvature of the bands at the gap edges is much sharper than the free-space one, giving for the *effective masses* $m^* = \hbar\,(d^2\omega/dk^2)^{-1}_{(k=0)}$ the values

$$\frac{1}{m^*_{c,v}} = \frac{1}{m}\left(1 \pm \frac{4(\hbar k_l)^2}{mV_l}\right) \simeq \pm\frac{1}{m}\frac{8\hbar\omega_{Br}}{V_l}; \tag{5.6}$$

which are both much smaller in modulus than the free-space mass m. As usual, the mass of *conduction* band particles is positive, while the mass of *valence* band ones is negative.

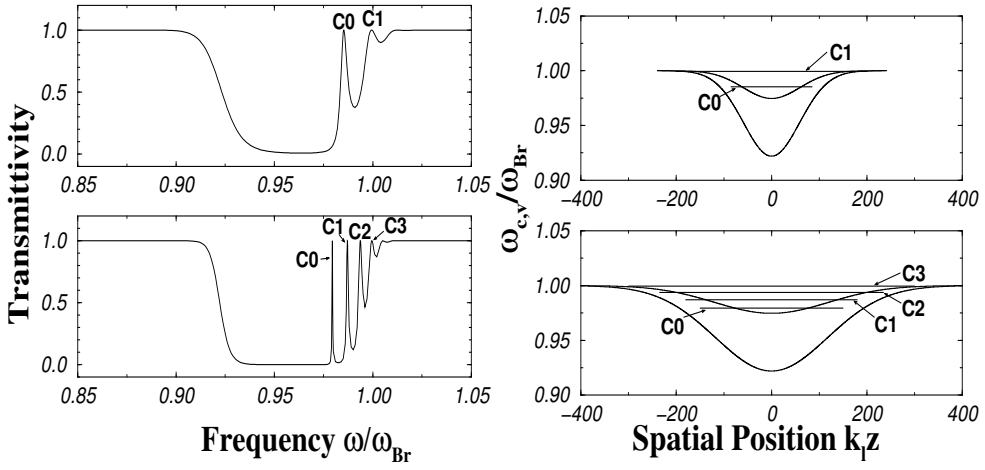

FIGURE 5.4: Linear atom optical properties of simple lattices. Left panel: transmission spectra as function of the kinetic energy of the incident matter field. Right panel: local potential for conduction and valence atoms as function of the spatial coordinate z. The horizontal lines give the frequencies of the resonant peaks in the spectra and correspond to the bound states of the potential. Used parameters: $\Omega_o/\omega_{Br} = 0.1$, $k_L w = 60$ (upper panels) and $\Omega_o/\omega_{Br} = 0.1$, $k_L w = 120$ (lower panels).

Since the spatial variation of the lattice parameters is supposed to occur on a length scale much longer than period of the lattice, we expect that an *envelope function* description should be able to explain the spectra[(b)]. In such an approach, the atomic wave function is approximated by the product of the fast-oscillating band edge Bloch wavefunction and a slow envelope, which satisfy a sort of Schrödinger equation with an effective mass m^* and a local potential given by the (slowly varying)

[(b)]The envelope function approach is used in order to give a physical interpretation to the results which have been numerically obtained by solving equation eq.(4.19) with the true optical potential eq.(5.3).

band edge energy; in the right panel of fig.5.4 we have plotted the band edge frequencies $\omega_{c,v}$ as function of the spatial coordinate z, as they result from the *nearly free atom* expressions eq.(5.5) once we substitute the specific values of $V_{av}(z) = V_l(z)/2 = \hbar\Omega_o/2$:

$$\hbar\omega_{c,v}(z) = \frac{\hbar^2 k_l^2}{2m} + V_{av}(z) \pm \frac{V_l(z)}{4} = \hbar\omega_{Br} - \hbar\Omega_o \left(\frac{1}{2} \mp \frac{1}{4}\right) e^{-z^2/2w^2} \tag{5.7}$$

The Gaussian lattice profile reflects in the inverted Gaussian shape of both $\omega_{c,v}(z)$: outside the lattice they tend to ω_{Br} and they show a single minimum at the lattice center. Give their negative effective mass, valence band atoms are repelled by such a potential minimum, while conduction band atoms, whose mass is positive, are instead attracted and can eventually be trapped in it. Since the effective mass is much smaller (of a factor of about 80 for the chosen parameters) than the free-space one, the quantized motion in such a potential well show energy spacings much larger than the ones expected for a comparable spatial size but in free-space.

Such a simple model is able to explain the main features of the spectra reproduced in the left panel of fig.5.4; for kinetic energies ω located below the minimum value of the valence band edge frequency (i.e. its value at the lattice center $\omega_v(z = 0)$), transmission is almost complete: incident atoms can in fact couple to valence band states and freely propagate through the lattice. Since the lattice edges are smooth, reflections at the interfaces can not occur; hence the absence of the sidebands in the transmission spectrum which were instead present in fig.1.4. For energies above the Bragg frequency $\omega > \omega_{Br}$, transmission is again almost complete, since conduction band states are available for the atomic propagation through the lattice. For energies comprised in the gap at the lattice center $\omega_v(z = 0) < \omega < \omega_c(z = 0)$, there is complete reflection, since the propagation in valence band can occur only up to the point where the valence band edge becomes equal to ω. Afterwards, propagation is forbidden and atoms have to be reflected back.

Starting from analogous considerations we would expect a complete reflection also for incident frequencies comprised between the Bragg frequency and the minimum value of the conduction band edge frequency $\omega_c(z = 0) < \omega < \omega_{Br}$; if the envelope function approximation were exact, this would be the case, since the discrete state in the conduction band potential would not be coupled to the incident states. But the fact the lattice is not uniform gives a small but finite amplitude to non-adiabatic *interband* transitions which can couple the valence band incident atoms to the conduction band discrete states in the potential well. Resonant tunneling processes

through these bound states can thus occur, giving the resonant peaks in the transmission that can be observed in fig.5.4. The resonant enhancement compensates for the small amplitude of the interband jumps, giving transmission peaks which, in our case of a symmetric potential, grow from a nearly vanishing transmission up to a nearly complete one; since the coupling to the continuum of incident and transmitted states is very weak, the peak linewidth is however very narrow and its integrated intensity very small; this implies a high sensitivity to eventual asymmetries in the optical potential eq.(5.3).[105]

An increase in the lattice width w has two main consequences: the increase in the spatial size of the potential well implies a reduced spacing of quantized modes and an increase in their total number; at the same time, the slower spatial modulation of the lattice reduces the amplitude of non-adiabatic jumps, meaning a weaker coupling to the localized mode.

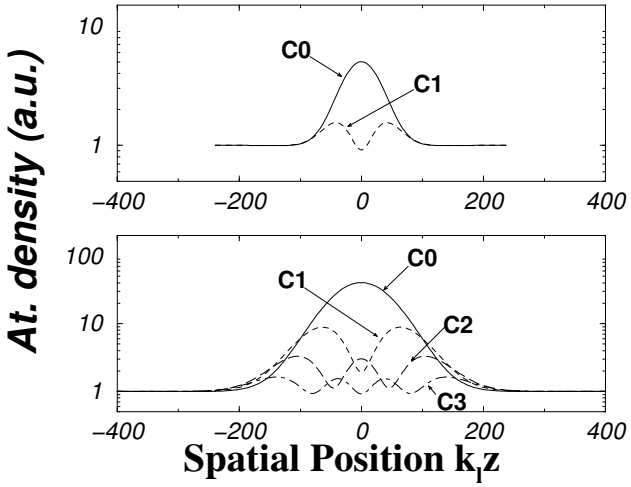

FIGURE 5.5: Density profile of the localized mode wavefunctions. The parameters are the same as in fig.5.4.

In fig.5.5, we have plotted the density profiles of the atomic wavefunctions when the incident frequency is tuned at exact resonance with the quantized modes: the behaviour is the typical one of a quantum-mechanical particle in a one-dimensional potential well: the order of the mode reflects in the spatial extension of the wavefunction and, in particular, in the number of its nodes. The enhanced particle density in the potential well for a unity incident flux is a clear signature of resonant behaviour: the peak density is in fact strictly related to the Q-factor of the localized

mode; in our specific case, the linewidth results a decreasing function of the mode order.

An improved version of this scheme will be presented in the next section; using a bichromatic optical lattice, it will be possible to achieve a tighter confinement of the discrete mode wavefunction, as well as a more efficient coupling to the incident and transmitted beams. The more complicate shape of the potential will allow for localized states also in valence band, for which the coupling to propagating modes is based on resonant tunneling processes across a potential barrier.

5.2 The bichromatic optical lattice

Consider now a more complicated optical lattice,[124] in which the laser field contains two distinct frequencies $\omega_{1,2} = \omega_L \pm \delta\omega_L/2$ ($\delta\omega_L \ll \omega_L$), both far off-resonance from the atomic transition at ω_{at}; provided the energy separation $\hbar\,\delta\omega_L$ of the two components of the light field is much larger than both the hyperfine splitting of the electronic ground state and the typical kinetic energies of the atoms, the optical potential can be written as an incoherent sum of the potentials due to the two frequency components

$$V_{\text{ext}}(z) = \left\{\hbar\Omega_1 \cos^2\left[(k_L + \delta k_L/2)z\right] + \hbar\Omega_2 \cos^2\left[(k_L - \delta k_L/2)z + \phi_o\right]\right\} e^{-z^2/2w^2} \quad (5.8)$$

where the effective Rabi frequencies $\Omega_{1,2}$ depend on the Rabi frequencies of the single beams and detunings according to $\hbar\Omega_{1,2} = 2\left|E_{1,2}d\right|^2/\hbar(\omega_{1,2} - \omega_{at})$. Interference terms due to processes in which the atom absorbs a photon at ω_1 and reemits a photon at ω_2 can be safely neglected on the base of energy conservation arguments.

The superposition of standing waves patterns given by eq.(5.8) gives a periodically modulated optical lattice, in which both the amplitude and the lattice constant are periodic functions of the spatial coordinate z with a period $l_{mod} = \pi/\delta k_L$ and a phase given by the relative phase ϕ_o of the two standing wave patterns, which can be controlled acting by the position of the back-reflecting mirror. As previously, the Gaussian envelope of the laser beams imposes an overall Gaussian profile to the lattice, setting the total length to w and limiting the number of oscillations actually present. By choosing the appropriate values for the lattice parameters ($\phi_o = \pi/2$, $\Omega_1 \geq \Omega_2$), a symmetric configuration like the one in the upper panel of fig.5.6 can be obtained, in which the lattice amplitude has a single minimum at its center.

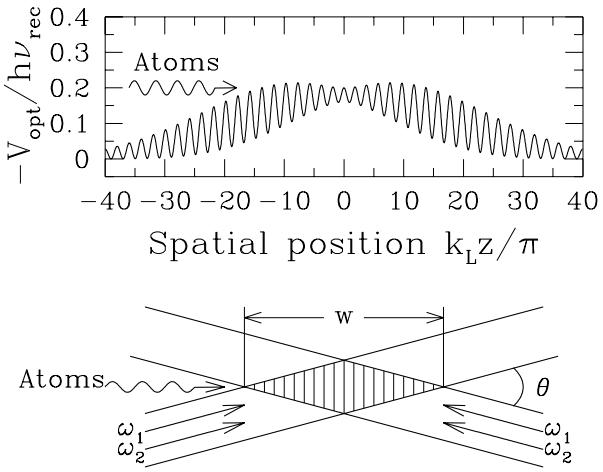

FIGURE 5.6: The bichromatic optical lattice. Lower panel: sketch of the proposed configuration. Upper panel: qualitative behaviour of the optical potential experienced by the atoms.

As we have previously done for the monochromatic lattice, the transmission properties of this bichromatic lattice can be determined by means of a numerical integration of the Schrödinger equation eq.(4.19) with the appropriate optical potential eq.(5.8); two examples of spectra are shown in the left panel of fig.5.7.

From eq.(5.8), we can define the mean potential V_{av}, the lattice amplitude $V_l(z)$ and the phase $\phi(z)$ of the optical lattice according to

$$V_{av}(z) = \hbar(\Omega_1 + \Omega_2)/2 \tag{5.9}$$

$$V_l(z) = \hbar \left| \Omega_1 e^{i\delta k_L z} - \Omega_2 e^{-i\delta k_L z} \right| \tag{5.10}$$

$$\phi(z) = \mathrm{Arg}\left(\Omega_1 e^{i\delta k_L z} - \Omega_2 e^{-i\delta k_L z} \right); \tag{5.11}$$

a spatially varying phase of the lattice means that also the effective wavevector of the lattice is a spatially periodic quantity, given by

$$2k_{\mathrm{eff}}(z) = 2k_l + \frac{d}{dz}\phi(z). \tag{5.12}$$

Inserting these results into eq.(5.7), we are immediately led to the band edges spatial profiles plotted in the right panel of fig.5.7. The spectra of the left panel can be qualitatively explained looking at these potentials, together with the correct signs of the effective masses, which are positive for the conduction band and negative for the valence one.

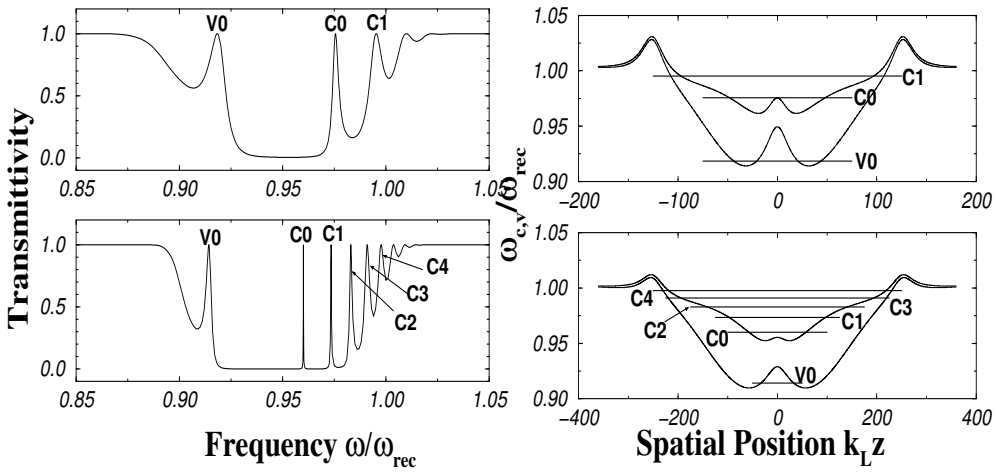

FIGURE 5.7: Linear atom optical properties of bichromatic optical lattices. Left panel: transmission spectra as function of the the kinetic energy of the incident matter field. Right panel: local potential for conduction and valence atoms as function of the spatial coordinate z. The horizontal lines give the frequencies of the resonant peaks in the spectra and correspond to the bound states of the potential. Used parameters $\Omega_1/\omega_{Br} = 0.1$, $\Omega_2/\omega_{Br} = 0.05$ and $\phi_o = \pi/2$; $\delta\omega_L/\omega_L = 1.25 \cdot 10^{-2}$ and $k_L w = 120$ (upper panels), $\delta\omega_L/\omega_L = 2.5 \cdot 10^{-2}$ and $k_L w = 60$ (lower panels).

For frequencies above the maximum value of the conduction band edge frequency $\omega > \omega_c^{(max)}$ and below the minimum of the valence band edge frequency $\omega < \omega_v^{(min)}$ transmission is complete, since atoms find propagating states at such frequency for every z. For frequencies comprised between these two values, transmission is forbidden at a classical regime, i.e. if tunneling processes as well as interband jumps are neglected. Since both conduction and valence band atoms can be confined in a neighborhood of the lattice center by the potential, atomic motion will present two series of discrete quantized bound states, coupled to the propagating external states by processes of two different kinds: as we can observe in the right panel of fig.5.7, for valence band states, tunneling across a potential barrier is sufficient, while for conduction band states, interband transitions are required. As usual, such states appear in transmission spectra as narrow resonance peaks, whose linewidths and integrated intensities are proportional to the coupling strength.

A simultaneous variation of both w and $\omega_L/\delta\omega_L$ by the same factor induces a scale transformation in the lattice: from the point of view of atomic transmission, a shorter lattice means a wider spacing of the discrete states as well as larger linewidths: in-

deed, the amplitude of both tunneling processes (valence band states) and interband transitions (conduction band states) is enhanced by the reduced characteristic length of the lattice; all such features can be easily verified comparing the upper and lower plots of fig.5.7.

In fig.5.8, we have reproduced the transmission spectrum of a different bichromatic lattice, in which we have tried to improve the mode spacing by using a larger value of the laser intensities and a smaller length scale. The zero order valence band *V0* mode, results now separated from all other peaks by a frequency difference of the order of $0.1\omega_{Br}$.

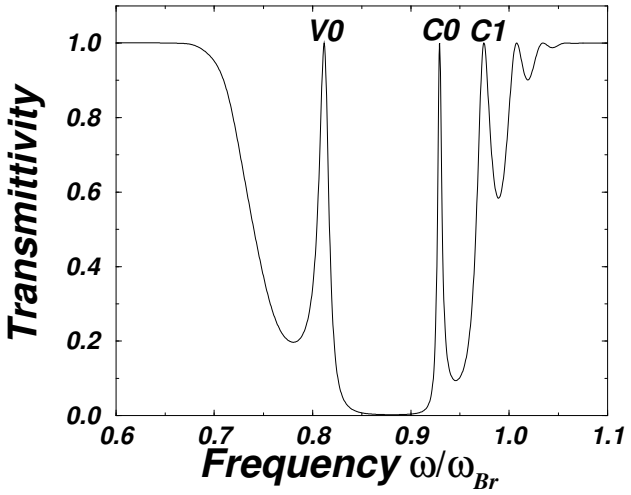

FIGURE 5.8: Linear atom optical properties of a bichromatic optical lattice: transmission spectra as function of the the kinetic energy of the incident matter field. Parameters $\Omega_1/\omega_{Br} = 0.2$, $\Omega_2/\omega_{Br} = 0.15$ and $\phi_o = \pi/2$; $\delta\omega_L/\omega_L = 0.05$ and $w = 30/k_L$.

Since the lowest gap of the optical lattice always opens up around ω_{Br}, this value shows up to be the characteristic frequency of the FP modes which can be obtained using optical lattices; this implies that other arrangements would have to be envisaged, if we need a mode spacing larger than a fraction of ω_{Br}. The use of lattices with a shorter spatial period can lead to higher values of ω_{Br}: this can be obtained either using n^{th} ($n > 1$) order Bragg scattering processes, which involve n absorption and stimulated emission cycles[226] with the consequent n^2 increase in ω_{Br}, or a higher frequency laser source. This latter possibility has two main limitations imposed by the off-resonance condition of the laser field with the atomic transitions and by the practical feasibility of the laser source. Also the frequency range of the atomic beam

is experimentally limited: the output coupling mechanisms which have been developed up to now can not provide atomic beams with wavevectors larger than twice the wavevector of the laser beams used to drive the Raman transitions;[198] such a constraint is however easily circumvented by letting the atoms accelerate under the effect of gravity[199] or by using higher order Raman processes to couple atom out from the trap.

5.3 Nonlinear atom optics: optical limiting and optical bistability

In sec.5.1 and 5.2, we have discussed the atom optical properties of monochromatic and bichromatic optical lattices at linear regime and we have characterized the narrow peaks which arise in the transmission spectra from resonant tunneling processes on localized states confined inside the lattice. Such modes are the atomic analogs of the photonic modes in DBR microcavities which have been discussed at length in the first part of the thesis and are expected to show a similar behaviour when driven by the coherent field of an atom laser.

As in the photonic case, the linear regime corresponds to the limit of very weak atomic flux in which the particles can be considered as independently propagating in the external potential $V^{\rm ext}(z)$ and their interaction energy is so weak that it can be neglected. For larger atom fluxes, the dependence of the transmission spectra on the flux may result in effects similar to the ones discussed in chapter 2. Within the *mean-field* approximation, which assumes a factorizability condition for the nonlinear interaction term in the wave equation eq.(4.10), the calculations can be performed by numerically integrating the Gross-Pitaevskii equation eq.(4.21) with the appropriate boundary conditions; in the most relevant case of repulsive interactions, all the features of the transmission spectrum result blue-shifted for growing incident flux by the mean-field energy. Depending on the sign of the detuning of the incident atom laser frequency ω_{inc} with respect to the empty cavity Fabry-Perot mode frequency ω_{lin}, the nonlinear feedback on the transmission can be either positive (if $\omega_{inc} > \omega_{lin}$) or negative (if $\omega_{inc} \leq \omega_{lin}$); an opposite result holds if the interactions are instead attractive. In the former case we can have *(atom) optical bistability*, while in the latter case we have *(atom) optical limiting*.

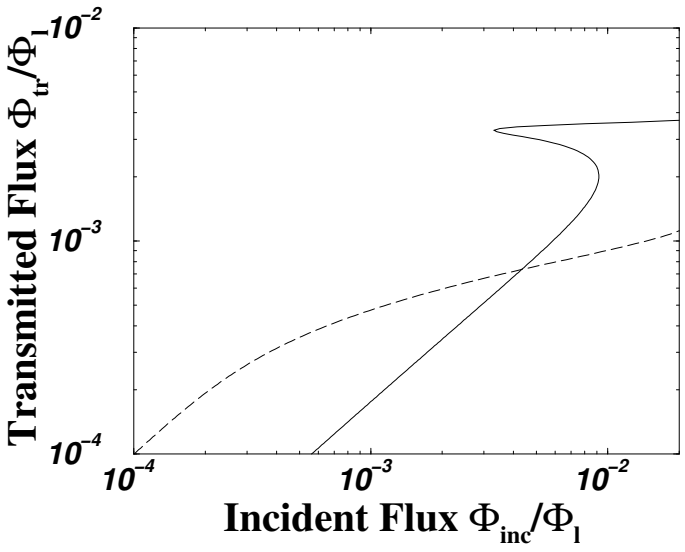

FIGURE 5.9: Transmitted flux as function of the incident flux for different detunings of the incident frequency ω_{inc} with respect to the C0 quasi-bound state frequency $\omega_{lin}/\omega_{Br} = 0.976$. Solid line: optical bistability case ($\omega_{inc}/\omega_{Br} = 0.986$); dashed line: optical limiter case ($\omega_{inc} = \omega_{lin}$). Same lattice parameters as in the upper panels of fig.5.7.

In fig.5.9, we have reproduced the characteristic dependence of the transmitted flux Φ_{tr} on the incident flux Φ_{inc} for two different values of the frequency ω_{inc} close to a resonance peak: for $\omega_{inc} \leq \omega_{lin}$, in fact, the transmission suffers a negative feedback for increasing fluxes, giving an optical limiter behaviour, i.e. a transmitted intensity which grows less than linearly with respect to the incident one (dashed line). For $\omega_{inc} > \omega_{lin}$, the feedback is instead positive and bistability can eventually occur (solid line): this means that for a given value of the incident flux, more than one transmitted flux values are possible; as usual, the central branch of the hysteresis loop is dynamically unstable, since it has negative differential transmittivity.

In the plot all the intensities have been normalized to the characteristic flux $\Phi_l = \hbar k_l^3/8\pi m|a_o|$, defined as the flux at which the mean-field frequency shift equal to the Bragg frequency ω_{Br} of the lattice. In order to reduce the incident atom flux required for observing nonlinear features such as atom optical bistability le behaviour, it can be useful to work with a very narrow transmission peak; indeed, as discussed in sec.2.1, both the resonance enhancement of the atom density in the cavity mode and the sharpness of the spectral dependence of the transmittivity are inversely proportional to the mode linewidth γ. On the other hand, if the cavity mode being is

Atom	^{7}Li	^{23}Na	^{87}Rb
Optical Transition	$2\,^2\mathrm{S}_{1/2} - 2\,^2\mathrm{P}_{3/2}$	$3\,^2\mathrm{S}_{1/2} - 3\,^2\mathrm{P}_{3/2}$	$5\,^2\mathrm{S}_{1/2} - 5\,^2\mathrm{P}_{3/2}$
λ_{tr} (nm)	671	589	780
$\omega_{rec} = \hbar k_{tr}^2/2m$ (kHz)	400	160	24
$v_{rec} = \hbar k_{tr}/m$ (cm/s)	8.5	2.95	0.6
a_o (nm)	-1.45	2.75	5.77
$\Phi_o = \hbar k_{tr}^3/8\pi m\lvert a_o\rvert$ (atoms/s cm^2)	$2.06 \cdot 10^{16}$	$4.94 \cdot 10^{15}$	$2.67 \cdot 10^{14}$

TABLE 5.1: Summary of experimental[3,182] values for atomic parameters. The Bragg frequency of the optical lattice ω_{Br} is generally comparable to the recoil frequency $\omega_{rec} \geq \omega_{Br}$.

very weakly coupled to the external propagating modes, the in- and out-coupling processes can present difficulties, since just a slight asymmetry in the in- and out-coupling amplitudes can result in a strongly depressed transmission.[50,105] In addition, the atom laser frequency spread have to be reduced to less than the mode linewidth; this means that, even if the atom laser output is assumed to be perfectly coherent, an atom pulse longer than the cavity relaxation time $\tau = \gamma^{-1}$ is necessary: with the actual non-refilled atom sources this may be a serious problem.

Using the experimental parameters of tab.5.1 for ^{23}Na and ^{87}Rb atoms, the switching on threshold of the hysteresis loop of fig.5.9 correspond to intensities respectively equal to $4.5 \cdot 10^{13}\mathrm{at/cm^2s}$ and $2.4 \cdot 10^{12}\mathrm{at/cm^2s}$; such values are hopefully achievable by the cw ^{87}Rb atom laser actually being developed in Paris.[202,228]

Very remarkably, a comparable flux for the case visible light would correspond to an intensity of the order of a few $\mu\mathrm{W/cm^2}$, which is several order of magnitude weaker than any light beam actually used for conventional nonlinear optics; this enormously larger nonlinearity of matter waves suggests that the observation of nonlinear effects at the low quanta level could be more easily obtained with atomic matter waves than with light waves. In other terms, provided the confinement of the matter wave in the atomic FP cavity is tight enough and cavity linewidth is narrow enough, a regime in which the mean-field theory underlying eq.(4.21) is no more valid can be achieved; in this case, the coherence properties of both the cavity and the transmitted atomic fields are not the classical ones and a complete theory which takes into account quantum correlations has to be used. The next chap.6 is devoted

to a detailed study of such effects within a single-mode model for the atomic cavity which allows for an exact and complete numerical calculation to be performed.

5.4 Atom laser coherence length determination

The calculations that have been reported in the previous sections have assumed that the incident beam is a perfectly coherent one and can therefore be described as a monochromatic classical wave. Although optical laser sources are in general well described by such an approximation, fluctuations in both the intensity and the phase of the emitted field may play an important role in limiting the attainable accuracy of measurements; for this reason their characterization results very important for practical applications.

While the coherence properties of optical lasers have been well understood for already a couple of decades,[49,152,178] the study of the atom laser output still deserves attention from both the theoretical and the experimental points of view. Actual coherent matter sources are in fact limited by the finite number of atoms initially present in the trapped BEC: since no continuous refilling mechanism has been realized yet, it is not possible to obtain a continuous wave coherent atomic beam, but only a pulsed one; nonetheless, the stability of the magnetic traps has attained very good levels so that the extracted atomic pulses can coherently last for a rather long time provided their intensity is weak enough.

As we have already discussed, mean-field theory predicts that the atomic field in a trapped BEC is a perfectly coherent one, for which the correlation functions factorize at all orders. First order coherence has been recently explored by a pair of groups using two different variants of the classical two-slit arrangement.[229,230] For very low-temperature samples, both groups found no decay of the fringe visibility but for the one which obviously came from a reduced overlap of the two interfering channels.[231] In optical terms, this means that the coherence length of the condensate is at least equal to its size. At higher temperatures, a substantial reduction of the first-order coherence length was observed, which has been interpreted as due to the presence of thermal atoms in the trap.[232,233] Recently, several papers have appeared which discuss such features in both trapped[234–236] and propagating[208,237] atomic samples and try to give a complete description of their first and second order coherence properties at zero as well as at finite temperatures.

However, a conclusive measurement of the coherence length of actual quasi-cw atom laser beams has not been reported yet, so that the problem of whether their coherence length can be considerably longer than the size of the parent condensate is still an experimentally open question. In the present section, we shall show how the interaction of a weak atom laser beam with an optical lattice can be used for the experimental determination of the first-order coherence properties of an atom laser beam.[238]

5.4.1 A simple atom laser model

Keeping in mind the very long (quasi-cw) atomic pulses which have been recently reported, the atom laser output can be modeled as a weak and stationary plane wave of (weak) intensity $|a_o|^2$, wavevector k_b, frequency $\omega_b = \hbar k_b^2/2m$ and group velocity $v_b = \hbar k_b/m$ with a slowly diffusing phase ϕ

$$a_b(x,t) = a_o e^{i(k_b x - \omega_b t)} e^{i\phi(x - v_b t)}; \tag{5.13}$$

provided phase coherence is maintained over a characteristic length l_c much longer than the atom laser wavelength, the parabolic atomic dispersion can be approximated as a linear one in a neighborhood of ω_b so that (5.13) is a good solution of the atomic Schrödinger equation within a sort of slowly varying envelope approximation [6, pag.216 and ff.].

Phase diffusion can be modeled by the stochastic differential equation

$$d\phi(x) = \sqrt{\eta}\, dB \tag{5.14}$$

with $\langle dB \rangle = 0$, $\langle dB^2 \rangle = dx$; its strength is fixed by the η parameter.

Using standard techniques[239] for the manipulation of stochastic differential equations, it can be shown that the first-order correlation function $C_b^{(1)}(x,t;x',t')$ of such a beam is equal to

$$C_b^{(1)}(x,t;x',t') = \langle a_b^*(x,t) a_b(x',t') \rangle = |a_o|^2 \, e^{i[k_b(x'-x) - \omega_b(t'-t)]} e^{-\frac{\eta}{2}|(x - v_b t) - (x' - v_b t')|} \tag{5.15}$$

and the phase diffusion constant η is related to the equal time ($t = t'$) coherence length l_c as well as to the equal point ($x = x'$) coherence time $t_c = l_c/v_b$ by $\eta = 2/l_{coh} = 2/v_b t_c$.

Since our beam is a stationary one $C^{(1)}(x,t+T;x',t'+T) = C^{(1)}(x+X,t;x'+X,t') = C^{(1)}(x,t;x',t')$, Wiener-Khintchine theorem[178] can be applied; it follows that the different frequency components are uncorrelated to each other

$$\langle \hat{a}_b^*(\omega)\hat{a}_b(\omega')\rangle = \delta(\omega-\omega')S_b(\omega) \tag{5.16}$$

and the spectral distribution $S_b(\omega)$ is the Fourier transform of the first-order correlation function $C_b^{(1)}(t;0)$ at a given spatial position $x = x'$

$$S_b(\omega) = \frac{1}{2\pi}\int dt\; e^{i\omega t} C_b^{(1)}(t;0) = \frac{1}{2\pi}\int dt\; e^{i\omega t}\,\langle a_b^*(t)a_b(0)\rangle\,. \tag{5.17}$$

In our specific model, the atom laser has a Lorentzian lineshape

$$S_b(\omega) = \frac{|a_o|^2}{\pi}\frac{\gamma}{(\omega-\omega_b)^2+\gamma_b^2} \tag{5.18}$$

with a linewidth $\gamma_b = \eta v_b/2$ proportional to the phase diffusion constant η.

In the following two subsections we shall discuss two possible methods for the determination of l_c or,equivalently, γ_b; both of them are based on the coherent reflection of an atomic beam on an optical lattice.

The first method, discussed in sec.5.4.2, makes use of the peculiar frequency dependence of the reflectivity of an optical lattice in order to determine the spectral distribution of the incident beam by filtering out the different frequency components. This can be done using either the narrow Fabry-Perot resonances described in the previous section, or even the sharp lower edge of the reflecting window of a simple lattice: in both cases, in fact, the frequency position of the different spectral features strongly depends on the lattice intensity Ω_o; by monitoring the density of the transmitted beam while varying Ω_o, it is in fact possible to get information on the spectral distribution $S_b(\omega)$ of the incident beam.

The second method (sec.5.4.3) is instead based on the diffraction of a probe laser beam on the atomic standing wave which is present in front of a nearly perfectly reflecting atomic mirror. Since the spatial period of the matter standing wave is generally as small as an optical wavelength, a direct experimental observation of the fringes would require a spatial resolution well beyond the possibilities of any absorptive imaging system; this difficulty can be overcome by diffracting light on the phase grating provided by the oscillatory refractive index profile of the atomic standing wave. The coherence length of the atom laser can be inferred from the

angular lineshape of the first-order diffracted peak: the longer the coherence time of the incident beam, the larger the number of coherent density oscillations and thus the narrower the peak.

5.4.2 Velocity filtering

Owing to the assumption of a weak atom laser beam and therefore negligible atom-atom interactions, the system is well described by an exactly solvable single-particle theory. In our specific case of an atom laser beam with known statistical properties which incides onto an optical lattice, eq.(4.20) is best studied in frequency space, where the different components are decoupled from each other. In other terms, the amplitude of the transmitted beam a_{tr} at a given frequency ω is uncorrelated from all the others and is given by

$$a_{tr}(\omega) = \tau(\omega) a_b(\omega) \tag{5.19}$$

where $\tau(\omega)$ is the transmission amplitude of the mirror which summarizes all the information on its detailed structure.

Since the total densities in the incident and transmitted beams are related to the corresponding spectral densities by

$$\rho_{b,tr} \propto \int S_{b,tr}(\omega)\, d\omega, \tag{5.20}$$

the effective transmittivity $T_{\text{eff}} = \rho_{tr}/\rho_b$ can be evaluated using eq.(5.19).

In the case of a red-detuned optical lattice, the upper edge of the reflecting window is fixed at ω_{Br}, while the position of the lower edge is a linear function of the lattice intensity Ω_o. If ω_b is located below the Bragg frequency ω_{Br}, the atomic beam is well transmitted for small values of Ω_o, while it is mainly reflected for large values of Ω_o.

The width of the crossover region provides information on the atom laser linewidth γ_b: the broader such a linewidth, the smoother the step. In fig.5.10a we have plotted the effective transmittivity T_{eff} as a function of the lattice intensity Ω_o, while in fig.5.10b we have plotted the maximum of the slope $dT_{\text{eff}}/d\Omega_o$, i.e. its value at Ω_o such as $\omega_v^{(min)}(\Omega_o) = \omega_b$, as a function of γ_b. Using this latter dependence, the linewidth γ_b of a given source can be easily inferred from the experimentally measured T_{eff} as a function of Ω_o.

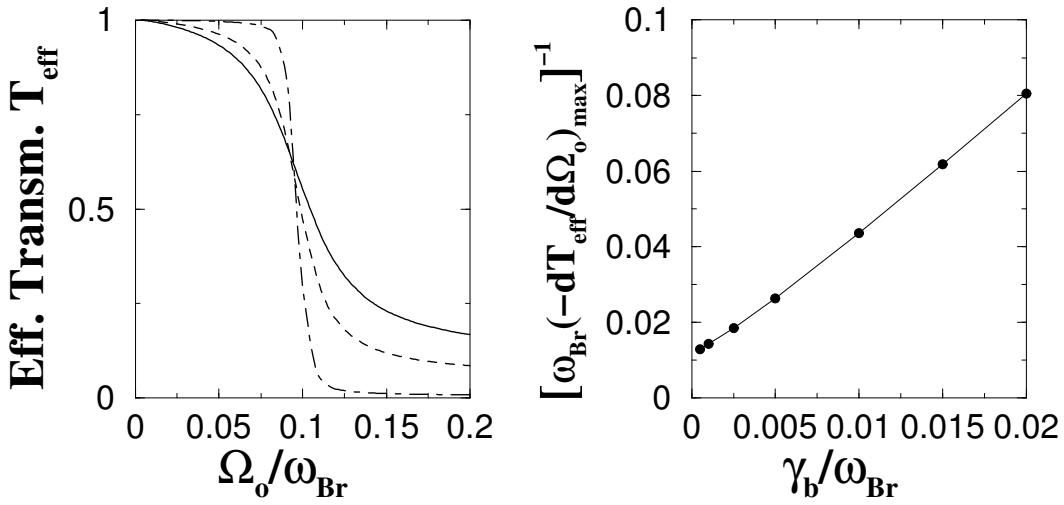

FIGURE 5.10: Left panel: transmitted fraction as a function of the lattice intensity Ω_o for different values of the atom laser *Lorentzian* linewidth γ_b. Solid, dashed and dot-dashed lines respectively correspond to $\gamma_b = 0.02, 0.01, 0.001\omega_{Br}$. Right panel: dependence of the maximum of the slope $dT_{\rm eff}/d\Omega_o$ on the atomic source linewidth γ_b. The central frequency $\omega_b = 0.925\omega_{Br}$ is such that $\omega_v^{(min)} = \omega_b$ for $\Omega_o/\omega_{Br} = 0.1$; lattice length $w = 120/k_L$.

The results of analogous calculations performed for a Gaussian atom laser lineshape[238] are plotted in fig.5.11: from the qualitative point of view, the behaviour looks very similar. As the only difference, reflection in the strong Ω_o limit is now complete, since the weight of the high frequency tail which overlaps with the $\omega > \omega_{Br}$ transmitting part of spectrum is negligible for a Gaussian lineshape.

In the language of X-ray diffraction,[240] the opening of a finite frequency window with nearly total reflection can be interpreted as a signature of a *dynamical* diffraction process rather than a simple *kinematical* diffraction one. The crossover from a transmitting to a reflecting regime situation can be reformulated in spatial terms as the crossover from a $l_c < l_e$ to a $l_c > l_e$ regime, l_e being the extinction length of the optical lattice[4] and l_c the coherence length of the source. If $l_c > l_e$, the reflected waves at all planes of the optical lattice involved in the reflection process are mutually coherent giving constructive interference and consequently a nearly perfect reflection. In the opposite $l_c < l_e$ case, the limited coherence length of the source washes out the constructive interference so that the reflection is only partial. The same effect occurs in X-ray diffraction: dynamical diffraction effects are in fact washed out when the size of the scattering monocrystals is smaller than the extinc-

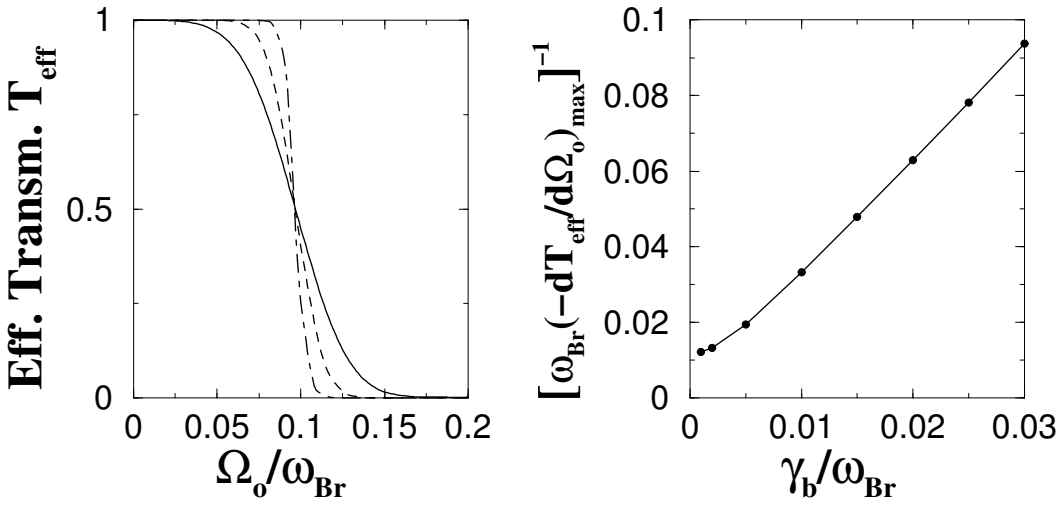

FIGURE 5.11: Left panel: transmitted fraction as a function of the lattice intensity Ω_o for different values of the atom laser *Gaussian* linewidth γ_b. Solid, dashed and dot-dashed lines respectively correspond to $\gamma_b = 0.02, 0.01, 0.001\omega_{Br}$. Right panel: dependence of the maximum of the slope $dT_{\rm eff}/d\Omega_o$ on the atomic source linewidth γ_b. The central frequency $\omega_b = 0.925\omega_{Br}$ is such that $\omega_v^{(min)} = \omega_b$ for $\Omega_o/\omega_{Br} = 0.1$; lattice length $w = 120/k_L$.

tion length.[240] In the X-ray case, the incident beam can generally be considered as perfectly coherent while the diffracting lattice has a finite coherence length; in the atomic case, the incident beam does have a finite coherence length while the optical lattice is perfect.

If the linewidth of the source is sufficiently smaller than the frequency separation of adjacent FP modes, the corresponding resonance peaks can also be used for a spectral analysis of the incident beam. As we can see in fig.5.12, the spectral position ω_{FP} of the Fabry-Perot modes in an optical lattice can be tuned by varying the intensity Ω_o of the lattice and therefore swept across the atom laser lineshape. In the most relevant case in which the FP mode linewidth is much smaller than the atom laser linewidth γ_b, the former can be approximated by a delta-function; hence, for each value of Ω_o, the effective transmittivity $T_{\rm eff}$ results proportional to the value of the spectral distribution function S_b evaluated at the FP mode frequency $\omega_{FP}(\Omega_o)$.

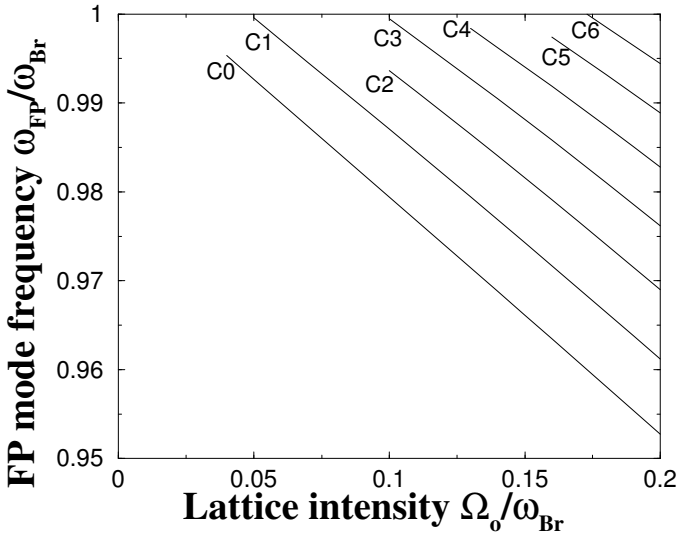

FIGURE 5.12: Simple optical lattice: spectral position of the conduction band FP modes as a function of lattice intensity; $k_L w = 120$

5.4.3 Atomic standing wave

Consider a weak atomic beam with the statistical properties described in 5.4.1 normally incident on a nearly perfectly reflecting atomic mirror with a frequency bandwidth much larger than the linewidth γ_b of the atomic source.

If the beam propagates along the negative x direction and the mirror is located at $x = 0$ (see fig.5.13), the atomic field amplitude in front of the mirror can be written as the sum of the incident and the reflected beam amplitudes

$$a(x,t) = a_b(-x - v_b t) + a_b(x - v_b t + 2l_{pen})e^{i\phi_r}; \tag{5.21}$$

the penetration depth l_{pen} in the mirror is related to the reflection retardation time t_{ret} by $2l_{pen} = v_b t_{ret}$; for an actual mirror, t_{ret} can be evaluated[61] as the frequency derivative $d\phi_r(\omega)/d\omega$ of the reflection phase ϕ_r [241, Chap.J$_I$].

Interference effects between the incident and the reflected matter waves creates in front of the mirror a standing wave profile in the atomic density

$$\rho(x,t) = 2\left|a_o\right|^2 \left\{1 + \mathrm{Re}\left[e^{2ik_L x} e^{i\theta(x,t)}\right]\right\} \tag{5.22}$$

whose contrast is fixed and unity at all positions, but whose phase $\theta(z,t) = \phi(z - v_g t + 2l_{pen}) + \phi_r - \phi(-z - v_g t)$ slowly fluctuates in both space and time [(c)].

[(c)] We are indebted to Markus Greiner for illuminating discussions on this point

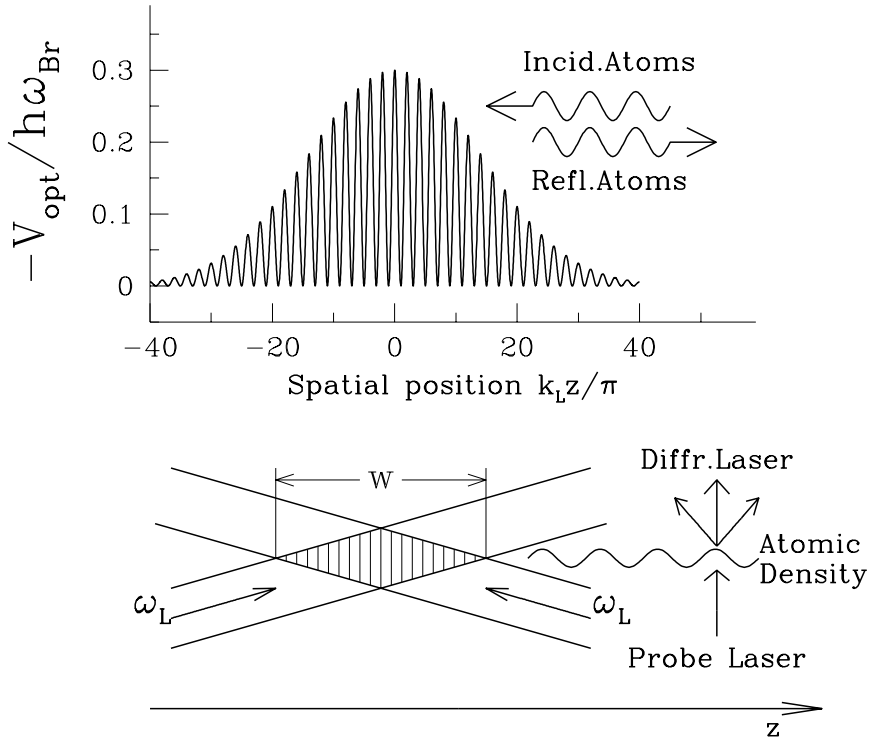

FIGURE 5.13: Lower panel: scheme of the proposed arrangement. Upper panel: qualitative plot of the optical potential experienced by the atoms.

If we introduce the evolution equation eq.(5.14) for $\phi(x)$ in the definition of θ and we solve the resulting stochastic equation,[239] we are led to a simple expression for the correlation function of the phase $\theta(x,t)$ of the standing wave at a given time t

$$\left\langle e^{i\theta(x,t)} e^{-i\theta(x',t)} \right\rangle = e^{-\eta|x-x'|}, \tag{5.23}$$

which means that the characteristic length over which the phase of the standing wave decoheres is equal to half the atom laser coherence length $l_c/2$. As we can see in fig.5.14, sufficiently close to the mirror (i.e. for $x < (l_c - l_{pen})$), the phase $\theta(x,t)$ is locked to the reflection phase of the mirror; farther away it is instead freely fluctuating and the oscillations in the density profile are washed out in the *average*: at each location x for which $x \gg (l_c - l_{pen})$, the standing wave position fluctuates in fact within a characteristic time scale set by l_c/v_b.

Since the spatial period of such density fringes is fixed by the wavelength of the mat-

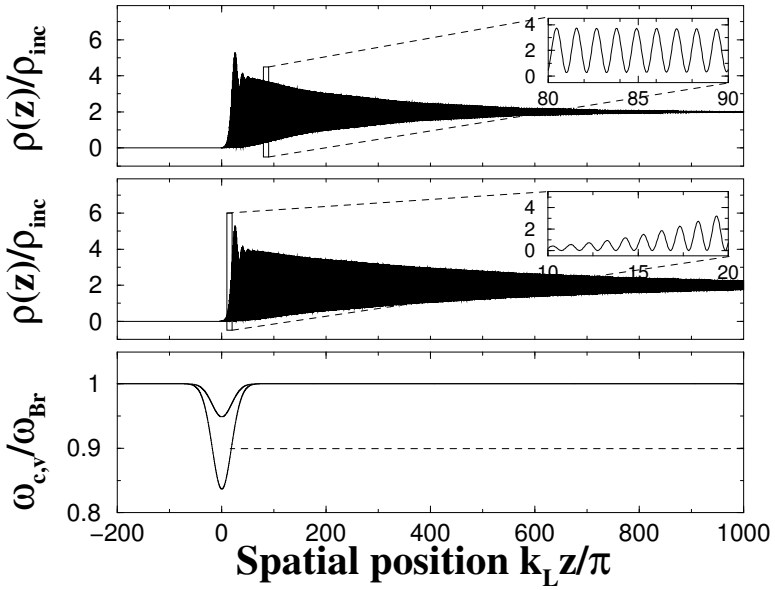

FIGURE 5.14: Mean value of the atomic density profile for an incident atomic beam Lorentzian linewidth $\gamma_a/\omega_{Br} = 6 \times 10^{-4}$ (upper) and $\gamma_a/\omega_{Br} = 3 \times 10^{-4}$ (middle). The broader the linewidth, the faster the phase decoherence of the standing wave leading to the effective decay of the oscillations in the *mean* atomic density. Spatial profile of the local band edges (lower panel). The central frequency $\omega_a/\omega_{Br} = 0.9$ of the Lorentzian source lineshape (horizontal dashed line) lies well inside the reflecting window of the DBR atomic mirror with $\Omega_o/\omega_{Br} = 0.2$.

ter wave, typically as small as an optical wavelength, the experimental observation of the fringes would require a spatial resolution well beyond the possibilities of any direct imaging system. This difficulty can be overcome looking at the diffraction of the light of a probe laser beam on the phase grating provided by the atomic density $\rho(x)$ profile: the spatially modulated refraction index is determined by the refractive properties of the atoms and is proportional to the atomic density $\rho(x)$.[242] If the probe beam is taken to be far off resonance from any atomic transition, the optical density of the matter wave turns out to be very small and the diffraction process can be treated in the first Born approximation, which takes into account only single scattering processes.

Denoting with $E_p(x)$ the transverse profile of the incident probe beam (k_p is its central wavevector), assumed not to spatially overlap with the atomic mirror, the

emerging beam profile can be written (at lowest order in $\beta\rho$) as

$$E_e(x,t) = [1 + i\beta\rho(x,t)]\, E_p(x) \tag{5.24}$$

where β is a numerical coefficient proportional to the atomic polarizability times the atom laser beam waist. The scattered amplitude E_s at an angle α is therefore given by

$$\begin{aligned} E_s(\alpha,t) &= \int \frac{dx}{2\pi} E_e(x,t) e^{-ik_t x} = \left[1 + 2i\beta\left|a_o\right|^2\right] \tilde{E}_p(k_t) + \\ &+ \frac{i\beta\left|a_o\right|^2}{2\pi} \left\{ \int e^{2ik_b x} e^{i\theta(x,t)} e^{-ik_t x} E_p(x)\, dx + \int e^{-2ik_b x} e^{-i\theta(x,t)} e^{-ik_t x} E_p(x)\, dx \right\} \end{aligned} \tag{5.25}$$

where the transferred wavevector k_t is defined as $k_t = k_p \sin\alpha$ and $\tilde{E}_p(k)$ is the Fourier transform of the transverse profile $E_p(x)$ of the probe beam.

If we assume the waist σ_p of the incident probe beam to be much larger than the coherence length l_c of the atom laser and we consider only the scattering at an angle close to the Bragg condition $k_t = 2k_b$, eq.(5.25) can be rewritten in the simpler form

$$E_s(\alpha,t) \simeq \beta\left|a_o\right|^2 \int \frac{dx}{2\pi}\, e^{i(2k_b - k_t)x} e^{i\theta(x,t)} E_p(x). \tag{5.26}$$

Experimentally, a detector placed at an angle α would give a signal proportional to the mean intensity of the scattered light

$$\begin{aligned} I(\alpha) &= \left\langle \left|E_s(\alpha)\right|^2 \right\rangle = \\ &= \left|\beta\left|a_o\right|^2\right|^2 \left[\int dk''\, dk'''\, D(k - k'' - 2k_b, k' - k''' - 2k_b) \tilde{E}_p(k'') \tilde{E}_p(k''') \right]_{k=k'=k_t} \end{aligned} \tag{5.27}$$

with $D(k,k')$ defined as the Fourier transform of the standing wave phase correlation function

$$D(k,k') = \int\int \frac{dx}{2\pi} \frac{dx'}{2\pi}\, e^{i(k'x' - kx)} \left\langle e^{i\theta(x,t)} e^{-i\theta(x',t)} \right\rangle = \frac{\eta/\pi}{k^2 + \eta^2} \delta(k - k'). \tag{5.28}$$

In our $\sigma_p \gg l_c$ case, the broadening due to the finite coherence of the standing wave profile described by $D(k,k')$ is much larger than the broadening due to the finite laser waist σ_p, so that the scattering lineshape can be rewritten as

$$I(\alpha) \propto \frac{\eta}{((k_p \sin\alpha - 2k_b)^2 + \eta^2}. \tag{5.29}$$

This means that the coherence length of the atom laser is easily inferred from the angular linewidth of the scattered peak.

In physical terms, this result can be explained just by thinking of the standing wave in front of the atomic mirror as a succession of different and uncorrelated pieces of length $l_c/2$, each of them scattering light in the $k_t \simeq 2k_b$ with a different and random phase; from the indetermination principle, a finite length $l_c/2$ corresponds to an uncertainty in the momentum roughly equal to $\Delta k_t = \eta = 2/l_c$. From a condensed-matter point of view, such an effect can be related to the broadening of the diffraction peaks from crystals which occurs in the presence of disorder; our specific model for the phase diffusion corresponds to the case of an uneven separation of lattice planes [243, chap.7.4].

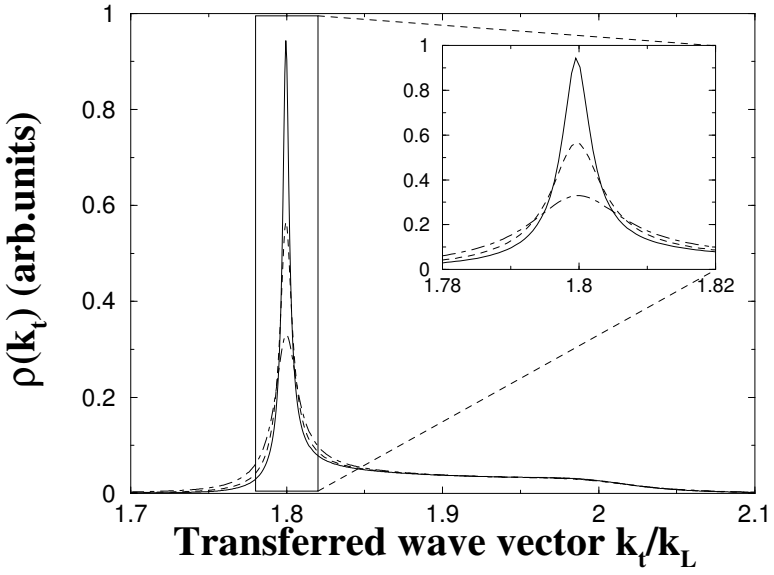

FIGURE 5.15: Angular diffraction pattern for different values of the atom laser linewidth: $\gamma_a/\omega_{Br} = 3\times10^{-4}$ (solid), $\gamma_a/\omega_{Br} = 6\times10^{-4}$ (dashed) and $\gamma_a/\omega_{Br} = 1.2\times10^{-3}$ (dot-dashed). Inset: enlargement of the Bragg peak at $k_t \simeq 2\times0.9k_L$ which corresponds to the standing wave pattern in front of the DBR atomic mirror.

If the probe beam has a non-negligible overlap with the optical potential of the mirror, the atomic density profile experienced by the probe is not simply the sinusoidal one given by eq.(5.22) but presents additional features due to the complicate shape of the atomic wavefunction inside the DBR mirror. The corresponding lineshape for the scattered light is plotted in fig.5.15: in addition to the Lorentzian peak at $k_t \simeq 2k_a$

corresponding to the diffraction on the standing wave pattern in front of the DBR atomic mirror, there is a broad plateau extending up to $k_t \simeq 2k_L$ due to the sharp decay of the atomic density as well as to its additional periodicity inside the mirror (see fig.5.14 and in particular the inset of the second panel).

Conclusions and perspectives

This second part of the thesis has been devoted to the study of atom optical effects from the point of view of photon optics: the strict parallelism between the behaviour of matter waves in external potentials and the behavior of light waves in dielectric structures has been emphasized and exploited in order to get a deeper insight on both systems via cross-fertilization effects.

In the first chap.4, we have given a general overview on interacting atomic matter waves in external potentials: the effect of the atom-atom interaction potential turns out to be analogous to an intensity-dependent refractive index for light waves, the external potential behaves as a linear dielectric constant for matter waves and the atomic spin is equivalent to the polarization of electromagnetic waves. Thanks to this strict analogy, the same theoretical approaches can be used for the description of both systems: after a general review on the main features of some of the most relevant approaches, a specific attention is paid to the mean-field theory, which is actually one of the most important tools for the study of the dynamics of the coherent matter waves of Bose-condensed samples. Very remarkably, the photonic version of mean-field theory is nothing else than the classical electrodynamics in nonlinear dielectric media which has been extensively used in the first part of the thesis; as it is well-known, such a theory well describes the dynamics of coherent laser light in conventional material.

In chap.5, we exploit the analogy between the behavior of matter waves in optical potentials and the behavior of light waves in dielectric structures in order to study the atomic reflection from optical lattices: as in the case of the electrons moving in a crystal or in the case of light propagating along a DBR mirror, the atomic dispersion in the periodic optical potential is characterized by allowed bands and forbidden gaps and the effective mass at band edge can be much lighter than the free-space mass. This suggests that a slow modulation of the optical lattice parameters could

act as a confining potential on atomic waves and eventually give rise to quasi-bound states similar to the localized modes of a DBR microcavity.[124,125] The very light atomic mass leads to an enhanced spacing of such cavity modes with respect to free-space and the confinement can be provided within a characteristic length scale of the order of a few optical wavelengths: this two facts cooperate in giving Fabry-Perot modes with spacings as large as one tenth of the atomic recoil energy. In addition, such modes can be easily driven by an external atom laser beam inciding on the lattice and give rise to very narrow features in the transmission spectra which can be exploited either as velocity filters or as resonant modes for the observation of nonlinear atom optical effects.

Two possible applications[238] of atomic reflection on optical lattices to the measurement of the atom laser coherence properties have been discussed in sec.5.4: a first method exploits the frequency dependence of the optical lattice transmittivity in order to filter the different atomic velocities in the beam and therefore determine its spectral distribution. The second method is instead based on the diffraction of light on the phase grating created by the atomic standing wave profile which is present in front of a good atomic mirror.

Given the narrow linewidth and the tight confinement of the mode wavefunction which can be obtained for matter waves using atomic Fabry-Perot interferometers based on modulated optical lattices, nonlinear atom optical effects are expected to occur at rather low intensities; with respect to the photonic counterpart, atom-atom interactions are generally much stronger and, for the specific arrangement of sec.5.3, the atomic flux value required for the switching on of the atomic bistable element has been estimated to be of the order of $10^{13}\mathrm{at/cm^2s}$; a similar value for the case of visible light would correspond to an intensity of the order of a few $\mu\mathrm{W/cm^2}$.

As new kinds of optical cavities are being actively studied so as to observe nonlinear optical effects at a low light level and therefore have the possibility to taylor the coherence properties of the transmitted beam down to the single photon level, the very low threshold atomic fluxes which are required for the observation of nonlinear atom optical effects look very promising from the point of view of controlling the quantum correlations of a beam down to the single atom level. Very remarkably, the modulated optical lattice arrangement proposed in chap.5 should be able to give interaction energies large enough for the nonlinearity parameter $N_o = \gamma/\omega_{nl}$ to be appreciably smaller than 1.

The third part of the thesis is devoted to the study of effects which go beyond the mean-field description of the (atomic or photonic) Bose field. In chap.6, a single-mode system will be discussed, whose formal simplicity allows for a numerical study in terms of quantum master equation; in particular, we shall check the accuracy of the mean-field results in the weak nonlinearity limit. In the opposite strong nonlinearity case, the discrete nature of the field turns out to be instead important and peculiar nonclassical correlations appear in the transmitted beam.

While for the simplified single-mode problem a numerical solution of the quantum master equation is a tractable problem, it quickly becomes unfeasible if the problem involves even just a few modes of the field. In particular, such an approach can not be used for planar systems such as DBR microcavities, in which confinement is present only in one dimension and the particles are free to move along the two other dimensions. Similar difficulties are encountered also in the study of current Bose condensed atomic clouds, for which the trapping frequencies are definitely not strong enough for a single-mode approximation to be valid and interactions may give rise to a small but finite non-condensed fraction even at zero temperature.

The absence of simple and efficient analytical or numerical schemes allowing for calculations to be performed in the general case of multimode systems with strong interactions has encouraged the quest for different formulations of the quantum Bose field problem. In chap.7 we shall discuss the principles of a novel approach based on the stochastic evolution of a macroscopic wavefunction; after proving on a mathematical basis its validity and stability properties in the most general case, we shall present first examples of its application to simple physical systems.

Part III

Quantum (atom) optics

Introduction

After having given in the previous two parts a detailed account of the mean-field dynamics of matter and light fields in respectively optical lattices and semiconductor DBR microcavities, this third part will cope with effects which can not be described in the framework of a mean-field theory since they involve the detailed quantum statistical properties of the Bose field under examination.

Although quantum optics of the light field has been an active field of research already for several decades, the weakness of the optical nonlinearity of current materials has in most cases forbidden the observation of quantum effects which are much more than a correction to the classical mean-field result. For this reason, much of the calculations have been performed with approximate theories which keep track of quantum fluctuations around the mean-field in a linearized way; only very recently, an active interest has been focussed on the possibility of achieving a regime in which photons interact strongly with each other: optical materials with very strong nonlinearities as well as very high Q-valued cavities have been investigated so as to realize systems in which the optical nonlinearity is triggered by a very small number of photons. In this case, the quantum state of the field can be manipulated down to the single quantum level so as to generate nonclassical and even entangled states of the field.

On the other hand, recent theoretical work on atomic Fabry-Perot interferometers has shown that the use of spatially modulated optical lattices allows for well separated cavity modes with narrow linewidths and tight longitudinal confinement and, in particular, atom-atom interactions have been predicted to give rise to atom optical bistability with a very low threshold value of the order of 10^{13}at/cm^{2}s for the incident atomic flux. Provided transverse motion is appropriately frozen by means of a single-mode atomic waveguide, the isolated cavity resonance can show a nonlinear coupling ω_{nl} comparable or even larger than the mode linewidth γ so as give a criti-

cal number N_o smaller than one. Since in this regime a very small number of atoms is required in the cavity mode to substantially affect its transmission properties, the mean-field approach can not be accurate and the peculiar coherence properties of the cavity field have to be described by a complete quantum theory.

This third part of the thesis is devoted to the discussion of effects which go beyond the mean-field description of the atomic or photonic Bose field. In the first chap.6 we consider a single-mode system which, thanks to its simplicity, allows for an exact numerical solution of the quantum master equation directly in the Fock state basis. Our calculations confirm the expectation that mean-field theory gives results which are correct in the weak nonlinearity ($N_o \gg 1$) case, i.e. when a large number of field quanta in the cavity mode are necessary for appreciable nonlinear effects; in this case, quantum fluctuations can be accurately described in a linearized way by the stochastic differential equations of Positive-P representation in their linearized version. The discrete nature of the field results instead important in the opposite strong nonlinearity ($N_o \leq 1$) case, in which peculiar nonclassical correlations appear in the transmitted beam in both the optical limiting and the optical bistability cases.

While the evolution in terms of quantum master equation in a Fock state basis is a numerically tractable problem in the case of the single-mode cavity, it quickly becomes unfeasible if the problem involves even just a few modes of the field; in particular, it can not be applied to planar geometries such as DBR microcavities in which confinement is present in just one dimension and the particles are free to move along the two other dimensions. Although at mean-field level the symmetry of the system guarantees conservation of the momentum along the plane for all particles, collisional effects beyond the mean-field are expected to produce correlated pairs of quanta with non-vanishing relative momentum; this means that all the modes of the field have to be simultaneously considered in the calculations, which results into a Hilbert space of an enormous dimensionality. A similar problem is encountered in the study of current trapped Bose condensates, in which the rather weak confinement frequency of the magnetic or optical trap prevents the single-mode approximation from being valid. In addition to the thermal cloud of uncondensed atoms unavoidably present at finite temperature, interactions can themselves give a small quantum depletion of the condensate even at zero temperature.

Several techniques have recently been developed for the determination of the dynamical and coherence properties of such a multimode quantum field. Besides the quantum kinetic theories of Gardiner and Zoller and the classical many-body

techniques, the complexity of which falls beyond the scope of the present thesis, a straightforward generalization of the Positive-*P* representation to multi-mode systems has been applied to strongly interacting systems; although some interesting results have been obtained with such a technique, the usual divergence problems have forbidden it from being applied in full generality.

For this reason, an intense quest for new formulations of the bosonic many-body problem have been pursuited by several groups: in chap.7, we shall present a novel approach based on the stochastic evolution of a macroscopic wavefunction. The general idea of the method consists in generalizing the Gross-Pitaevskii equation introducing a new stochastic term in the evolution of the macroscopic wavefunction so as to recover the exact dynamics after the average over the stochastic noise. Under appropriate conditions on the specific form of the stochastic terms, we shall prove that the time evolution described by the stochastic dynamics is equivalent to the complete many-body problem and therefore able to recover all the quantum correlations which appear in the quantum gas following atom-atom interactions. Thanks to the fact that the conditions for recovering the exact dynamics do not completely determine the form of the stochastic equation, different schemes with profoundly different statistical and stability properties can be chosen. One of such schemes is a reformulation of the Positive-*P* representation: since the solution of the stochastic equations are subject to divergences within a finite time, this scheme has a limited practical utility. Our approach being very general, it has been possible to find schemes which have regular solutions for all times; in this case, the only limitation turns out to be the computational time required for an accurate Monte Carlo sampling of the observables. The chapter is concluded with the presentation of two examples of application of the method to simple physical systems such as a two-mode model of a Josephson junction and a one dimensional Bose gas. For the two-mode system, a direct numerical integration of the Schrödinger equation in the Fock basis can also be performed: the successful comparison with Monte Carlo calculation has provided further confirmation to our stochastic wavefunction method.

Chapter 6

Quantum theory of the single-mode nonlinear (atomic) Fabry-Perot cavity

In the present chapter, we investigate the coherence properties of the atomic beam which is transmitted through a single-mode atomic cavity when the cavity is driven by a monochromatic and coherent atom laser beam: the field dynamics is numerically studied by solving the full quantum master equation for the cavity mode and the results are physically interpreted in comparison with the available approximate theories. Given the strict analogies between the behaviour of light waves in DBR microcavities and matter waves in optical lattices, these predictions are definitely not limited to atomic systems, but can be freely transferred to photonic systems as well.

As expected, mean-field theory is found to be accurate in the weak nonlinearity limit in which an appreciable nonlinear modulation of the transmission requires the presence of a large number of atoms in the cavity mode. Within MFT, the atomic Bose field is considered as a classical C-number field and its fluctuations around the classical steady-state are treated in a linearized way by means of the stochastic differential equations of Positive-P representation in their linearized form.

In the opposite strong nonlinearity case, when the transmission state is substantially modified by the presence of a single atom in the cavity mode, the discrete nature of the matter field results important: MFT, which is based on a classical field assumption, breaks down and a full quantum calculation results necessary in order to accurately describe the peculiar nonclassical properties of the transmitted beam.

For the specific case of an incident field at resonance with the empty cavity mode, the numerical solution of the full master equation predicts a sort of *atom blockade* effect, which closely reminds the well-known Coulomb blockade effect of electronic transport through microscopic structures: if the electrostatic potential change following the injection of a single carrier is able to substantially affect the injection of the successive carriers, the current shot-noise results strongly suppressed. Analogously, atom-atom interactions in our FP cavity can be so strong that the presence of a single atom shifts the mode frequency off-resonance from the incident atom laser beam and the following atoms are effectively forbidden from resonantly entering the cavity before the first atom has left. For moderate incident intensities, the cavity therefore behaves as a two-level system and the transmitted atomic beam has the usual nonclassical properties of resonance fluorescence light, such as a strong antibunching.

Only at very large incident intensities –much larger than the saturation intensity of the effective two-level system– more than one atom can be forced to be in the cavity mode at the same time and a peculiar dependence on the incident intensity is found for both the coherent and the incoherent transmission. In this regime, some of the most peculiar features resulting from the numerical calculation are well explained by a dressed cavity model, in particular the frequencies of the incoherent transmission peaks.

For the case of a blue detuned incident atom laser beam and repulsive atom-atom interactions, the feedback of the nonlinearity on the transmission is instead positive and optical bistability is predicted by mean-field theory. Given the discrete nature of the field, quantum fluctuations may however allow for tunneling events from one branch of the bistability curve to the other so that the mean-field steady states are not true steady states for an indefinite time any more; as expected, the larger the critical number N_o, the smaller the tunneling rate. From the point of view of the density matrix, there is just one steady state of the system which consists of a (generally statistical) mixture of the two mean-field steady states, the "transmitting" and the "non-transmitting" ones; the slow tunneling rate from one of them to the other reflects into the appearance of a slow time scale τ_s in the correlation functions, much slower than the characteristic damping time of the cavity γ^{-1}.

If the detuning is such that the energy of the cavity filled of N atoms is exactly on resonance with the injection process of N atoms, a sort of N-atom transmission process occurs, which is the atom optical analog of N-photon absorption; in the

weak incident intensity limit, atoms are therefore most likely transmitted in bunches containing a number of atoms of the order of N and separated by intervals in which no atom is present; this reflects into peculiar coherence properties of the transmitted beam.

In sec.6.1, we shall introduce the Hamiltonian of the model and we shall describe the physical processes involved, as well as the physical parameters which control them.

In sec.6.2 we shall address the weak nonlinearity case, in which the full numerical calculation is well reproduced by the mean-field theory with a linearized treatment of fluctuations.

In the two following sections, we shall discuss the numerical results obtained for the opposite case of a strong nonlinearity: the former (sec.6.3) deals with the case of a resonant incident atom laser, for which MFT would predict optical limiting. The latter (sec.6.4) deals instead with an incident beam blue detuned with respect to the empty cavity so as to give a positive feedback on the transmission; for this case, MFT would predict optical bistability.

6.1 The model

Consider a quasi-cw beam of atoms coherently extracted from a trapped Bose Einstein condensate (BEC) by means of a radio-frequency field or of a pair of optical beams in a Raman configuration. As we have discussed in detail in chap.4, given the coherent nature of the outcoupling mechanism used to transfer atoms from the trapped BEC to the propagating beam, the all-order coherence of the BEC is expected to transfer into a similar property for the *atom laser* beam. If the intensity of the outcoupled beam is weak enough not to deplete substantially the trapped BEC or this is continuously replenished, the atom laser can be modeled as a monochromatic classical C-number wave; phase fluctuations (sec.5.4) are neglected assuming their characteristic time scale to be much longer than all other characteristic times of the problem.

As shown in fig.6.1, suppose to inject such an outcoupled wave into a single mode atomic waveguide[215–225] in order to freeze the transverse atomic motion; in this way, the system behaves as a one-dimensional one. At the same time, the use of

a horizontal waveguide allows to counteract the effect of gravity, so that the longitudinal wavefunction of the outcoupled beam is simply a plane wave $\psi(x,t) = \psi_{inc}e^{i(k_L x - \omega_L t)}$ of frequency ω_L and momentum k_L.

Suppose now to send such a cw coherent atomic beam onto an atomic Fabry-Perot (FP) cavity, formed by a pair of parallel atomic mirrors which confine atomic matter waves in the space between them; atomic motion between the mirrors is quantized in discrete cavity modes, which are coupled to externally propagating modes because of the non-perfect reflectivity of the cavity mirrors. The most interesting schemes which realize such a device have been analyzed in detail in the chap.5: they are in general based on the optical potential applied to the atoms by far off-resonance laser fields: some of them[209–211] use a blue detuned laser field to create potential hills between which the atoms are confined; some others[124,125,212,213] use optical lattices in order to create the atomic analog of DBR microcavities and give features which are generally more favorable from the nonlinear atom optics point of view.

If the frequency ω_L of the incident atom laser beam is far from resonance with all the cavity modes, the atomic beam is effectively forbidden from entering the cavity and therefore is nearly completely reflected back. On the other hand, if ω_L is close to the frequency ω_o of one of the cavity modes, this latter is resonantly excited: a substantial fraction of the incident atoms resonantly enter the cavity and are transmitted on the other side where they form the transmitted beam.

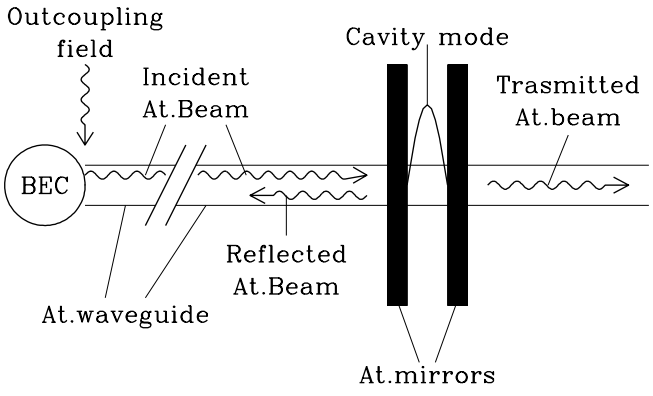

FIGURE 6.1: Sketch of the experimental scheme under examination

If we assume that the frequency spacing of the different cavity modes is much larger than both the laser linewidth and the atom-atom interaction energy, and if we suppose the atom laser frequency ω_L to be close to a cavity resonance, only this mode is effectively excited, while the other ones are safely neglected. If we develop the atomic field inside the cavity on its eigenstates

$$\hat{\psi}(x) = \sum_{\alpha} \phi_{\alpha}(x)\hat{c}_{\alpha}, \tag{6.1}$$

this *single-mode* approximation is equivalent to assuming all the $\hat{c}_{\alpha}$ to be effectively negligible but for one of them, which will be called in the following $\hat{a}$; let $\phi(x)$ be the wavefunction of such mode.

Under this approximation, the driven atomic cavity can be described by the same model Hamiltonian used for the single-mode nonlinear Fabry-Perot interferometer in sec.2.2

$$\mathcal{H} = \hbar\omega_o \hat{a}^{\dagger}\hat{a} + \hbar\omega_{nl}\hat{a}^{\dagger}\hat{a}^{\dagger}\hat{a}\hat{a} + i\hbar k_{inc}\psi_{inc}\hat{a}^{\dagger}e^{-i\omega_L t} + \text{h.c.} \tag{6.2}$$

where $\hat{a}$ and $\hat{a}^{\dagger}$ are respectively the destruction and creation operators for the localized cavity mode; thanks to the Bose nature of the atomic species under examination, such operators satisfy the usual Bose commutation relation $\left[\hat{a}, \hat{a}^{\dagger}\right] = 1$.

The first term of the Hamiltonian eq.(6.2) describes linear oscillations at frequency ω_o; the second term keeps track of the (collisional) atom-atom interactions, whose strength is quantified by the ω_{nl} parameter. This is easily related to the cavity mode wavefunction $\phi(\boldsymbol{x})$ and the s-wave scattering length a_o:[135]

$$\omega_{nl} = \frac{2\pi\hbar a_o}{m}\int d^3x \left|\phi(x)\right|^4; \tag{6.3}$$

as expected, its sign is positive (negative) for repulsive (attractive) interactions. Since the atomic density inside the cavity is, at resonance, much larger than the density in the incident atom laser beam, atom-atom interactions outside the cavity are safely neglected; in addition, the single-mode approach neglects all those processes in which atoms are transferred from the mode $\hat{a}$ to the other modes of the cavity by the interactions; such an approximation is generally justified provided the interaction energy is much smaller than the spacing of adjacent cavity modes and parametric resonances of the kind $2\omega_{\alpha} = \omega_{\alpha'} + \omega_{\alpha''}$ are absent.

The driving of the cavity mode by the incident atom laser beam is taken into account by the last two terms; thanks to the all-order coherence assumption, the driving

field is well modeled as a monochromatic and classical $\boldsymbol{C}$-number field $\psi_{inc}e^{-i\omega_L t}$ which forces the cavity mode to oscillate; in particular, the coupling coefficient k_{inc} is proportional to the transmission amplitude of the front cavity mirror. Analogously, the amplitude of the transmitted field through the cavity $\hat{\psi}_{tr}$ is proportional to the internal amplitude $\hat{a}$ times a η_{tr} coefficient proportional to transmission amplitude of the back mirror; all the statistical properties of the transmitted field can therefore be expressed in terms of the internal field ones.[1,49]

From the point of view of the sole cavity, the coupling to the continuum of propagating external modes through the non-perfectly reflecting mirrors, which underlies the driving of the cavity mode by the incident beam as well as the formation of the transmitted beam, is a dissipative process and thus can not be included in a simple Hamiltonian formalism.

From the general theory of quantum damping, it follows that the dynamics of the single-mode cavity under examination is completely described by the following *master equation* for the density matrix $\hat{\rho}$

$$\frac{\partial \hat{\rho}}{\partial t} = \frac{i}{\hbar}\left[\hat{\rho}, \mathcal{H}\right] + \gamma D\left[\hat{a}\right]\hat{\rho}; \tag{6.4}$$

the first (Hamiltonian) term keeps track of the driving, the linear oscillations and the atom-atom interactions, while the second term keeps track of the dissipative effects. This latter has been written in terms of the superoperator $D\left[\hat{a}\right]\hat{\rho}$, defined as usually as

$$D\left[\hat{a}\right]\hat{\rho} = \hat{a}\hat{\rho}\hat{a}^{\dagger} - \frac{1}{2}\left(\hat{a}^{\dagger}\hat{a}\hat{\rho} + \hat{\rho}\hat{a}^{\dagger}\hat{a}\right); \tag{6.5}$$

the coefficient γ has the usual meaning of damping rate of the cavity excitation.

In our actual calculations, the steady-state of the density matrix $\hat{\rho}_{\mathrm{eq}}$ is determined by letting $\hat{\rho}$ evolve according to eq.(6.4) for a time much longer than the characteristic relaxation time of the system under examination. The expectation values $\left\langle \hat{O} \right\rangle$ of the observables $\hat{O}$ of interest are calculated as mean values over the steady-state density matrix $\mathrm{Tr}\left[\hat{\rho}_{\mathrm{eq}}\hat{O}\right]$; for the determination of a two-time correlation function $\left\langle \hat{O}_2(t)\hat{O}_1(0) \right\rangle$, we have first to apply the observable $\hat{O}_1$ to the left of $\hat{\rho}_{\mathrm{eq}}$, then to let the resulting density matrix $\hat{O}_1\hat{\rho}_{\mathrm{eq}}$ evolve for a time t according to the master equation eq.(6.4) and finally to take the expectation value of second observable $\hat{O}_2$.

From a numerical point of view, several different representations can be chosen for $\hat{\rho}$;[49,157,244] our actual simulations have been performed using a Fock representation

in which the density matrix is expanded in the number-state basis $M_{n,n'} = \langle n|\hat{\rho}|n'\rangle$. The time evolution is numerically performed using a standard fourth order Runge-Kutta method and then checking the numerical stability of the result with respect to a reduction in the integration time step.

In the case of symmetric systems, in which the front and back mirrors have the same transmission properties, the k_{inc} and η_{tr} coefficients are related to the damping γ by the relations $k_{inc} = (\gamma v/2)^{1/2}$ and $\eta_{tr} = (\gamma/2v)^{1/2}$, which follow from the well-known property that the transmission through any linear, symmetric and non-absorbing cavity is, at exact resonance, exactly one [50, chap.9]; $v = (2\hbar\omega_o/m)^{1/2}$ denotes the (group) velocity of free atoms which incide on the cavity at resonance.

Depending on the specific scheme adopted for the cavity, processes of different kinds can be responsible of additional incoherent non-radiative losses which are the atomic analog of light absorption in materials; as we have seen in sec.4.1, if the confinement is a magnetic one, Majorana spin flips may occur, while spontaneous emission of light may take place in presence of an optical confinement. Such effects have to be handled by means of additional terms in eq.(6.4) of the same form $\gamma_{\rm abs} D\left[\hat{a}\right]\hat{\rho}$: their main consequences are a broadening of the resonance and a reduction of the peak transmittivity by a factor $(\gamma + \gamma_{\rm abs})/\gamma$.

When the single-mode nonlinear cavity model is applied to the optical case, the field operator $\hat{a}$ describes the amplitude of the electromagnetic field in the cavity mode and the nonlinear interaction between photons results from eq.(2.11) proportional to the third-order nonlinear polarizability $\chi^{(3)}$ of the cavity material. The main difference consists in the strength of the nonlinear coupling, which can be quantified by the *critical number* $N_o = \gamma/\omega_{nl}$ of quanta which are necessary for having an appreciable nonlinear effect on the transmittivity. Since the optical nonlinearity of usual materials is very weak, conventional optical resonators are characterized by $N_o \gg 1$, which means that a huge number of photons have to be excited inside the cavity before the effect of optical nonlinearity to be apparent. For the description of such systems, the mean-field approximation performed in sec.2.2 is expected to give accurate results; in the next sec.6.2 we shall confirm this statement by directly comparing the mean-field predictions with the results of the exact numerical calculation.

Very recently, an active interest has been focussed on the possibility of achieving the $N_o \leq 1$ regime with light: optical materials with very strong nonlinearities as well as

very high Q-valued cavities have been investigated in order to generate nonclassical states of the field and even entangled ones.

First of all, high finesse optical cavities containing a small number of atoms have been investigated in the realm of cavity quantum electrodynamics:[245] in this case, the nonlinearity mechanism is the intrinsic one of two-level atoms: with a smaller number of atoms, a smaller number of photons is required for the saturation of the transition, but at the same time the weaker polarizability imposes a stronger requirement on cavity finesse. Furthermore, an additional loss channel is introduced by the spontaneous decay of excited atoms.

Secondly, quantum coherence effects in multilevel atoms dressed by strong pump fields have been theoretically shown to give enhanced nonlinear susceptibilities as well as depressed absorptions:[246–250] apart from some difficulties related to the specific level scheme chosen,[251–255] such arrangements are now beginning to be exploited for low intensity nonlinear optics experiments[256,257] as well as for the study of very slow pulse propagation.[258]

Finally, new cavity geometries with enhanced Q-factors are also being investigated: in particular, the whispering gallery modes of cylindrical or spherical resonators look very promising, since fused silica spheres and disks with spatial sizes of the order of micrometer and very weak surface roughness are currently available; unfortunately, the nonlinear susceptibility of fused silica is very weak and the insertion of active impurities may result necessary for the study of nonlinear processes.[28,259]

On the other hand, recent theoretical work on atomic Fabry-Perot interferometers[124,125] has shown that the use of spatially modulated optical lattices allows for well separated cavity modes with narrow linewidths and tight longitudinal confinement: in particular, it has been shown that atom-atom interactions can give rise to atom optical bistability with a very low threshold intensity of the order of $10^{13}\mathrm{at/cm^2s}$. Provided transverse motion is appropriately frozen by means of a single-mode atomic waveguide,[215–225] such systems behave as effectively one dimensional ones; thanks to the transverse confinement, the isolated cavity resonance can show a nonlinear coupling ω_{nl} comparable or even larger than the mode linewidth γ and therefore a critical number $N_o \leq 1$. In this regime, MFT breaks down and a full quantum calculation based on the master equation eq.(6.4) is required; the peculiar coherence properties which result from the calculations will be discussed in sec.6.3.

6.2 Weak nonlinearity case: mean field theory and linearized fluctuations

In the mean-field theory, the atomic field is described by a classical $\boldsymbol{C}$-number field equal to the mean value of the quantum field $\psi(\boldsymbol{x},t) = \left\langle \hat{\psi}(\boldsymbol{x},t) \right\rangle$ and factorization is assumed for the operator products involved in the motion equation for the macroscopic wavefunction $\psi(\boldsymbol{x},t)$.

Using the many-body theory of 3D Bose gases,[182,260] this approach can be proven to be accurate in the case of dilute systems for which the mean interparticle distance $n^{-1/3}$ is much larger than the scattering length a_o; current trapped atomic condensates well satisfy such a inequality. In other terms, for a constant mean-field interaction energy (proportional to na_o), MFT is valid in the $a_o \to 0$ and $n \to \infty$ limit in which the interaction energy per particle is vanishing small and the discrete nature of the matter field effectively washed out.

For the single mode cavity actually under examination, the mean-field approach leads to a single differential equation for the mean value of the cavity field $a(t) = \langle \hat{a}(t) \rangle$ of the form

$$\frac{da}{dt} = -i\left(\omega_o + 2\omega_{nl}\left|a\right|^2\right)a + k_{inc}\psi_{inc}e^{-i\omega_L t} - \frac{\gamma}{2}a \tag{6.6}$$

from which we can immediately obtain the steady state value $a(t) = \bar{a}e^{-i\omega_L t}$ with

$$\bar{a} = \frac{ik_{inc}\,\psi_{inc}}{\omega_L - \omega_o - 2\omega_{nl}\left|\bar{a}\right|^2 + i\gamma/2}. \tag{6.7}$$

If fluctuations of the cavity field are completely neglected, the transmitted field $\hat{\psi}_{tr} = \eta_{tr}\hat{a}$ has the same all-order coherence properties as the incident one.

For a given value of the mean-field interaction energy $\omega_{\rm mf} = 2\omega_{nl}\left|\bar{a}\right|^2$, this approximation is valid in the limit of very a small interaction energy ω_{nl} per atom; in this case, in fact, fluctuations are irrelevant and the discreteness of the atomic field is canceled by the very large number of atoms present in the cavity.

Although the application of Positive-P representation to the present system suffers from the usual divergence problems,[169] lowest-order fluctuations around the mean value can however be obtained by studying the linearized[160] version of the same stochastic equations for which the solution is mathematically defined at any time. In some sense, this linearization procedure generalizes to driven dissipative systems

the well-known Bogoliubov approach[260] for the description of the lowest-order fluctuations in Bose condensates.

Within the Positive-*P* representation of the quantum field, the dynamics of the field in a nonlinear single-mode cavity is described by a pair of stochastic differential equations

$$d\alpha = \left[-i\left(\omega_o + 2\omega_{nl}\alpha^*\alpha\right)\alpha + k_{inc}\psi_{inc}e^{-i\omega_L t} - \frac{\gamma}{2}\alpha\right]dt + \sqrt{-2i\omega_{nl}\alpha^2}d\eta_1 \tag{6.8}$$

$$d\alpha^* = \left[i\left(\omega_o + 2\omega_{nl}\alpha\alpha^*\right)\alpha^* + k^*_{inc}\psi^*_{inc}e^{i\omega_L t} - \frac{\gamma}{2}\alpha^*\right]dt + \sqrt{2i\omega_{nl}\alpha^{*2}}d\eta_2 \tag{6.9}$$

for the field variables α and α^*, which are now complex conjugate of each other only in the mean. The noise terms $d\eta_i$ are independent Gaussian noise terms ($\overline{d\eta_i} = 0$, $\overline{d\eta_i\, d\eta_j} = \delta_{i,j}dt$).[239] In terms of the stochastic field variables α and α^*, the mean value of any normally ordered observable can be expressed as

$$\left\langle \hat{a}^{\dagger m}\hat{a}^m \right\rangle = \overline{\alpha^{*m}\alpha^m}. \tag{6.10}$$

Linearizing the stochastic equations eqs.(6.8) and (6.9) around the steady-state $\alpha = \bar{a}e^{-i\omega_L t}$, $\alpha^* = \bar{a}^* e^{i\omega_L t}$ of the deterministic evolution, we get to a pair of linear stochastic equations for the slowly-varying field fluctuations $\delta\alpha = \alpha e^{i\omega_L t} - \bar{a}$ and $\delta\alpha^* = \alpha^* e^{-i\omega_L t} - \bar{a}^*$

$$d\,\delta\alpha = \left[-i\left(-\Delta\omega + 4\omega_{nl}\left|\bar{a}\right|^2\right)\delta\alpha - 2i\omega_{nl}\bar{a}^2\,\delta\alpha^* - \frac{\gamma}{2}\delta\alpha\right]dt + \sqrt{-2i\omega_{nl}\bar{a}^2}d\eta_1 \tag{6.11}$$

$$d\,\delta\alpha^* = \left[i\left(-\Delta\omega + 4\omega_{nl}\left|\bar{a}\right|^2\right)\delta\alpha^* + 2i\omega_{nl}\bar{a}^{*2}\,\delta\alpha - \frac{\gamma}{2}\delta\alpha^*\right]dt + \sqrt{2i\omega_{nl}\bar{a}^{*2}}d\eta_2. \tag{6.12}$$

from which all the stationary moments can be extracted using the standard techniques for the solution of linear stochastic differential equations.[239] We shall not reproduce here all the details of the calculations, which can be found in the original paper,[160] but we shall only give the final results and compare them with the exact result of our numerical calculations.

The mean transmitted intensity results given by

$$I_{\rm tr} = I_{\rm coh} + I_{\rm nc} = \frac{\gamma}{2}\left\langle \hat{a}^\dagger\hat{a}\right\rangle = \frac{\gamma}{2}\left[N + \frac{\omega^2_{\rm mf}}{2\left|\lambda(\omega_L)\right|}\right]; \tag{6.13}$$

the first term $I_{\rm coh}$, which describes the coherently (i.e. elastically) transmitted intensity, corresponds to the mean-field amplitude $\bar{a}$; the second one $I_{\rm nc}$ accounts for quantum fluctuations and therefore describes the incoherently (inelastically) transmitted intensity. With $\Delta\omega = \omega_L - \omega_o$ we have denoted the detuning of the incident

atom laser beam with respect to the empty cavity mode; $N = |\bar{a}|^2$ is the mean-field number of quanta in the cavity mode and $\omega_{\rm mf} = 2\omega_{nl}N$ is the corresponding frequency shift of the cavity mode; finally, for notational simplicity, we have set

$$\lambda(\omega) = \left\{ i\left[(\omega - \omega_L) + (\Delta\omega - 2\omega_{\rm mf})\right] + \frac{\gamma}{2} \right\} \cdot \\ \cdot \left\{ i\left[(\omega - \omega_L) - (\Delta\omega - 2\omega_{\rm mf})\right] + \frac{\gamma}{2} \right\} - \omega_{\rm mf}^2 \quad (6.14)$$

As expected, for a fixed value of the mean-field interaction energy $\omega_{\rm mf}$, the contribution of fluctuations is inversely proportional to the number of atoms in the cavity mode and thus vanishing small in the classical limit ($\omega_{nl} \to 0$, $N \to \infty$). With a similar procedure we can determine the one-time second order correlation function $g^{(2)}(0)$:

$$g^{(2)}(0) = \frac{\left\langle \hat{a}^\dagger \hat{a}^\dagger \hat{a} \hat{a} \right\rangle}{\left\langle \hat{a}^\dagger \hat{a} \right\rangle^2} = 1 + \frac{\omega_{\rm mf}}{|\lambda(\omega_L)|\, N} \left(\Delta\omega - \omega_{\rm mf}\right). \quad (6.15)$$

Finally, a Fourier transform of the two-times first order correlation function leads to the spectrum of the transmitted intensity

$$S(\omega) = S_{\rm coh}(\omega) + S_{\rm nc}(\omega) = \frac{\gamma}{2}\mathcal{F}_t \left\langle \hat{a}^\dagger(t)\hat{a}(0) \right\rangle = \\ = \frac{\gamma}{2} \left\{ N\delta(\omega - \omega_L) + \frac{\omega_{\rm mf}^2}{2\pi\, |\lambda(\omega)|^2} \right\} \quad (6.16)$$

in which we again recognize the elastic and inelastic contributions; the former corresponds to the delta-function peak at ω_L, while the latter gives a pair of (inelastic) Lorentzian peaks at the frequencies

$$\omega^{\pm} = \omega_L \pm \sqrt{\Delta\omega^2 - 4\Delta\omega\, \omega_{\rm mf} + 3\omega_{\rm mf}^2}; \quad (6.17)$$

which correspond to the dressed states of the driven system. As we have discussed in sec.3.3, poles at these same frequencies appear in the linear response of the driven system to additional probe beams. Whenever the argument of the square root is negative, the two peaks coalesce into a single one at ω_L.

These results are to be compared to the exact solution of the full master equation eq.(6.4) obtained using the numerical technique sketched in the previous section. In fig.6.2, we have plotted the coherent and the incoherent transmitted intensities $I_{\rm coh}$ and $I_{\rm nc}$ vs. the incident intensity $I_{\rm inc} = v\,|\psi_{inc}|^2$ for different values of the critical number $N_o = \gamma/\omega_{nl}$ at zero detuning $\Delta\omega = 0$. In the plots, the intensities have been

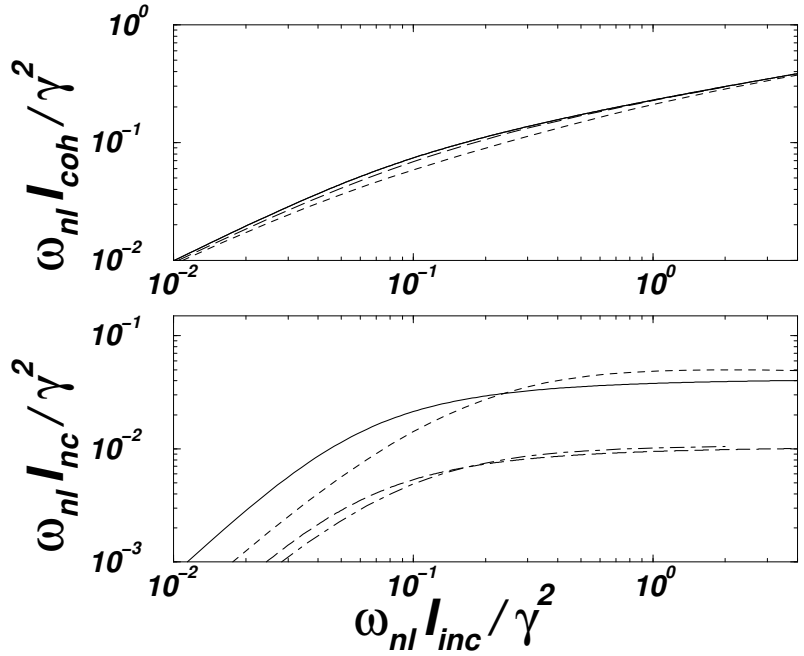

FIGURE 6.2: Transmission properties of a nonlinear Fabry-Perot interferometer in the weak nonlinearity (large N_o) regime: in the upper panel, coherent intensity $I_{\rm coh}$ as a function of the incident intensity $I_{\rm inc}$; in the lower one, incoherent intensity $I_{\rm nc}$. All intensities have been normalized to the characteristic intensity γ^2/ω_{nl}. In the upper panel, the solid curve is the result of the linearized approach, while the long- and short-dashed ones correspond to the exact calculations respectively for $N_o = 8$ and $N_o = 2$. In the lower panel, the solid and the long-dashed lines are again the approximate results, while the short-dashed and the dot-dashed are the exact ones. The upper curves are for $N_o = 2$ the lower ones are for $N_o = 8$.

normalized in units of the characteristic intensity $\gamma^2/\omega_{nl} = \gamma N_o$, so that the mean-field curves for the coherently transmitted intensity superimpose on each other exactly.

In the zero detuning $\Delta\omega = 0$ case we are considering, MFT (eq.(6.7)) predicts an optical limiter behavior for the transmitted intensity: for growing intensities, in fact, the mean-field interaction energy $2\hbar\omega_{nl}\,|a|^2$ tends to shift the cavity mode out off resonance with respect to the incident beam and thus to lower the effective transmittivity. In particular, while at low intensity the transmitted intensity grows linearly with the incident intensity, in the large intensity limit the transmitted intensity grows only as its power $1/3$. In a log-log scale, the transition between these two

regimes can be observed as a rather smooth bending.

The discrepancy of the MF result for the coherently transmitted intensity with respect to the exact one is concentrated mostly in the crossover region and, as expected, tends to disappear in the classical limit $N_o \to \infty$ (see upper panel of fig.6.2). An analogous comparison can be made for the incoherently transmitted intensity (see lower panel of the same figure): at lowest order (eq.(6.13)), such a quantity is a factor of N lower than the coherent contribution and thus its relative weight vanishes in the classical limit. As expected, the discrepancy of the MF result with respect to the exact one is of higher order in N_o^{-1}.

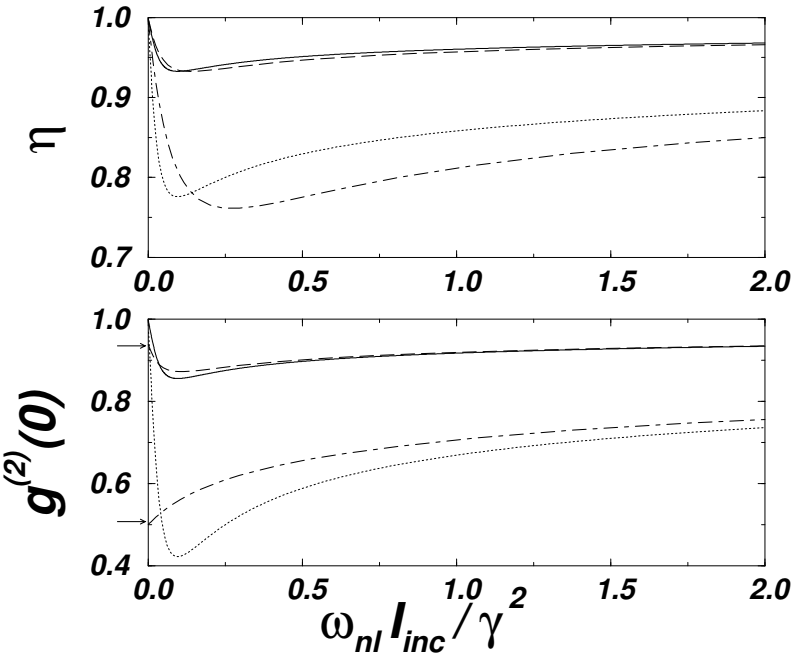

FIGURE 6.3: Coherence properties of the transmitted beam as a function of the incident intensity $I_{\rm inc}$: in the upper panel, long-time first-order coherence $\eta = I_{\rm coh}/I_{\rm tr}$; in the lower panel, one-time second-order coherence $g^{(2)}(0) = \langle \hat{a}^\dagger \hat{a}^\dagger \hat{a} \hat{a} \rangle / \langle \hat{a}^\dagger \hat{a} \rangle^2$. The solid and the dotted curves are the approximated results of linearized theory respectively for $N_o = 8$ and $N_o = 2$, while the long-dashed and the dot-dashed are the exact ones for the same parameter choices. The arrows in the lower panel are the predictions of the analytical expression eq.(6.21) for $g^{(2)}(0)$ in the low-intensity limit.

In the upper panel of fig.6.3, we have plotted the first order long time coherence of

the transmitted beam

$$\eta = \frac{I_{\rm coh}}{I_{\rm tr}} = \frac{\lim_{t\to\infty} \left|\langle \hat{a}^\dagger(t)\hat{a}(0)\rangle\right|}{\langle \hat{a}^\dagger(0)\hat{a}(0)\rangle} \tag{6.18}$$

as a function of the (normalized) incident intensity for different values of the critical number N_o. All curves show a single minimum at a value of the incident intensity which, being related to the crossover in the optical limiter response curve, results approximately proportional to γN_o; the depth of such a minimum is approximately inversely proportional to N_o. Perfect coherence $\eta = 1$ is recovered in the classical limit $N_o \to \infty$.

A similar behavior is found also for the one-time second-order coherence $g^{(2)}(0)$ which is plotted in the lower panel of the same figure; a value for $g^{(2)}(0)$ smaller than 1 means that the transmitted beam is antibunched, i.e. has reduced intensity fluctuations as compared to a classical coherent beam. Such a quantum property is a consequence of the optical limiter response and is at lowest order inversely proportional to N_o.

As previously, the MF result is found to keep track in a correct way of the lowest order fluctuations: the discrepancy with the exact result is in fact of higher order in N_o^{-1} for any incident intensity. In particular, for the low intensity limit $I_{\rm inc} \to 0$ the mean field theory predicts $g^{(2)} \to 1$ (see eq.(6.15)), since in this regime the system behaves as an effectively linear one. On the other hand, the exact calculation gives a value lower than 1, which is an unambiguous signature of the discrete nature of the field: while the $\boldsymbol{C}$-number variable which describes the field in the linearized treatment can assume any value, the quantum system can only be in a discrete ladder of states. For an incident beam at exact resonance with the empty cavity, the $|n=1\rangle$ state is on resonance, while the second excited one $|n=2\rangle$ is already out of resonance of a finite frequency $2\omega_{nl}$. A straightforward but somewhat lengthy analytical calculation for the steady state value of the density matrix $\hat{\rho}_{\rm eq}$ at lowest order in $I_{\rm inc}$ leads to the expressions

$$\rho_{11}^{\rm eq} \simeq \frac{4\left|k_{inc}\psi_{inc}\right|^2}{\gamma^2} \tag{6.19}$$

and

$$\rho_{22}^{\rm eq} \simeq \frac{8\left|k_{inc}\psi_{inc}\right|^4}{\gamma^2\left(\gamma^2+4\omega_{nl}^2\right)} \tag{6.20}$$

for the matrix elements $\rho_{11}^{\rm eq} = \langle n=1|\hat{\rho}_{\rm eq}|n=1\rangle$ and $\rho_{22}^{\rm eq} = \langle n=2|\hat{\rho}_{\rm eq}|n=2\rangle$. From these expressions, it is immediate to obtain an expression of the one-time second

order coherence function

$$g^{(2)}(0) = \frac{2\rho_{22}^{\rm eq}}{(\rho_{11}^{\rm eq})^2} = \frac{1}{1+4/N_o^2}, \tag{6.21}$$

which is valid in the low-intensity limit for any value of N_o. This exact analytical prediction is marked with horizontal arrows in the lower panel of fig.6.3 and the agreement with the numerical result is excellent. As expected, in the classical $N_o \to \infty$ limit, the analytical expression eq.(6.21) tends to the mean-field prediction of 1 and, at lowest order, the discrepancy is proportional to N_o^{-2}.

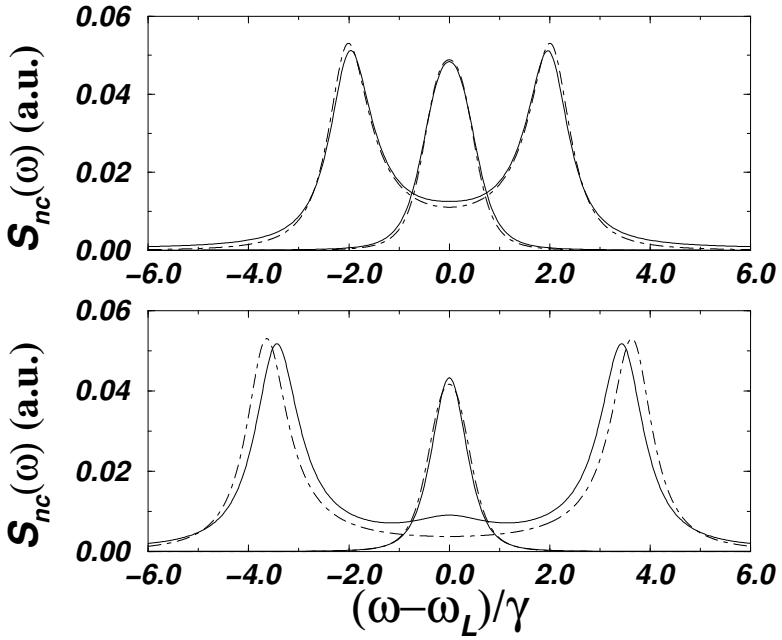

FIGURE 6.4: Incoherently transmitted intensity spectra: in the upper panel, $N_o = 8$; in the lower one, $N_o = 2$. The solid lines refer to the exact calculations, while the dot-dashed ones are the result of the linearized approach. The incident intensities are equal to $I_{\rm inc} = 0.64$ and $I_{\rm inc} = 16$ for the upper panel spectra, and to $I_{\rm inc} = 0.1$ and $I_{\rm inc} = 20$ for the lower panel ones.

Finally, in fig.6.4 we have plotted a few spectra of the inelastically transmitted intensity in the zero detuning ($\Delta\omega = 0$) case and we have compared the approximate result of MFT to the exact one. Apart from the small central peak at $\omega = \omega_L = \omega_o$ which appears at smaller values of N_o, both the position and the intensities of the external peaks as predicted by the MFT are in excellent agreement with the exact result. As previously, the larger the N_o parameter, the closer the similarity.

In the present section, we shall not specifically address the case of a detuned driving field $\Delta\omega \neq 0$ and we shall limit ourselves to a few remarks. In the case where the detuning has opposite sign with respect to the nonlinear frequency shift of the cavity mode, the feedback of the nonlinearity on the transmission is still negative and leads to the same optical limiter behavior previously described; only the frequencies of the dressed modes eq.(6.17) result different. On the other hand, when the detuning has the same sign as the nonlinear shift, the feedback of the nonlinearity results positive and MFT predicts the possibility of multiple steady-state solutions of eq.(6.7) for a single value of the incident intensity.[63] In this case, the linearized theory can account only for the fluctuations occurring in the neighborhood of each steady-state,[160] but it does not keep track of effects related to quantum tunneling from one steady-state to another.[49,156,244,261,262] Nevertheless, the numerical solution of the full master equation eq.(6.4) can provide us exact results for the coherence properties of the transmitted beam; this topic will be matter of sec.6.4.

6.3 Strong nonlinearity: the *(atom) blockade* effect

In the previous section we have discussed the solution of the quantum master equation eq.(6.4) in the weak nonlinearity $N_o \gg 1$ regime in which the exact numerical solution is accurately approximated by the analytic mean-field result. In that case, in fact, the behavior of the quantum field has been shown to be well reproduced by a classical field while the discrete nature of the field was taken into account simply by means of noise terms in the stochastic motion equations eq.(6.11)-(6.12). Unfortunately, an exact solution of the complete Positive-P equations eq.(6.8)-(6.9) does not mathematically exist for small values of the critical number N_o because of the well-known divergences of the wavefunction.[169] Since a relatively small value of the critical number N_o implies that only a moderate number of Fock states are actually involved in the dynamics, a numerical calculation in the Fock basis can be easily performed within a reasonable computation time; moreover, the results of the numerical calculations are themselves best understood in the number-state basis $|n\rangle$.

In this basis, the Hamiltonian of the driven nonlinear single-mode cavity has the

form:

$$\frac{\mathcal{H}}{\hbar} = \begin{pmatrix} 0 & \mathcal{E}_i e^{-i\omega_L t} & 0 & 0 & \\ \mathcal{E}_i^* e^{i\omega_L t} & \omega_o & \sqrt{2}\mathcal{E}_i e^{-i\omega_L t} & 0 & \\ 0 & \sqrt{2}\mathcal{E}_i^* e^{i\omega_L t} & 2\omega_o + 2\omega_{nl} & \sqrt{3}\mathcal{E}_i e^{-i\omega_L t} & \vdots \\ 0 & 0 & \sqrt{3}\mathcal{E}_i^* e^{i\omega_L t} & 3\omega_o + 6\omega_{nl} & \\ & & \cdots & & \end{pmatrix} \tag{6.22}$$

For a vanishing driving $\mathcal{E}_i = ik_{inc}\psi_{inc}$, the eigenvectors of $\mathcal{H}$ are the Fock states $|n\rangle$ themselves, and their eigenenergies are equal to $n\omega_o + n(n-1)\omega_{nl}$; because of the presence of nonlinear interactions, the energy splitting of adjacent modes, given by $\omega_o + 2n\omega_{nl}$, is a monotonically increasing (decreasing) function of n for repulsive (attractive) interactions.

In the zero-detuning ($\Delta\omega = 0$) case, only the transition $|n=0\rangle \rightarrow |n=1\rangle$ is on resonance with the driving field; indeed, the higher states are shifted off the n-atom resonance of a frequency $(n-1)\omega_{nl}$. In particular, an incident intensity of the order of $8\omega_{nl}^2/\gamma = 8\gamma/N_o^2$ is required for the Rabi frequency $|\mathcal{E}_i|$ of the driving field to be equal to the detuning of the $|n=2\rangle$ level and thus for this to be effectively populated.

This physical picture is confirmed by the results of the numerical calculations reproduced in fig.6.5 and 6.6: for moderate intensities $I_{\rm inc} \ll I_2 = \gamma/N_o^2$, the cavity shows a behavior analogous to the one of a driven two-level system; in particular, the transmitted atomic beam has the same statistical properties as the resonance fluorescence from a single two-level atom.[1,49] Such an effect is the atom optical analog of the well-known *Coulomb blockade* of electronic systems[263–266] in which the change in the electrostatic potential following the injection of a single carrier inside the device is able to bring the energy of its electronic states above the Fermi level of the injector and thus forbid the injection of other carriers. In the atomic case, the collisional interaction energy following the presence of a single atom is able to shift the cavity mode frequency of an amount equal to $2\omega_{nl}$; if the incident beam is initially on resonance with the cavity, and if we are in a strong nonlinearity regime $\omega_{nl} \gg \gamma$, the entrance of a second atom in the cavity is an off-resonant process, and thus it is strongly suppressed. This means that before a second carrier can enter the cavity, the first one must have left. As usual, the antibunching of the transmitted beam which follows from this *atomic blockade* effect results in a suppression of intensity fluctuations well below the shot-noise limit.

For strong nonlinearities ($N_o \ll 1$), the characteristic incident intensity scale $I_{\rm sat}$ for

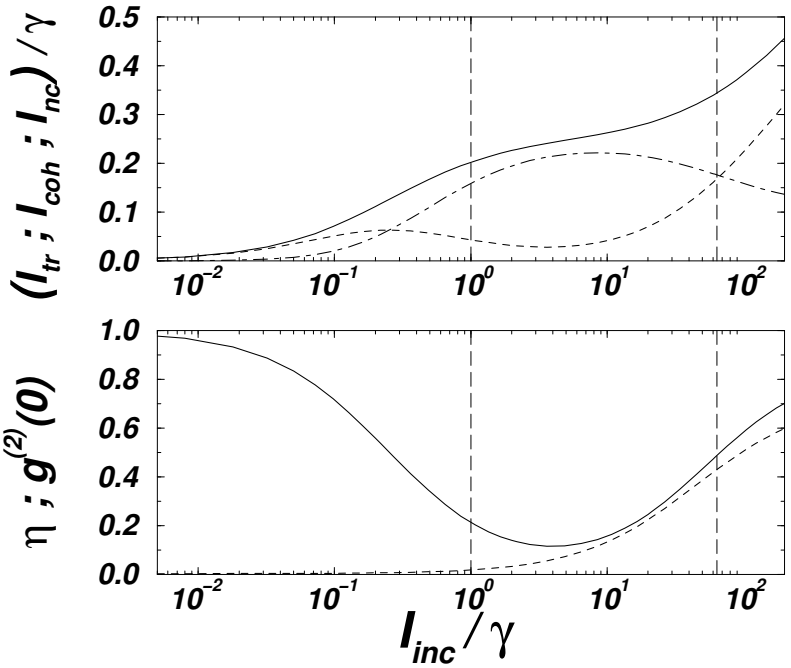

FIGURE 6.5: Transmission and coherence properties of a nonlinear Fabry-Perot interferometer in the strong nonlinearity regime ($N_o = 0.125$) as a function of the incident intensity: in the upper panel, transmitted intensity $I_{\rm tr}$ (solid line), coherent $I_{\rm coh}$ (dashed line) and incoherent $I_{\rm nc}$ (dot-dashed) components. In the lower panel, long time first order coherence η (solid line) and one-time second order coherence $g^{(2)}(0)$ (dashed line). *Atom Blockade* behavior occurs for $I_{\rm inc}$ comprised between $I_{\rm sat} = \gamma$ and $I_2 = 64\gamma$ (vertical dashed lines).

the saturation of the two-level system, which is of the order of γ, is well separated from the characteristic intensity $I_2 = \gamma/N_o^2$ for substantial population of the $|n = 2\rangle$ state. Hence it exists an intensity window $I_{\rm sat} \ll I_{\rm inc} \ll I_2$ in which the two-level system is effectively saturated but the higher excited states are still unpopulated: in this window (denoted by the vertical dashed lines in fig.6.5) the atom blockade is most effective in imposing the strict upper limit $I_{\rm tr} \leq \gamma/4$ to the total transmitted intensity. In this same intensity window, the spectral distribution of the transmitted intensity is characterized by the usual coherent delta-like peak at ω_L due to coherent (elastic) transmission plus a triplet of peaks (the so-called Mollow triplet[91]) resulting from incoherent transmission (see fig.6.6).

The intensity scale separation $I_{\rm sat} \ll I_2$ translates into the characteristic dependence of the total transmitted intensity on the incident intensity that can be observed in

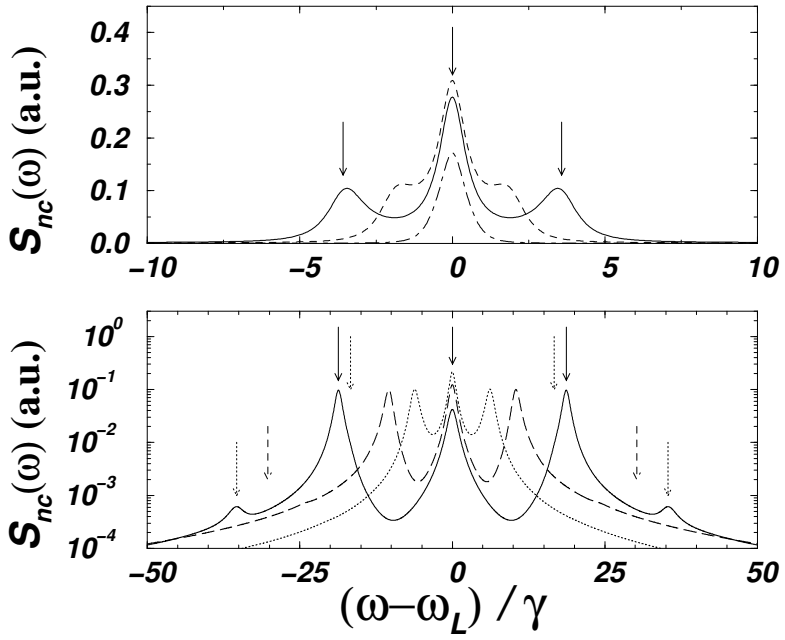

FIGURE 6.6: Incoherently transmitted intensity spectra in the strong nonlinearity regime ($N_o = 0.125$) for growing values of the incident intensity: in the upper panel, $I_{\rm inc} = 0.2, 2, 6.5$; in the lower one, $I_{\rm inc} = 20, 60, 240$. The arrows correspond to the transition frequencies resulting from the dressed cavity approach; the chosen parameters are the same ($I_{\rm inc} = 6.5, 240$) as for the solid line spectra. In the lower panel, solid arrows correspond to transitions involving only the $|n = 0, 1\rangle$ states, while the dotted and dashed ones correspond to weaker transitions which involve respectively the $|n = 2\rangle$ and the $|n = 3\rangle$ states.

the upper panel of fig.6.5: first of all, when the two-level system is not saturated, the transmitted intensity is a linear function of the incident one; then, for $I_{\rm inc}$ of the order of γ, saturation of the two-level system occurs and the response flattens. Finally, for $I_{\rm inc}$ of the order of γ/N_o^2, the transmitted intensity starts to grow again thanks to the contribution of the $|n = 2\rangle$ state.

The behavior of the single coherent and incoherent contributions to the transmitted intensity as functions of the incident intensity can also be interpreted within this same picture. As in the classical two-level system,[1] at low incident intensities most of the transmission is coherent, since the coherent fraction $I_{\rm coh}$ is a linear function of $I_{\rm inc}$ and the incoherent fraction $I_{\rm nc}$ a quadratic one. When the two-level system is appreciably saturated, the incoherent fraction starts to dominate, while the coherent one drops to nearly zero. As the incident intensity grows even further, more than

one atom can be simultaneously stored in the cavity mode, so that the $|n=2\rangle$ state results populated as well; therefore the coherent component starts to grow again, while the incoherent one to decrease. In other terms, the first order coherence η shows a minimum as a function of the incident intensity at a value corresponding to the saturation plateau of the two-level transition. The population of the $|n=2\rangle$ state can be singled out just by looking at the one-time second-order coherence function $g^{(2)}(0)$: for the ideal two-level system this quantity is rigorously zero for any value of $I_{\rm inc}$; any departure from this value is a unambiguous signature of a population of the $|n\geq 2\rangle$ levels. For low incident intensities $g^{(2)}(0)$ has the very small value $N_o^2/4$ (see eq.(6.21)), while it is substantially larger than zero only above the saturation plateau.

In order to explain the incoherent transmission spectra reproduced in fig.6.6, it can be useful to apply the dressed states technique to the physical system formed by the cavity plus the driving field.[1,267] In analogy to what is usually done in the dressed atom model, we shall label the quantum states of such system with a pair of integer numbers $(\mathcal{N},n)$, respectively denoting the number of atoms in the driving field and in the cavity mode. In the dressed atom model, the integer number n is generally replaced by a discrete index running over the different internal states of the fluorescing atom and $\mathcal{N}$ has the physical meaning of number of photons in the incident laser beam.

Neglecting for the moment the radiative damping of the cavity mode, the total number of atoms $N_T=\mathcal{N}+n$ is a conserved quantity; since $\mathcal{N}$ is assumed to be very large, adjacent manifolds have the same structure and are spaced from each other by an amount equal to the incident laser frequency ω_L; in particular, the corresponding eigenstates only differ for the number $\mathcal{N}$ of atoms in the driving field. Within each constant N_T manifold, the Hamiltonian of the dressed system in the Fock $|n\rangle$ basis has the simple form

$$\frac{\mathcal{H}}{\hbar}=\begin{pmatrix} 0 & \mathcal{E}_i & 0 & 0 & \\ \mathcal{E}_i^* & -\Delta\omega & \sqrt{2}\mathcal{E}_i & 0 & \\ 0 & \sqrt{2}\mathcal{E}_i^* & -2\Delta\omega+2\omega_{nl} & \sqrt{3}\mathcal{E}_i & \vdots \\ 0 & 0 & \sqrt{3}\mathcal{E}_i^* & -3\Delta\omega+6\omega_{nl} & \\ & & \cdots & & \end{pmatrix}. \tag{6.23}$$

As it is sketched in fig.6.7a, transitions between one manifold to the immediately lower one occur because of radiative losses through the non-perfectly reflecting mir-

rors and give rise to the incoherent component of the transmitted beam. Denoting with ω_α the energy of the $|\psi_\alpha\rangle$ eigenstate of a manifold, we expect that the spectrum of incoherently transmitted atoms will be peaked at the frequencies $\omega_L + (\omega_\alpha - \omega_\beta)$; the intensity of each peak is proportional to the matrix element of the corresponding transition $|\langle\psi_\alpha|\hat{a}|\psi_\beta\rangle|^2$ times the population N_α of the departure level $|\psi_\alpha\rangle$.

For moderate intensities $I_{\rm inc} \ll \gamma/N_o^2$ the mixing of the bare states into the new dressed states is limited to the two lowest states of the manifold, while the upper states nearly coincide with the $|n \geq 2\rangle$ states and are nearly unpopulated; for this reason transitions involving these upper states give a negligible contribution to the incoherent transmission spectra. In this regime, these spectra are thus the usual Mollow spectra of resonance fluorescence from driven two-level systems: at very low intensity, there is a single peak at ω_o; for intensities at least of the order of the saturation intensity $|\mathcal{E}_i| \simeq \gamma$, there starts to be a symmetric triplet of peaks at respectively ω_o and $\omega_o \pm |\mathcal{E}_i|$, the central peak having a height three time larger than the lateral ones (see fig.6.6b).

At stronger intensities, when a larger number of states of the cavity begins to be effectively populated, the structure of the manifolds becomes more complex and additional peaks can be found in the wings of the fluorescence spectra; the stronger the driving field, the larger the mixing of $|n \geq 2\rangle$ states with the lower ones and consequently the stronger the intensity of the peaks corresponding to transitions involving such states.

A simple numerical diagonalization of the Hamiltonian eq.(6.23) gives the frequencies of the peaks: in fig.6.7b we have reproduced the dependence of the frequency of the lowest dressed states on the driving strength. Obviously, since the higher state population is very small as well as the matrix elements of the transitions reaching them, only a few peaks are visible in the actual spectra plotted in fig.6.6. Comparison between the two approaches is easily made: the transition frequencies as they are predicted by the dressed state picture have been marked by vertical arrows; the agreement with the numerical peaks is excellent. Solid arrows refer to the transitions involving only $|n = 0\rangle$ and $|n = 1\rangle$, which are visible at any intensity; on the other hand, dotted (dashed) arrows denote transitions which involve the $|n = 2\rangle$ ($|n = 3\rangle$) state as well; given their weakness, the corresponding peaks can be distinguished from the underlying pedestal only at high intensities.

Remarkably, the intensity of the central peak at ω_o decreases for growing intensity

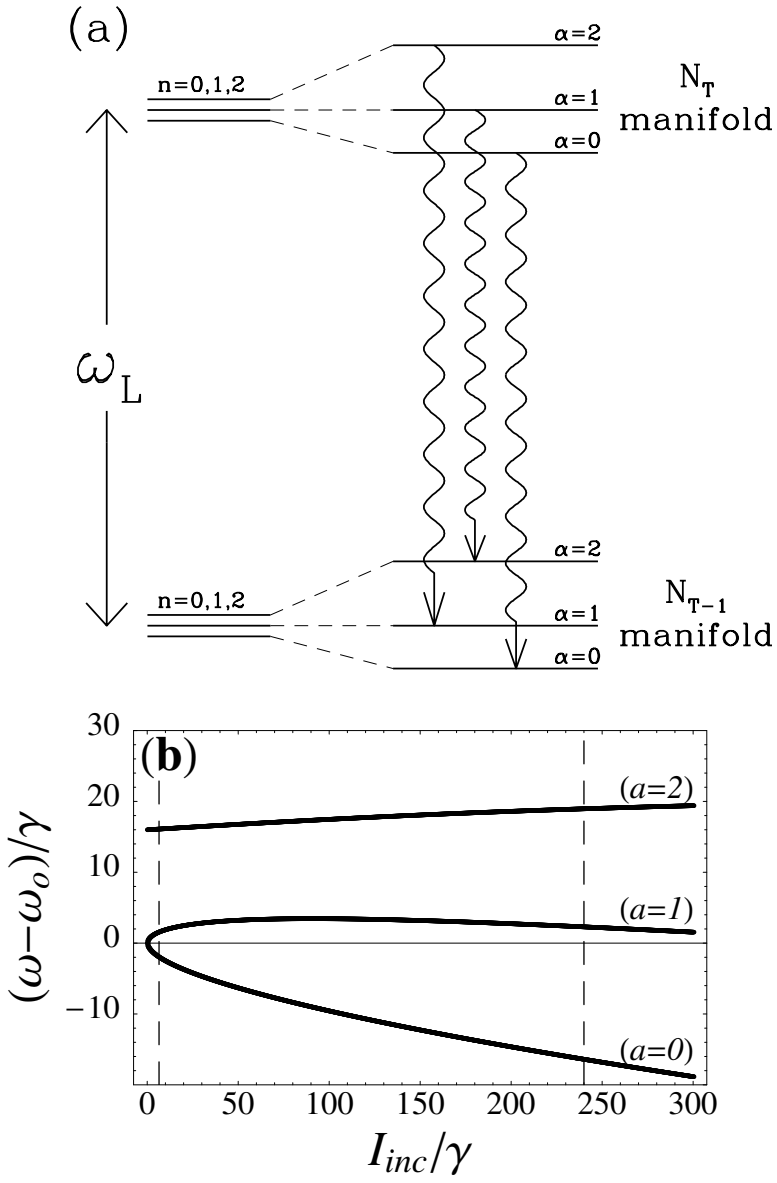

FIGURE 6.7: Strong nonlinearity regime ($N_o = 0.125$): sketch of the dressed cavity level scheme (panel a); dressed state frequencies (panel b) as a function of the incident intensity $I_{\rm inc}$ for the $\Delta\omega = 0$ case. The vertical dashed lines correspond to the intensity values used in fig.6.6.

with respect to the first pair of side peaks: this evolution suggests a smooth transition towards the two-peaked spectra obtained by means of the semiclassical approach described in the previous section; at very high driving intensity, in fact, when the mean occupation number of the cavity is much larger than one, fluctuations result again well described by the linearized theory of the previous section.

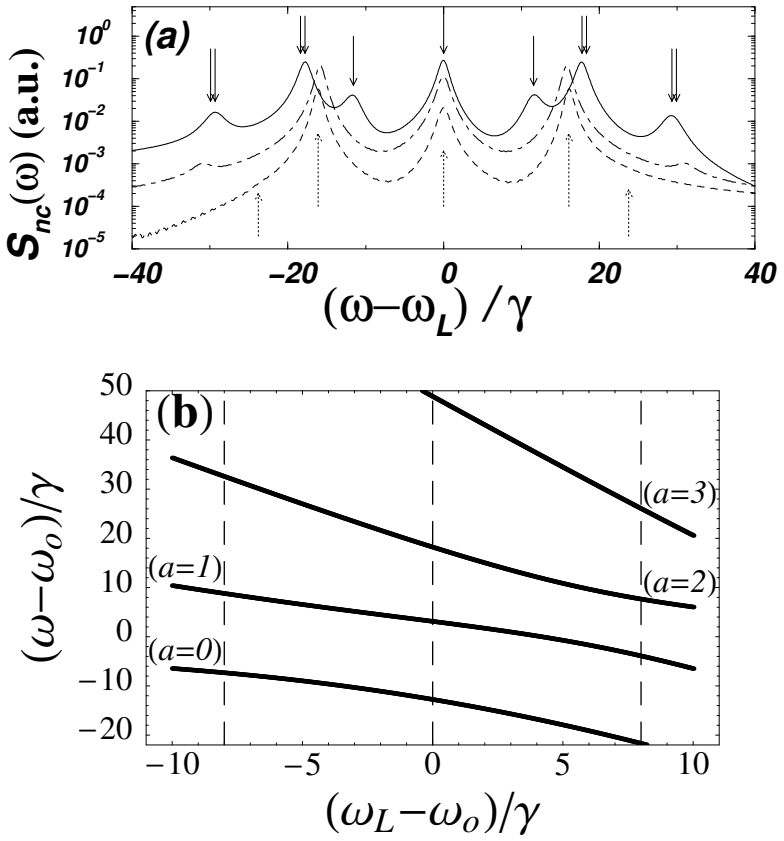

FIGURE 6.8: Effect of a finite detuning $\Delta\omega$ on the incoherently transmitted intensity spectra in the strong nonlinearity regime ($N_o = 0.125$, $I_{\rm inc} = 160$): in the upper panel, spectra for $\Delta\omega/\gamma = -8, 0, 8$ (respectively, dashed, dot-dashed and solid lines); arrows indicate the transition frequencies according to the dressed cavity model: solid arrows refer to the $\Delta\omega/\gamma = 8$ spectrum, dotted arrows to the $\Delta\omega/\gamma = -8$ one. In the lower panel, plot of the dressed state frequencies as function of the detuning $\Delta\omega$. The vertical dashed lines correspond to the values of the detuning which have been used in panel (a).

The dressed cavity model can be extended to the case of a non-vanishing detuning $\Delta\omega$ as well: the positions of the peaks are again well reproduced in terms of transitions connecting dressed states of adjacent manifolds. In the upper panel of fig.6.8

we have plotted a series of spectra for different detunings: the spectra are centered at the incident frequency ω_L, i.e. the spacing between adjacent manifolds.

When $\Delta\omega$ and ω_{nl} have opposite signs, the nonlinear feedback on transmission is negative and the population of the upper states of the manifold is further reduced with respect to the $\Delta\omega = 0$ case; the lateral peaks in the spectra are therefore even weaker. On the other hand, when $\Delta\omega$ and ω_{nl} have the same sign and the nonlinear feedback is positive, the population of the upper states of the manifold is enhanced and the spectra show a larger number of peaks. As previously, their frequencies result in good agreement with the predictions of the dressed cavity model, which are marked with arrows in the figure. In the lower panel of the same fig.6.8, we have specifically plotted the position of the different dressed states as function of the detuning as they have been determined by numerically diagonalizing the Hamiltonian eq.(6.23).

6.4 Quantum tunneling effects in optical bistability

In the previous section we have studied the coherence properties of the transmitted atomic beam in the case the incident beam is exactly on resonance with the empty cavity; these effects are the generalization to the quantum $N_o \leq 1$ regime of the well-known optical limiting effect which is observed whenever the nonlinearity gives a negative feedback on the transmittivity.

For the case of repulsive interactions, the nonlinear shift $\omega_{\rm mf}$ of the cavity resonance is a positive quantity and optical limiting occurs if $\omega_L \leq \omega_o$; on the other hand, optical bistability is expected to occur in the opposite $\omega_L > \omega_o$ case, when the nonlinear feedback on the transmission is positive.

In this case, the mean-field steady-state equation eq.(6.7) possesses multiple solutions for a given range of incident intensities; if all fluctuations are neglected, such solutions correspond to true steady states which last for an indefinite time. This picture is clearly correct only for sufficiently large values of N_o: as we have discussed in the previous section, the amplitude of quantum fluctuations is inversely proportional to N_o, so that a large N_o means that the fluctuations explore only a small neighborhood of the steady state and the probability of a fluctuation large enough to induce a tunneling event from one steady state to another is exponentially small.[156,261,262]

For smaller values of the critical number N_o, tunneling effects from one branch of the bistability curve to the other start to be important even for a perfectly coherent incident beam; in this case, a linearized treatment of fluctuations is not sufficient any more and a full quantum calculation has to be performed by numerically solving the complete quantum master equation in some representation;[244] given the range of parameters we are interested in, our numerical calculations have been performed in the same Fock state basis as before.

From the point of view of the master equation, optical bistability emerges in the steady-state of the density matrix simply as a statistical mixture of the two steady-states of the mean-field approach, the "transmitting" and the "non-transmitting" ones; formally, the density matrix can therefore be written in the form

$$\rho_{ss} = \alpha_1 \rho_{ss}^{(1)} + \alpha_2 \rho_{ss}^{(2)} \tag{6.24}$$

where each of the components $\rho_{ss}^{(1,2)}$ describes a state in which the number of quanta in the cavity is almost constant and equal to the corresponding mean-field solution; the fact that the steady-state density matrix is a mixture physically follows from the tunneling events which connect one state to the other and determine the relative weights $\alpha_{1,2}$ of the two components. From the point of view of the correlation functions of the cavity field, optical bistability reflects into the appearance of two different time scales in the relaxation dynamics: a fast $\tau_f \approx \gamma^{-1}$ time scale corresponds to the equilibration of each of the $\rho^{(1,2)}$ towards its steady-state $\rho_{ss}^{(1,2)}$, while the slow τ_s time scale corresponds instead to the final equilibration of the weights of the two components $\alpha_{1,2}$ through the tunneling events.

In the left panel of fig.6.9, we have plotted the characteristic transmitted vs. incident intensity curve for an example of nonlinear cavity: unlike the mean-field result, the full quantum calculation for the mean transmitted intensity does not show any bistable behaviour, the resulting value being the average over the two $\rho_{ss}^{(1,2)}$ components. This can be better observed in the probability distribution for the number of quanta in the cavity that has been plotted in the right panel: as expected, this shows two maxima for incident intensities within the mean-field bistability loop;[156] the smooth transition from a single peak around the empty cavity ("non-transmitting" state) towards a single peak at a non-zero value ("transmitting" state) follows the smooth rearrangement of the weights $\alpha_{1,2}$ of the two components.

The characteristic bi-peaked shape of the atom-number probability distribution reflects into a peculiar behaviour (fig.6.10) of the second-order coherence function: at

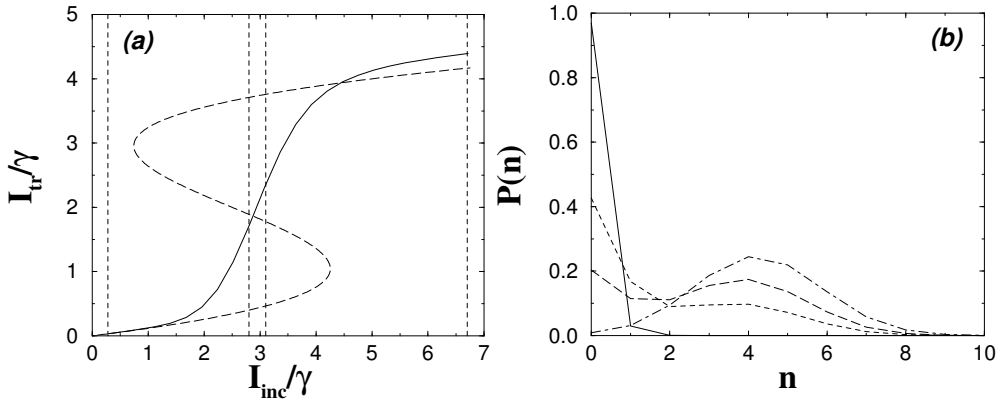

FIGURE 6.9: Left panel: Characteristic transmitted vs. incident intensity curve; $\Delta\omega = 3\gamma$, $\omega_{nl} = 0.5\gamma$. Solid line: quantum calculation. Dashed line: mean-field result. Vertical lines correspond to the incident intensities used in the right panel and in fig.6.10. The disagreement at large incident intensities is due to quantum fluctuations around the (single) mean-field steady state. Right panel: Atom-number probability distribution for different values of the incident intensity $I_{inc}/\gamma = 0.28$ (solid), 2.8 (dashed), 3.1 (long-dashed), 6.7 (dot-dashed).

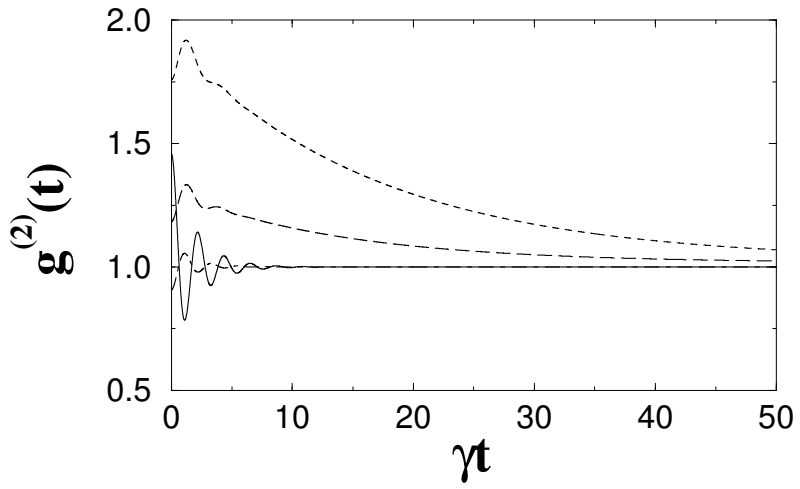

FIGURE 6.10: Second-order coherence function $g^{(2)}(t)$ for different values of the incident intensity $I_{inc}/\gamma = 0.28$ (solid), 2.8 (dashed), 3.1 (long-dashed), 6.7 (dot-dashed). Same cavity parameters as in fig.6.9.

very short times $g^{(2)}(t \simeq 0)$ shows a value definitely larger than one; after a few oscillations, quickly damped on a time scale of the order of τ_f, $g^{(2)}(t)$ exponentially relax to the long-time value of 1 within a slow characteristic time $\tau_s \gg \tau_f$ determined by the tunneling rate. This behaviour is easily explained: the detection of a first atom projects the density matrix mainly on its large n component; the observation of a second atom after a short time has now an enhanced probability; the fast relaxation follows from the fact the projected density matrix is not exactly equal to the steady-state $\rho_{ss}^{(2)}$. At longer times, tunneling events tend to reequilibrate ρ to the steady state ρ_{ss}; as we can see in fig.6.11, for incident intensities within the mean-field hysteresis loop, the characteristic time τ_s of the exponential decay turns out to be much longer than the cavity damping time γ^{-1}.

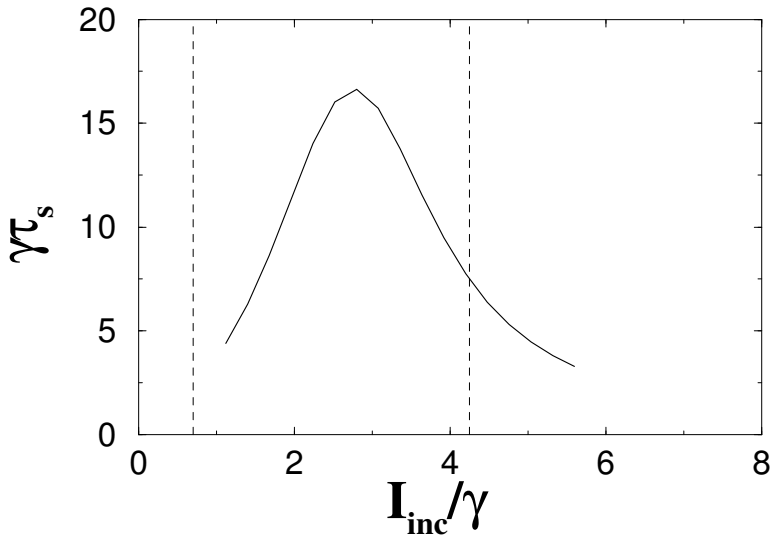

FIGURE 6.11: Tunneling time τ_s as a function of the incident intensity. Same cavity parameters as in fig.6.9. Vertical lines correspond to the boundaries of the mean-field bistability region.

If the detuning of the incident beam $\Delta\omega = \omega_L - \omega_o$ is such that the cavity energy $n\omega_o + n(n-1)\omega_{nl}$ is on resonance with the incident beam after the injection of $n = N_r$ atoms

$$N_r = 1 + \frac{\Delta\omega}{\omega_{nl}}, \tag{6.25}$$

a sort of n-atom transmission process is expected, in much the same way as n-photon absorption occurs if a laser beam is resonant with a n-photon atomic transition at $\omega_a = n\omega_L$. In physical terms, we expect that the transmitted beam in the

limit of very low incident intensity will be formed by a sort of discrete bunches containing a number of atoms of the order of N_r and separated by intervals of time in which no atom is present; since there is no physical binding between the atoms in the transmitted beam, the bunches are quickly spred out because of the curvature of the atomic dispersion and thus can be observed only at moderate distances from the cavity.

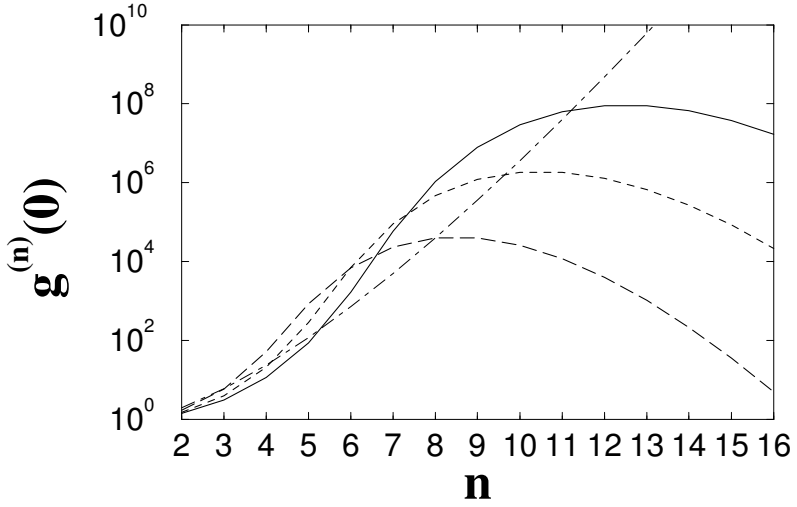

FIGURE 6.12: Value of the n^{th} order coherence function $g^{(n)}(0)$ as a function of n in the weak incident intensity limit. $\Delta\omega/\omega_{nl} = 3$ (solid: $N_r = 7$), 2.5 (dashed: $N_r = 6$), 2 (long-dashed: $N_r = 5$); $\omega_{nl} = 0.5\gamma$. Dot-dashed line: $g^{(n)}(0)$ for the case of a thermal beam.

This physical idea can be formalized[268] in terms of the coherence functions of the transmitted beam: if we plot the value of the n^{th}-order coherence function $g^{(n)}(t = 0)$ as a function of the order n, we expect it to be peaked around the number of atoms within the bunch. From the numerical calculations summarized in fig.6.12 it is immediate to observe that the value of $g^{(n)}$ can be substantially larger than the corresponding value for a chaotic thermal beam: this is a clear signature of a strong bunching effect. Furthermore, the maximum of $g^{(n)}$ is found around $n \approx 2N_r$ and the maximum of its slope is around $n \approx N_r$; these last results are in qualitative agreement with the simple physical picture of the discrete bunches.

6.5 Conclusions and perspectives

In the present chapter we have investigated the nonlinear atom optical effects which arise from atom-atom collisional interactions in a single-mode atomic Fabry-Perot cavity driven by a coherent atom laser beam; in particular, we have numerically solved the full quantum master equation in a number-state basis and we have given a physical interpretation of the obtained results.[269]

Provided the nonlinear interaction energy per atom is small, the exact results are well reproduced by the mean-field theory in which the atomic field is described as a classical C-number field and quantum fluctuations are taken into account using a linearized version of the stochastic differential equations of Positive-P representation.

In the opposite limit of strong nonlinearity, the mean-field theory breaks down; for an incident beam exactly on resonance with the empty cavity, a sort of *atom blockade* effect is predicted: the presence of a single atom in the cavity mode pushes the mode frequency off-resonance from the incident field so that a second atom can not enter the cavity but at very large incident intensities. The statistical properties predicted by the numerical calculations are very similar to the resonance fluorescence ones from a two-level system. A very strong incident beam is necessary for several atoms to be simultaneously forced into the cavity mode; this is reflected in a peculiar behavior of the transmitted intensity a function of the incident intensity. The multiplet of peaks which characterizes the spectral distribution of the incoherently transmitted atoms can be interpreted as arising from radiative transitions between dressed states of the driven cavity: the agreement between the predictions of the dressed cavity model and the frequencies of the numerical peaks is excellent.

For the case of a positive nonlinear feedback on transmission, mean-field is well-known to predict atom optical bistability. A complete treatment of the problem in terms of the density matrix has confirmed the expectation that the steady state density matrix is a statistical mixture of the two mean-field steady states (the "transmitting" and the "non-transmitting" ones) and tunneling events allow for transitions from one of them to the other in a finite time τ_s; the larger the critical number N_o, the longer the tunneling time and therefore the more "classical" the behaviour of the system. From the point of view of the coherence functions, in addition to the usual damping time $\tau_f \approx \gamma^{-1}$, a longer time scale appears, corresponding to the tunneling

time τ_s; as an example, the second-order coherence shows a long-time exponential tail with a time constant equal to τ_s.

If the detuning of the atom laser from the cavity mode is such that the simultaneous injection of N_r atoms is a resonant process since $N_r\omega_L = N_r\omega_o + N_r(N_r-1)\omega_{nl}$, a sort of N_r-atom transmission phenomenon occurs, in which the atoms are most likely transmitted in bunches containing a number of atoms of the order of N_r separated by time intervals in which no atoms are present. Such a simple physical picture is confirmed by numerical calculations for the coherence function $g^{(n)}(0)$ of the transmitted beam as a function of n.

Although all the discussion is mainly focussed on the case of atomic Fabry-Perot cavities, similar results hold for optical resonators filled of a nonlinear medium; in this latter case, since the intrinsic optical nonlinearity of current materials is generally very weak, clever schemes have to be adopted in order to enhance the nonlinear coupling per photon and depress losses so to attain the quantum $N_o \leq 1$ regime. On the other hand, the Fabry-Perot cavity for atomic matter waves proposed in chap.5 is expected to be already close to this condition.

Chapter 7

A stochastic macroscopic wavefunction approach to the interacting Bose gas

In the previous chapter we have studied the quantum dynamics of an interacting Bose field spatially localized in a Fabry-Perot cavity driven by an external coherent field: the discrete mode structure of the cavity has suggested a single-mode approximation which has allowed for calculations to be performed in a reasonably small Hilbert space.

Here we shall address the much more difficult case of a spatially distributed field for which a large number of modes has to be taken into account: for instance, this is the case of a trapped atomic Bose condensates. A brute force approach to the $N-$body problem inside a trap would require to cope with a Hilbert space with a dimension equal to m^N, m being the number of field modes to be considered; for any practical case, such a task is numerically untractable and other techniques have to be developed; the calculations described in the previous chapter have been possible only thanks to the $m = 1$ condition.

At very low temperature, a simple theoretical description of the dynamics of these multimode systems is obtained by making the usual mean-field approximation, in which all the atoms are assumed to share a single quantum state and the uncondensed fraction is completely neglected. In this approach, the wave function of the condensate obeys the Gross-Pitaevskii equation eq.(4.21) in which the interactions

between the atoms are described by a simple cubic term; such an approach neglects two- and more-particle correlations and is valid at zero temperature under a diluteness condition which is usually stated in terms of the density n and the scattering length a of the gas as $(na^3)^{1/2} \ll 1$; current gaseous condensates satisfy such a condition but finite temperature phenomena are not included in this mean field approach.

In the present chapter, we shall describe the principles of a novel approach to the exact time-evolution of an interacting Bose gas: we shall discuss how a generalization of the Gross-Pitaevskii equation including a stochastic term leads to an exact reformulation of the time-dependent N-body bosonic problem in terms of the stochastic evolution of single particle wavefunctions. In this way, an exact and numerically tractable approach to the problem of the interacting Bose gas is obtained, an approach not restricted to thermal equilibrium case but which allows for the study of the time evolution of any observable of the quantum gas under examination.

The principle of the method is based on the stochastic evolution of an Hartree state ansatz in which all atoms share the same wavefunction and this latter evolves according to a stochastic partial differential equation. Depending on the specific form of the Hartree states – either Fock states with a fixed number of atoms or coherent states can be used – different forms of the stochastic evolution can be obtained with completely different statistical properties. Since the exactness conditions do not completely determine the form of the stochastic evolution within a given ansatz, a further freedom in the choice of the specific form of the stochastic equations is available for the optimization of the statistics and the stability of an actual simulation. As a particular solution within the coherent state ansatz, we have recovered the stochastic scheme of the positive-P representation;[49,170,270] although this specific choice is well-known to have serious instability problems,[169] other schemes have been found to give differential equations with a regular solution for all times; in these cases, the efficiency of the method is only limited by the computational time.

In sec.7.1, we shall present the stochastic formulation of the many-body problem and we shall determine the conditions for recovering the exact evolution after the average over the stochastic noise. The following sec.7.2 is devoted to the presentation of two particular schemes implementing this stochastic formulation: we first present a *simple* scheme, which minimizes the statistical spread of the calculated N-atom density matrix, and then a more elaborate scheme in which the trace of the calculated density matrix is strictly fixed in the evolution so as to reduce the statistical error of an actual simulation. With this latter constraint, we recover for the

coherent state ansatz the known stochastic simulation associated with the positive-P representation;[170] unfortunately, such *constant trace* simulations are subject to divergences of the norm of the wavefunction which explodes to infinity after a finite time.

In secs.7.3 and 7.4 we finally investigate two examples (a two-mode model and a one-dimensional Bose gas) which illustrate the accuracy and the limitations of the methods. Generally speaking, we find that the *simple* simulations are only limited by the computation power: the number of realizations needed for a good statistical accuracy increases exponentially with the time with an exponent $\gamma \propto NV(0)$. For this reason, these simple schemes are not well suited to determine small deviations from the mean-field approximation in the large N limit but can be more efficiently applied to systems with a small number of particles, such as small atomic clouds tightly trapped at the nodes or antinodes of an optical lattice. On the other hand, the divergences of the norm of the wavefunction which characterize the *constant trace* simulations impose serious limitations to their practical use.

Although the discussion of the present chapter is mainly focussed on the dynamics of trapped atomic ensembles, there is no reason not to extend the approach to multimode nonlinear photonic systems such as planar microcavities: thanks to the analogy between interacting matter and light waves, the same interaction Hamiltonian used for the collisional atom-atom interactions can be applied to describe the third order polarizability of nonlinear optical materials with an intensity-dependent refraction index.

In particular, the stochastic techniques developed in the present chapter can be applied to the study of the quantum correlations among the different transverse modes of the light field of a planar system: in this case, in fact, the transverse modes are not well spaced in energy and a single mode approximation is not allowed; as the quantum depletion of the condensate or the damping of large amplitude collective excitations can give rise to a cloud of non-condensed atoms, in the same way nonlinear photon-photon interactions can populate modes other than the driven one.

7.1 Stochastic formulation of the N-boson problem using Hartree functions

The Hamiltonian of the trapped interacting Bose gas under examination can be written in terms of the Bose field operator $\hat{\Psi}(x)$ as:

$$\mathcal{H} = \int dx\, \hat{\Psi}^\dagger(x) h_0 \hat{\Psi}(x) + \frac{1}{2}\int\int dx\, dx'\, \hat{\Psi}^\dagger(x)\hat{\Psi}^\dagger(x') V(x-x')\hat{\Psi}(x')\hat{\Psi}(x) \tag{7.1}$$

where x is the set of spatial coordinates of a particle, $h_0 = -\frac{\hbar^2}{2m}\nabla^2 + V_{\rm ext}(x)$ is the single particle Hamiltonian in the external confining potential $V_{\rm ext}$ and where interactions are assumed to occur via a two-body potential $V(x-x')$.

In practice we consider the dilute gas and the low temperature regimes, which correspond respectively to $n|a|^3 \ll 1$ and $|a| \ll \lambda$ for a three-dimensional problem ($\lambda = h/(2\pi m k_B T)^{1/2}$ is the thermal de Broglie wavelength). The true interaction potential can then be replaced by a simpler model potential leading to the same scattering length a provided that the range b of this model potential is much smaller than the healing length $\xi = (8\pi n a)^{-1/2}$ and than λ. This ensures that the physical results do not depend on b. For simplicity we will use here repulsive Gaussian potentials corresponding to a positive scattering length $a > 0$.

7.1.1 A stochastic Hartree Ansatz with Fock states

From a mathematical point of view, the exact evolution of the N-body density matrix ρ can be obtained from the Hamiltonian eq.(7.1) using the quantum-mechanical equation of motion

$$\dot{\rho}(t) = \frac{1}{i\hbar}\,[\mathcal{H}, \rho(t)] \tag{7.2}$$

but any concrete calculation is impracticable even for moderate particle numbers N, due to the multi-mode nature of the problem leading to a huge dimensionality of the $N-$body Hilbert space.

For this reason approximate theories have been developed in order to get useful results at least in some specific ranges of parameters; the simplest one is the so-called mean-field theory, in which the N-particle density matrix is approximated by a Fock state Hartree ansatz

$$\rho(t) = |N : \phi(t)\,\rangle\langle\, N : \phi(t)|. \tag{7.3}$$

The evolution of the normalized *condensate wave function* ϕ is determined using a variational procedure. The result of such a procedure is the well-known mean-field equation

$$i\hbar\frac{\partial\phi(x)}{\partial t} = \left(-\frac{\hbar^2\nabla^2}{2m} + V_{\rm ext}(x)\right)\phi(x) + (N-1)\left(\int dx'\, V(x-x')\,|\phi(x')|^2\right)\phi(x). \quad (7.4)$$

For an interaction potential $V(x-x')$ modeled by a contact term $g\delta(x-x')$ (where $g = 4\pi\hbar^2 a/m$ in a three-dimensional problem) it reduces to the Gross-Pitaevskii equation commonly used to analyze the dynamics of pure Bose-Einstein condensed gases.

A first attempt to improve the accuracy of the Hartree ansatz eq.(7.3) is to allow for a stochastic contribution dB in the evolution of the macroscopic wave function ϕ:

$$\phi(t+dt) = \phi(t) + F\,dt + dB \quad . \quad (7.5)$$

In all this chapter the noise dB is treated in the standard Ito formalism:[239] it is assumed to have a zero mean $\overline{dB} = 0$ and to have a variance $\overline{dB^2} \propto dt$; a deterministic contribution is given by the force term Fdt. In this framework, the N-body density matrix would result from the stochastic mean over noise or, in other terms, from a mean over the probability distribution $\mathcal{P}(\phi)$ in the functional space of the wave functions ϕ:

$$\rho(t) \stackrel{?}{=} \Big\langle |N:\phi(t)\rangle\langle N:\phi(t)| \Big\rangle_{\rm stoch} = \int \mathcal{D}\phi\, \mathcal{P}(\phi)\, |N:\phi(t)\rangle\langle N:\phi(t)|. \quad (7.6)$$

An immediate advantage of this prescription over the pure state ansatz eq.(7.3) is that it can deal with finite temperature problems.[271] However as shown in sec.7.1.4, the simple generalization eq.(7.5) of the Gross-Pitaevskii equation cannot lead to an exact solution of the N-body problem [(a)]. We have therefore to enlarge the family of dyadics over which we expand the density operator; more precisely we use Hartree dyadics in which the wave functions in the bra and in the ket are different:

$$\sigma(t) = |N:\phi_1(t)\rangle\langle N:\phi_2(t)| \quad . \quad (7.7)$$

The two wave functions $\phi_1(x)$ and $\phi_2(x)$ are assumed to evolve according to Ito stochastic differential equations:

$$\phi_\alpha(t+dt) = \phi_\alpha(t) + F_\alpha\,dt + dB_\alpha \qquad (\alpha = 1,2). \quad (7.8)$$

[(a)] One can show that the distribution $\mathcal{P}(\phi)$ evolves according to a functional Fokker-Planck equation with a non-positive diffusion coefficient and therefore cannot be simulated by a Brownian motion of ϕ. In quantum optics this problem is known to occur in the Glauber-Sudarshan P-representation of the density matrix [239, chap.10, §7].

The expansion eq.(7.6) is then replaced by

$$\rho(t) = \left\langle |N:\phi_1(t)\rangle\langle N:\phi_2(t)| \right\rangle_{\text{stoch}} = \\ = \int\!\!\int \mathcal{D}\phi_1\, \mathcal{D}\phi_2\, \mathcal{P}(\phi_1,\phi_2)\, |N:\phi_1(t)\rangle\langle N:\phi_2(t)|. \quad (7.9)$$

We will see in the following that within this extended Hartree ansatz one can find a stochastic evolution for $\phi_{1,2}$ reproducing the exact time evolution.

Actual calculations (sec.7.3 and 7.4) will be performed with a Monte-Carlo technique, in which the evolution of the probability distribution $\mathcal{P}$ is simulated by a large but finite number $\mathcal{N}$ of independent realizations $\phi_{1,2}^{(i)}(t)$, $i = 1,\ldots,\mathcal{N}$. At any time the (approximate) density matrix ρ is given by the mean over such an ensemble of wave functions:

$$\rho(t) \simeq \frac{1}{\mathcal{N}} \sum_{i=1}^{\mathcal{N}} |N:\phi_1^{(i)}(t)\rangle\langle N:\phi_2^{(i)}(t)|. \quad (7.10)$$

The expectation value of any operator $\hat{O}$ is thus expressed by:

$$\left\langle \hat{O} \right\rangle \simeq \frac{1}{\mathcal{N}} \sum_{i=1}^{\mathcal{N}} \left\langle N:\phi_2^{(i)}(t)|\hat{O}|N:\phi_1^{(i)}(t) \right\rangle. \quad (7.11)$$

For an Hermitian operator one can equivalently consider only the real part of this expression since the imaginary part is vanishingly small in the large $\mathcal{N}$ limit.

Consider as an example the one-particle density matrix of the gas, usually defined as:

$$\rho^{(1)}(x,x') = \left\langle \hat{\Psi}^\dagger(x')\hat{\Psi}(x) \right\rangle. \quad (7.12)$$

Inserting in this expression our form of the complete density matrix eq.(7.10), we obtain the simple result

$$\rho^{(1)}(x,x') = N \left\langle \phi_1(x)\phi_2^*(x')\, \langle\phi_2|\phi_1\rangle^{N-1} \right\rangle_{\text{stoch}} \quad (7.13)$$

from which it is easy to obtain the spatial density $n(x) = \rho^{(1)}(x,x)$ and the correlation function $g^{(1)}(x,x') = \rho^{(1)}(x,x')/(n(x)n(x'))^{1/2}$. Also, the condensate fraction can be obtained from the largest eigenvalue of $\rho^{(1)}(x,x')$.

Remarks:

1. The desired stochastic evolution, which has to satisfy $\text{Tr}[\rho] = 1$, cannot preserve the normalization of $\phi_{1,2}$ to unity; we can write indeed

$$\text{Tr}[\rho(t)] = \left\langle \langle\phi_2(t)|\phi_1(t)\rangle^N \right\rangle_{\text{stoch}} = 1 \quad (7.14)$$

which for $|\phi_1\rangle \neq |\phi_2\rangle$ imposes $||\phi_1||\ ||\phi_2|| > 1$.

2. The expansion eq.(7.9) is always possible with a positive distribution function $\mathcal{P}_t(\phi_1, \phi_2)$. We prove this statement by showing that a general density operator ρ can be written as in eq.(7.10) in the limit $\mathcal{N} \to +\infty$. Using the identity

$$\mathrm{Id}_N = \lim_{\mathcal{M}\to+\infty} \frac{1}{\mathcal{M}} \sum_{j=1}^{\mathcal{M}} |N : \psi^{(j)}\rangle\langle N : \psi^{(j)}| \tag{7.15}$$

where the functions $\psi^{(j)}$ have a uniform distribution over the unit sphere in the functional space, we obtain

$$\rho = \lim_{\mathcal{M}\to+\infty} \frac{1}{\mathcal{M}^2} \sum_{j_1,j_2=1}^{\mathcal{M}} |N : \psi^{(j_1)}\rangle\langle N : \psi^{(j_2)}|\ \langle N : \psi^{(j_1)}|\rho|N : \psi^{(j_2)}\rangle. \tag{7.16}$$

This expression is not yet in the form of eq.(7.10) since the matrix elements $\langle N : \psi^{(j_1)}|\rho|N : \psi^{(j_2)}\rangle$ are complex. Fortunately we can always write this matrix element as the $2N$-th power of the complex number $\xi_{(j_1,j_2)}$. It is then sufficient to set $\phi_1^{(j_1,j_2)} = \psi^{(j_1)}\xi_{(j_1,j_2)}$ and $\phi_2^{(j_1,j_2)} = \psi^{(j_2)}\xi^*_{(j_1,j_2)}$, to put $\mathcal{N} = \mathcal{M}^2$ and to reindex (j_1, j_2) as a single index i, in order to recover the expansion eq.(7.10). Note that this expansion is not unique and does not have the pretension to be the most efficient one. For instance if the system is initially in a Hartree state $|N : \phi_0\rangle$, such a procedure is clearly not needed since one has just to set $\phi_1^{(i)}(t = 0) = \phi_2^{(i)}(t = 0) = \phi_0$. This will be the case of the numerical examples in sections 7.3 and 7.4.

7.1.2 Stochastic evolution of a Fock state Hartree dyadic

In this subsection we calculate the stochastic time evolution during an infinitesimal time interval dt of the dyadic $\sigma(t)$ given in eq.(7.7). This will be used later in a comparison with the exact master equation.

After dt, the dyadic σ has evolved into:

$$\sigma(t + dt) = |N : \phi_1 + d\phi_1\rangle\langle N : \phi_2 + d\phi_2|, \tag{7.17}$$

where $d\phi_1$ and $d\phi_2$, defined according to eq.(7.8), contain both the deterministic contribution $F_\alpha dt$ and the stochastic one dB_α. Splitting each contribution into a lon-

gitudinal and an orthogonal component with respect to ϕ_α and isolating a Gross-Pitaevskii term in the deterministic contribution, we can write:

$$dB_\alpha(x) = \phi_\alpha(x)\, d\gamma_\alpha + dB_\alpha^\perp(x) \tag{7.18}$$

$$F_\alpha(x) = F_\alpha^{GP}(x) + \lambda_\alpha \phi_\alpha(x) + F_\alpha^\perp(x). \tag{7.19}$$

Our choice of the Gross-Pitaevskii term is the following one:

$$\begin{aligned} F_\alpha^{GP}(x) = \quad & \frac{1}{i\hbar}\left[h_0 + \frac{(N-1)}{\|\phi_\alpha\|^2}\int dx'\; V(x-x')\,|\phi_\alpha(x')|^2\right]\phi_\alpha(x) \\ - \quad & \frac{1}{i\hbar}\left[\frac{(N-1)}{2}\frac{\langle\phi_\alpha\phi_\alpha|V|\phi_\alpha\phi_\alpha\rangle}{\|\phi_\alpha\|^4}\right]\phi_\alpha(x). \end{aligned} \tag{7.20}$$

The first term gives the standard Gross-Pitaevskii evolution, i.e. the kinetic term, the potential energy of the trap and the mean-field interaction energy; the second term, which arises naturally because we are considering Fock states (rather than coherent states as commonly done) takes into account the difference between the total mean-field energy per particle of the condensate and its chemical potential μ.[272]

We split the field operator in its longitudinal and transverse components, keeping in mind that the wave functions ϕ_α are not of unit norm:

$$\hat\Psi^\dagger(x) = \frac{\phi_\alpha^*(x)}{\|\phi_\alpha\|^2} a_{\phi_\alpha}^\dagger + \delta\hat\Psi_\alpha^\dagger(x) \tag{7.21}$$

with

$$a_{\phi_\alpha}^\dagger = \int dx\; \phi_\alpha(x)\; \hat\Psi^\dagger(x). \tag{7.22}$$

The relevant bosonic commutation relations then read:

$$[a_{\phi_\alpha}, a_{\phi_\alpha}^\dagger] = \|\phi_\alpha\|^2 \qquad \text{and} \qquad [a_{\phi_\alpha}, \delta\hat\Psi_\alpha^\dagger(x)] = 0. \tag{7.23}$$

We will also need the projector $\mathcal{Q}_\alpha$ onto the subspace orthogonal to ϕ_α:

$$\mathcal{Q}_\alpha^{(x)}[\psi(x,x',\ldots)] = \psi(x,x',\ldots) - \frac{\phi_\alpha(x)}{||\phi_\alpha||^2}\int dy\; \phi_\alpha^*(y)\,\psi(y,x',\ldots). \tag{7.24}$$

This projector arises in the calculation as we have introduced a component of the field operator orthogonal to ϕ_α. Using $\int dx\; \phi_\alpha(x)\; \delta\hat\Psi_\alpha^\dagger(x) = 0$ we shall transform integrals involving $\delta\hat\Psi_\alpha^\dagger(x)$ as follows:

$$\int dx\; \psi(x,x',\ldots)\delta\hat\Psi_\alpha^\dagger(x) = \int dx\; \mathcal{Q}_\alpha^{(x)}[\psi(x,x',\ldots)]\delta\hat\Psi_\alpha^\dagger(x). \tag{7.25}$$

Inserting these definitions in eq.(7.17) the expression for σ at time $t+dt$ can be written as

$$\begin{aligned}\sigma(t+dt) &- \sigma(t) = S_1^{(0)}|N:\phi_1\rangle\langle N:\phi_2| + \text{e.c.} \\ &+ \int dx\; S_1^{(1)}(x)\delta\hat{\Psi}_1^\dagger(x)|N-1:\phi_1\rangle\langle N:\phi_2| + \text{e.c.} \\ &+ \iint dx\; dx'\; S_1^{(2)}(x,x')\delta\hat{\Psi}_1^\dagger(x)\delta\hat{\Psi}_1^\dagger(x')|N-2:\phi_1\rangle\langle N:\phi_2| + \text{e.c.} \\ &+ \iint dx\; dx'\; S^{(1,1)}(x,x')\delta\hat{\Psi}_1^\dagger(x)|N-1:\phi_1\rangle\langle N-1:\phi_2|\delta\hat{\Psi}_2(x')\end{aligned} \tag{7.26}$$

where the notation *e.c.* stands for the *exchanged* and *conjugate* of a quantity, *i.e.* the complex conjugate of the same quantity after having exchanged the indices 1 and 2. The explicit expressions for the $S_\alpha^{(i)}$ are:

$$S_1^{(0)} = N\frac{\langle\phi_1|F_1^{GP}\rangle}{\|\phi_1\|^2}dt + N\lambda_1\,dt + Nd\gamma_1 + \frac{N(N-1)}{2}d\gamma_1^2 + \frac{N^2}{2}d\gamma_1\,d\gamma_2^* \tag{7.27}$$

$$\begin{aligned}S_1^{(1)}(x) &= \sqrt{N}\Big\{\mathcal{Q}_1^{(x)}\left[F_1^{GP}(x)\right]dt + F_1^\perp(x)dt + dB_1^\perp(x) + \\ &\quad +(N-1)d\gamma_1\,dB_1^\perp(x) + N\,dB_1^\perp(x)\,d\gamma_2^*\Big\}\end{aligned} \tag{7.28}$$

$$S_1^{(2)}(x,x') = \frac{\sqrt{N(N-1)}}{2}dB_1^\perp(x)\,dB_1^\perp(x') \tag{7.29}$$

$$S^{(1,1)}(x,x') = N\,dB_1^\perp(x)\,dB_2^{\perp *}(x'). \tag{7.30}$$

Analogous expressions for $S_2^{(0)}$, $S_2^{(1)}$, $S_2^{(2)}$ are obtained by exchanging the indices 1 and 2. In the next subsection, we evaluate the exact evolution of the same dyadic during a time interval dt, so that we can determine the constraints on the force and noise terms entering into these equations.

7.1.3 Exact evolution of a Fock state Hartree dyadic

To make the stochastic scheme described in the previous sections equivalent to the exact dynamics as it is given by eq.(7.1), the final result of the previous subsection eqs.(7.26-7.30) has to be compared with the exact evolution of the density matrix $\sigma(t)$. Consider a dyadic $\sigma = |N:\phi_1\rangle\langle N:\phi_2|$ at time t; according to the equation of

motion eq.(7.2), after an infinitesimal time step dt it has evolved into:

$$\begin{aligned}\sigma(t+dt) &= \sigma(t) + \frac{dt}{i\hbar}\left(H\sigma(t) - \sigma(t)H\right) = \\ &= \sigma(t) + E_1^{(0)}|N:\phi_1\rangle\langle N:\phi_2| + \text{e.c.} + \\ &+ \int dx\; E_1^{(1)}(x)\delta\hat{\Psi}_1^\dagger(x)|N-1:\phi_1\rangle\langle N:\phi_2| + \text{e.c.} \\ &+ \iint dx\; dx'\; E_1^{(2)}(x,x')\delta\hat{\Psi}_1^\dagger(x)\delta\hat{\Psi}_1^\dagger(x')|N-2:\phi_1\rangle\langle N:\phi_2| + \text{e.c.}\end{aligned} \tag{7.31}$$

where the $E_\alpha^{(i)}$ are given by

$$E_1^{(0)} = \frac{N\,dt}{i\hbar}\left[\frac{\langle\phi_1|h_0|\phi_1\rangle}{\|\phi_1\|^2} + \frac{(N-1)}{2}\frac{\langle\phi_1\phi_1|V|\phi_1\phi_1\rangle}{\|\phi_1\|^4}\right] \tag{7.32}$$

$$E_1^{(1)}(x) = \frac{dt\sqrt{N}}{i\hbar}\mathcal{Q}_1^{(x)}\left[\left(h_0 + \frac{(N-1)}{\|\phi_1\|^2}\int dx'\; V(x-x')\,|\phi_1(x')|^2\right)\phi_1(x)\right] \tag{7.33}$$

$$E_1^{(2)}(x,x') = \frac{dt\sqrt{N(N-1)}}{2i\hbar}\;\mathcal{Q}_1^{(x)}\mathcal{Q}_1^{(x')}[V(x-x')\phi_1(x)\phi_1(x')]. \tag{7.34}$$

Analogous expressions for $E_2^{(0)}$, $E_2^{(1)}$, $E_2^{(2)}$ are obtained by exchanging the indices 1 and 2.

7.1.4 Validity conditions for the stochastic Fock state Hartree ansatz

The similarity of the structures of eq.(7.26) and eq.(7.31) suggests the possibility of a stochastic scheme equivalent to the exact evolution: to achieve this, it is necessary to find out specific forms of deterministic eq.(7.19) and stochastic eq.(7.18) terms for which the mean values of the $S_\alpha^{(i)}$ equal the $E_\alpha^{(i)}$:

$$\overline{S_1^{(0)} + S_2^{(0)*}} = E_1^{(0)} + E_2^{(0)*} \tag{7.35}$$

$$\overline{S_\alpha^{(1)}(x)} = E_\alpha^{(1)}(x) \tag{7.36}$$

$$\overline{S_\alpha^{(2)}(x,x')} = E_\alpha^{(2)}(x,x') \tag{7.37}$$

$$\overline{S^{(1,1)}(x,x')} = 0. \tag{7.38}$$

From the last equation eq.(7.38), it follows immediately why independent bras and kets are needed in the ansatz eq.(7.7): in the case $\phi_1 = \phi_2 = \phi$ such a condition

would in fact lead to a vanishing orthogonal noise and finally to the impossibility of satisfying eq.(7.37).

In terms of the different components, these conditions can be rewritten as:

$$(\lambda_1 + \lambda_2^*)\, dt + \frac{(N-1)}{2}\left[d\gamma_1^2 + d\gamma_2^{2^*}\right] + N d\gamma_1 d\gamma_2^* = 0 \tag{7.39}$$

$$F_1^\perp(x)\; dt + (N-1) dB_1^\perp(x)\, d\gamma_1 + N dB_1^\perp(x)\, d\gamma_2^* = 0 \tag{7.40}$$

$$F_2^\perp(x)\; dt + (N-1) dB_2^\perp(x)\, d\gamma_2 + N dB_2^\perp(x)\, d\gamma_1^* = 0 \tag{7.41}$$

$$dB_\alpha^\perp(x) dB_\alpha^\perp(x') = \frac{dt}{i\hbar}\mathcal{Q}_\alpha^x \mathcal{Q}_\alpha^{x'}\left[V(x-x')\phi_\alpha(x)\phi_\alpha(x')\right] \tag{7.42}$$

$$dB_1^\perp(x) dB_2^{\perp *}(x') = 0. \tag{7.43}$$

As we shall discuss in detail in sec.7.2, several different stochastic schemes can be found satisfying eqs.(7.39-7.43); each of them gives an evolution identical in average to the exact one, but the statistical properties can be much different.

7.1.5 A stochastic Hartree ansatz with coherent states

Up to now we have worked out the case of a Fock state ansatz $|N:\phi_1\rangle\langle N:\phi_2|$. Both in quantum optics and in condensed matter physics, coherent states are often used rather than Fock states We now show that a stochastic approach can be developed using a coherent state ansatz of the form:

$$\sigma(t) = \Pi(t)\; |\mathrm{coh}:\phi_1\rangle\langle\,\mathrm{coh}:\phi_2|, \tag{7.44}$$

where

$$|\mathrm{coh}:\phi_\alpha\rangle = \exp\left(\bar{N}^{1/2}\int dx\; \phi_\alpha(x)\hat{\Psi}^\dagger(x)\right)|\mathrm{vac}\rangle \tag{7.45}$$

and $\bar{N}$ is the mean number of particles. We have included here a prefactor $\Pi(t)$ which was absent in the case of the Fock state ansatz eq.(7.7); in the Fock state case indeed such a prefactor could be reincluded into the definition of ϕ_1 and ϕ_2. The wave functions $\phi_\alpha(x)$ and the prefactor factor Π evolve according to Ito stochastic differential equations

$$\begin{aligned} d\phi_\alpha &= F_\alpha dt + dB_\alpha \\ d\Pi &= f\, dt + db. \end{aligned} \tag{7.46}$$

Splitting the field operator as

$$\hat{\Psi}(x) = \bar{N}^{1/2}\; \phi_\alpha(x) + \delta\hat{\Psi}_\alpha(x) \tag{7.47}$$

and using

$$\delta\hat{\Psi}_\alpha(x)\ |\mathrm{coh}:\phi_\alpha\rangle = 0. \tag{7.48}$$

we find that the equivalence of the stochastic scheme and the exact evolution translates into the set of conditions:

$$f = 0 \tag{7.49}$$

$$F_1(x)dt + \frac{1}{\Pi}db\, dB_1(x) = \frac{dt}{i\hbar}h_0\phi_1(x) \tag{7.50}$$

$$F_2(x)dt + \frac{1}{\Pi^*}db^*\, dB_2(x) = \frac{dt}{i\hbar}h_0\phi_2(x) \tag{7.51}$$

$$dB_\alpha(x)dB_\alpha(x') = \frac{dt}{i\hbar}V(x-x')\phi_\alpha(x)\phi_\alpha(x') \tag{7.52}$$

$$dB_1(x)dB_2^*(x') = 0. \tag{7.53}$$

As we shall see in sec.7.2, such conditions are satisfied by several stochastic schemes. Very remarkably, the stochastic evolution deduced from the positive-P representation arises naturally as one of them.

Within this coherent state ansatz the one-particle density matrix is evaluated using

$$\rho^{(1)}(x,x') = \bar{N}\Big\langle \phi_1(x)\phi_2^*(x')\ \Pi(t)\ \exp(\bar{N}\ \langle\phi_2|\phi_1\rangle\ \Big\rangle_{\mathrm{stoch}}. \tag{7.54}$$

In a practical implementation of the simulation it turns out to be numerically more efficient to represent $\Pi(t)$ as the exponential of some quantity

$$\Pi(t) = e^{\bar{N}S(t)} \tag{7.55}$$

and to evolve $S(t)$ according to the stochastic equation

$$\begin{aligned} dS = &-\int dx\ [dB_1(x)\phi_1^*(x) + dB_2^*(x)\phi_2(x)] + \\ &-\frac{\bar{N}dt}{2i\hbar}\int dx \int dx'\ V(x-x')\left[|\phi_1(x)|^2|\phi_1(x')|^2 - |\phi_2(x)|^2|\phi_2(x')|^2\right]. \end{aligned} \tag{7.56}$$

7.2 Particular implementations of the stochastic approach

In the previous section we have derived the conditions that a stochastic scheme has to satisfy in order to recover the exact evolution given by the Hamiltonian eq.(7.1); in the case of the Fock state ansatz eq.(7.7), we get to the system eqs.(7.39-7.43), while in the case of the coherent state ansatz eq.(7.44) we get to the conditions eqs.(7.49-7.53).

As the number of these equations is actually smaller than the number of unknown functions there is by no mean uniqueness of the solutions, that is of the simulation schemes. We need a strategy to identify interesting solutions.

We therefore start this section by considering various indicators of the statistical error of the simulation (sec.7.2.1 which can be used as guidelines in the search for simulation schemes. These indicators are defined as variances of relevant quantities which are conserved in the exact evolution but which may fluctuate in the simulation. We show that these indicators are non decreasing functions of time; attempts to minimize the time derivative of a specific indicator will lead to particular implementations of the general stochastic method, such as the *simple* scheme (sec.7.2.2) and the *constant trace* scheme (sec.7.2.3).

7.2.1 Growth of the statistical errors

The first indicator that we consider measures the deviation of the stochastic operator $\sigma(t)$ from the exact density operator $\rho(t)$:

$$\Delta(t) = \Big\langle \mathrm{Tr}[(\sigma^\dagger(t) - \rho(t))(\sigma(t) - \rho(t))] \Big\rangle_{\mathrm{stoch}} = \\ = \Big\langle \mathrm{Tr}[\sigma^\dagger(t)\sigma(t)] \Big\rangle_{\mathrm{stoch}} - \mathrm{Tr}\left[\rho(t)^2\right]. \quad (7.57)$$

We now show that $\Delta(t)$ is a non-decreasing function of time. When the stochastic scheme satisfies the validity conditions derived in the previous section, we can write the stochastic equation for σ as:

$$d\sigma = \frac{dt}{i\hbar}[\mathcal{H}, \sigma] + d\sigma_s \quad (7.58)$$

where $d\sigma_s$ is a zero-mean noise term linear in dB_α (and db for the coherent state simulation). In the case of simulation with Fock states it is given by

$$d\sigma_s = N^{1/2} \Big\{ \int dx\, dB_1(x) \hat{\Psi}^\dagger(x) |N-1:\phi_1\rangle\langle N:\phi_2| + \\ + \int dx\, dB_2^*(x) |N:\phi_1\rangle\langle N-1:\phi_2| \hat{\Psi}(x) \Big\}. \quad (7.59)$$

In the case of simulation with coherent states it is given by

$$d\sigma_s = db|\text{coh } :\phi_1\rangle\langle\text{ coh } :\phi_2| + \\ + \bar{N}^{1/2}\Pi\left\{\int dx\; dB_1(x)\hat{\Psi}^\dagger(x)|\text{coh } :\phi_1\rangle\langle\text{ coh } :\phi_2| + \right. \\ \left. + \int dx\; dB_2^*(x)|\text{coh } :\phi_1\rangle\langle\text{ coh } :\phi_2|\hat{\Psi}(x)\right\}. \quad (7.60)$$

We calculate the variation of Δ during dt, replacing σ by $\sigma + d\sigma$ in eq.(7.57) and keeping terms up to order dt. Using the invariance of the trace in a cyclic permutation and averaging over the noise between t and $t + dt$ we finally obtain

$$d\Delta = \left\langle \text{Tr}[d\sigma_s^\dagger d\sigma_s]\right\rangle_{\text{stoch}}, \quad (7.61)$$

which is a positive quantity. Minimization of this quantity is the subject of sec.7.2.2. Physically $d\Delta \geq 0$ means that the impurity of the stochastic density operator σ always increases in average, while the exact density operator has a constant purity $\text{Tr}\,[\rho^2]$.

The second kind of indicator that we consider measures the statistical error on constants of motion of the exact evolution. Consider a time independent operator X commuting with the Hamiltonian. The stochastic evolution leads to an error on the expectation value of X with a variance given by the ensemble average of

$$\Delta_X(t) = \left\langle \left|\text{Tr}[X\sigma(t)] - \text{Tr}[X\rho(t)]\right|^2\right\rangle_{\text{stoch}} = \\ = \left\langle \left|\text{Tr}[X\sigma(t)]\right|^2\right\rangle_{\text{stoch}} - \left|\text{Tr}[X\rho(t)]\right|^2. \quad (7.62)$$

From eq.(7.58) we obtain the variation after a time step dt of the expectation value of X along a stochastic trajectory:

$$d(\text{Tr}[X\sigma]) = \frac{dt}{i\hbar}\text{Tr}\,(X[\mathcal{H},\sigma]) + \text{Tr}[Xd\sigma_s]. \quad (7.63)$$

Using the invariance of the trace under cyclic permutation and the commutation relation $[\mathcal{H}, X] = 0$ we find that the first term in the right hand side of eq.(7.63) vanishes so that

$$d\Delta_X = \left\langle \left|\text{Tr}[Xd\sigma_s]\right|^2\right\rangle_{\text{stoch}}, \quad (7.64)$$

a quantity which is always non-negative.

Using expression eq.(7.64) one can *design* simulations preserving exactly the conserved quantity, the constraint to meet being $\mathrm{Tr}[X d\sigma_s] = 0$: for instance in the Fock state simulation, one first chooses the transverse noises $dB_\alpha^\perp$ satisfying eqs.(7.42-7.43); then one simply has to take for the longitudinal noise of ϕ_1:

$$d\gamma_1 = -\frac{1}{\sqrt{N}}\Big(\langle N:\phi_2|X|N:\phi_1\rangle\Big)^{-1} \int dx\; dB_1^\perp(x)\langle N:\phi_2|X\delta\hat{\Psi}_1^\dagger(x)|N-1:\phi_1\rangle \quad (7.65)$$

and a similar expression for $d\gamma_2$; finally the force terms F_α are adjusted in order to satisfy eqs.(7.39-7.41). As natural examples of conserved quantities one can choose $X = 1$ or $X = H$; the former case is discussed in detail in sec.7.2.3.

7.2.2 The *simple* schemes

This scheme is characterized by the minimization of the incremental variation of the statistic spread of the N-particle density matrix $\sigma(t)$, a spread that we have already quantified in eq.(7.57) by $\Delta(t)$. To be more specific we assume that we have evolved a dyadic up to time t, and we look for the noise terms that minimize the increase of $\mathrm{Tr}[\sigma^\dagger\sigma]$ between t and $t + dt$.

Simulation with Fock states

In the case of the Fock state ansatz, we calculate explicitly the variation of $\mathrm{Tr}[\sigma^\dagger\sigma]$ from eq.(7.59) and we get:

$$\frac{d\mathrm{Tr}[\sigma^\dagger\sigma]}{N\mathrm{Tr}[\sigma^\dagger\sigma]} = N\left(d\gamma_1 + d\gamma_2^*\right)\left(d\gamma_1^* + d\gamma_2\right) + \\ + \sum_{\alpha=1,2}||\phi_\alpha||^{-2}\int dx\; dB_\alpha^\perp(x)dB_\alpha^{\perp *}(x) + \left[d\gamma_1 + d\gamma_2^* + \text{c.c.}\right]. \quad (7.66)$$

We now look for the noise terms $d\gamma_\alpha$ and $dB_\alpha^\perp$ minimizing this quantity under the constraints eqs.(7.39-7.43).

We first note that we can choose $d\gamma_1 = d\gamma_2 = 0$ without affecting the transverse noises, as shown by eqs.(7.39-7.43): the correlation function of the transverse noises do not involve the $d\gamma_\alpha$, and we can accommodate for any choice of $d\gamma_\alpha$ by defining appropriately the force terms $F_\alpha^\perp, \lambda_\alpha$. In the particular case defining our simple scheme we take all these force terms equal to zero; note that the choice of vanishing

$d\gamma$'s immediately leads to a vanishing noise term in eq.(7.66). Since the deterministic part of the evolution is described by Gross-Pitaevskii equations which preserve the norm of $\phi_{1,2}$, and the eigenvalues $\zeta_{1,2}$ of the noise covariance operator $dB_\alpha(x)dB^*_\alpha(x')$ have the upper bound $\zeta_{1,2} \leq V(0)dt||\phi_{1,2}||^2/\hbar$, the stochastic equations do possess a regular and non-exploding solution valid for all times so that no divergences can occur within a finite time [273, §4.5].

Secondly the terms involving the transverse noise in eq.(7.66) are bounded from below: As the modulus of a mean is less than or equal to the mean of the modulus, we have

$$\left| \, dB^\perp_\alpha(x)dB^\perp_\alpha(x) \, \right| \leq \; dB^\perp_\alpha(x)dB^{\perp *}_\alpha(x) \; , \tag{7.67}$$

with the left hand side of this inequality fully determined by condition eq.(7.42).

For the remaining part of the present section sec.7.2.2 we assume that the interaction potential $V(x)$ has a positive Fourier transform:

$$\tilde{V}(k) \geq 0 \quad \text{for all } k \tag{7.68}$$

where the Fourier transform of $V(x)$ is defined as

$$\tilde{V}(k) = \int dx \; V(x) e^{-ikx}; \tag{7.69}$$

the repulsive Gaussian interaction potential used in sec.7.4 satisfies the condition eq.(7.68). Note that as a consequence of eq.(7.68) and of the inverse Fourier transform formula the model interaction potential is maximal and positive in $x = 0$:

$$V(0) \geq |V(x)| \quad \text{for all } x. \tag{7.70}$$

Under the assumption eq.(7.68) we have found for the transverse noise a choice which both fulfills eqs.(7.42-7.43) and saturates the inequality eq.(7.67). We first discretize the Fourier space with an arbitrarily small wavevector step dk and we set

$$dB^\perp_\alpha(x) = \left(\frac{dt}{i\hbar}\right)^{1/2} \mathcal{Q}^{(x)}_\alpha \left[\phi_\alpha(x) \sum_k \frac{\sqrt{dk}}{(2\pi)^{d/2}} \left(\tilde{V}(k)\right)^{1/2} e^{ikx} e^{i\theta_\alpha(k)} \right] \tag{7.71}$$

where d is the dimension of position space. The phases θ_α have the following statistical property:

$$\overline{e^{i\theta_\alpha(k)} e^{i\theta_\alpha(k')}} = \delta_{k,-k'} \tag{7.72}$$

and θ_1, θ_2 are uncorrelated. In practice for half of the k-space (e.g. $k_z > 0$) $\theta_\alpha(k)$ is randomly chosen between 0 and 2π; for the remaining k's we take $\theta_\alpha(-k) = -\theta_\alpha(k)$.

One can then check that this choice for the transverse noise reproduces the correlation function eqs.(7.42-7.43).

We show now that the implementation eq.(7.71) saturates the inequality eq.(7.67) and therefore leads to the minimal possible value for $d\mathrm{Tr}[\sigma^\dagger\sigma]$ within the validity constraints of the stochastic approach. We calculate explicitly the right hand side of eq.(7.67):

$$dB_\alpha^\perp(x)dB_\alpha^{\perp *}(x) = \frac{dt}{\hbar}\left(\mathcal{Q}_\alpha^{(x)*}\mathcal{Q}_\alpha^{(x')}[V(x-x')\phi_\alpha^*(x)\phi_\alpha(x')]\right)_{x=x'} = \\ = \frac{dt}{\hbar}|\phi_\alpha(x)|^2\left[V(0) - 2\int dy\ \frac{|\phi_\alpha(y)|^2}{||\phi_\alpha||^2}V(x-y) + \frac{\langle\phi_\alpha,\phi_\alpha|V|\phi_\alpha,\phi_\alpha\rangle}{||\phi_\alpha||^4}\right] \quad (7.73)$$

where $\mathcal{Q}_\alpha^*$ projects onto the subspace orthogonal to ϕ_α^* and where we have used the positivity of the Fourier transform $\tilde{V}$ of the model interaction potential. The left hand side of eq.(7.67) is calculated using eq.(7.42):

$$dB_\alpha^\perp(x)^2 = \frac{dt}{i\hbar}\phi_\alpha^2(x)\left[V(0) - 2\int dy\ \frac{|\phi_\alpha(y)|^2}{||\phi_\alpha||^2}V(x-y) + \frac{\langle\phi_\alpha,\phi_\alpha|V|\phi_\alpha,\phi_\alpha\rangle}{||\phi_\alpha||^4}\right]. \quad (7.74)$$

As the expressions between square brackets in eqs.(7.74-7.73) are real we deduce the equality in eq.(7.67).

We can now calculate explicitly the variation of $\mathrm{Tr}[\sigma^\dagger\sigma]$ by integrating eq.(7.73) over x:

$$\frac{d\mathrm{Tr}[\sigma^\dagger\sigma]}{N\mathrm{Tr}[\sigma^\dagger\sigma]} = \frac{dt}{\hbar}\left[2V(0) - \sum_{\alpha=1,2}\frac{\langle\phi_\alpha,\phi_\alpha|V|\phi_\alpha,\phi_\alpha\rangle}{||\phi_\alpha||^4}\right]. \quad (7.75)$$

This expression is particularly useful since it allows one to derive an upper bound on the increase of $\mathrm{Tr}[\sigma^\dagger\sigma]$: as we assume here a positive Fourier transform of the potential $V(x-x')$, the matrix element $\langle\phi_\alpha,\phi_\alpha|V|\phi_\alpha,\phi_\alpha\rangle$ is also positive so that the right hand side of eq.(7.75) is smaller than $2V(0)dt/\hbar$. After time integration we obtain

$$\mathrm{Tr}[\sigma^\dagger\sigma](t) \leq \mathrm{Tr}[\sigma^\dagger\sigma](0)e^{2NV(0)t/\hbar}. \quad (7.76)$$

Using eq.(7.57) and the fact that the trace of the squared density operator ρ^2 is a constant under Hamiltonian evolution we can deduce an upper bound on the squared statistical error $\Delta(t)$:

$$\Delta(t) + \mathrm{Tr}[\rho^2] \leq \left[\Delta(0) + \mathrm{Tr}[\rho^2]\right]e^{2NV(0)t/\hbar}. \quad (7.77)$$

Note that it involves the model dependent quantity $V(0)$ and not only the physical parameters of the problem such as the chemical potential or the scattering length. It may be therefore important to adjust the model interaction potential $V(x-x')$ in order to minimize the growth of the statistical error for given physical parameters.

Simulation with coherent states

In the case of the coherent state ansatz, an explicit calculation of $d\,\mathrm{Tr}\left[\sigma^\dagger\sigma\right]$ from eq.(7.60) gives:

$$\begin{aligned}\frac{d\mathrm{Tr}[\sigma^\dagger\sigma]}{\mathrm{Tr}[\sigma^\dagger\sigma]} = \left|\frac{db}{\Pi} + \bar{N}\int dx\; dB_1(x)\phi_1^*(x) + dB_2^*(x)\phi_2(x)\right|^2 + \\ + \left[\frac{db}{\Pi} + \bar{N}\sum_{\alpha=1,2}\int dx\; dB_\alpha(x)dB_\alpha^*(x) + \text{c.c}\right] + \\ + \bar{N}\int dx\; dB_1(x)\phi_1^*(x) + dB_2^*(x)\phi_2(x). \quad (7.78)\end{aligned}$$

We now proceed to the minimization of the increment of $\mathrm{Tr}[\sigma^\dagger\sigma]$ within the coherent state ansatz along the same lines as the previous subsection. First we optimize the noise db on the normalization factor Π:

$$db = -\bar{N}\Pi\left(\int dx\; dB_1(x)\phi_1^*(x) + dB_2^*(x)\phi_2(x)\right). \quad (7.79)$$

This choice leads to a vanishing noise term in eq.(7.78). We insert this expression for db in the validity conditions eq.(7.50) and eq.(7.51) and we obtain:

$$F_\alpha(x) = \frac{1}{i\hbar}\left[h_0 + \bar{N}\int dx'\, V(x-x')|\phi_\alpha(x')|^2\right]\phi_\alpha(x). \quad (7.80)$$

Finally minimization of the contribution of the noise terms dB_α with the constraint eq.(7.52) is achieved with the choice

$$dB_\alpha(x) = \left(\frac{dt}{i\hbar}\right)^{1/2}\phi_\alpha(x)\sum_k \frac{\sqrt{dk}}{(2\pi)^{d/2}}\left(\tilde{V}(k)\right)^{1/2} e^{ikx}e^{i\theta_\alpha(k)} \quad (7.81)$$

where the phases $\theta_\alpha(k)$ are randomly generated as in eq.(7.72).

The first equation eq.(7.80) fixes the deterministic evolution to the usual mean-field equation eq.(7.4). We note here that the mean-field term in eq.(7.80) does not contain

the normalization of the spatial density $\bar{N}|\phi_\alpha(x')|^2$ by $||\phi_\alpha||^2$, a feature present in the Fock state simulation (see eq.(7.20)). This is a disadvantage of the coherent state simulation since this normalization factor appearing in the Fock state simulation has a regularizing effect: the norms $||\phi_\alpha||$ may indeed deviate significantly from unity in the stochastic evolution. The second equation eq.(7.81) determines the stochastic noise on the wave functions in a way very similar to the Fock state case eq.(7.71). In particular the evolutions of ϕ_1 and ϕ_2 are still uncorrelated. The only difference is the disappearance of the projector $\mathcal{Q}_\alpha$ in the expression of the noise, which leads to an increased noise with respect to the simulation with Fock states.

As in the Fock state case, the deterministic evolution of the present scheme has a Gross-Pitaevskii form and therefore conserves the norms $||\phi_{1,2}||$; this means that the stochastic equations are again regular at all times and no divergences occur within a finite time.

As in the previous subsection we now estimate the squared error Δ. We calculate the variation of $\mathrm{Tr}[\sigma^\dagger\sigma]$ for the choice of noise eq.(7.81):

$$\frac{1}{\mathrm{Tr}[\sigma^\dagger\sigma]}\frac{d\mathrm{Tr}[\sigma^\dagger\sigma]}{dt} = \frac{\bar{N}V(0)}{\hbar}\sum_{\alpha=1,2}||\phi_\alpha||^2. \tag{7.82}$$

The average over all stochastic realizations of the norm squared of the wave functions can be calculated exactly:

$$\Big\langle ||\phi_\alpha||^2 \Big\rangle_{\mathrm{stoch}}(t) = e^{tV(0)/\hbar}\Big\langle ||\phi_\alpha||^2 \Big\rangle_{\mathrm{stoch}}(0). \tag{7.83}$$

This leads to a remarkable identity on the trace of $\sigma^\dagger\sigma$:

$$\begin{aligned}\Big\langle \ln \mathrm{Tr}[\sigma^\dagger\sigma] \Big\rangle_{\mathrm{stoch}}(t) = \\ = \Big\langle \ln \mathrm{Tr}[\sigma^\dagger\sigma] \Big\rangle_{\mathrm{stoch}}(0) + \bar{N}\left(e^{tV(0)/\hbar}-1\right)\Big\langle \sum_{\alpha=1,2}||\phi_\alpha||^2 \Big\rangle_{\mathrm{stoch}}(0).\end{aligned} \tag{7.84}$$

Using finally the concavity of the logarithmic function, leading to the logarithm of a mean being larger than the mean of the logarithm we obtain a lower bound on the squared error Δ on the $N-$body density matrix:

$$\Delta(t) + \mathrm{Tr}[\rho^2] \geq A\exp\left[2B\bar{N}\left(e^{tV(0)/\hbar}-1\right)\right] \tag{7.85}$$

where we have introduced the constant quantities

$$A = \exp\left[\Big\langle \ln \mathrm{Tr}[\sigma^\dagger\sigma] \Big\rangle_{\mathrm{stoch}}(0)\right] \tag{7.86}$$

$$B = \frac{1}{2}\Big\langle \sum_{\alpha=1,2}||\phi_\alpha||^2 \Big\rangle_{\mathrm{stoch}}(0) \tag{7.87}$$

We recall that a vanishing $V(0)$ would correspond here to an identically vanishing interaction potential $V(x)$, according to eq.(7.70).

Final remark on the *simple* schemes

In the simple schemes the $N-$body density operator is obtained as a stochastic average of dyadics such as $|\text{coh} : \bar{N}^{1/2}\phi_1\rangle\langle\text{coh} : \bar{N}^{1/2}\phi_2|$ or $|N : \phi_1\rangle\langle N : \phi_2|$, where the evolutions of ϕ_1 and ϕ_2 are fully decoupled and uncorrelated. This allows for an interesting reinterpretation of our representation of the $N-$body density operator: if the initial density operator is given by $\rho(t=0) = |N : \phi_0\rangle\langle N : \phi_0|$, at a time t it will be given by

$$\rho(t) = |\Psi(t)\rangle\langle\Psi(t)| \tag{7.88}$$

where the $N-$particle state vector is equal to

$$|\Psi(t)\rangle = \lim_{\mathcal{N}\to\infty}\frac{1}{\mathcal{N}}\sum_{j=1}^{\mathcal{N}}|N : \phi^{(j)}(t)\rangle; \tag{7.89}$$

here $\phi^{(j)}$ are stochastic realizations with the initial condition $\phi^{(j)}(t=0) = \phi_0$.

7.2.3 The *constant trace* schemes

We have given the expression of the one-body density matrix $\rho^{(1)}$ in terms of $\phi_\alpha(x)$ for the simulation with Fock states eq.(7.13). This expressions shows that $\rho^{(1)}$ is very sensitive in the large N limit to fluctuations of $\langle\phi_2|\phi_1\rangle$. The same remark applies to two-body observables. In order to improve the statistical properties of the simulation one can consider the possibility of a simulation scheme exactly preserving $\langle\phi_2|\phi_1\rangle = 1$ at any time. This actually corresponds to a conserved trace of each single dyadic $\sigma(t)$. For the case of the coherent state ansatz, such a requirement leads to the well-known positive-*P* representation.

Simulation with Fock states

Within the Fock state ansatz, the conservation of the trace of the dyadic $\text{Tr}[\sigma]$ can be achieved by (i) choosing the transverse noises $dB_\alpha^\perp$ according to the formula

eq.(7.71) and (ii) using the expression eq.(7.65) for the longitudinal noise with $X = 1$. Point (ii) gives:

$$d\gamma_1 = -\langle\phi_2|\phi_1\rangle^{-1} \int dx\ \phi_2^*(x) dB_1^\perp(x). \tag{7.90}$$

The forces terms λ_α and F_α are fixed by the conditions eqs.(7.39-7.41):

$$\lambda_1\ dt = -\frac{N-1}{2}\langle\phi_2|\phi_1\rangle^{-2} \int dx\ dx'\ \phi_2^*(x)\phi_2^*(x') dB_1^\perp(x) dB_1^\perp(x') \tag{7.91}$$

and

$$F_1^\perp(x)\ dt = (N-1)\langle\phi_2|\phi_1\rangle^{-1} \int dx'\ \phi_2^*(x') dB_1^\perp(x') dB_1^\perp(x). \tag{7.92}$$

The expressions for $d\gamma_2, \lambda_2$ and $F_2^\perp(x)$ are obtained by exchanging the indices 1 and 2 in these results.

Simulation with coherent states

In the case of the coherent state ansatz, the value of $d\sigma_s$, which is the zero-mean noise term entering the variation of the dyadic σ during a time step dt, is given in eq.(7.60). The requirement of a constant trace $\mathrm{Tr}[\sigma] = \Pi e^{\bar{N}\langle\phi_2|\phi_1\rangle}$ leads to the following condition on the noise terms

$$db + \bar{N}\Pi \int dx\ \left(\phi_2^*(x) dB_1(x) + dB_2^*(x)\phi_1(x)\right) = 0. \tag{7.93}$$

We choose the noise terms dB_α as in eq.(7.81). The remaining parameters F_α are now unambiguously determined by eqs.(7.50-7.51):

$$F_1(x) = \frac{1}{i\hbar}\left[h_0 + \int dx'\ \bar{N}\phi_2^*(x') V(x-x')\phi_1(x')\right]\phi_1(x) \tag{7.94}$$

$$F_2(x) = \frac{1}{i\hbar}\left[h_0 + \int dx'\ \bar{N}\phi_1^*(x') V(x-x')\phi_2(x')\right]\phi_2(x). \tag{7.95}$$

This scheme exactly recovers the stochastic evolution in the positive-P representation, which was originally obtained with a different mathematical procedure.[157]

7.3 Stochastic vs. exact approach for a two-mode model

In order to test the convergence of the stochastic schemes developed in the previous section we now apply this method to a simple two-mode system for which the

exact solution of the N-body Schrödinger equation can also be obtained by a direct numerical integration. This allows (i) to check that the stochastic methods when averaged over many realizations give the correct result indeed, and (ii) to determine the statistical error for each of the four implementations of the stochastic approach (*constant trace* vs. *simple*, Fock vs. coherent states).

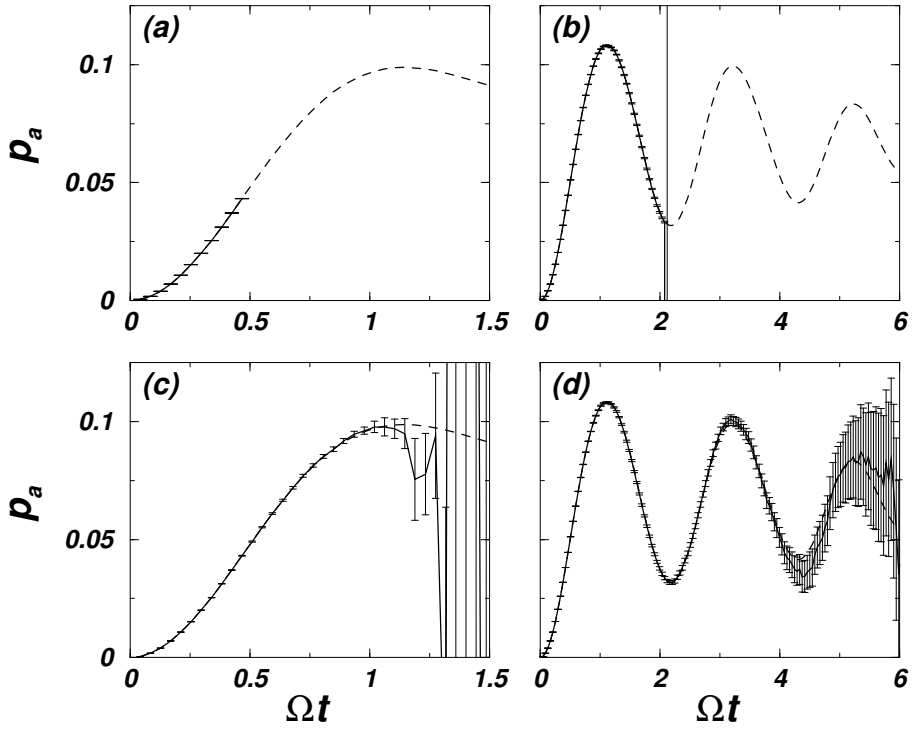

FIGURE 7.1: Two-mode model: mean fraction of atoms in the mode a as function of time, obtained with (a) the positive-P representation, (b) the Fock state simulation with constant trace, (c) the simple simulation with coherent states, and (d) the simple simulation with Fock states. The solid line represents the average over $\mathcal{N} = 2 \times 10^5$ simulations, with corresponding error bars. The dashed line is the direct numerical solution of the Schrödinger equation. The number of atoms is $N = 17$, initially all in mode b. The interaction constant is $\kappa = 0.1\Omega$. The calculations in (a) and (b) have been stopped after the divergence of one realization.

The toy-model that we consider describes the dynamics of two self-interacting condensates coherently coupled one to the other. It can be applied to the case of two condensates separated by a barrier[193] (Josephson-type coupling) or condensates in two different internal states coupled by an electromagnetic field[274] (Rabi-type coupling). In this model we restrict the expansion of the atomic field operator to two

orthogonal modes,

$$\hat{\psi}(x) = \hat{a}\, u_a(x) + \hat{b}\, u_b(x). \tag{7.96}$$

The Hamiltonian eq.(7.1) takes the simple form:

$$\mathcal{H} = \frac{\hbar\Omega}{2}\left(\hat{a}^\dagger\hat{b} + \hat{b}^\dagger\hat{a}\right) + \hbar\kappa\left(\hat{a}^{\dagger 2}\hat{a}^2 + \hat{b}^{\dagger 2}\hat{b}^2\right) \tag{7.97}$$

where $\hat{a}, \hat{b}$ annihilate a particle in modes A and B, κ characterizes the strength of the atomic interactions inside each condensate and Ω is the Rabi coupling amplitude between the two condensates. Here we have restricted for simplicity to the case where (i) the condensates have identical interaction properties, (ii) the interactions between atoms in different modes are negligible, and (iii) the Rabi coupling is resonant. The most general two-mode case could be treated along the same lines.

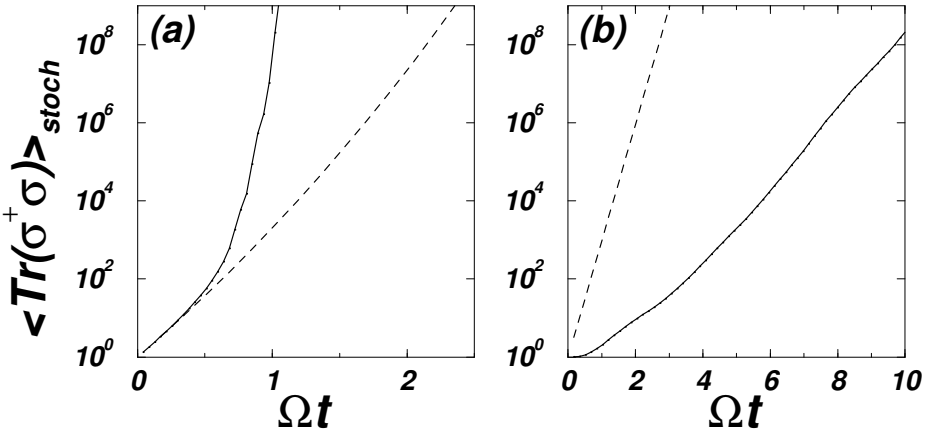

FIGURE 7.2: Statistical error on the $N-$body density matrix for the two-mode model: (a) *simple* scheme with coherent states and (b) *simple* scheme with Fock states. The solid line is the numerical result of the simulations. The dashed lines in (a) and (b) correspond respectively to the lower and upper bounds eq.(7.85) and eq.(7.77). The parameters are the same as in figure 7.1.

The direct numerical solution of the Schrödinger equation is performed in a basis of Fock states $|n_a, n_b\rangle$ with $n_{a,b}$ particles in modes A, B. The numerical integration is simplified by the fact that $n_a + n_b$ is a quantity conserved by the Hamiltonian evolution. We start with a state in which all atoms are in mode B, either in a Fock state $|n_a = 0, n_b = N\rangle$ (for the Fock state simulations) or in a coherent state $\propto \exp(N^{1/2}\hat{b}^\dagger)|0,0\rangle$ (for the coherent state simulations). We watch the time evolution of the mean fraction of particles in mode A, $p_a \equiv \langle\hat{a}^\dagger\hat{a}\rangle/N$.

Mean-field theory (the Gross-Pitaevskii equation), valid in the limit $N \gg 1$ with a fixed $\kappa N/\Omega$,[275,276] predicts periodic oscillations of $\langle \hat{a}^\dagger \hat{a} \rangle / N$; the peak-to-peak amplitude of the oscillations is equal to unity if $\kappa N/\Omega < 1$, and is smaller than one otherwise.[135] In the exact solution the oscillations are no longer periodic due to emergence of incommensurable frequencies in the spectrum of $\mathcal{H}$.

In the simulation method we evolve sets of two complex numbers representing the amplitudes of the functions $\phi_1(x)$ and $\phi_2(x)$ on the modes $u_{a,b}(x)$ (plus the Π coefficient in the coherent state case). The results are presented in figure 7.1 for $N = 17$ particles which $\kappa/\Omega = 0.1$ together with the result of the direct integration of the Schrödinger equation.

The first row in the figure concerns the constant trace simulations. Figure 7.1a shows results of the simulation based on the positive-*P* representation, that is the constant trace simulation with coherent states. As well known[169] this scheme leads to divergences of the norm $||\phi_1||\,||\phi_2||$ for some realizations of the simulation. We have cut the plot in figure 7.1 at the first divergence. The same type of divergences occurs in the constant trace simulation with Fock states. Note however that the characteristic time for the first divergence to occur is somewhat longer. We have checked that the probability distribution of $||\phi_1||\,||\phi_2||$ broadens with time, eventually getting a power law tail. The corresponding exponent α decreases in time below the critical value $\alpha_{\rm crit} = 3$ for which the variance of $||\phi_1||\,||\phi_2||$ becomes infinite. This scenario is identical to the one found with the positive-*P* representation.[169]

The simple simulation schemes plotted on the second row of figure 7.1 provide results which are at all time in agreement with the direct integration within the error bars. Contrarily to the constant trace schemes we do not observe finite time divergences in the simple schemes. For a given evolution time we have checked that the error bars scale as $1/\sqrt{\mathcal{N}}$ where $\mathcal{N}$ is the number of stochastic realizations. For a given $\mathcal{N}$ we found that the error bars increase quasi-exponentially with time.

The noise in the simple simulation schemes is investigated in more details in figure 7.2 which shows the error estimator $\left\langle \mathrm{Tr}[\sigma^\dagger \sigma] \right\rangle_{\rm stoch}$ as function of time, for coherent states in figure 7.2a and for Fock states in figure 7.2b. The coherent state result confirms the prediction eq.(7.85). The Fock state result is found to be notably smaller than the upper bound eq.(7.77). This is due to the fact that the terms proportional to $\langle \phi_\alpha, \phi_\alpha | V | \phi_\alpha, \phi_\alpha \rangle$ in eq.(7.75) are not negligible as compared to the term $V(0)$. We have checked these conclusions for various values of N and κ/Ω.

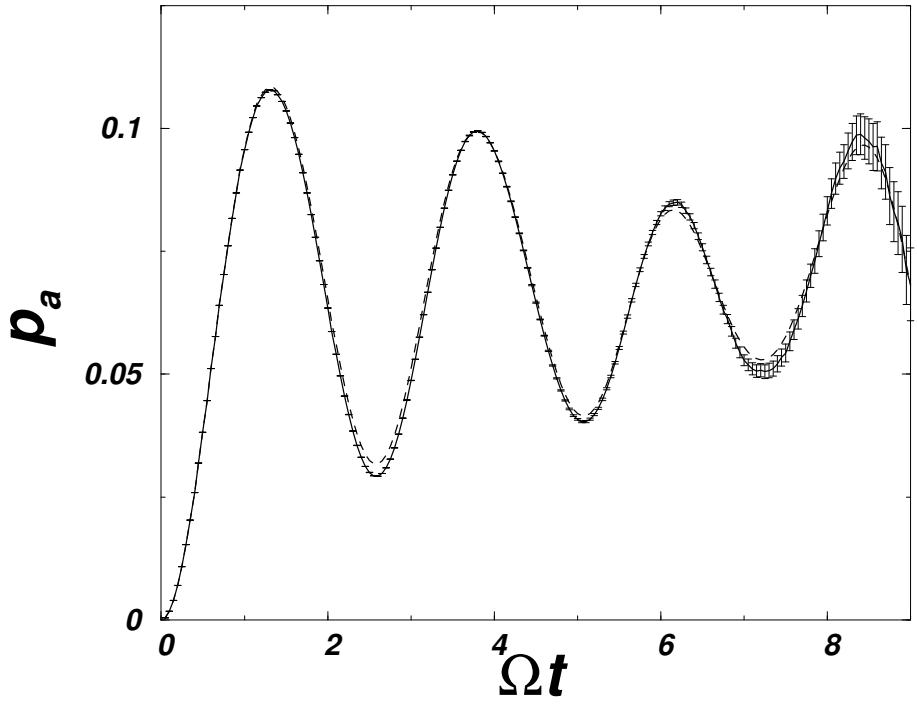

FIGURE 7.3: Fraction of atoms in mode a in the two-mode model, for the parameters of figure 7.1. The solid line with error bars is the result of the *simple* scheme simulation with Fock states with $\mathcal{N} = 10^8$ realizations. The dashed line is the direct numerical solution of the Schrödinger equation. The quantum phenomenon of collapse and revival of the oscillation amplitude clearly apparent on the exact result is well reproduced by the simulation.

For a large number of particles it is known[277] that the oscillations of $\langle \hat{a}^\dagger \hat{a} \rangle$ experience a collapse followed by revivals. These revivals are purely quantum phenomena for the field dynamics and they cannot be obtained in classical field approximation such as the Gross-Pitaevskii equation. We expect to see a precursor of this phenomenon even for the small number of particles $N = 17$. As the simple scheme simulation with Fock states is the most efficient of the four schemes for the investigation of the long time limit, we have pushed it to the time at which a *revival* can be seen, as shown in figure 7.3. This figure is obtained with $\mathcal{N} = 10^8$ simulations.

7.4 Stochastic approach for a one-dimensional Bose gas

The physical problem of the interacting Bose gas is in general a multi-mode problem, and the simulation schemes may have in this case a behavior different from the one in a few-mode model such as in sec.7.3. We have therefore investigated a model for a one-dimensional Bose gas. The atoms are confined in a harmonic trap with an oscillation frequency ω. They experience binary interactions with a Gaussian interaction potential of strength g and range b:

$$V(x-x') = \frac{g}{(2\pi)^{1/2}b} \exp\left[-(x-x')^2/(2b^2)\right]. \tag{7.98}$$

At time $t = 0$ all the atoms are in the same normalized state ϕ solution of the time independent Gross-Pitaevskii equation

$$\mu\phi(x) = -\frac{\hbar^2}{2m}\frac{d^2\phi}{dx^2} + \frac{1}{2}m\omega^2x^2\phi(x) + (N-1)\int dx'\, V(x-x')|\phi(x')|^2\phi(x). \tag{7.99}$$

At time $t = 0^+$ the trap frequency is suddenly increased by a factor two, which induces a breathing of the cloud.[278–280]

This expected breathing is well reproduced by the numerical simulations. The mean squared spatial width R^2 of the cloud as function of time is obtained by taking $\hat{O} = \sum_{k=1}^{N}\hat{x}_k^2/N$ in eq.(7.11) where $\hat{x}_k$ is the position operator of the $k-$th particle. The quantity R^2 is shown in figure 7.4 for the simulation schemes with Fock states. One recovers the key feature of the constant trace simulation, that is a divergence of the norm $||\phi_1||\,||\phi_2||$ in finite time for some realizations. Before the occurrence of the first divergence the stochastic variance of the size squared of the cloud, defined as

$$\mathrm{Var}(R^2)_{\mathrm{stoch}} = \frac{1}{\mathcal{N}}\sum_{i=1}^{\mathcal{N}}\left[R_i^2(t) - R^2(t)\right]^2 \tag{7.100}$$

with

$$R_i^2(t) = \mathrm{Re}\left[\langle N:\phi_2^{(i)}(t)|\hat{O}|N:\phi_1^{(i)}(t)\rangle\right] \tag{7.101}$$

is notably smaller in the constant trace scheme than in the simple scheme, as shown in figure 7.5a. This contrast between the two schemes for the statistical error on one-body observables was absent in the two-mode model of sec.7.3.

We have also investigated the noise on the $N-$body density matrix characterized by $\left\langle \mathrm{Tr}[\sigma^\dagger\sigma]\right\rangle_{\mathrm{stoch}}$ (see figure 7.5b). As expected this error indicator is smaller with

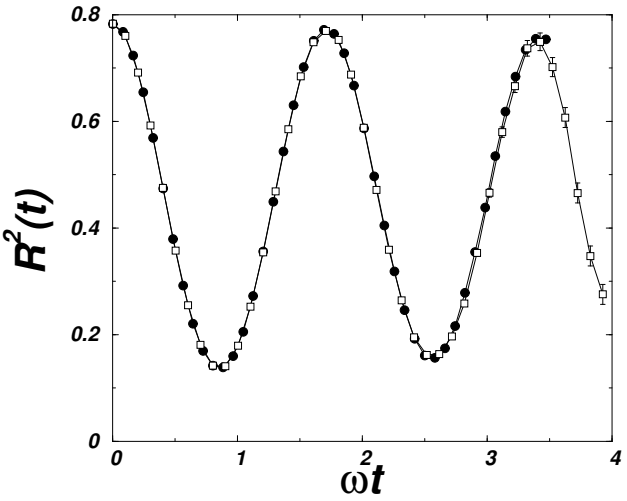

FIGURE 7.4: Mean squared spatial width R^2 of a harmonically confined cloud of $N = 10$ atoms as function of time. The breathing of the cloud is induced by an abrupt change of the trap frequency from ω to 2ω. The width R is measured in units of the harmonic oscillator length $a_{\rm ho} = (\hbar/(m\omega))^{1/2}$. The interaction potential is chosen such that $b = 0.5a_{\rm ho}$ and $g = 0.4\hbar\omega a_{\rm ho}$ leading to a chemical potential $\mu = 1.7\hbar\omega$ in the Gross-Pitaevskii equation eq.(7.99). The calculation is performed on a spatial grid with 32 points ranging from $-6a_{\rm ho}$ to $+6a_{\rm ho}$ (with periodic boundary conditions). •: constant trace simulation with $\mathcal{N} = 1000$ realizations. For $\omega t > 3.5$ a divergence has occured for one of the realizations and the calculation has been stopped. □: simple scheme simulation with $\mathcal{N} = 40000$ realizations.

the simple scheme. For this simple scheme it varies quasi exponentially with time with an exponent $\gamma \simeq 4\omega$, which is smaller by a factor roughly 2 than the one of the upper bound eq.(7.77). This difference is due to the fact that the range b of the interaction potential is chosen here of the same order as the size R of the cloud so that the terms $\langle\phi_\alpha, \phi_\alpha|V|\phi_\alpha, \phi_\alpha\rangle$ neglected in the derivation of the upper bound are actually significant. We have checked for various ranges b much smaller than R that γ then approaches the upper bound $2NV(0)/\hbar$.

7.5 Conclusions and perspectives

In this chapter we have developed a new approach to the time-dependent bosonic $N-$body problem.[177] The principle of the approach is to add to the usual mean-field

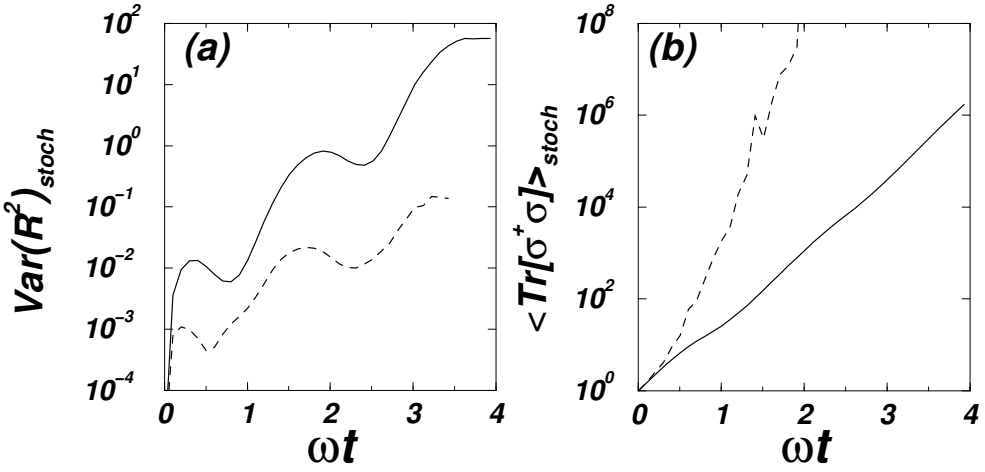

FIGURE 7.5: For the one-dimensional Bose gas in the conditions of figure 7.4, (a) stochastic variance of the size squared of the cloud and (b) noise on the $N-$body density matrix. Solid lines: simple scheme with Fock states. Dashed lines: constant trace scheme with Fock states.

Gross-Pitaevskii equation a stochastic term which recovers in the average the effect of the atoms in modes other than the condensate. The general conditions ensuring that the average over all possible realizations of this stochastic equation reproduces the exact $N-$body Schrödinger equation have been determined and some of the possible solutions characterized; each of them corresponds to a simulation scheme with different statistical and stability properties.

Among the many possible ones, schemes which evolve either a Fock state (i.e. number states) ansatz or a coherent states one have been investigated, as well as schemes which either minimize the statistical error on the N-body density matrix (*simple* schemes) or keep the trace of the density matrix constant during the whole evolution (*constant trace* schemes). Fock states are in fact best suited for dealing with situations in which the total number of particles is conserved, such as a trapped atomic Bose condensate, while coherent states are most likely to be useful when there is a coherent external driving; the *simple* schemes are mathematically regular at all times, while a practical use of the *constant trace* ones is made difficult by the occurrence of divergences. In particular, the constant trace scheme with coherent states recovers from a different point of view the well-known positive-P representation of quantum optics, which is here obtained following a procedure which is alternative to the usual derivation based on analyticity properties.

These simulation schemes have been applied to a two-mode model and to a one-dimensional Bose gas. In both cases we have found that the constant trace schemes lead to some diverging realizations, while the simple schemes lead to a statistical spread on the $N-$body density operator increasing exponentially with time with an exponent $\gamma \propto NV(0)$. The simple schemes are therefore not well suited to determine small deviations from the mean-field approximation in the large N limit but can be more efficiently applied to systems with a small number of particles, such as small atomic clouds tightly trapped at the nodes or antinodes of an optical lattice. Although in the numerical calculations of the present work we have limited ourselves to simple one-body observable such as the size of the atomic cloud, the same technique is immediately generalized to more elaborate observables such as the first and second order correlation functions of the field. We have not presented here numerical results for such quantities since the Hartree state taken as the initial state of the system gas does not make much physical sense for what concerns higher order correlations. More realistic initial states such as thermal equilibrium ones could however be implemented simply by performing some evolution in imaginary time in order to get the correct initial state and then a real time evolution in order to follow the dynamics.

As a further possible extension of the present work, one could also try to use more sophisticated ansatz than the simple Hartree state, such as squeezed states, or even multimode ansatz, such as coherent superpositions of number states in several adjustable modes of the field.

Conclusions and future developments

Although the physical systems which have been considered in the present thesis are apparently completely different from each other, all of them can be considered as different realizations of the same physical concept, the *interacting quantum Bose field*; the propagation of light waves in nonlinear semiconducting microstructures and of collisionally interacting atomic matter waves can be described within very similar theoretical frameworks and the strict analogies have allowed for a very fruitful exchange of ideas between the two fields.

The first part of the thesis contains a detailed discussion of nonlinear (photon) optical effects which can be observed in semiconducting dielectric structures; the linear refractive index profile of the system modifies the mode structure of the photonic field, while the optical nonlinearities give additional coupling terms between modes. In particular, we have addressed the case of DBR microcavities, which show energetically well-spaced and spatially localized cavity modes (chap.1); if the cavity is grown with a material showing an intensity-dependent refractive index (chap.2), optical bistability and optical limiting can be observed at reasonable values of the incident light intensity.[26,64] With an eye to all-optical signal processing, we have discussed configurations which could result useful for either the amplification of an optical signal (optical transistor) or the realization of a bit of optical memory.[70,75]

The following chap.3 is devoted to the analysis of a different kind of optical nonlinearities, which arise in DBR microcavities from resonant two-photon processes such as resonant second-harmonic generation and resonant two-photon absorption.[76,77] Specific signatures of the optical nonlinearity have been discussed in the transmission spectra of the cavity, such as a two-photon Rabi splitting of the resonant tunneling peak. In addition, we have considered the linear optical response to a weak probe beam when the cavity is dressed by a strong and coherent pump beam; in analogy with the usual optical Stark effect, the resulting shifts and splittings of

the excitonic spectral features for growing pump intensity have been interpreted as a two-photon optical Stark effect. A quantitative estimate of the light intensities needed for the actual observation of such effects in GaAs based systems has been given.

The second part of the thesis is focussed on the propagation of interacting matter waves through optical lattices: thanks to the strict analogy between the coherent light field of an optical laser and the coherent matter waves of Bose-condensates and atom lasers which is described in full detail in chap.4, the same ideas described in the first part of the thesis for the case of semiconducting structures can be applied to the propagation of matter waves in optical lattices. The periodic optical potential can be interpreted as forming a distributed Bragg reflector for matter waves; an atomic Fabry-Perot cavity is readily obtained by using a spatially modulated optical lattice.[124,125] Localized discrete quasi-bound states are apparent in the corresponding transmission spectra and can be used in nonlinear atom optical experiments to observe atom optical limiting and atom optical bistability. Furthermore, we have shown how the reflection of matter waves on optical lattices can be used for the experimental determination of the coherence length of an atom laser.[238]

Thanks to the much stronger collisional atom-atom interactions with respect to the effective photon-photon ones in nonlinear dielectric media, nonlinear optical effects at low intensities should be more likely to be observed with matter waves than with light waves; this means that the Gross-Pitaevskii equation for the atomic field is more likely to fail than the wave equation of classical Maxwell's electrodynamics in nonlinear dielectric media. In particular (chap.6), if the transmission properties of a single-mode nonlinear device are substantially modified by the presence of a very small number of quanta, the transmitted field can have definitely nonclassical properties, while it is well approximated by a classical field if the nonlinearity threshold corresponds instead to a large number of quanta.[269]

While the simplicity of the single mode model has allowed for a complete solution of the quantum optical properties in terms of the quantum master equation in the Fock basis, an analogous approach for a multimode system is practically unfeasible because of the huge dimensionality of the corresponding Hilbert space. We conclude the thesis (chap.7) with a detailed account of a novel reformulation of the interacting Bose gas problem in terms of the stochastic evolution of Hartree states:[177] such an approach is expected to be able to handle the non-trivial correlations which appear in a non-dilute magnetically trapped Bose condensed cloud as well as the photon

statistics in a strongly nonlinear planar cavity; in particular, it looks most promising for the numerical study of multimode systems involving a relatively small number of strongly interacting particles. Among the many possible implementations of the method, schemes have been found which are not subject to the divergences typical of Positive-P calculations since the corresponding stochastic differential equations have a regular solution for all times; Positive-P representation naturally arises as the constant trace scheme with coherent states. First examples of application of the approach to simplest physical systems such as a two-mode model of a Josephson junction and a one-dimensional Bose gas have been discussed.

At the end of these lengthy discussions, we may be tempted to conclude that physics is a sort of Sysiphus torment: the more problems you solve, the more unsolved problems you will find yourself interested in. But, as it is well known by any atomic physicist, Sysiphus is a good guy who can never disappoint us, so let's try to enumerate the most interesting steps to do in the next future.

Most of the subjects discussed in the thesis allow for a number of possible developments: first of all, while nonlinear optical effects are currently observed with light waves, the development of nonlinear atom optics will be matter of intense investigations in the next years both from the theoretical and the experimental points of view. The discussion of the atomic Fabry-Perot cavity contained in chap.5 has dealt with a very simplified one-dimensional model with a continuous wave coherent driving; since a cw atom laser has not been realized yet and truly single-mode atomic waveguides are difficult to obtain, an extension of our calculations to more realistic geometries could reserve interesting surprises. In particular, since the loading of a BEC in a magnetic waveguide has been recently obtained, predictions for the behaviour of a finite pulse of atoms interacting with an optical lattice within a waveguide will hopefully be soon necessary for the interpretation of experimental data; such a geometry corresponds to the propagation of a strong light pulse through a nonlinear optical cavity: thanks to the nonlinear atom-atom interactions, pulse compression and reshaping via mode-locking effects could eventually be observed.

In the last years there has been a renewed interest for two-quantum nonlinear processes such as the second harmonic generation and the two-photon absorption considered in chap.3: the forthcoming realization of molecular condensates coherently coupled to atomic ones via photo-association transitions can in fact be considered

as a sort of second harmonic generation of matter waves. While the mean-field theory of such a system can be easily developed as a set of Gross-Pitaevskii equations mutually coupled by quadratic terms, a complete characterization of the quantum effects which may arise is far from being available; as in the case of the quartic interaction term in the Hamiltonian, only a linearized analysis has been done so far and a discussion of the correlations within each of the modes as well as between the modes still has to be done. If we are allowed to perform a few-modes approximation like in chap.3, an exact calculation can be performed in terms of the quantum master equation in a simple Fock basis as in chap.6; in this way, all the coherence properties of the system can be completely characterized. However, since conventional magnetic and optical traps are not tight enough for only a small number of field modes to be relevant, a theory capable to handle a multimode and spatially distributed field is necessary but, unfortunately, is not available yet. For this reason, an extension of the stochastic approach of chap.7 to other forms of nonlinear coupling could therefore have important applications for the study of the quantum correlations in coupled atomic and molecular condensates.

As we have previously discussed, the stochastic wavefunction method itself deserves further developments both from the point of view of the improvement of its efficiency and from the point of view of its application to concrete problems. On one hand, a generalization of the initial ansatz by including squeezed states or multimode Fock states from the beginning should give an even larger freedom in the choice of the simulation scheme and therefore improve the efficiency of practical numerical calculations: a wider ansatz allows in fact for a reconstruction of a given quantum state in terms of a smaller number of states and therefore requires a smaller number of Monte Carlo realizations for an efficient sampling of the observables. In order to correctly implement the initial state of the system as either the ground state of the many-body system or a thermodynamical equilibrium state at temperature T, a straightforward extension of the stochastic approach to imaginary time evolution can be used. Unlike conventional quantum Monte Carlo techniques, the stochastic wavefunction approach should be able to handle all kinds of observables and all kinds of Hamiltonians; in particular, it could be applied also to many-body problems of large actual relevance such as the enucleation and the stability of vortices in Bose-condensed clouds.

In the domain of optics, our stochastic method could for example be applied to the dynamics of the light field in planar microcavities: while a weak nonlinearity

regime can be successfully handled in terms of the linearized equations of Positive-P representation, the strong nonlinearity regime requires a treatment able to recover all the peculiar coherence properties of such a strongly-interacting two-dimensional Bose gas. From the experimental point of view, planar microcavities provide in fact an alternative route towards the realization of two-dimensional Bose gases and the strong coupling of light to delocalized excitonic states can be exploited to enhance the strength of the nonlinear interaction. With respect to atomic systems, experimental access to the coherence properties of the gas can be obtained simply by looking at the transmitted light through the cavity: as a simplest example, the Bogoliubov dispersion of the fluctuations should reflect in the angular pattern of incoherently transmitted light. In addition, solid-state samples allow for the investigation of the response of the interacting photon gas to external disturbances such as cavity roughness, phonons and even localized optical transitions: the modification of the dispersion relation from the one of a non-interacting gas to the Bogoliubov-like one of the interacting gas is expected to have profound consequences on such effects, which could be interpreted as the photonic analog of the superfluidity of ^{4}He.

Related publications

- I.Carusotto and G.C.La Rocca, *Optical response of linear and nonlinear photonic superlattices near the first photonic band gap*, Phys.Stat.Sol.(a) **164**, 377 (1997) (proceedings of the OECS-5 conference in Göttingen, august 1997).
- I.Carusotto and G.C.La Rocca, *Nonlinear optics of coupled semiconductor microcavities*, Phys.Lett.A **243**, 236 (1998).
- I.Carusotto and G.C.La Rocca, *Coupled semiconductor microcavities with distributed Kerr optical nonlinearities*, proceedings of the ICPS-24 conference in Jerusalem, ed. D.Gershoni, World Scientific, 1998
- I.Carusotto and G.C.La Rocca, *Two photon Rabi splitting and optical Stark effect in semiconductor microcavities*, Phys.Rev.B **60**, 4907 (1999).
- I.Carusotto and G.C.La Rocca, *Two photon Rabi splitting and optical Stark effect in semiconductor microcavities*, Phys.Stat.Sol.(a) **178**, 173 (2000) (proceedings of the OECS-6 conference in Ascona, august 1999)
- I.Carusotto and G.C.La Rocca, *The modulated optical lattice as an atomic Fabry-Perot interferometer*, Phys.Rev.Lett. **84**, 399 (2000)
- I.Carusotto and G.C.La Rocca, *The atomic Fabry-Perot interferometer*, Proceedings of the XXVII International School of Quantum Electronics on Bose-Einstein condensates and atom lasers (Erice-Sicily, October 1999), Kluwer Academic / Plenum Publishers, New York, 2000.
- I.Carusotto, M.Artoni and G.C.La Rocca, *Atom laser coherence length and atomic standing waves*, submitted for publication on Phys.Rev.A (2000)
- I.Carusotto, *The nonlinear atomic Fabry-Perot interferometer: from the mean-field theory to the atom blockade effect*, submitted for publication on Phys.Rev.A (2000)

- I.Carusotto, Y.Castin and J.Dalibard, *The N boson time dependent problem: a reformulation with stochastic wave functions*, accepted for publication on Phys.Rev.A (2000); cond-mat/0003399.

Other research activities

Brevity and clarity reasons have forced me to skip in the present thesis several interesting topics which have been subject of intense work during this three-year period, but do not fit in the main development of my research activity.

The first of them is certainly the theoretical analysis of prof.M.Inguscio's experiment for the measure of the fine structure constant α on ^{4}He atoms, from which my interest in atomic physics has begun: in the first months of 1998, the helium experimental group at LENS (Firenze), which was spectroscopically measuring some transition frequency, had remarked a slight dependence of the linecenter position on the parameters of the experimental setup and, in particular, on the interaction time between the atoms and the light. Since the purpose of the experiment was a precision measure of the transition frequency in order to infer a reliable value of the α fine-structure constant,[281] such a slight frequency shift had an interest not only from a fundamental point of view, but also from an applicative one, since it risked to compromise the precision of the measure. In close connection with numerical simulations performed by G.Giusfredi and in collaboration with M.Artoni, a theoretical model has been developed, which has been able to account for the experimental results and to give a simple physical picture of the effect in terms of Doppler cooling and heating.

- F.Minardi, M.Artoni, P.Cancio, M.Inguscio, G.Giusfredi and I.Carusotto, *Frequency-shift in saturation spectroscopy induced by mechanical effects of light*, Phys. Rev. A **60**, 4164 (1999)
  Abstract: We report on a substantial light-force-induced line-center shift of the sub-Doppler dip in a saturation spectroscopy configuration where mechanical effects are expected to be negligible. We observe the shift on the $2^3S_1 \rightarrow 2^3P_1$ open transition of 4He that is relevant for a determination of the fine-structure constant [Phys. Rev. Lett. 82, 1112 (1999)]. We discuss the physical origin

of the shift and we provide a numerical analysis to support our interpretation. The shift can be quite important for various other high-precision spectroscopy measurements

- M.Artoni, I.Carusotto and F.Minardi, *Light-force induced fluorescence line-center shifts in high precision optical spectroscopy: simple model and experiment*, Phys. Rev. A **62**, 023402 (2000)
  Abstract: We calculate the effect of light–induced forces on the fluorescence line–shape of a two–level atom crossing at right angle a lin $\parallel$ lin polarized standing wave laser field in a common configuration for ultra-high precision optical spectroscopy. For an incident atomic beam with a narrow spread of transverse velocities the dipole force induces a *red*–shift of the fluorescence maximum while in the reverse case of a wide spread of transverse velocities the radiation–pressure force induces a *blue*–shift of the saturation dip minimum. We then use our theory to explain a blue-shift of the saturation line–center dip occurring for the closed transition $2\,^3S_1 \rightarrow 2\,^3P_2$ of a ^{4}He beam. The observed shift, which is in quite good agreement with the theory, can be of the order of 1/10 of the transition natural linewidth and hence quite important for ultra high–precision spectroscopy measurements.

In the last months of 1998, a collaboration with prof.F.Beltram's experimental group has taken place on the subject of resonant second-harmonic generation in ZnSe DBR microcavities: as we have discussed in detail in chap.3, resonant enhancement of the generated harmonic intensity is a key tool both for obtaining high conversion efficiencies in the generation of blue-green light and for the observation of novel nonlinear optical effects. Our work has consisted in a quantitative estimation of the generated harmonic intensity and, specifically, of the enhancement factor introduced by the resonance of the harmonic frequency with a cavity mode in the actual experimental setup.

- V.Pellegrini, R.Colombelli, I.Carusotto, F.Beltram, S.Rubini, R.Lantier, A.Franciosi, C.Vinegoni and L.Pavesi, *Resonant second harmonic generation in ZnSe bulk microcavity*, Appl.Phys.Lett **74**, 1945 (1999)
  Abstract: Room-temperature resonant second harmonic generation is demonstrated in a ZnSe bulk microcavity with Si_3N_4/SiO_2 Bragg reflectors. The resonance occurs at the second harmonic wavelength in the blue-green spec-

tral region and yields an enhancement of one order of magnitude in the second harmonic process. Tunability of the resonant effect between 480nm and 500nm is achieved by varying the angle of incidence.

In the first half of 1999, during my stay at the *Laboratoire Kastler-Brossel* in Paris, my research activity has been followed by prof.J.Dalibard and prof.Y.Castin and has been mainly focussed on two theoretical projects in the field of quantum atom optics and atom lasing. The first project, which has absorbed the greatest portion of my time, consists in the development of a novel reformulation of the interacting bosonic N-body problem in terms of the stochastic evolution of Hartree states and has been described in full detail in chap.7. The other project consists in the study of evaporative cooling of an atomic beam which is propagating along a magnetic atomic waveguide; cooling is provided by transverse evaporation and thermalization of the third degree of freedom is guaranteed by elastic collisions. Calculations have been performed mainly by E.Mandonnet, A.Minguzzi and R.Dum using two different and complementary methods, an approximate analytical solution of the Boltzmann equation and an atom dynamics Monte-Carlo simulation; the results of the two approaches are in very good agreement with each other. My main task has been the study of the final stage of the evaporation at the onset of quantum degeneracy, when stimulation of the collisional cross-section begins to be important; at the moment, a complete theory has not been developed yet, but interesting results have already been obtained both for the case of single-mode waveguide and for the case of a multi-mode one. The experiment has recently started in the same laboratory and seems very promising from the point of view of a obtaining a continuous wave atom laser.

- E.Mandonnet, A.Minguzzi, R.Dum, I.Carusotto, Y.Castin and J.Dalibard, *Evaporative cooling of an atomic beam*, Eur.Phys.J.D **10**, 9 (2000)
  Abstract: We present a theoretical analysis of the evaporative cooling of an atomic beam propagating in a magnetic guide. Cooling is provided by transverse evaporation. The atomic dynamics inside the guide is described by solving the Boltzmann equation with two different approaches: an approximate analytical ansatz and a Monte-Carlo simulation. Within their domain of validity, these two methods are found to be in very good agreement with each other. They allow us to determine how the phase-space density and the flux of the beam vary along its direction of propagation. We find a significant increase for

the phase-space density along the guide. By extrapolation, we estimate the length of the beam needed to reach quantum degeneracy.

- Y.Castin, R.Dum, E.Mandonnet, J.Dalibard, A.Minguzzi and I.Carusotto, *Coherence properties of a continuous atom laser*, submitted for publication on Journal of Modern Optics (2000)
  Abstract: We have recently proposed to evaporatively cool an atomic beam in a magnetic guide to produce a continuous "atom laser". The coherence properties of the atomic beam in the quantum degenerate regime are investigated here at thermal equilibrium. The gas experiences two-dimensional, transverse Bose-Einstein condensation rather than a full three-dimensional condensation because of the very elongated geometry of the magnetic guide, First order and second order correlation functions of the atomic field are used to characterize the coherence properties of the gas along the axis of the guide. The coherence length of the gas is found to be much larger than the thermal de Broglie wavelength in the strongly quantum degenerate regime. Large intensity fluctuations present in the ideal Bose gas model are found to be strongly reduced by repulsive atomic interactions; this conclusion is obtained with a one-dimensional classical field approximation valid when the temperature of the gas is much higher than its chemical potential $k_B T \gg |\mu|$.

In the first months of 2000, we have started to study the propagation dynamics of ultra-slow light pulses in coherently driven Bose condensed atomic gases and, in particular, the effect of atomic recoil on the group velocity of light. Calculations performed in collaboration with M.Artoni have shown that, depending on the chosen geometry and level scheme, a lower bound to the observable group velocities can be observed as well as pulse propagation at negative group velocities without appreciable absorption.

- I.Carusotto, M.Artoni and G.C.La Rocca, *Atomic recoil effects in slow light propagation*, JETP letters **72**, 420 (2000).
  Abstract: We theoretically investigate the effect of atomic recoil on the propagation of ultra-slow light pulses through a coherently driven Bose-Einstein condensed gas. For a sample at rest, the group velocity of the light pulse is the sum of the group velocity that one would observe in the absence of mechanical effects (infinite mass limit) plus the velocity of the recoiling atoms

(light dragging effect). We predict that atomic recoil may give rise to a lower bound for the observable group velocities as well as to pulse propagation at negative group velocities without appreciable absorption.

Bibliography

[1] C.Cohen-Tannoudji, J.Dupont-Roc and G.Grynberg, *Processus d'interaction entre photons et atomes* (InterEditions/Editions du CNRS, Paris) (1988).

[2] M.D.Levenson and S.S.Kano, *Introduction to nonlinear laser spectroscopy* (Academic Press) (1987).

[3] C.S.Adams and E.Riis, *Laser cooling and trapping of neutral atoms*, Prog.Quant.Electr. **21**, 1 (1997).

[4] E.Burstein and C.Weisbuch, eds., *Confined electrons and photons* (Plenum Press, New York) (1995).

[5] H.Haug and S.W.Koch, *Quantum theory of the optical and electronic properties of semiconductors* (World Scientific, Singapore) (1993).

[6] P.N.Butcher and D.Cotter, *The elements of nonlinear optics* (Cambridge Univ.Press) (1993).

[7] N.W.Ashcroft and N.D.Mermin, *Solid state physics* (Saunders College Publishing, Orlando) (1976).

[8] P.Yu and M.Cardona, *Fundamentals of semiconductors: physics and material properities* (Springer, Berlin) (1996).

[9] F.Bassani and G. Parravicini, *Electronic states and optical transitions in solids* (Pergamon Press, Oxford) (1975).

[10] Ph.St.J.Russell, *Photonic band gaps*, Physics World p. 37 (August 1992).

[11] E.Yablonovitch, *Photonic band-gap crystals*, J.Phys.:Condens.Matter **5**, 2443 (1993).

[12] E.Yablonovitch and T.J.Gmitter, *Photonic band structure: the face-centered-cubic case*, Phys.Rev.Lett.**63**, 1950 (1989).

[13] S.Satpathy, Z.Zhang and M.R.Salehpour, *Theory of photon bands in three-dimensional periodic dielectric structures*, Phys.Rev.Lett.**64**, 1239 (1990).

[14] K.M.Leung and Y.F.Liu, *Full vector wave calculation of photonic band structures in face-centered-cubic dielectric media*, Phys.Rev.Lett.**65**, 2646 (1990).

[15] Z.Zhang and S.Satpathy, *Electomagnetic wave propagation in periodic structures: Bloch wave solution of Maxwell's equations*, Phys.Rev.Lett.**65**, 2650 (1990).

[16] K.M.Ho, C.T.Chan and C.M.Soukoulis, *Existence of a photonic gap in periodic dielectric structures*, Phys.Rev.Lett.**65**, 3152 (1990).

[17] E.Yablonovitch, T.J.Gmitter and K.M.Leung, *Photonic band structure: the face-centered-cubic case employing nonspherical atoms*, Phys.Rev.Lett.**67**, 2295 (1991).

[18] N.A.Clark, A.J.Hurd and B.J.Ackerson, *Single colloidal crystals*, Nature **281**, 57 (1979).

[19] I.Inanç Tarhan and G.H.Watson, *Photonic band structure of fcc colloidal crystals*, Phys.Rev.Lett.**76**, 315 (1996).

[20] Yu.A.Vlasov, V.N.Astratov, O.Z.Karimov, A.A.Kaplyanskii, V.N.Bogomolov and A.V.Prokofiev, *Existence of a photonic pseudo gap for visible light in synthetic opals*, Phys.Rev.B**55**, R13357 (1997).

[21] D. van Coevorden, R.Sprik, A.Tip and A.Lagendijk, *Photonic band structure of atomic lattices*, Phys.Rev.Lett.**77**, 2412 (1996).

[22] K.-P. Marzlin and W.Zhang, *Bose-Einstein condensates in optical lattices: spontaneous emission in the presence of photonic band gaps*, cond-mat/0004326 (2000).

[23] A.M.Hawryluk, N.M.Ceglio and D.G.Stearns, *Applications of microfabrication technology to x-ray laser cavities*, J.Vac.Sci.Technol.B **6**, 2153 (1988).

[24] J.D.Jackson, *Classical Electrdynamics* (J.Wiley & Sons) (1962).

[25] P.Yeh, *Optical waves in layered media* (Wiley, New York) (1988).

[26] I.Carusotto, *Ottica lineare e nonlineare in cristalli fotonici unidimensionali*, Tesi di Laurea, Università di Pisa (1997).

[27] V.Berger, *Second harmonic generation in monolithic cavities*, J.Opt.Soc.Am.B **14**, 1351 (1997).

[28] L.Collot, V.Lefèvre-Seguin, M.Brune, J.M.Raimond and S.Haroche, *Very high-Q whispering-gallery mode resonances observed on fused silica microspheres*, Europhys.Lett. **23**, 327 (1993).

[29] P.V.Kelkar, V.G.Kozlov, A.V.Nurmikki, C.-C.Chu, J.Han and R.L.Gunshor, *Stimulated emission, gain and coherent oscillations in II-VI semiconductor microcavities*, Phys.Rev.B **56**, 7564 (1997).

[30] V.Pellegrini, R.Colombelli, I.Carusotto, F.Beltram, S.Rubini, R.Lantier, A.Franciosi, C.Vinegoni and L.Pavesi, *Resonant second harmonic generation in ZnSe bulk microcavity*, Appl.Phys.Lett. **74**, 1945 (1999).

[31] S.E.Burns, G.Denton, N.Tessler, M.A.Stevens, F.Cacialli and R.H.Friend, *High finesse organic microcavities*, Optical Materials **9**, 18 (1998).

[32] L.A.Graham, Q.Deng, D.G.Deppe and D.L.Huffaker, *Exciton spectral splitting near room temperature from high contrast semiconductor microcavities*, Appl.Phys.Lett. **70**, 814 (1997).

[33] A.Convertino, A.Valentini, T.Ligonzo and R.Cingolani, *Organic-inorganic dielectric multilayer systems as high reflectivity distributed Bragg reflectors*, Appl.Phys.Lett. **71**, 732 (1997).

[34] G. L.Pavesi and L.C.Andreani, *All-porous silicon-coupled microcavities: Experiment versus theory*, Phys.Rev.B**58**, 15974 (1998).

[35] V.Savona, *Linear optical properties of semiconductor microcavities with embedded quantum wells*, in *Confined photon systems*, edited by H.Benisty, J.-M.Gérard, R.Houdré, J.Rarity and C.Weisbuch (Springer) (1999).

[36] R.P.Stanley, R.Houdré, U.Oesterle, M.Gailhanou and M.Ilegems, *Ultrahigh finesse microcavity with distributed Bragg reflectors*, Appl.Phys.Lett. **65**, 1883 (1994).

[37] C.Weisbuch, M.Nishioka, A.Ishikawa and Y.Arakawa, *Observation of the coupled exciton-photon mode splitting in a semiconductor microcavity*, Phys.Rev.Lett. **69**, 3314 (1992).

[38] R.Houdré, C.Weisbuch, R.P.Stanley, U.Oesterle, P.Pellandini and M.Ilegems, *Measurement of cavity-polariton dispersion curve from angle-resolved photoluminescence experiments*, Phys.Rev.Lett.**73**, 2043 (1994).

[39] R.Houdré, R.P.Stanley, U.Oesterle, M.Ilegems and C.Weisbuch, *Room-temperature polaritons in a semiconductor microcavity*, Phys.Rev.B**49**, 16761 (1994).

[40] R.P.Stanley, R.Houdré, C.Weisbuch, U.Oesterle and M.Ilegems, *Cavity-polariton photoluminescence in semiconductor microcavities. Experimental evidence*, Phys.Rev.B**53**, 10995 (1996).

[41] E.Yablonovitch, T.J.Gmitter, R.D.Meade, A.M.Rappe, K.D.Brommer and J.D.Joannopoulos, *Donor and acceptor modes in photonic band structure*, Phys.Rev.Lett.**67**, 3380 (1991).

[42] R.P.Stanley, R.Houdré, U.Oesterle, M.Ilegems and C.Weisbuch, *Impurity modes in one-dimensional periodic systems: the transition from photonic band gaps to microcavities*, Phys.Rev.A**48**, 2246 (1993).

[43] P.R.Villeneuve, S.Fan and J.D.Joannopoulos, *Microcavities in photonic crystals: mode symmetry, tunability and coupoling efficiency*, Phys.Rev.B**54**, 7837 (1996).

[44] E.Özbay, G.Tuttle, M.Sigalas, C.M.Soukoulis and K.M.Ho, *Defect structures in a layer-by-layer photonic band-gap crystal*, Phys.Rev.B**51**, 13961 (1995).

[45] S.Y.Lin, V.M.Hietala, S.K.Lyo and A.Zaslavsky, *Photonic band gap quantum well and quantum box structures: a high-Q resonant cavity*, Appl.Phys.Lett.**68**, 3233 (1996).

[46] G.C.La Rocca, F.Bassani and V.M.Agranovich, *Biexcitons and dark states in semiconductor microcavities*, J.Opt.Soc.Am.B **15**, 652 (1998).

[47] Y.Kadoya, K.Kameda, M.Yamanishi, T.Nishikawa, T.Kannari and T.Ishihara, *Oscillator strength dependence of cavity-polariton mode splitting in semiconductor microcavities*, Appl.Phys.Lett. **68**, 281 (1996).

[48] G.S.Agarwal, *Vacuum-field Rabi splitting in microwave absorption by Rydberg atoms in a cavity*, Phys.Rev.Lett.**53**, 1732 (1984).

[49] D.F.Walls and G.J.Milburn, *Quantum Optics* (Springer-Verlag, Berlin) (1994).

[50] W.H.Steel, *Interferometry* (Cambridge University Press) (1967).

[51] A.Imamoglu, *Interference of radiatively broadened resonances*, Phys.Rev.A**40**, 2835 (1989).

[52] M.G.Raizen, R.J.Thompson, R.J.Brecha, H.J.Kimble and H.J.Carmicheal, *Normal-mode splitting and linewidth averaging for two-state atoms in an optical cavity*, Phys.Rev.Lett.**63**, 240 (1989).

[53] F.Tassone, F.Bassani and C.Andreani, *Resonant and surface polaritons in quantum wells*, Nuovo Cimento D **12**, 1673 (1990).

[54] A.Honold, L.Schultheis, J.Kuhl and C.W.Tu, *Collision broadening of two-dimensional excitons in a Ga As single quantum well*, Phys.Rev.B**40**, 6442 (1989).

[55] G.Bastard, *Wave mechanics applied to semiconductor heterostructures* (Les editions de physique) (1988).

[56] S.E.Harris, *Electromagnetically induced transparency*, Physics Today p. 36 (July 1997).

[57] E.Arimondo, *Coherent population trapping in laser spectroscopy*, in *Progress in Optics*, edited by E.Wolf, vol. XXXV, p. 257 (Elsevier Science, Amsterdam) (1996).

[58] U.Fano, *Effects of configuration interaction on intensities and phase shifts*, Phys.Rev. **124**, 1866 (1961).

[59] B.Lounis and C.Cohen-Tannoudji, *Coherent population trapping and Fano profiles*, J.Phys II (France) **2**, 579 (1992).

[60] R.P.Stanley, R.Houdré, U.Oesterle, M.Ilegems and C.Weisbuch, *Coupled semiconductor microcavities*, Appl.Phys.Lett. **23**, 120 (1997).

[61] G.Panzarini, L.C.Andreani, A.Armitage, D.Baxter, M.S.Skolnick, V.N.Astratov, J.S.Roberts, A.K.Kavokin, M.R.Vladimirova and M.A.Kaliteevskii, *Exciton-light coupling in single and coupled semiconductor*

microcavities: polariton dispersion and polarization splitting, Phys.Rev.B**59**, 5082 (1999).

[62] A.Armitage, M.S.Skolnick, A.V.Kavokin, D.M.Whittaker, V.N.Astratov, G.A.Gehring and J.S.Roberts, *Polariton-induced optical asymmetry in semiconductor microcavities*, Phys.Rev.B**58**, 15367 (1998).

[63] R.W.Boyd, *Nonlinear optics* (Academic Press, San Diego) (1992).

[64] I.Carusotto and G.C.La Rocca, *Optical response of linear and nonlinear photonic superlattices near the first photonic band gap*, Phys.Stat.Sol. **164**, 377 (1997), proceedings of the OECS-5 conference in Göttingen, august 1997.

[65] S.Schmitt-Rink, D.S.Chemla and D.A.B.Miller, *Theory of transient excitonic nonlinearities in semiconductor quantum-well structures*, Phys.Rev.B**32**, 6601 (1995).

[66] H.Haug and S.Schmitt-Rink, *Basic mechanism of the optical nonlinearities of semiconductors near the band-edge*, J.Opt.Soc.Am.B **2**, 1135 (1985).

[67] D.S.Chemla and D.A.B.Miller, *Room-temperature excitonic nonlinear-optical effects in semiconductor quantum-well structures*, J.Opt.Soc.Am.B **2**, 1155 (1985).

[68] E.D.Palik, *Handbook of optical constants of solids* (Academic Press, Orlando) (1985).

[69] Y.H.Lee, A.Chavez-Pirson, S.W.Koch, H.M.Gibbs, S.H.Park, J.Morhange, A.Jeffery, N.Peyghambarian, L.Banyai, A.C.Gossard and W.Wiegmann, *Room-temperature optical nonlinearities in GaAs*, Phys.Rev.Lett.**57**, 1446 (1986).

[70] I.Carusotto and G.C.La Rocca, *Coupled semiconductor microcavities with distributed Kerr nonlinearity*, in *The physics of semiconductors*, edited by D.Gershoni, Proceedings of the 24th ICPS, Jerusalem (World Scientific) (1998).

[71] D.G.Lidzey, T.Virgili, D.D.C.Bradley, M.S.Skolnick, S.Walker and D.M.Whittaker, *Strong exciton-photon coupling in an organic semiconductor microcavity*, Nature (London) **395**, 53 (1998).

[72] T.Fujita, Y.Sato, T.Kuitani and T.Ishihara, *Tunable polariton absorption of distributed feedback microcavities at room temperature*, Phys.Rev.B**57**, 12428 and 7456 (1998).

[73] A.Tredicucci, Y.Chen, V.Pellegrini, M.Börger and F.Bassani, *Optical bistability of semiconductor microcavities in the strong-coupling regime*, Phys.Rev.A**54**, 3493 (1996).

[74] J.Gripp, S.L.Mielke, L.A.Orozco and H.J.Carmicheal, *Anharmonicity of the vacuum Rabi peaks in a many-atom system*, Phys.Rev.A**54**, R3746 (1996).

[75] I.Carusotto and G.C.La Rocca, *Nonlinear optics of coupled semiconductor microcavities*, Phys.Lett.A **243**, 236 (1998).

[76] I.Carusotto and G.C.La Rocca, *Two-photon Rabi splitting and optical Stark effect in semiconductor microcavities*, Phys.Rev.B**60**, 4907 (1999).

[77] I.Carusotto and G.C.La Rocca, *Two-photon Rabi splitting and optical Stark effect in semiconductor microcavities*, Phys.Status Solidi (a) **178** (2000), proceedings of the OECS-6 conference in Ascona, august 1999.

[78] K.J.McNeil, P.D.Drummond and D.F.Walls, *Self-pulsing in second harmonic generation*, Opt.Comm. **27**, 292 (1978).

[79] P.D.Drummond, K.J.McNeil and D.F.Walls, *Bistability and photon antibunching in sub/second harmonic generation*, Opt.Comm. **28**, 255 (1979).

[80] P.D.Drummond, K.J.McNeil and D.F.Walls, *Non-equilibrium transitions in sub/second harmonic generation. I: semiclassical theory*, Optica Acta **27**, 321 (1980).

[81] P.D.Drummond, K.J.McNeil and D.F.Walls, *Non-equilibrium transitions in sub/second harmonic generation. II: quantum theory*, Optica Acta **28**, 211 (1981).

[82] P.Mandel, N.P.Pettiaux, W.Kaige, P.Galatola and L.A.Lugiato, *Periodic attractors in two-photon processes*, Phys.Rev.A**43**, 424 (1991).

[83] P. D.F.Walls and K.J.McNeil, *Bistable systems in nonlinear optics*, in *Optical bistability*, edited by C.M.Bowden, M.Ciftan and H.R.Robl, p. 51 (Plenum Press, New York) (1981).

[84] M.J.Collett and D.F.Walls, *Squeezing spectra for nonlinear optical systems*, Phys.Rev.A**32**, 2887 (1985).

[85] G.S.Agarwal, *Strong coupling induced splitting of dynamical response of the optical parametric oscillator*, Phys.Rev.Lett.**73**, 522 (1994).

[86] C.Zimmermann, R.Kallenbach, T.W.Hänsch and J.Sandberg, *Doubly-resonant second-harmonic generation in β-barium borate*, Opt.Comm. **71**, 229 (1989).

[87] C.Simonneau, J.P.Debray, J.C.Harmand, P.Vidaković, D.J.Lovering and J.A.Levenson, *Second-harmonic generation in a doubly resonant semiconductor microcavity*, Opt.Lett. **22**, 1775 (1997).

[88] E.Rosencher, B.Vinter and V.Berger, *Second-harmonic generation in nonbirefringent semiconductor optical microcavities*, J.Appl.Phys. **78**, 6042 (1995).

[89] R.Paschotta, K.Fiedler, P.Kürz and J.Mlynek, *Nonlinear mode coupling in doubly resonant frequency doublers*, Appl.Phys.B **58**, 117 (1994).

[90] H.J.Kreuzer, *Nonequilibrium thermodynamics and its statistical foundations* (Clarendon Press, Oxford) (1981).

[91] B.R.Mollow, *Power spectrum of light scattered by two-level systems*, Phys.Rev. **188**, 1969 (1969).

[92] F.Y.Wu, R.E.Grove and S.Ezekiel, *Measurement of the spectrum of resonance fluorescence from a two-level atom in an intense monochromatic field*, Phys.Rev.Lett.**35**, 1426 (1975).

[93] S.Haroche and F.Hartmann, *Theory of saturated-absorption line-shapes*, Phys.Rev.A**6**, 1280 (1972).

[94] B.R.Mollow, *Stimulated emission and absorption near resonance for driven systems*, Phys.Rev.A**5**, 2217 (1972).

[95] F.Y.Wu, S.Ezekiel, M.Ducloy and B.R.Mollow, *Observation of amplification in a strongly driven two-level atomic system at optical frequencies*, Phys.Rev.Lett.**38**, 1077 (1977).

[96] F.Quochi, G.Bongiovanni, A.Mura, J.L.Staehli, B.Deveaud, R.P.Stanley, U.Oesterle and R.Houdré, *Strongly driven semiconductor microcavities: from the polariton doublet to an AC-Stark triplet*, Phys.Rev.Lett.**80**, 4733 (1998).

[97] C.Ciuti and F.Quochi, *Theory of the excitonic Mollow spectrum in semiconductors*, Solid State Commun. **107**, 715 (1998).

[98] A.Shimizu, *Two-photon absorption in quantum-well structures near half the direct band gap*, Phys.Rev.B**40**, 1403 (1989).

[99] E.Rosencher and Ph.Bois, *Model systems for optical nonlinearities: asymmetric quantum wells*, Phys.Rev.B**44**, 11315 (1991).

[100] V.Pellegrini, A.Parlangeli, M.Börger, R.D.Atanasov, F.Beltram, L.Vanzetti and A.Franciosi, *Interband second-harmonic generation in $Zn_{1-x}Cd_xSe/ZnSe$ strained quantum wells*, Phys.Rev.B**52**, R5527 (1995).

[101] C.Ciuti and G.C.La Rocca, *Excitonic resonant self-electro-optic-device configuration in polytype double-quantum-well structures*, Phys.Rev.B**58**, 4599 (1998).

[102] J.P.Likforman, M.Joffre and D.Hulin, *Hyper-Raman gain due to excitons coherently driven with femtosecond pulses*, Phys.Rev.Lett.**70**, 3716 (1997).

[103] F.Bassani and S.Scandolo, *Dispersion relations and sum rules in nonlinear optics*, Phys.Rev.B**44**, 8446 (1991).

[104] S.Scandolo and F.Bassani, *Nonlinear sum rules: the three-level and the anharmonic-oscillator models*, Phys.Rev.B**45**, 13257 (1992).

[105] M.Born and E.Wolf, *Principles of Optics* (Pergamon Press, London) (1964).

[106] S.Scandolo and F.Bassani, *Miller's rule and the static limit for second-harmonic generation*, Phys.Rev.B**51**, 6928 (1994).

[107] K.Tai, A.Mysyrowicz, R.J.Fischer, R.E.Slusher and A.Y.Cho, *Two-photon absorption spectroscopy in GaAs quantum wells*, Phys.Rev.Lett.**62**, 1784 (1989).

[108] A.Pasquarello and A.Quattropani, *Gauge-invariant two-photon transitions in quantum wells*, Phys.Rev.B**38**, 6206 (1988).

[109] I.M.Catalano, A.Cingolani, R.Cingolani, M.Lepore and K.Ploog, *Two-photon spectroscopy in $GaAs/Al_xGa_{1-x}As$ multiple quantum wells*, Phys.Rev.B**40**, 1312 (1989).

[110] E.V.Goldstein and P.Meystre, *Phase conjugation of trapped Bose-Einstein condensates*, Phys.Rev.A**59**, 1509 (1999).

[111] J.H.Müller, O.Morsch, D.Ciampini, M.Anderlini, R.Mannella and E.Arimondo, *Atomic micromotion and geometric forces in a triaxial magnetic trap*, cond-mat/0005081 (2000).

[112] E.V.Goldstein, M.G.Moore, O.Zobay and P.Meystre, *Nonlinear optics of matter waves*, cond-mat/9807392 (1998).

[113] J.Vigué, *Index of refraction of dilute matter in atomic interferometry*, Phys.Rev.A**52**, 3973 (1995).

[114] Y.Castin, lecture at the Euroschool on *Bose condensates and atom lasers*, Cargèse, July 2000.

[115] D.E.Pritchard, *Cooling neutral atoms in a magnetic trap for precision spectroscopy*, Phys.Rev.Lett.**51**, 1336 (1983).

[116] Y.V.Gott, M.S.Iotte and V.G.Telkovsky, in *Nuclear Fusion*, p. 1045 (Int.Atomic Ag., Vienna) (1962).

[117] T.Bergeman, G.Erez and H.J.Metcalf, *Magnetostatic trapping fields for neutral atoms*, Phys.Rev.A**35**, 1535 (1987).

[118] C.R.Monroe, E.A.Cornell, C.A.Sackett, C.J.Myatt and C.E.Wieman, *Measurement of Cs-Cs elastic scattering at T=30μK*, Phys.Rev.Lett.**70**, 414 (1993).

[119] W.Petrich, M.H.Anderson, J.R.Ensher and E.A.Cornell, *Stable, tightly confining magnetic trap for evaporative cooling of neutral atoms*, Phys.Rev.Lett.**74**, 3352 (1995).

[120] D.M.Stamper-Kurn, M.R.Andrews, A.P.Chikkatur, S.Inouye, H.-J.Miesner, J.Stenger and W.Ketterle, *Optical confinement of a Bose-Einstein condensate*, Phys.Rev.Lett.**80**, 2037 (1998).

[121] D.M.Stamper-Kurn, H.-J.Miesner, A.P.Chikkatur, S.Inouye, J.Stenger and W.Ketterle, *Reversible formation of a Bose-Einstein condensate*, Phys.Rev.Lett.**81**, 2194 (1998).

[122] I.Bouchoule, H.Perrin, A.Kuhn, M.Morinaga and C.Salomon, *Neutral atoms prepared in Fock states of a one-dimensional harmonic potential*, Phys.Rev.A**59**, R8 (1999).

[123] M.Morinaga, I.Bouchoule, J.-C.Karam and C.Salomon, *Manipulation of motional quantum states of neutral atoms*, Phys.Rev.Lett.**83**, 4037 (1999).

[124] I.Carusotto and G.C.La Rocca, *The modulated optical lattice as an atomic Fabry-Perot interferometer*, Phys.Rev.Lett.**84**, 399 (2000).

[125] I.Carusotto and G.C.La Rocca, *The atomic Fabry-Perot interferometer*, in *Proceedings of the 27th International School of quantum electronics, Erice, October 1999*, edited by S.Martellucci and A.N.Chester (Kluwer Academic / Plenum Publishers) (2000).

[126] G.Ferrari, *Collision-assisted Zeeman cooling of neutral atoms*, cond-mat/0004236 (2000).

[127] Ph.Courteille, R.S.Freeland, D.J.Heinzen, F. Abeelen and B.J.Verhaar, *Observation of a Feshbach resonance in cold atom scattering*, Phys.Rev.Lett.**81**, 69 (1998).

[128] J.L.Roberts, N.R.Claussen, J.P.Burke, C.H.Greene, E.A.Cornell and C.E.Wieman, *Resonant magnetic field control of elastic scattering in cold* ^{85}Rb, Phys.Rev.Lett.**81**, 5109 (1998).

[129] S.Inouye, M.R.Andrews, J.Stenger, H.-J.Miesner, D.M.Stamper-Kurn and W.Ketterle, *Observation of Feshbach resonances in a Bose-Einstein condensate*, Nature **392**, 151 (1998).

[130] P.O.Fedichev, Yu.Kagan, G.V.Shlyapnikov and J.T.M.Walraven, *Influence of nearly resonant light on the scattering length in low-temperature atomic gases*, Phys.Rev.Lett.**77**, 2913 (1996).

[131] D.J.Heinzen, R.Wynar, P.D.Drummond and K.V.Kheruntsyan, *Superchemistry: dynamics of coupled atomic and molecular Bose-Einstein condensates*, Phys.Rev.Lett.**84**, 5029 (2000).

[132] J.Stenger, S.Inouye, M.R.Andrews, H.-J.Miesner, D.M.Stamper-Kurn and W.Ketterle, *Strongly Enhanced Inelastic Collisions in a Bose-Einstein Condensate near Feshbach Resonances*, Phys.Rev.Lett.**82**, 2422 (1999).

[133] P.O.Fedichev, M.W.Reynolds and G.V.Shlyapnikov, *Three-body recombination of ultracold atoms to a weakly bound s level*, Phys.Rev.Lett.**77**, 2921 (1996).

[134] J.Dalibard, *Collisional dynamics of ultra-cold atomic gases*, in *Proceedings of the international School of physics E.Fermi on* Bose-Einstein condensation in atomic gases, edited by M.Inguscio, S.Stringari and C.E.Wieman (1998).

[135] G.J.Milburn, J.Corney, E.W.Wright and D.F.Walls, *Quantum dynamics of an atomic Bose-Einstein condensate in a double-well potential*, Phys.Rev.A**55**, 4318 (1997).

[136] E.V.Goldstein and P.Meystre, *Quantum theory of atomic four-wave mixing in Bose condensates*, Phys.Rev.A**59**, 3896 (1999).

[137] D.M.Ceperley, *Path integrals in the theory of condensed helium*, Rev.Mod.Phys. **71**, S438 (1999).

[138] W.Krauth, *Quantum Monte Carlo calculations for a large number of bosons in a harmonic trap*, Phys.Rev.Lett.**77**, 3695 (1996).

[139] S.Giorgini, J.Boronat and J.Casulleras, *Ground state of a homogeneous Bose gas: a diffusion Monte-Carlo calculation*, Phys.Rev.A**60** (1999).

[140] M.Holzmann and W.Krauth, *Transition temperature of the homogeneous, weakly interacting Bose gas*, Phys.Rev.Lett.**83**, 2687 (1999).

[141] C.W.Gardiner and P.Zoller, *Quantum kinetic theory: a quantum kinetic master equation for condensation of a weakly interacting Bose gas without a trapping potential*, Phys.Rev.A**55**, 2902 (1997).

[142] D.Jaksch, C.W.Gardiner and P.Zoller, *Quantum kinetic theory. II. Simulation of the quantum Boltzmann master equation*, Phys.Rev.A**56**, 575 (1998).

[143] C.W.Gardiner and P.Zoller, *Quantum kinetic theory. III. Quantum kinetic master equation for strongly condensed trapped systems*, Phys.Rev.A**58**, 536 (1998).

[144] D.Jaksch, C.W.Gardiner, K.M.Gheri and P.Zoller, *Quantum kinetic theory. IV. Intensity and amplitude fluctuations of a Bose-Einstein condensate at finite temperature including trap loss*, Phys.Rev.A**58**, 1450 (1998).

[145] C.W.Gardiner and P.Zoller, *Quantum kinetic theory. V. Quantum kinetic master equation for mutual interaction of condensate and noncondensate*, Phys.Rev.A**61**, 033601 (2000).

[146] M.D.Lee and C.W.Gardiner, *Quantum kinetic theory. VI. The growth of a Bose-Einstein condensate*, Phys.Rev.A**62**, 033606 (2000).

[147] C.W.Gardiner, P.Zoller, R.J.Ballagh and M.J.Davis, *Kinetics of Bose-Einstein condensation in a trap*, Phys.Rev.Lett.**79**, 1793 (1997).

[148] C.W.Gardiner, M.D.Lee, R.J.Ballagh, M.J.Davis and P.Zoller, *Quantum kinetic theory of condensate growth: comparison of experiment and theory*, Phys.Rev.Lett.**81**, 5266 (1997).

[149] H.T.C.Stoof, J.Low Temp.Phys. **114**, 11 (1999).

[150] M.Imamović-Tomasović and A.Griffin, *Coupled Hartree-Fock-Bogoliubov kinetic equations for a trapped Bose gas*, Phys.Rev.A**60**, 494 (1999).

[151] M.O.Scully and M.S.Zubairy, *Quantum optics* (Cambridge University Press) (1997).

[152] W.H.Louisell, *Quantum statistical properties of radiation* (J.Wiley and sons) (1973).

[153] R.J.Glauber, *The quantum theory of optical coherence*, Phys.Rev. **130**, 2529 (1963).

[154] R.J.Glauber, *Photon correlations*, Phys.Rev.Lett.**10**, 84 (1963).

[155] E.C.G.Sudarshan, *Equivalence of semiclassical and quantum mechanical descriptions of statistical light beams*, Phys.Rev.Lett.**10**, 277 (1963).

[156] K.Vogel and H.Risken, *Quantum-tunneling rates and stationary solutions in dispersive optical bistability*, Phys.Rev.A**38**, 2409 (1988).

[157] P.D.Drummond and C.W.Gardiner, *Generalised P-representations in quantum optics*, J.Phys.A: Math.Gen. **13**, 2353 (1980).

[158] P.D.Drummond, C.W.Gardiner and D.F.Walls, *Quasiprobability methods for nonlinear chemical and optical systems*, Phys.Rev.A**24**, 914 (1981).

[159] S.L.Braunstein, C.M.Caves and G.J.Milburn, *Interpretation for a positive* P *representation*, Phys.Rev.A**43**, 1153 (1991).

[160] P.D.Drummond and D.F.Walls, *Quantum theory of optical bistability. I:Nonlinear polarizability model*, J.Phys.A: Math. Gen. **13**, 725 (1980).

[161] M.Wolinsky and H.J.Carmicheal, *Quantum noise in the parametric oscillator: from squeezed states to coherent-state superpositions*, Phys.Rev.Lett.**60**, 1836 (1988).

[162] P.Kinsler and P.D.Drummond, *Quantum dynamics of the parametric oscillator*, Phys.Rev.A**43**, 6194 (1991).

[163] S.J.Carter, P.D.Drummond, M.D.Reid and R.M.Shelby, *Squeezing of quantum solitons*, Phys.Rev.Lett.**58**, 1841 (1987).

[164] P.D.Drummond and S.J.Carter, *Quantum-field theory of squeezing in solitons*, J.Opt.Soc.Am.B **4**, 1565 (1987).

[165] A.M.Smith and C.W.Gardiner, *Simulations of nonlinear quantum damping using the postive* P *representation*, Phys.Rev.A**39**, 3511 (1989).

[166] I.J.D.Craig and K.J.McNeil, *Quantum simulations of nonlinear optical damping: an exact solution for the stochastic differential equations and an interpretation of "spiking"*, Phys.Rev.A**39**, 6267 (1989).

[167] K.J.McNeil and I.J.D.Craig, *Positive-*P *representation for second-harmonic generation: analytic and computational results*, Phys.Rev.A**41**, 4009 (1990).

[168] R.Schack and A.Schenzle, *Positive* P *representation*, Phys.Rev.A**44**, 682 (1991).

[169] A.Gilchrist, C.W.Gardiner and P.D.Drummond, *Positive* P *representation: application and validity*, Phys.Rev.A**55**, 3014 (1997).

[170] M.J.Steel, M.K.Olsen, L.I.Plimak, P.D.Drummond, S.M.Tan, M.J.Collett, D.F.Walls and R.Graham, *Dynamical quantum noise in trapped Bose-Einstein condensates*, Phys.Rev.A**58**, 4824 (1998).

[171] P.D.Drummond and J.F.Corney, *Quantum dynamics of evaporatively cooled Bose-Einstein condensates*, Phys.Rev.A**60**, R2661 (1999).

[172] J.Dalibard, Y.Castin and K. lmer, *Wave-function approach to dissipative processes in quantum optics*, Phys.Rev.Lett.**68**, 580 (1992).

[173] K.Mølmer, Y.Castin and J.Dalibard, *Monte Carlo wave-function method in quantum optics*, J.Opt.Soc.Am.B **10**, 524 (1993).

[174] C.W.Gardiner, A.S.Parkins and P.Zoller, *Wave-function quantum stochastic differential equations and quantum-jump simulation methods*, Phys.Rev.A**46**, 4363 (1992).

[175] R.Dum, A.S.Parkins, P.Zoller and C.W.Gardiner, *Monte Carlo simulation of master equations in quantum optics for vacuum, thermal, and squeezed reservoirs*, Phys.Rev.A**46**, 4382 (1992).

[176] P.Zoller and C.W.Gardiner, *Quantum noise in quantum optics: the stochastic Schrödinger equation*, in *Quantum fluctuations*, edited by S.Reynaud, E.Giacobino and J.Zinn-Justin, p. 79 (Elsevier Science B.V.) (1995).

[177] I.Carusotto, Y.Castin and J.Dalibard, *The N boson time dependent problem: a reformulation with stochastic wave functions*, accepted for publication on Phys.Rev.A; cond-mat/0003399 (2000).

[178] R.Loudon, *The quantum theory of light* (Clarendon Press, Oxford) (1973).

[179] E.P.Gross, *Structure of a quantized vortex in boson systems*, Nuovo Cimento **20**, 454 (1961).

[180] E.P.Gross, *Hydrodynamics of a superfluid condensate*, J.Math.Phys. **4**, 195 (1963).

[181] L.P.Pitaevskii, *Vortex lines in an imperfect Bose gas*, Zh.Eksp.Teor.Fiz. [Sov.Phys.JETP] **13**, 451 (1961).

[182] F.Dalfovo, S.Giorgini, L.P.Pitaevskii and S.Stringari, *Theory of trapped Bose-condensed gases*, Rev.Mod.Phys. **71**, 463 (1999).

[183] W.Ketterle and H.-J.Miesner, *Coherence properties of Bose-Einstein condensates and atom lasers*, Phys.Rev.A**56**, 3291 (1997).

[184] H.M.Wiseman, *Defining the (atom) laser*, Phys.Rev.A**56**, 2068 (1997).

[185] E.V.Goldstein, O.Zobay and P.Meystre, *Coherence of atomic matter-wave fields*, Phys.Rev.A**53**, 2373 (1998).

[186] E.V.Goldstein and P.Meystre, *Atomic detection and matter-wave coherence*, Phys.Rev.Lett.**80**, 5036 (1998).

[187] M.Yasuda and F.Shimizu, *Observation of two-atom correlation of an ultracold neon atomic beam*, Phys.Rev.Lett.**77**, 3090 (1996).

[188] E.A.Burt, R.W.Ghrist, C.J.Myatt, M.J.Holland, E.A.Cornell and C.E.Wieman, *Coherence, correlations and collisions: what one learns about Bose-Einstein condensates from their decay*, Phys.Rev.Lett.**79**, 337 (1997).

[189] A.Röhrl, M.Naraschewski, A.Schenzle and H.Wallis, *Transition from phase locking to the interference of independent Bose condensates: theory versus experiment*, Phys.Rev.Lett.**78**, 4143 (1997).

[190] J.Williams, R.Walser, J.Cooper, E.Cornell and M.Holland, *Nonlinear Josephson-type oscillations of a driven, two-component Bose-Einstein condensate*, Phys.Rev.A**59**, R31 (1999).

[191] D.S.Hall, M.R.Matthews, J.R.Ensher, C.E.Wieman and E.A.Cornell, *Dynamics of component separation in a binary mixture of Bose-Einstein condensate*, Phys.Rev.Lett.**81**, 1539 (1998).

[192] M.Kozuma, L.Deng, E.W.Hagley, J.Wen, R.Lutwak, K.Helmerson, S.L.Rolston and W.D.Phillips, *Coherent splitting of Bose-Einstein condensates with optically induced Bragg diffraction*, Phys.Rev.Lett.**82**, 871 (1999).

[193] B.P.Anderson and M.A.Kasevich, *Macroscopic Quantum Interference from Atomic Tunnel Arrays*, Science **282**, 1686 (1998).

[194] M.L.Chiofalo, S.Succi and M.P.Tosi, *Output coupling of Bose condensates from atomic tunnel arrays: a numerical study*, Phys.Lett.A **260**, 86 (1999).

[195] M.Trippenbach, Y.B.Band and P.Julienne, *Four-wave mixing in the scattering of Bose-Einstein condensates*, Opt.Express **3**, 530 (1998).

[196] L.Deng, E.W.Hagley, J.Wen, M.Trippenbach, Y.Band, P.S.Julienne, J.E.Simsarian, K.Helmerson, S.L.Rolston and W.D.Phillips, *Four-wave mixing with matter waves*, Nature **398**, 218 (1999).

[197] H.Steck, M.Naraschewski and H.Wallis, *Output of a pulsed atom laser*, Phys.Rev.Lett.**80**, 1 (1998).

[198] E.W.Hagley, L.Deng, M.Kozuma, J.Wen, K.Helmerson, S.L.Rolston and W.D.Phillips, *A well-collimated quasi-continuous atom laser*, Science **283**, 1706 (1999).

[199] I.Bloch, T.W.Hänsch and T.Esslinger, *An atom laser with a cw output coupler*, Phys.Rev.Lett.**82**, 3008 (1999).

[200] M.O.Mewes, M.R.Andrews, D.M.Kurn, D.S.Durfee, C.G.Townsend and W.Ketterle, *Output coupler for Bose-Einstein condensed atoms*, Phys.Rev.Lett.**78**, 582 (1997).

[201] H.Wiseman, A.Martins and D.F.Walls, *An atom laser based on evaporative cooling*, Quant.Semiclass.Opt. **8**, 737 (1996).

[202] E.Mandonnet, A.Minguzzi, R.Dum, I.Carusotto, Y.Castin and J.Dalibard, *Evaporative cooling of an atomic beam*, Eur.Phys.J.D **10** (2000).

[203] M.Olshanii, Y.Castin and J.Dalibard, *A model for an atom laser*, in *Proc.XII Conf. on Laser Spectroscopy*, edited by M.Inguscio, M.Allegrini and A.Sasso, p. 7 (World Scientific, Singapore) (1995).

[204] H.M.Wiseman and M.J.Collett, *An atom laser based on dark-state cooling*, Phys.Lett.A **202**, 246 (1995).

[205] W.Zhang and D.F.Walls, *Phonon-induced quantum pair correlation in the diffraction of an ultracold atomic beam by a crystalline solid surface*, Phys.Rev.A**50**, 4069 (1994).

[206] W.Zhang and D.F.Walls, *Bosonic-degeneracy-induced quantum correlation in a nonlinear atomic beam splitter*, Phys.Rev.A**52**, 4696 (1995).

[207] M.G.Moore and P.Meystre, *Optical control and entanglement of atomic Scrödinger fields*, Phys.Rev.A**59**, R1754 (1999).

[208] Y.Japha, S.Choi, K.Burnett and Y.B.Band, *Coherent output, stimulated quantum evaporation and pair breaking in a trapped atomic Bose gas*, Phys.Rev.Lett.**82**, 1079 (1999).

[209] M.Wilkens, E.Goldstein, B.Taylor and P.Meystre, *Fabry-Perot interferometer for atoms*, Phys.Rev.A**47**, 2366 (1993).

[210] L.Tribe, W.Zhang and B.C.Sanders, *Resonant atomic tunneling through a laser beam*, Phys.Rev.A**54**, 5447 (1996).

[211] L.Santos and L.Roso, *Fabry-Pérot-like transmission spectrum of an atom through a two-Gaussian laser arrangement*, Phys.Rev.A**57**, 432 (1998).

[212] L.Santos and L.Roso, *Multilayer "dielectric" mirror for atoms*, Phys.Rev.A**58**, 2407 (1998).

[213] L.Santos and L.Roso, *Bloch-like quantum multiple reflections of atoms*, Phys.Rev.A**60**, 2312 (1999).

[214] N.Friedman, R.Ozeri and N.Davidson, *Quantum reflection of atoms from a periodic potential*, J.Opt.Soc.Am. B **15**, 1749 (1998).

[215] M.A.Ol'shanii, Yu.B.Ovchinnikov and V.S.Letokhov, *Laser guiding of atoms in a hollow optical fiber*, Opt.Commun. **98**, 77 (1993).

[216] S.Marksteiner, C.M.Savage, P.Zoller and S.L.Rolston, *Coherent atoms waveguides from hollow optical fibers: quantized atomic motion*, Phys.Rev.A**50**, 2680 (1994).

[217] M.J.Renn, D.Montgomery, O.Vdovin, D.Z.Anderson, C.E.Wieman and E.A.Cornell, *Laser-guided atoms in hollow-core optical fibers*, Phys.Rev.Lett.**75**, 3253 (1995).

[218] D.Müller, E.A.Cornell, D.Z.Anderson and E.R.I.Abraham, *Guiding laser-cooled atoms in hollow-core fibers*, Phys.Rev.A**61**, 033411 (2000).

[219] H.Ito, K.Sakaki, T.Nakata, W.Jhe and M.Ohtsu, *Optical potential for atom guidance in a cylindrical-core hollow fiber*, Opt.Comm. **115**, 57 (1995).

[220] J.D.Weinstein and K.G.Libbrecht, *Microscopic magnetic traps for neutral atoms*, Phys.Rev.A**52**, 4004 (1995).

[221] C. J.Fortagh, A.Grossmann and T.W.Hänsch, *Miniaturized wire trap for neutral atoms*, Phys.Rev.Lett.**81**, 5310 (1998).

[222] J.Schmiedmayer, *Quantum wires and quantum dots for neutral atoms*, Eur.Phys.J.D **4**, 57 (1998).

[223] J.Denschlag, D.Cassettari and J.Schmiedmayer, *Guiding neutral atoms with a wire*, Phys.Rev.Lett.**82**, 2014 (1999).

[224] D.Müller, D.Z.Anderson, R.J.Grow, P.D.D.Schwindt and E.A.Cornell, *Guiding neutral atoms around curves with lithographically patterned current-carrying wires*, Phys.Rev.Lett.**83**, 5194 (1999).

[225] D.Müller, E.A.Cornell, M.Prevedelli, P.D.D.Schwindt, A.Zozulya and D.Z.Anderson, *A waveguide atom beamsplitter for laser-cooled neutral atoms*, cond-mat/0003091 (2000).

[226] M.Wilkens, E.Schumacher and P.Meystre, *Band theory of a common model in atom optics*, Phys.Rev.A**44**, 3130 (1991).

[227] J.J.Hope and C.M.Savage, *Band gaps fpr atoms in light-based waveguides*, Phys.Rev.A**53**, 3449 (1996).

[228] Y.Castin, R.Dum, E.Mandonnet, J.Dalibard, A.Minguzzi and I.Carusotto, *Coherence properties of a continuous atom laser*, Submitted to J.Mod.Opt. (2000).

[229] I.Bloch, T.W.Hänsch and T.Esslinger, *Measurement of the spatial coherence of a trapped Bose gas at the phase transition*, Nature **403**, 166 (2000).

[230] E.W.Hagley, L.Deng, M.Kozuma, M.Trippenbach, Y.B.Band, M.Edwards, M.Doery, P. Julienne, K.Helmerson, S.L.Rolston and W.D.Phillips, *Measurement of the coherence of a Bose-Einstein condensate*, Phys.Rev.Lett.**83**, 3112 (1999).

[231] M.Trippenbach, Y.B.Band, M.Edwards, M.Doery and P.S.Julienne, *Coherence properties of an atom laser*, cond-mat/0002119 (2000).

[232] J.Schneider and A.Schenzle, *Output from an atom laser: theory vs. experiment*, Appl.Phys.B: Laser Opt. **69**, 353 (2000).

[233] J.Schneider and A.Schenzle, *Investigations of a two-mode atom laser model*, Phys.Rev.A**61**, 053611 (2000).

[234] M.Naraschewski and R.J.Glauber, *Spatial coherence and density correlations of trapped Bose gases*, Phys.Rev.A**59**, 4595 (1999).

[235] M.Holzmann and Y.Castin, *Pair correlation function of an inhomogeneous interacting Bose-Einstein condensate*, Eur.Phys.J.D **7** (1999).

[236] R.Graham, *Decoherence of Bose-Einstein condensates in traps at finite temperature*, Phys.Rev.Lett.**81**, 5262 (1998).

[237] S.Choi, Y.Japha and K.Burnett, *Adiabatic output coupling of Bose gas at finite temperatures*, Phys.Rev.A**61**, 063606 (2000).

[238] I.Carusotto, M.Artoni and G.C.La Rocca, *Atom laser coherence length and atomic standing waves*, accepted for publication on Phys.Rev.A(2000).

[239] C.W.Gardiner, *Handbook of stochastic methods* (Springer Verlag, Berlin) (1985).

[240] B.W.Batterman and H.Cole, *Dynamical diffraction of X-rays by perfect crystals*, Rev.Mod.Phys. **36**, 681 (1964).

[241] C.Cohen-Tannoudji, B.Diu and F.Laloë, *Quantum mechanics* (Wiley-Interscience) (1977).

[242] M.R.Andrews, M.-O.Mewes, N. Druten, D.S.Durfee, D.M.Kurn and W.Ketterle, *Direct, nondestructive observation of a Bose condensate*, Science **273**, 84 (1996).

[243] J.M.Cowley, *Diffraction physics* (North-Holland) (1981).

[244] K.Vogel and H.Risken, *Quasiprobability distributions in dispersive optical bistability*, Phys.Rev.A**39**, 4675 (1989).

[245] P.R.Berman, ed., *Cavity quantum electrodynamics* (Academic Press) (1993).

[246] H.Schmidt and A.Imamoglu, *Giant Kerr nonlinearities obtained by electromagnetically induced transparency*, Opt.Lett. **21**, 1936 (1996).

[247] G.S.Agarwal and W.Harshawardhan, *Inhibition and enhancement of two photon absorption*, Phys.Rev.Lett.**77**, 1039 (1996).

[248] W.Harshawardhan and G.S.Agarwal, *Controlling optical bistability using electromagnetic-field-induced transparency and quantum interferences*, Phys.Rev.A**53**, 1812 (1996).

[249] Y.Yamamoto, *A photon in solitary confinement*, Nature **390**, 17 (1997).

[250] A.Imamoglu, H.Schmidt, G.Woods and M.Deutsch, *Strongly interacting photons in a nonlinear cavity*, Phys.Rev.Lett.**79**, 1467 (1997), see also the comment ref.251 and the erratum ref.252.

[251] P.Grangier, D.F.Walls and K.M.Gheri, *Comment on "Strongly interacting photons in a nonlinear cavity"*, Phys.Rev.Lett.**81**, 2833 (1998).

[252] A.Imamoglu, H.Schmidt, G.Woods and M.Deutsch, *Erratum: Strongly interacting photons in a nonlinear cavity*, Phys.Rev.Lett.**81**, 2836 (1998).

[253] M.D.Lukin, M.Fleischhauer, M.O.Scully and V.L.Velichansky, *Intracavity electromagnetically induced transparency*, Opt.Lett. **23**, 295 (1998).

[254] K.M.Gheri, W.Alge and P.Grangier, *Quantum analysis of the photonic blockade mechanism*, Phys.Rev.A**60**, R2673 (1999).

[255] M.J.Werner and A.Imamoglu, *Photon-photon interactions in cavity electromagnetically induced transparency*, Phys.Rev.A**61**, R11801 (1999).

[256] S.E.Harris and Y.Yamamoto, *Photon switching by quantum interfererence*, Phys.Rev.Lett.**81**, 3611 (1998).

[257] S.E.Harris and L.H.Hau, *Nonlinear optics at low light levels*, Phys.Rev.Lett.**82**, 4611 (1999).

[258] L.V.Hau, S.E.Harris, Z.Dutton and C.H.Behroozi, *Light speed reduction to 17 metres per second in an ultracold atomic gas*, Nature **397**, 594 (1999).

[259] V.B.Braginsky, M.L.Gorodetsky and V.S.Ilchenko, *Quality-factor and nonlinear properties of optical whispering-gallery modes*, Phys.Lett.A **137**, 393 (1989).

[260] K.Huang, *Statistical mechanics* (Wiley, New York) (1963).

[261] H.Risken, C.Savage, F.Haake and D.F.Walls, *Quantum tunneling in dispersive optical bistability*, Phys.Rev.A**35**, 1729 (1987).

[262] H.Risken and K.Vogel, *Quantum tunneling rates in dispersive optical bistability for low cavity damping*, Phys.Rev.A**38**, 1349 (1988).

[263] A.Imamoglu and Y.Yamamoto, *Noise suppression in semiconductor* p-i-n *junctions: transition from macroscopic squeezing to mesoscopic Coulomb blockade of electron emission processes*, Phys.Rev.Lett.**70**, 3327 (1993).

[264] M.Reznikov, M.Heiblum, H. Shtrikman and D.Mahalu, *Temporal correlation of electrons: suppression of shot noise in a ballistic quantum point contact*, Phys.Rev.Lett.**75**, 3340 (1995).

[265] J.Kim, O.Benson, H.Kan and Y.Yamamoto, *A single-photon turnstile device*, Nature **397**, 500 (1999).

[266] A.Imamoglu and Y.Yamamoto, *Turnstile device for heralded single photons: Coulomb blockade of electron and hole tunneling in quantum confined* p-i-n *heterojunctions*, Nature **390**, 17 (1997).

[267] C.Cohen-Tannoudji and S.Reynaud, *Dressed-atom description of resonance fluorescence and absorption spectra of a multi-level atom in an intense laser beam*, J.Phys.B: Atom.Molec.Phys. **10**, 345 (1977).

[268] P.D.Drummond, K.J.McNeil and D.F.Walls, *Statistical properties of an incoherently driven nonlinear interferometer*, Phys.Rev.Ap. 1672 (1980).

[269] I.Carusotto, *The nonlinear atomic Fabry-Perot interferometer: from the mean-field theory to the* atom blockade *effect* (2000), submitted to Phys.Rev.A.

[270] C.W.Gardiner, *Quantum noise* (Springer Verlag, Berlin) (1991).

[271] Yu.Kagan and B.Svistunov, *Evolution of correlation properties and appearance of broken symmetry in the process of Bose-Einstein condensation*, Phys.Rev.Lett.**79**, 3331 (1997).

[272] A.Sinatra and Y.Castin, *Binary mixtures of Bose-Einstein condensates: Phase dynamics and spatial dynamics*, Eur.Phys.J.D **8**, 319 (2000).

[273] McKean, *Stochastic integrals* (Academic Press, New York) (1969).

[274] M.R.Matthews, B.P.Anderson, P.C.Haljan, D.S.Hall, M.J.Holland, J.E.Williams, C.E.Wieman and E.A.Cornell, *Watching a superfluid untwist itself: recurrence of Rabi oscillations in a Bose-Einstein condensate*, Phys.Rev.Lett.**83**, 3358 (1999).

[275] C.W.Gardiner, *Particle-number-conserving Bogoliubov method which demonstrates the validity of the time-dependent Gross-Pitaevskii equation for a highly condensed Bose gas*, Phys.Rev.A**56**, 1414 (1997).

[276] Y.Castin and R.Dum, *Low-temperature Bose-Einstein condensates in time-dependent traps: beyond the* U(1) *symmetry-breaking approach*, Phys.Rev.A**57**, 3008 (1998).

[277] J.H.Eberly, N.B.Narozhny and J.J.Sanchez-Mondragon, *Periodic spontaneous collapse and revival in a simple quantum model*, Phys.Rev.Lett.**44**, 1323 (1980).

[278] Y. Kagan, E. Surkov and G. Shlyapnikov, *Evolution of a Bose-condensed gas under variations of the confining potential*, Phys.Rev.A**54**, R1753 (1996).

[279] V.M.Pérez-García, H.Michinel, J.I.Cirac, M.Lewenstein and P. Zoller, *Low energy excitations of a Bose-Einstein condensate: A time-dependent variational analysis*, Phys.Rev.Lett.**77**, 5320 (1996).

[280] Y.Castin and R.Dum, *Bose-Einstein condensates in time dependent traps*, Phys.Rev.Lett.**77**, 5315 (1996).

[281] F.Minardi, G.Bianchini, P. Pastor, G.Giusfredi, F.S.Pavone and M.Inguscio, *Measurement of the helium* $2\,^3P_0 - 2\,^3P_1$ *fine structure interval*, Phys.Rev.Lett.**82**, 1112 (1999).

Acknowledgments

Caro lettore,

chiunque tu sia, sappi che io ho provato in tutti i modi a rendere questa tesi il più divertente possibile per te che, volente o nolente, te la sei dovuta leggere.

Ti capisco bene se sei rimasto spaventato da tutte queste pagine scritte fitte fitte, con poche figure e troppe formule, ma spero che tu ti sia fatto coraggio e che, come forse ti è capitato col *Nome della Rosa*, alla fine tu sia ritrovato addosso una tale curiosità di sapere chi è l'assassino che quasi quasi ... sei stato tentato di saltare alle conclusioni! Devi comunque sapere che l'autore (che forse tu conoscerai soltanto come tuo predecessore nelle grinfie di un famelico relatore) si è molto divertito nel ragionare per tre anni di fotoni, eccitoni, collisioni, atomoni e anche ... bicchieroni! E' infatti ben noto (Zichichi docet) che le discussioni di fisica vengono meglio se inumidite con golosità varie, a partire dalle prelibatezze dei ristoranti ericini fino alle più modeste (e famigerate) paste *alla Yak*. La mia sapienza triennale mi dice infatti che la buona compagnia è essenziale per fare della buona fisica; e di questo non posso che ringraziare tutte le persone con cui ho avuto l'onore e il piacere di discutere e lavorare in questi primi anni da (aspirante) fisico.

Primo fra tutti, il prof. Giuseppe La Rocca, il cui ruolo nell'indirizzare i miei (spesso dispersivi) interessi è stato essenziale: la sua inespugnabile cultura fisica si è sempre rivelata a prova di domanda e, in tutti i lavori, anche quelli forse più lontani dai suoi originari interessi, il suo intuito fisico si è rivelato impareggiabile nell'indicare le vie più fruttuose e i collegamenti più arditi. Unici poi la sua disponibilità e il suo incoraggiamento ad allargare le mie vedute facendo conoscenza e collaborando con i gruppi più disparati, anche se questo mi ha spesso reso uno studente un po' evanescente!

Segue da presso il prof. Massimo Inguscio, il cui trascinante sostegno ed entusiasmo non sono venuti mai meno; in particolare, non posso che ringraziarlo per la

stimolante collaborazione con il suo laboratorio a Firenze e, soprattutto, per avermi offerto la possibilità di andare a farmi le ossa a Parigi.

I sei mesi parigini sono certamente stati fra i più fecondi di nuove idee: sia le continue chiacchierate con i vari membri del *Laboratoire Kastler-Brossel* in occasione dei seminari e dei frequenti pots di festeggiamento, sia le impegnative discussioni con Jean Dalibard e Yvan Castin hanno dato un contributo essenziale sia alla mia cultura generale che al raffinamento delle tecniche concrete di lavoro; molti dei risultati discussi in questa tesi non sarebbero mai stati ottenuti senza i pomeriggi passati con loro a discutere seduti per terra davanti alla lavagna con in mano una cialda di Montecatini o davanti al fido tom.lkb.ens.fr a debuggare i mitici "TwoModes.f90" e "GPstoch.f90" che hanno popolato i miei incubi notturni fino a quando non ho imparato ad apprezzare la birra tedesca.

E come non ricordare tutti i vari compagni di studio, mensa e avventure che mi hanno continuamente stimolato con discussioni di ogni tipo ad interessarmi degli argomenti più diversi. Solo qualche nome in ordine più o meno cronologico: Cristiano C., Simone L., Anna M., Alessandra F., Galimba, Davide C., Riccardo S., Denis B., Markus H. Gabri F., Corinna U. e Paolo G., senza i quali il lavoro di fisico non sarebbe di sicuro stato cosí appassionante!

E, per concludere in modo degno questi ringraziamenti (*in cauda venenum*), come non rendere omaggio a tutti coloro che hanno cercato in tutti i modi di osteggiare lo svolgimento del mio lavoro da fisico e salvare il mio pencolante equilibrio mentale con discorsi del tipo:

• La mamma: "La mia amica xxx ti ha visto per la strada: dice che quest'estate sei più pallido e rifinito del solito; perché non te ne vai a trovare i tuoi amici al mare, invece di startene in terrazza tra i tuoi fogli"

• Il babbo: "Non è possibile che tu con la bici da corsa non mi stacchi neppure in salita, sei proprio una ... (edulc. polenta)"

• Le gatte: "Miao miao!" (trad. simult. dal gattesco: "Ma ti decidi a comprare qualcosa di decente da mangiare, invece delle solite scatolette")

• Certi (ingenui...) amici fisici: "Tu lavori troppo e ci fai sentire tutti in colpa"

• Certi (meno ingenui...) amici fisici: "Domenica gita in bici alle Cinque Terre. E non dire che hai da lavorare che tanto non ti crediamo!"

• L'*Armata Brancaleone* (dopo l'umiliante sconfitta con le matricole di *Scienze I*): "Sigh! Sob! Sigh! Sob! Forse dovremmo allenarci più spesso..."

• E infine certi amici non fisici: “Andiamo a pescare? Guarda che se no lo chiedo a tuo babbo; lui sí che ci verrebbe volentieri!”. Al ché il babbo mi toglieva i libri di mano e mi spediva forzatamente a pesca...